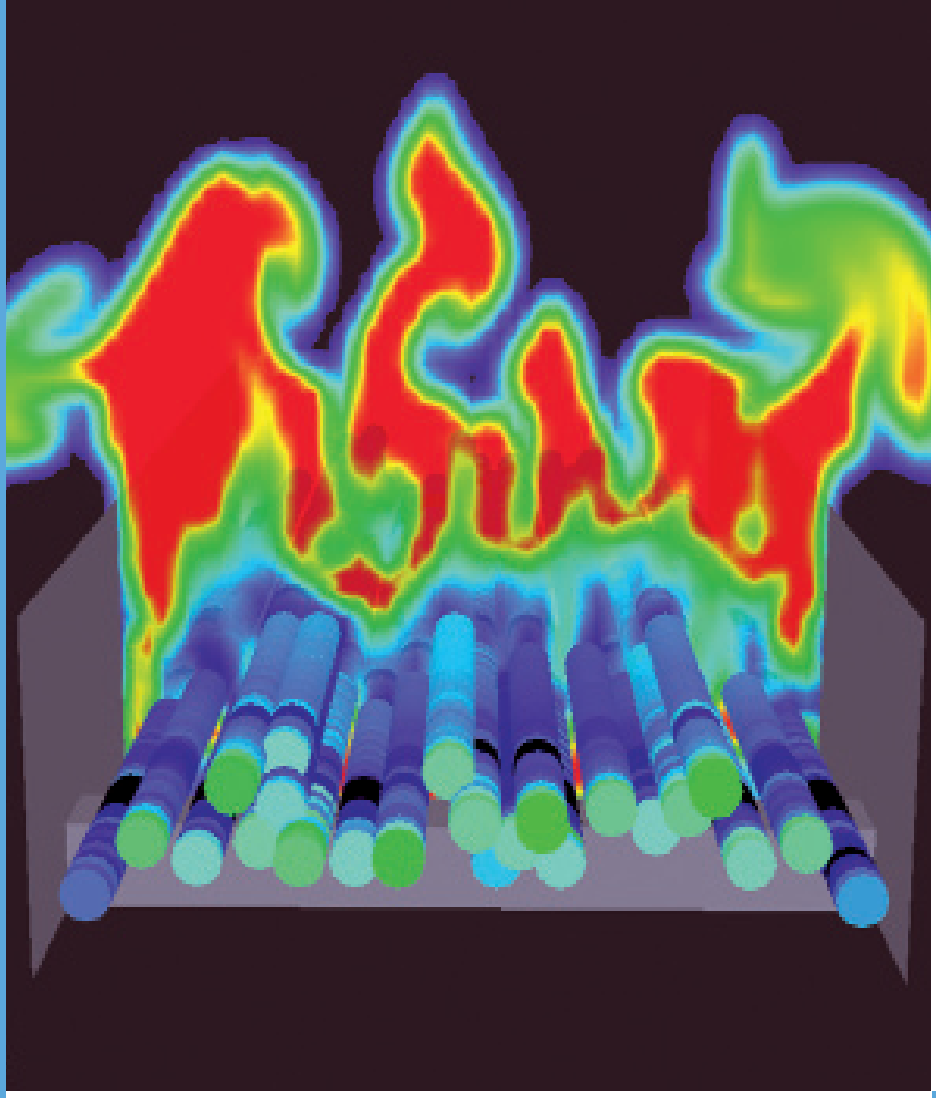

SCIENCE • TECHNOLOGY • RESEARCH HIGHLIGHTS • VISIONS •

Dissertation
44

Methods and applications of pyrolysis modelling for polymeric materials

Anna Matala

VTT

VTT SCIENCE 44

Methods and applications of pyrolysis modelling for polymeric materials

Anna Matala

Thesis for the degree of Doctor of Science (Technology) to be presented with due permission for public examination and criticism in Otakaari 1, at Aalto University School of Science, on the 15.11.2013 at 12 noon.

ISBN 978-951-38-8101-6 (Soft back ed.)
ISBN 978-951-38-8102-3 (URL: http://www.vtt.fi/publications/index.jsp)

VTT Science 44

ISSN-L 2242-119X
ISSN 2242-119X (Print)
ISSN 2242-1203 (Online)

JULKAISIJA – UTGIVARE – PUBLISHER

VTT
PL 1000 (Tekniikantie 4 A, Espoo)
02044 VTT
Puh. 020 722 111, faksi 020 722 7001

VTT
PB 1000 (Teknikvägen 4 A, Esbo)
FI-02044 VTT
Tfn. +358 20 722 111, telefax +358 20 722 7001

VTT Technical Research Centre of Finland
P.O. Box 1000 (Tekniikantie 4 A, Espoo)
FI-02044 VTT, Finland
Tel. +358 20 722 111, fax +358 20 722 7001

Kopijyvä Oy, Kuopio 2013

Methods and applications of pyrolysis modelling for polymeric materials

Pyrolyysimallinnuksen metodeita ja sovelluksia polymeereille. **Anna Matala.** Espoo 2013. VTT Science 44. 85 p. + app. 87 p.

Abstract

Fire is a real threat for people and property. However, if the risks can be identified before the accident, the consequences can be remarkably limited. The requirement of fire safety is particularly important in places with large number of people and limited evacuation possibilities (e.g., ships and airplanes) and for places where the consequences of fire may spread wide outside of the fire location (e.g., nuclear power plants).

The prerequisite for reliable fire safety assessment is to be able to predict the fire spread instead of prescribing it. For predicting the fire spread accurately, the pyrolysis reaction of the solid phase must be modelled. The pyrolysis is often modelled using the Arrhenius equation with three unknown parameters per each reaction. These parameters are not material, but model specific, and therefore they need to be estimated from the experimental small-scale data for each sample and model individually.

The typical fuel materials in applications of fire safety engineers are not always well-defined or characterised. For instance, in electrical cables, the polymer blend may include large quantities of additives that change the fire performance of the polymer completely. Knowing the exact chemical compound is not necessary for an accurate model, but the thermal degradation and the release of combustible gases should be identified correctly.

The literature study of this dissertation summarises the most important background information about pyrolysis modelling and the thermal degradation of the polymers needed for understanding the methods and results of this dissertation. The articles cover developing methods for pyrolysis modelling and testing them for various materials. The sensitivity of the model for the modelling choices is also addressed by testing several typical modeller choices. The heat release of unknown polymer blend is studied using Microscale Combustion Calorimetry (MCC), and two methods are developed for effectively using the MCC results in building an accurate reaction path. The process of pyrolysis modelling is presented and discussed. Lastly, the methods of cable modelling are applied to a large scale simulation of a cable tunnel of a Finnish nuclear power plant.

The results show that the developed methods are practical, produce accurate fits for the experimental results, and can be used with different materials. Using these methods, the modeller is able to build an accurate reaction path even if the material is partly uncharacterised. The methods have already been applied to simulating real scale fire scenarios, and the validation work is continuing.

Keywords pyrolysis modelling, simulation, polymer, cables, composites, probabilistic risk assessment (PRA)

Pyrolyysimallinnuksen metodeita ja sovelluksia polymeereille

Methods and applications of pyrolysis modelling for polymeric materials. **Anna Matala.** Espoo 2013. VTT Science 44. 85 s. + liitt. 87 s.

Tiivistelmä

Tulipalot aiheuttavat todellisen uhan ihmisille ja omaisuudelle. Mikäli riskit voidaan tunnistaa jo ennen onnettomuutta, tulipalon ikäviä seurauksia voidaan rajoittaa. Paloturvallisuuden merkitys korostuu erityisesti paikoissa, joissa on paljon ihmisiä ja rajoitetut evakuointimahdollisuudet (esim. laivat ja lentokoneet), ja laitoksissa, joissa tulipalon seuraukset voivat levitä laajalle palopaikan ulkopuolellekin (esim. ydinvoimalaitokset).

Jotta materiaalien palokäyttäytymistä voitaisiin luotettavasti tarkastella erilaisissa olosuhteissa, pitää palon leviäminen pystyä ennustamaan sen sijaan, että paloteho määrättäisiin ennalta. Palon leviämisen ennustamiseksi täytyy materiaalin kiinteän faasin pyrolyysireaktiot tuntea ja mallintaa. Pyrolyysi mallinnetaan usein käyttäen Arrheniuksen yhtälöä, jossa on kolme tuntematonta parametria jokaista reaktiota kohti. Nämä parametrit eivät ole materiaali- vaan mallikohtaisia, ja siksi ne täytyy estimoida kokeellisista pienen mittakaavan kokeista jokaiselle näytteelle ja mallille erikseen.

Paloturvallisuusinsinöörin kannalta erityisen hankalaa on, että palavat materiaalit eivät useinkaan ole hyvin määriteltyjä tai tunnettuja. Esimerkiksi sähkökaapeleiden polymeeriseokset voivat sisältää suuria määriä erilaisia lisäaineita, jotka vaikuttavat materiaalin palokäyttäytymiseen merkittävästi. Kemiallisen koostumuksen tunteminen ei ole välttämätöntä luotettavan mallin aikaansaamiseksi, mutta aineen lämpöhajoaminen ja erityisesti palavien kaasujen vapautuminen tulisi tuntea tarkasti.

Väitöskirjan tiivistelmäosa kokoaa yhteen tärkeimmät taustatiedot pyrolyysimallinnuksen ja polymeerien palokäyttäytymisen ymmärtämisen tueksi. Tässä väitöstyössä on kehitetty menetelmiä pyrolyysiparametrien estimoimiseksi ja näitä metodeita on testattu erilaisilla materiaaleilla. Mallinnusvalintojen merkitystä mallin tarkkuuteen on myös tutkittu herkkyysanalyysin keinoin. Osittain tuntemattomien polymeeriseosten lämmön vapautumista on tutkittu käyttäen mikrokalorimetria. Mikrokalorimetritulosten hyödyntämiseksi kehitettiin kaksi metodia, joiden avulla voidaan saada aikaan entistä tarkempia reaktiopolkuja. Lopuksi pyrolyysimallinnusta on hyödynnetty sovellusesimerkissä suomalaisen ydinvoimalan kaapelitilan täyden mittakaavan kaapelisimuloinneissa.

Tulokset osoittavat, että tässä työssä kehitetyt menetelmät ovat käytännöllisiä, tuottavat riittävän tarkkoja sovituksia koetuloksille ja niitä voidaan soveltaa monien erilaisten materiaalien mallintamiseen. Näitä menetelmiä käyttämällä mallintaja pystyy mallintamaan tuntemattomienkin materiaalien palokäyttäytymistä riittävän tarkasti. Menetelmiä on jo sovellettu todellisten, suuren mittakaavan palotilanteiden simuloimiseksi, ja validointityö jatkuu edelleen.

Avainsanat pyrolyysimallinnus, simulaatiot, polymeerit, kaapelit, komposiitit, todennäköisyyspohjainen riskianalyysi (PRA)

Preface

In spring 2007 I returned home from a job interview full of excitement; I had been offered a summer job at the fire research team of VTT. I did not know much about the work itself, but what could be "hotter" than a summer job playing with fire and even getting paid for it! That summer I implemented the first version of my genetic algorithm application for Matlab that has been extensively used throughout this dissertation work. After the summer job, I progressed to be a Master's thesis worker in the same team, and after graduation the work continued naturally towards the PhD dissertation (I don't think anyone even asked me if I was interested in doing a PhD, it just happened). During these years, I have had the opportunity to get familiar with the fascinating topic of fire and pyrolysis modelling, and had an opportunity to get to know many inspiring people. The learning has not been fully successful – I still burn my fingers regularly, both at work and at home, but I still love watching fire and burning things; who wouldn't?

There are so many great people I want to thank for contributing to my dissertation. First of all, I would like to acknowledge my Professor Harri Ehtamo from Aalto University School of Science, for supervising this PhD work, and the pre-examiners, Dr. Richard E. Lyon and Dr. Brian Lattimer, for their valuable comments. I would like to thank my thesis advisor and boss, Dr. Simo Hostikka from VTT, who has been supervising my work at VTT ever since the summer of 2007. He has provided continuous support, patiently provided answers to my never-ending questions and motivated me when my own ideas wained. At VTT, I'm also grateful to our technology manager Dr. Eila Lehmus, for making this doctoral work possible and for her encouragement, Dr. Esko Mikkola for his valuable comments on my dissertation manuscript and for being the best office mate, and Dr. Johan Mangs and Dr. Tuula Hakkarainen for guidance and company during the long hours of experimental work. My team (past and current) deserves a special acknowledgement for the great work ambience, and for making it easy and pleasant place to work; thank you Simo, Tuula, Esko, Johan, Topi, Antti, Terhi, Timo, Jukka, Kati, Tuomo, Peter and Tuomas. From VTT expert services, I would like to thank Mr. Konsta Taimisalo for sharing some of his endless knowledge on the experimental work and his help during the tests, and also Ms. Hanna Hykkyrä and Ms. Katja Ruotanen for their help with experimental work as well as the out of hours activities.

I had the opportunity to spend a year in the University of California, Berkeley, Department of Mechanical Engineering. I am grateful to Professor Carlos Fernandez-Pello for his supervision during that time, introducing me to many important people and for making sure I did not return home without getting tanned. I would also like to thank Dr. Chris Lautenberger for the cooperation, discussions and, most importantly, the trips to the Wine County and Lake Tahoe. Thanks to Nikki, for making Guifré and me feel so welcome. Thanks to David and Erin Rich for welcoming us to their house during the first week, for lending a bed and for the good times in their beautiful garden. I would like to thank Sonia and Laurence for being my 'Berkeley sisters', I miss you a lot. Thanks to everyone in and outside the lab (Diana!), you all made my stay in California very special!

I would like to thank Dr. Kevin McGrattan from NIST for the discussions, support and help related to FDS. I also greatly appreciate the experimental data I received from the CHRISTIFIRE project. I also acknowledge Dr. Tuula Leskelä from Aalto University School of Chemical Technology for performing the STA experiments for several materials. I would like to thank Dr. Sophie Cozien-Cazuc from Cytec, Dr. Per Blomqvist from SP, and Mr. Iván Sánchez from Gaiker, for providing samples, experimental results and support on the composites.

I'm grateful to my entire family for support, opportunities, and, most importantly, absolute love at all the phases of this work and of my life. Thank you Mum and Neville, Dad and Aulikki, Roser and Angel, Saara, Raakku, Guillem and Rommi, as well as my grandparents, cousins and other relatives. Thanks to all my friends for always being there for me, for the dinners and brunches, evenings with dance or guitar hero, walks and skiing, and all the other things I have had a pleasure to share with you. I couldn't have done this without you. Lastly, thanks to my awesome husband, Guifré, for his love and support. He believed in me when I lost the motivation, helped with all the details of this dissertation, and took me out to run when I started to climb the walls. You are the best thing that ever happened to me. T'estimo.

The work on this thesis has been mainly done in three major projects: SAFIR2010, SAFIR2014 and FIRE-RESIST. The two first are partially funded by The State Nuclear Waste Management Fund (VYR) and the third is part of the Seventh Framework Programme of European Commission. I'm also grateful to the strategic research funding of VTT for supporting the research and writing of this dissertation.

Espoo, October 10, 2013
Anna Matala

Academic dissertation

Supervisor	Professor Harri Ehtamo Aalto University School of Science Systems Analysis Laboratory Finland
Instructor	Doctor Simo Hostikka VTT Technical Research Centre of Finland
Reviewers	Doctor Richard E. Lyon, Federal Aviation Administration, USA Associate Professor Brian Y. Lattimer, Virginia Tech, USA
Opponent	Professor Richard Hull, University of Central Lancashire, UK

List of publications

This thesis is based on the following original publications which are referred to in the text as I–V. The publications are reproduced with kind permission from the publishers.

I. Matala, A., Hostikka, S. and Mangs, J. (2008) Estimation of Pyrolysis Model Parameters for Solid Materials Using Thermogravimetric Data. Fire Safety Science – Proceedings of the Ninth International Symposium, International Association for Fire Safety Science, pp. 1213–1224.

II. Matala, A., Lautenberger, C. and Hostikka, S. (2012) Generalized direct method for pyrolysis kinetic parameter estimation and comparison to existing methods. Journal of Fire Sciences, Vol. 30, No. 4, pp. 339–356.

III. Matala, A. and Hostikka, S. (2011) Pyrolysis Modelling of PVC Cable Materials. Fire Safety Science – Proceedings of the Tenth International Symposium, International Association for Fire Safety Science, pp. 917–930.

IV. Matala, A. and Hostikka, S. (2013) Modelling polymeric material using Microscale combustion calorimetry and other small scale data. Manuscript submitted to Fire and Materials in June 2013.

V. Matala, A. and Hostikka, S. (2011) Probabilistic simulation of cable performance and water based protection in cable tunnel fires. Nuclear Engineering and Design, Vol. 241, No. 12, pp. 5263–5274.

Author's contributions

Matala is the main author of all the publications I–V and has performed most of the work reported in the articles.

In Publication I, the author developed a Matlab tool for data processing and genetic algorithm application. She also performed the parameter estimations using the tool for several materials reported in the article.

In Publication II, the author developed an analytical method for estimating the kinetic parameters of pyrolysis reaction together with Lautenberger. Lautenberger was responsible for the parameter estimations using estimation algorithms while the author estimated the parameters using analytical methods.

In Publication III, the author estimated all the parameters, performed the sensitivity study of the modelling choices, and participated in performing the cone calorimeter experiments.

In Publication IV, the author developed the method for using the Microscale Combustion Calorimetry and tested it using generated and experimental data.

In Publication V, the author did the material parameter estimation for the cable, estimated the sprinkler parameters using experimental results and performed the Monte Carlo simulations using different water suppression configurations. She also participated to the cone calorimeter experiments of the cable, and designed and performed the water distribution tests for nozzles together with Hostikka.

Contents

List of Figures

List of Tables

List of Symbols

A	Pre-exponential factor
c_p	Specific heat
E	Activation energy
f	Reaction model
ΔH	Heat of reaction
ΔH_c	Heat of combustion
k	Thermal conductivity
k_r	Reaction constant
m	Mass
$\dot{m}$	Mass loss rate
M	Experimental result
N	Reaction order
N_k	Number of experimental results
N_{O_2}	Reaction order of oxygen concentration
Q	Total heat release
$\dot{q}$	Heat release rate
R	Universal gas constant
T	Temperature
t	Time
x	Depth
Y	Mass fraction / Oxygen concentration
y	yield
Z	Residue yield

Greek

α	Fractional conversion of mass
β	Heating rate
δ	Thickness / Scaling factor
ϵ	Emissivity
κ	Absorption coefficient
μ	Mean of the heating rates
ρ	Density

Subscripts

0	Initial value
exp	Experimental
F	Fuel gas
I	Inert gas
i	Component index / Time step
j	Reaction index
k	Exp. result index (in GA)
mod	Model
Z	Residue

List of Abbreviations

ATH	Alumina trihydrate
CaCl	Calcium Chloride
$CaCO_3$	Calcium Carbonate
CFD	Computational Fluid Dynamics
DM	Direct method
DOP	Diethylhexyl Phthalate
DPO	Diphenyl oxide
DSC	Differential Scanning Calorimetry
FDS	Fire Dynamics Simulator
FEM	Finite Element Method
GA	Genetic Algorithm
GDM	Generalized Direct Method
HCl	Hydrochloric acid
HGA	Hybrid Generic Algorithm
HRR	Heat release rate
LH	Latin Hypercubes
MC	Monte Carlo
MCC	Microscale Combustion Calorimeter
MD	Molecular dynamics
MDH	Magnesium hydroxide
MLR	Mass loss rate
NPP	Nuclear power plant
PFS	Probabilistic Fire Simulator
PMMA	Poly(methyl methacrylate)
PRA	Probabilistic Risk Assessment
PVC	Polyvinyl Chloride
SA	Simulated Annealing
SCE	Suffled Complex Evolution
SGS	Sub-grid-scale
SHC	Stochastic Hill Climber
TGA	Thermogravimetric Analysis

1. Introduction

1.1 Background

Fire causes significant harm to people and property. In Finland, on average 100 people (about 18 per million citizens) die every year through fire, although the trend has been descending in recent years. Deaths due to fires initiated from smoking or careless handling of fire decreased in 2007–2010, but the number of fires caused by vandalism rose [1]. Although most fires that lead to death occur in residential buildings, the potential consequences of fire become especially serious in public places with high occupation yet limited evacuation possibilities, such as on aeroplanes [2] or ships [3]. Fires in industry may arise for various reasons, including failing electronic components, dust, or vandalism, and cause significant expenses to the owners and insurance companies.

In general, the objective of fire safety engineering is to protect first people and animals, then property and the fire fighters. In some safety critical facilities, such as nuclear power plants (NPP), these objectives are not enough: one must also consider the environmental problems caused by leaking radioactive material or the economic losses of industry that are caused by the attendant lack of power. Fire at a nuclear power plant is considered to be among *initiating events* (events that could begin a chain of events leading to a serious accident) in *probabilistic risk assessment* (PRA); therefore it is a focus of extensive research [4].

In the earlier times, building materials were limited to those available more directly from nature: wood, stone, and metals. Entire cities of wooden houses easily burnt to the ground, and iron structures rust away and fall down. In the 20th century, however, new materials started to emerge. The use of polymers and synthetic fibres increased in the manufacturing of furnitures and other household goods. As electronics grew more and more commonplace, kitchens and living rooms became filled with new gadgets and cables of various types. Cables also account for a significant proportion of the fire load at factories and power plants.

The search for better materials led to the development of modern composites. In transportation, the composites were designed to be lighter, less expensive, stiffer, or stronger than the original metal. These qualities make composites very attractive, especially in, for example, the aviation industry. More than 50% of the structure of an Airbus 380 is made of composite materials [5]. Unfortunately, the fire performance of these new materials does not always improve

on (or even equal) that of the traditional materials. A laminate loses its structure when heated, and in a polymer composite only parts of the material survive the fire. A glass fibre reinforced phenolic composite after a fire is shown in Figure 1.1. The structure is weakened by the pyrolysis of the phenolic polymer and the subsequent delamination.

Clearly, the new materials needed protection from the heat. That is why several flame retardant additives have been developed over the years. Some materials are flame retardant by nature, such as charring wood or materials that release non-combustible gas that cools the surface and dilutes the combustion gases (as halogen in polyvinyl chloride (PVC) does). Halogenated flame retardants are not recommended nowadays, because of environmental concerns, but a similar mechanism has been adopted for new, non-corrosive flame retardants that release, for example, water [6, 7]. Wood charring has also inspired new, intumescent surfaces that protect the underlying surface from the heat [8].

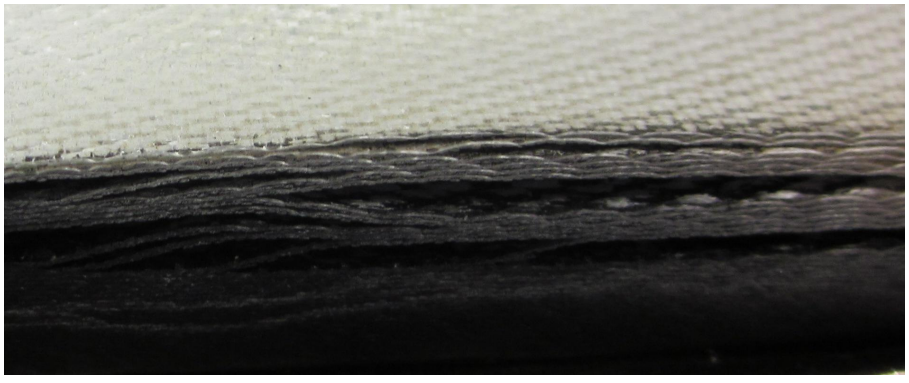

Figure 1.1. Glass fibre-Phenolic composite after fire.

Fire simulations are used extensively in the planning and design of new solutions for structures or interiors of buildings. They can be used as an element of performance-based design, wherein the designer has to prove that the new solution is at least as safe as the previously accepted solutions. They can also be used as part of the PRA of nuclear power plants [4].

Increased processing capacity and improvements to software have made extensive fire simulations possible. The simulations can be used to predict fire spread and/or its consequences and to study structural performance [9], the water suppression [10], evacuation safety [11], or even the human behaviour [12]. Studies of the thermal degradation at atomic level have been done by means of molecular dynamics (MD) [13].

Pyrolysis modelling is an important part of a modern fire simulation. Traditionally, the consequences of fire have been evaluated on basis of pre-described

fires and standard fire curves. Pyrolysis modelling is designed to predict the heat release rate and the response of the structures and materials that follows. It allows implementation of more realistic fire scenarios and study of the flame spread.

In the future, pyrolysis modelling may also be used in product development for new materials. Potential fire risks and the structures' performance in fire could be evaluated by means of simulations before manufacture of large samples. Pyrolysis modelling can also be part of the process of optimisation of the new materials' properties. This could be especially useful in development of new flame retardant materials or mechanisms.

Pyrolysis modelling consists of five steps:

1. The material is tested experimentally on small scale. Typical experimental methods in this connection are thermogravimetric analysis (TGA) [14,15] and cone calorimeter [16].
2. The experiments are described by a mathematical model. The pyrolysis is often modelled by means of Arrhenius equation in combination with data on heat transfer [17,18]. The model's validation is an important part of the process.
3. The model has to be solved numerically and this solution verified.
4. Model parameters are often unknown and have to be estimated by fitting of the model to the experimental results.
5. The pyrolysis model is taken in combination with the computational fluid dynamics (CFD) calculations. This is the case with the Fire Dynamics Simulator (FDS) [18].

The present work concentrates on finding methods for estimation of the pyrolysis parameters, an important topic since the model parameters are not always well-known or even well-defined sets for any given material. They may vary significantly, depending on the model's limitations and complexity. Therefore, they cannot be listed in any handbook or on a product sheet. The most significant difference between the work of a fire safety engineer and a product R&D engineer is that the fire safety engineer does not usually have precise information about the fuel or fire load. There is a demand for methods that are accurate enough for predicting the material degradation correctly and at the same time are simple and fast enough that they can be easily used by a practising fire engineer.

Several methods have been developed for extracting the reaction (or *kinetic*) parameters from the experimental data, some simple and fast and others more complicated but providing more accurate results. The other (*thermal*) parameters are typically estimated from bench scale data [19] or in some cases measured directly [20]. Publication I and Publication II cover the authors contri-

bution to the estimation methods and Publication III describes the sensitivity study for the modelling choices.

This dissertation provides methods for pyrolysis modelling of these complex materials. It also offers methods for calculating the reaction specific heat release rate that can in some cases be used in estimation of the material composition (in Publication IV).

Not only the material parameters, but also the geometry and structure, additives and flame retardants may cause challenges in larger scale simulations with complex materials such as cables or composites. The methods are applied to a real fire safety assessment for a nuclear power plant in Publication V.

The work on this dissertation was carried out primarily in two projects. The material modelling of the cables for improving nuclear power plant fire safety has been developed as part of the Finnish Research Programme on Nuclear Power Plant Safety (SAFIR 2010[1] and SAFIR 2014[2]) [4]. The work pertaining to composites is done as part of the European Union project FIRE-RESIST[3].

1.2 Outline of the dissertation

The dissertation is organised as follows:

Chapter 2 provides the background on the work done for this dissertation. First, the pyrolysis model and other important equations for the material modelling are reviewed. Then the experimental methods used for the parameter estimation are presented. Literature on some significant estimation methods is reviewed. Also, the Monte Carlo method is presented in brief.

Chapter 3 presents some special cases of pyrolysis modelling, including thermoplastic and thermoset polymers and intumescent surfaces. It also provides a literature review considering some complex materials (PVC, cables, and composites) and the associated modelling.

Chapter 4 summarises the methods developed by the author in the course of the doctoral research. First, the FDS models of the experimental methods are briefly described. After this, the applications of the two estimation methods (one analytical and one a curve fitting algorithm) are discussed, after which an application of new experimental method that can be used in parameter estimation, *microscale combustion calorimetry* (MCC), is presented.

Chapter 5 summarises the most important results emerging in Publications I–V and some additional discussion related to the topics of this work.

Chapter 6 presents conclusions and discussion of the topic of the dissertation. Future plans and possibilities for applications are presented.

[1] See http://virtual.vtt.fi/virtual/safir2010/
[2] See http://virtual.vtt.fi/virtual/safir2014/
[3] See http://www.fire-resist.eu/FireResist/index.xhtml

2. Pyrolysis modelling and fire simulations

2.1 Motivation

If one is to be able to predict the spread of fire, the pyrolysis model, starting with the solid phase degradation reactions, has to be defined. This chapter provides background information and the literature survey needed for understanding of the concepts of pyrolysis modelling. First, a brief review of the pyrolysis model and the equations needed for predicting the fire spread of a material are presented. Then the experimental methods essential to the pyrolysis modelling are described. An review of literature on existing parameter estimation methods is provided and discussed in brief. The methods applied and improved upon for Publication I and Publication II are based on these methods. Lastly, the Monte Carlo simulation method is presented as it is relevant for an understanding of Publication V.

2.2 The pyrolysis model

Pyrolysis is the thermal degradation that occurs in the solid phase of a material when it is heated. The bonds between the molecules start to break at elevated temperatures, leading to release of volatile compounds and changes from the original structure of the material. This is seen as mass loss. Technically, 'pyrolysis' refers only to thermal degradation without oxygen; in general (regardless of the oxygen concentration) the mechanism is called thermolysis. In the presence of air, the carbonous residue may oxidise. The combustible gases released during the pyrolysis may also ignite, leading to combustion in the gas phase. This increases the gas temperature, with the results being slightly faster degradation than in inert ambient. In this dissertation, the term 'pyrolysis' is used to describe the thermal degradation at elevated temperatures both in inert ambient and in the presence of oxygen.

The temperature dependent reaction rate of the pyrolysis is often described by the Arrhenius equation. This equation describes the temperature dependence of reaction constant

$$k_r = Ae^{-\frac{E}{RT}}, \tag{2.1}$$

where A is the pre-exponential factor, E the activation energy, R the universal gas constant, and T temperature. Originally developed by Svante Arrhenius

in 1884 in study of the dissociation of electrolytes [21], the equation has been applied since then in various fields of research, from chemical and physical processes to studies of quantum statistics and climate change [21–28]

In the fire community interest in the Arrhenius parameters grew in the late 20th century, first for describing the char oxidation [29–31] and then for predicting the thermal decomposition in the solid phase [17–19].

The equation gives a relationship between reaction rate and temperature and is often represented in the form

$$r_j = \frac{d\alpha}{dt} = A_j f(\alpha) e^{-\frac{E_j}{RT}}, \tag{2.2}$$

where $\alpha = (m_0 - m)/(m_0)$ is the fractional conversion from reactants to products ranging from 0 to 1, and T the temperature of the solid. The so called *kinetic triplet* consists of A_j, E_j, and reaction model $f(\alpha)$. Each reaction j has a different kinetic triplet. The reaction model often depends on reaction order N_k and may be expressed as

$$f(\alpha) = (1 - \alpha)^{N_j}. \tag{2.3}$$

The stoichiometric reaction orders of chemical reactions are integers (usually 1). The thermal degradation is a consequence of the chemical bonds breaking at elevated temperatures. The materials consist of several, different bonds, requiring different amounts of energy for breaking. The overall mass loss reaction is, therefore, a combination of several chemical reactions. In pyrolysis modelling, these reactions are lumped together and hence fractional reaction rates also are used. The model is not an attempt to describe each chemical reaction exactly; the parameters should be considered model specific elements that merge the net effect of several overlapping reactions.

The reaction rate depends on the temperature. The temperature at the front surface of the material rises through by radiation and convection, while inside the material the heat is transferred via conduction and internal radiation. A one dimensional heat conduction equation with internal heat generation/absorption is often sufficient to determine the temperature gradient, $T(x)$:

$$\rho c_p \frac{dT}{dt} = \frac{\partial}{\partial x} k \frac{\partial T}{\partial x} + \dot{q}_s^{'''}, \tag{2.4}$$

where ρ is the solid density, c_p the specific heat capacity, k thermal conductivity, x depth from the surface and $\dot{q}_s^{'''}$ a source term that consists of the chemical reactions ($\dot{q}_{s,c}^{'''}$) and the radiation and emission at depth ($\dot{q}_{s,r}^{'''}$). The chemical

source term is linked to the Arrhenius equation by the reaction rate:

$$\dot{q}_{s,c}^{'''} = -\rho_0 \sum_j r_j(x) \Delta H_j, \tag{2.5}$$

where ΔH_j is the heat of reaction of reaction j.

The boundary condition at front (F) surface is

$$-k \frac{\partial T}{\partial x}(0,t) = \dot{q}_c^{''} + \dot{q}_r^{''}, \tag{2.6}$$

where convective heat flux $\dot{q}_c^{''}$ is

$$\dot{q}_c^{''} = h(T_g - T_F); \tag{2.7}$$

constant h is the heat transfer coefficient, and the net radiative flux is

$$\dot{q}_r^{''} = \dot{q}_{r,in}^{''} - \epsilon \, \sigma \, T_F^4, \tag{2.8}$$

where ϵ is the emissivity and σ the Stefan-Boltzmann coefficient. [14, 18]

In the presence of air, the combustible gases released during pyrolysis may ignite and lead to combustion. This is modelled through assumption of a component specific heat of combustion (ΔH_c) that describes the heat released per unit mass. The heat release rate per unit area then becomes

$$\dot{q}^{''} = \dot{m}^{''} \Delta H_c = \Delta H_c \int_0^L \sum_j \sum_i A_{i,j} \rho_i e^{-E_{i,j}/RT(x)} dx, \tag{2.9}$$

where i is the component (material) index and j reaction index.

Materials that can sustain smouldering combustion are porous and form solid carbonaceous char when heated. Materials that melt do not exhibit this kind of combustion. The char is formed on the exposed surface. When the char is oxidised in this region, a glow at high temperatures (about $600°$C for wood) results. This exothermic process yields ash and residual char, along with volatile products (e.g., tar) that have high carbon monoxide content. These products are also flammable if accumulating in a closed space; hence, smouldering may lead to flaming after passage of considerable time. [14]

Surface oxidation is most significant after the flame is extinguished, but the surface is still hot, for example, after combustion of lignocellulosic material. An example of the surface oxidation is seen in Figure 2.1. A graphite sample was tested in TGA and differential scanning calorimetry (DSC) under both oxidative (air) and inert (nitrogen) ambient conditions (see Section 2.3 for more details). In the presence of oxygen, the sample degrades almost completely (leaving less than 1% as residue). Without oxygen, this degradation does not occur, even at

high temperatures and with a slow heating rate. Similarly, the DSC experiments show a clear exothermic reaction peak for the sample in air, while the same test in nitrogen does not show any reaction (except minor experimental fluctuation of the baseline).

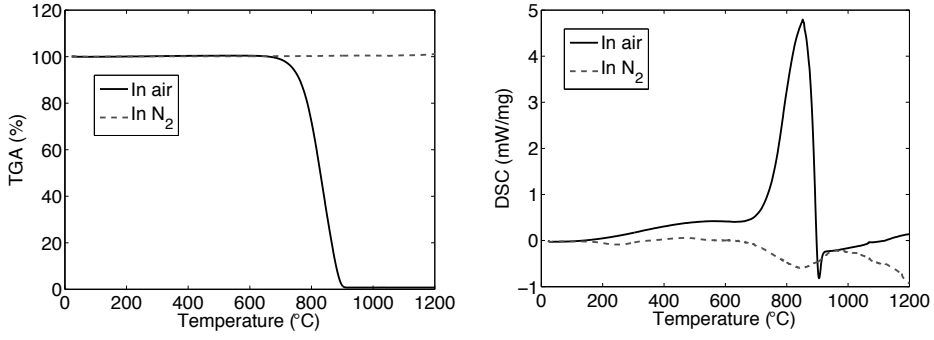

Figure 2.1. a) TGA and b) DSC experiments with graphite in air and in nitrogen at $2\,\mathrm{K/min}$.

A reaction depending on the oxygen concentration can be modelled by means of a modified Arrhenius equation:

$$r_{O_2,j} = A_j(1-\alpha_j)_j^N \exp\left(-\frac{E_j}{RT}\right) Y_{O_2}^{N_{O_2}}, \tag{2.10}$$

where Y_{O_2} is the oxygen concentration and N_{O_2} is the reaction order of the oxygen concentration. If reaction rate does not depend on oxygen concentration (as normal pyrolysis reaction), $N_{O_2} = 0$.

The material in the model consists of several *pseudo-components*. A pseudo-component (later also simply *component*) refers to a component in the model that represents one mass loss step in the model. It does not necessarily represent any particular chemical reaction, but it does serve as a way to model the net effect of all reactions occurring simultaneously. In total, there are at least 10 model parameters per reaction or component. Each component is described in terms of these parameters. Some components may encompass several reactions (or competing reactions), which increase the number of parameters still further. The parameters in the model are summarised in Table 2.1.
Several pieces of software have been developed in the fire community for modelling the thermal degradation of solids: FDS[1] [18], Gpyro[2] [19], Open Foam[3], and ThermaKin [32]. FDS and OpenFoam are CFD codes while Gpyro and

[1]See https://code.google.com/p/fds-smv/
[2]See http://code.google.com/p/gpyro/
[3]See http://www.openfoam.com/

Table 2.1. Summary of parameters of pyrolysis modelling. *Est* estimated from and *Mes* measured with. (*R*) reaction specific. (*C*) component specific.

Param.	Explanation (unit)	Eq.	Method of obtaining	**R**eaction/ **C**omponent
A	Pre-exponential factor (s^{-1})	2.2	*Est* TGA/MCC	*R*
c_p	Specific heat (kJ/(K·kg))	2.4	*Mes* DSC / *Est* cone calorimeter	*C*
E	Activation energy (J/mol)	2.2	*Est* TGA/MCC	*R*
ΔH	Heat of reaction (kJ/kg)	2.5	*Mes* DSC / *Est* cone calorimeter	*R*
ΔH_c	Heat of combustion (kJ/kg) / (MJ/kg)	2.9	*Mes* MCC / *Est* cone calorimeter	*R*
k	Thermal conductivity (W/(m· K))	2.4	*Mes* / *Est* cone calorimeter	*C*
N	Reaction order	2.2	*Est* TGA/MCC	*R*
N_{O_2}	Reaction order of oxidation	2.10	*Est* TGA results in air	*R*
ϵ	Emissivity	2.8	*Est* cone calorimeter	*C*
ρ	Density (kg/m^3)	2.4	*Meas* directly	*C*

ThermaKin are limited to the solid phase. Gpyro also includes an algorithm for estimation of the model's parameters.

2.3 Experimental methods

The experiments commonly employed in fire research can be divided into small (milligram), bench (gram to kilogram), and large/full (kilogram to metric ton) scale experiments on the basis of the sample size required. The small scale experiments are the easiest to model and involve less inaccuracy related to fire or experimental set up. The material models are typically built on the basis of small and bench scale experiments. Large scale fire tests are often very expensive, but important for code validation purposes.

2.3.1 Small scale experiments

In a small scale experiment, the sample mass is usually 1–30 mg. These experiments typically measure only one property at a time, such as mass, heat of reaction, specific heat, or heat release rate. The reaction parameters and sometimes even a good estimate as to the sample composition can be determined by means of small scale experimental results.

The most commonly used small scale experiment for pyrolysis modelling is the TGA. It uses a small furnace filled with either air or inert purge gas (often nitrogen). The sample is inside a small crucible that is placed over a load cell. During the experiment, the sample mass is measured. The experiment can be performed either *isothermally* (i.e., at a one constant temperature) or *non-isothermally* (with temperature increasing linearly). The non-isothermal experiment is often more suitable for the estimation of the pyrolysis parameters, since it also provides information about the reaction temperatures. The heating rates are relatively low (2–30 K/min), in order to keep the sample in thermal equilibrium with the furnace. [14,15] For pyrolysis modelling purposes, TGA experiments are often performed at several heating rates. This is necessary, because the chemical reactions may depend on heating rate, and using several rates enables the estimation of more general reaction parameters. An example of TGA results at several heating rates is seen in Figure 2.2. Often the increasing heating rate moves the reaction to higher temperatures. That means that the reaction takes place more slowly than the heating of the sample and therefore the temperature of the sample is higher when the mass loss occurs. At very high heating rates or with thermally thick samples the thermal equilibrium between the furnace and sample may be lost and the sample temperature no longer corresponds to the furnace temperature.

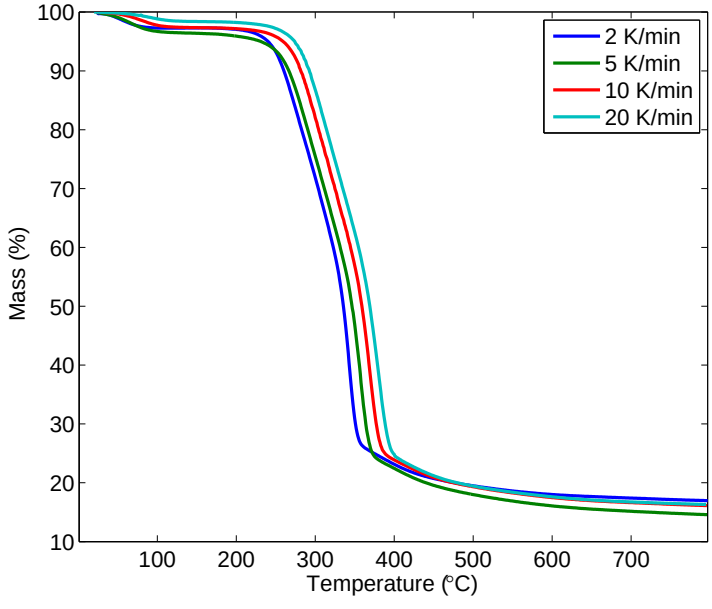

Figure 2.2. TGA results of birch wood at 2–20 K/min heating rates in nitrogen ambient.

More information about the reaction enthalpies and specific heat is provided by another small scale experiment, DSC. The furnace and the method of operation are similar those in TGA. In DSC, the sample temperature is regulated relative to a reference sample, and the required energy is measured. With DSC, one can perform experimental measurements in an individual experiment or simultaneously with TGA. From individually measured DSC, one can calculate the heat of reaction and the specific heat capacity. It is good to keep in mind that the measured value is actually the joint effect of possibly several simultaneous reactions. The results should then be scaled for the target application, more specifically, to its reaction path. [14, 15] For accurate calculation of the specific heat, three measurements are required in all: of the actual material, of a reference sample with known specific heat (often sapphire), and of an empty pan for setting of the baseline. The baseline value is subtracted from the results for the actual sample and the reference. The specific heat capacity of the reference sample is scaled by the ratio of the DSC measurements between the sample and the reference:

$$c_{p,s}(T) = \frac{\dot{q}_s/m_s(T)}{\dot{q}_r/m_r(T)} c_{p,r}(T), \tag{2.11}$$

where the subscript *r* refers to the reference and *s* to the sample.

A simpler but less accurate method is to calculate the specific heat by using only the baseline corrected heat flow of the sample. Then the heat flow for the initial mass is scaled by the current heating rate β:

$$c_{p,s} = \frac{\dot{q}_s/m_s}{\beta}. \tag{2.12}$$

A comparison of the results of these methods is shown in Figure 2.3.
The heat of reaction (or reaction enthalpy) is calculated as the integral over the reaction peak in DSC. An example of the definition of the heat of reaction is seen in Figure 2.4.

When DSC is performed simultaneously with a TGA experiment, the results are mostly more qualitative than quantitative. Often a significant, unpredictably behaving baseline can be observed in the simultaneous DSC results that make the calculation of reaction enthalpy extremely difficult. This is probably because of experimental uncertainty that comes from the set-up necessary for measuring the sample mass simultaneously with the heat flow. Qualitative results may, however, be very useful, since they reveal whether the reaction is endothermic or exothermic. In Figure 2.5, qualitative DSC results for heat flow in nitrogen and in air can be seen. Three reactions can be observed in air, two in nitrogen. The first one occurs at around $100°$C and is endothermic in both purge gas conditions. An endothermic reaction that occurs at low temperature

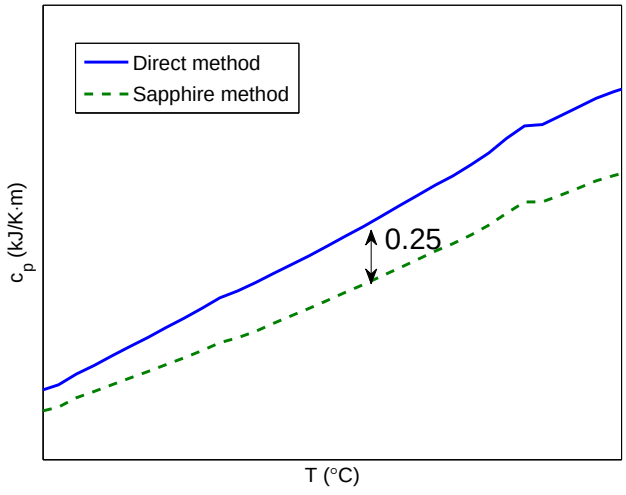

Figure 2.3. Comparison of direct method to sapphire method in calculation of specific heat from DSC results for a furane sample. Experimental data courtesy of Gaiker.

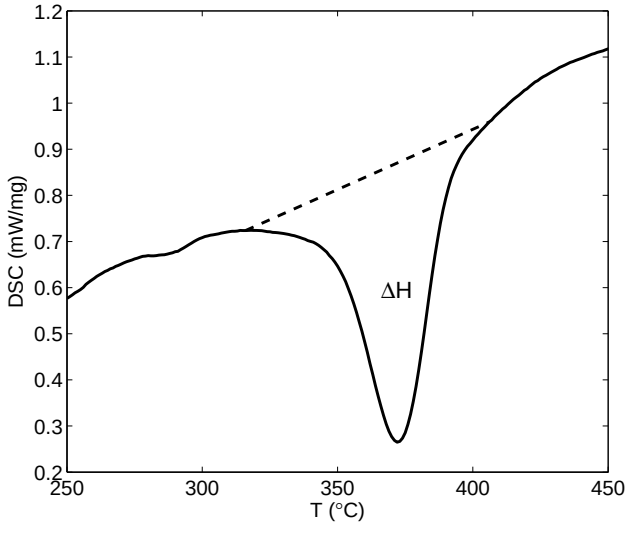

Figure 2.4. Integration over the reaction peak for determination of the heat of reaction.

can usually be identified as evaporation of moisture. The second reaction takes place after $300°$C and is exothermic in air and endothermic in nitrogen. The additional reaction only in air (peak at $440°$C) is defined as char oxidation. In the

presence of air, the exothermic peaks can indicate oxidative surface reactions or flaming combustion. It is difficult to know for certain if the combustion gases are ignited during the test or not, although self-ignition is not very probable at low temperatures. The possibility of ignition can be decreased by reducing sample size.

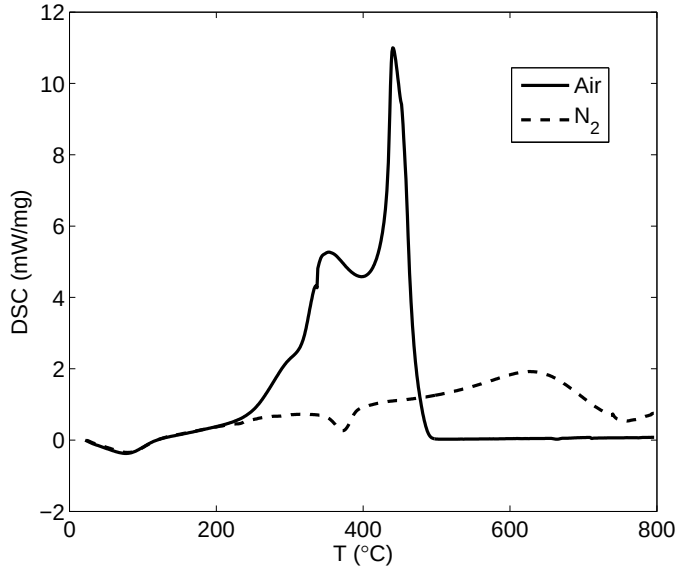

Figure 2.5. DSC results for birch at 10 K/min in air and nitrogen. Exothermic peaks are positive.

Microscale combustion calorimetry (MCC) can be used for measuring the heat release rate of a sample. It first pyrolyses the sample in a nitrogen environment, at a higher heating rate than in the TGA (typically around 60 K/min, although heating rates from 12 to 120 K/min are possible). Then the pyrolysis gases flow into a combustor, a tube whose high temperature and sufficient oxygen concentration cause all the combustible gases to burn immediately. The result is the heat of complete combustion as a function of temperature. [33, 34] The pyrolysis can alternatively be done in air, to study the oxidation of pyrolysis char. In this work, the MCC results are combined with the information from the TGA for determination of the heat of combustion values for each reaction. This information can be used when one is simulating complex materials, e.g., polymer samples. [35]

2.3.2 Bench-scale tools – the cone calorimeter

The cone calorimeter (ISO 5660-1, [16]) is the most commonly used bench-scale experimental tool in fire research. The sample usually has dimensions of 10 cm $\times$ 10 cm $\times$ 0.1–5 cm and has a substrate made of mineral-based insulation or calcium silicate board on the unexposed surface. The sample is placed under a cone shaped heater, which heats the sample with a radiant heat flux of 10–75 kW/m^2. The igniter is an electric spark that is kept on until the sample ignites, although spontaneous ignition may also be investigated without use of the spark igniter. The gases are collected in a hood, from which the various properties are measured. As a result, the cone calorimeter provides information about mass loss, heat release rate, and soot yield. Additionally, sample temperatures may be measured by means of thermocouples. The standard cone calorimeter operates in ambient air, but ambient controlled cone calorimeters are available also. They can be used for studying the effect of the oxygen in the atmosphere or the pyrolysis of the sample in an inert (nitrogen) ambient. [16, 36, 37]

2.4 Parameter estimation

The reaction rate of the thermal degradation of a material is often modelled by means of Arrhenius equation as explained in Section 2.2. The kinetic parameters cannot be measured directly; they need to be estimated somehow from the experimental data. An overview of methods to quantify kinetic parameters is provided in the following sections. The estimation algorithms presented in Subsection 2.4.2 can also be used in estimation of other (mainly thermal) model parameters.

2.4.1 Semi-analytical methods

The first methods, developed in the 1960s, included approximations, reference points, and graphical solutions [38–40]. The isoconversional (i.e. applying multiple heating rates) methods were soon discovered to be more useful because they provide more general results. They can be used for defining the reaction model ($f(\alpha)$) or the reaction parameters (A, E) [22–25]. Drawbacks to these analytical methods may be found in their limited accuracy; inconvenience of locating various reference points; limitations in reaction steps or order; or, in some cases, the fact that the complete kinetic triplet, (A, E) or $f(\alpha)$, cannot be solved from the same data set. The fire community's interest in the reaction parameters has led to some new, simple but reasonably accurate methods, aimed at encouraging modellers to base their kinetic parameters for their material

instead of using estimates from the literature [41–43].

The methods presented in this chapter assume that the pyrolysis reaction follows Eq. 2.2, or, in integral form,

$$F(\alpha) = \frac{A}{\beta} \int_{T_0}^{T} e^{-\frac{E}{RT}} dT. \tag{2.13}$$

In the 1960s, several methods were suggested for determination of the parameter pair (A,E) from experimental data [38–40]. Bell and Sizmann [38] presented an approximation for the integral,

$$\int e^{-\frac{E}{RT}} dT \approx \frac{RT^2}{E + 2RT} e^{-\frac{E}{RT}}, \tag{2.14}$$

which at two separate heating rates (β_1 and β_2 at the same conversion α, see Figure 2.6) leads to the following equation for activation energy

$$E = \frac{RT_1T_2}{T_2 - T_1} \ln\left(\frac{\beta_2}{\beta_1}\right)\left(\frac{T_1}{T_2}\right)^2. \tag{2.15}$$

They compared this approximation to an experimental method called *step annealing*. The latter is an iterative process wherein the sample is heated over time Δt_i from temperature T_i to T_{i+1} and sample concentration α_{i+1} is measured at each step i. The set (α_i, T_i) is then given by

$$\int_{\alpha_i}^{\alpha_{i+1}} \frac{d\alpha}{f(\alpha)} = e^{-\frac{E}{RT_{i+1}}} \cdot \Delta t. \tag{2.16}$$

Step annealing has since been developed into an estimation algorithm (further discussed in Subsection 2.4.2). Both methods are isoconversional, i.e., they require data at several heating rates. However, the step annealing can also be modified for just one heating rate.

Flynn and Wall [39] used an approximation technique to determine the activation energy. This method too is isoconversional. Similar to the previous method, the constant conversion is chosen for each heating rate, and the temperature is recorded (see Figure 2.6).

With the substitution $x = E/RT$, Eq. 2.13 becomes

$$F(\alpha) = \frac{AR}{\beta E} \int_{x_0}^{x_i} e^{-x} dx, \tag{2.17}$$

where $x_0 = E/RT_0$ and $x_i = E/RT_i$ and, after taking of a natural logarithm, this becomes

$$\ln(F(\alpha)) = \ln\left(\frac{AR}{E}\right) + \ln\left(\frac{1}{\beta}\right) + \ln\left(\int_{x_0}^{x_i} e^{-x} dx\right). \tag{2.18}$$

The above-mentioned authors found that for $E/RT \geq 20$, the integral can be approximated thus:

$$\ln\left(\int_{T_0}^{T_i} e^{-\frac{E}{RT}}\right) dT \approx -2.315 - 0.457\frac{E}{RT_i} \tag{2.19}$$

and therefore E becomes, after differentiation,

$$E \approx -\frac{R}{0.457}\frac{\Delta \ln(\beta)}{\Delta T^{-1}}. \tag{2.20}$$

This approximated value is then used for calculation of a more accurate estimate for E/RT and consequently its integral. This method was developed in a time when solving integrals numerically was not commonly performed. Instead, approximations and lists of integral values were used.

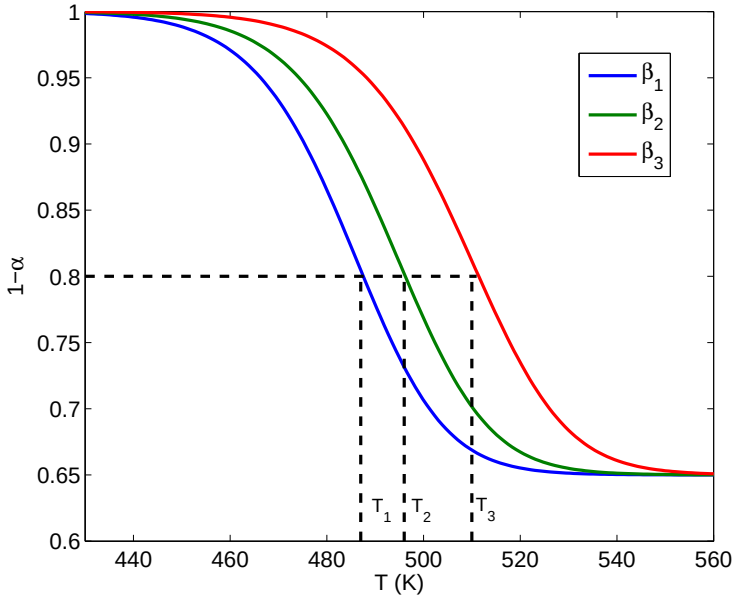

Figure 2.6. Demonstration of selecting different reference points for Flynn's isoconversional method.

Friedman [40] suggested several methods that are based on reference points and allow the use of reaction orders that are not equal to one. His methods are based on either reference points from two heating rates, or multiple points from the same data. In the simplest form, the reference point is chosen from

the point of the highest reaction rate ($\frac{d^2\alpha}{dT^2} = 0$):

$$E = NRT_p^2 \frac{(\frac{d\alpha}{dT})_p}{1-\alpha_p}. \tag{2.21}$$

Another relation, a slightly more elaborate one, requires two reference points for the same heating rate

$$E = -R \frac{\ln\left(\frac{(\frac{d\alpha}{dT})_2}{(\frac{d\alpha}{dT})_1}\right) + N\ln\left(\frac{1-\alpha_1}{1-\alpha_2}\right)}{T_2^{-1} - T_1^{-1}}. \tag{2.22}$$

Friedman also provided several relations for reaction order N that shall be discussed later in this section.

Since the 1980s, an isoconversional method that is based on linear fitting has been widely used in many fields of research in slightly different forms [22–25]. Methods in this family are also called the *model-free methods*, because they do not require an analytical form of the reaction model ($f(\alpha)$). The approach can be applied either for isothermal thermogravimetric data at several temperatures or to non-isothermal data at one heating rate.

The idea of the isothermal version is to take the natural logarithm of both sides of the Arrhenius equation. After rearrangement of the terms, it becomes

$$\ln\left(\frac{(\frac{d\alpha}{dT})}{f(\alpha)}\right) = \ln(A) - \frac{E}{RT}. \tag{2.23}$$

The left-hand side of the equation consists of the experimental values that should form a line when plotted against T^{-1} with $\ln(A)$ being the intercept and -E/R the slope. If $f(\alpha)$ depends on N, the best fit can be found through repeating of the calculation at several reaction orders, and the best fitting solution will be chosen. [22, 23]

In non-isothermal conditions, the above-mentioned method becomes a bit more complicated. If the measurement is done at only one heating rate, the results are often ambiguous. Keuleer et al. [23] suggest using the equation

$$\ln\left(\frac{\beta\,(\frac{d\alpha}{dT})}{f(\alpha)}\right) = \ln(A) - \frac{E}{RT} \tag{2.24}$$

at several heating rates (β) at fixed values of conversion α. Liu et al. [25] base their method on an approximation of the temperature integral yielding the linear relationship

$$\ln\left(\frac{\beta}{T^2}\right) = \ln\left(\frac{AR}{Eg(\alpha)}\right) - \frac{E}{RT}, \tag{2.25}$$

where $g(\alpha) = \int_0^\alpha \frac{d\alpha}{f(\alpha)} = \frac{AE}{\beta R} p(\frac{E}{RT})$.

Other related methods have been suggested and presented by several authors over the past few years [21, 24, 44–47].

The key parameter of $f(\alpha)$ for the reaction order model is the reaction order N. From the chemistry point of view for thermal degradation reactions reaction orders other than 1 do not have real meaning, as is discussed in Section 2.2. Many simplified reaction models are limited to the first order. However, the reaction order does affect the reaction rate shape significantly, so it is often used in modelling when the effects of several simultaneous reactions are approximated with just one kinetic reaction.

Friedman [40] presented several equations for calculation of N. The following equation is based on three well-separated reference points from the same data

$$N = \frac{\ln\left(\frac{(\frac{d\alpha}{dT})_3}{(\frac{d\alpha}{dT})_1}\right) - \frac{T_2(T_3-T_1)}{T_3(T_2-T_1)} \cdot \ln\left(\frac{(\frac{d\alpha}{dT})_2}{(\frac{d\alpha}{dT})_1}\right)}{\frac{T_2(T_3-T_1)}{T_3(T_2-T_1)} \cdot \ln\left(\frac{1-\alpha_1}{1-\alpha_2}\right) - \ln\left(\frac{1-\alpha_1}{1-\alpha_3}\right)} \tag{2.26}$$

This method works very well for smooth data and non-overlapping reactions but may be complicated for real data, as discussed in Publication II.

Gao [48] has provided a more practical approach by listing theoretical limits for the reaction order as a function of the conversion. Through a polynomial curve fit, those values convert into a very simple relationship (as demonstrated in Publication II):

$$N \approx 13.25(1-\alpha_p^*)^3 - 4.16(1-\alpha_p^*)^2 + 2.3(1-\alpha_p^*) - 0.077, \tag{2.27}$$

where α_p^* is the reaction progress variable at the peak of the reaction.

The isoconversional method provides also a good way of defining N. Li and Järvelä [24] suggest that the reaction rate can be expressed as

$$r = \frac{(\frac{d\alpha}{dt})}{(1-\alpha)^N}. \tag{2.28}$$

After one takes a natural logarithm and rearranges this, it results in

$$\ln\left(\frac{d\alpha}{dt}\right) = \ln(r) + N\ln(1-\alpha). \tag{2.29}$$

If $\ln(d\alpha/dt)$ is now plotted against $\ln(1-\alpha)$ at several temperatures, the N value is equal to the average slope of these lines.

2.4.2 Optimization algorithms

The analytical methods solve the parameters by using reference points, and the results depend only on the choice of method and the location of the reference point. Another approach is to consider the parameter estimation as an optimisation problem wherein the model is fitted to the experimental data. Several curve-fitting algorithms have been developed over the years. The traditional gradient methods tend to converge at the closest local minimum (not necessarily the global optimum) and therefore generally do not operate well with this kind of problem. Accordingly, evolutionary algorithms were considered. The first attempts used *genetic algorithms* (GA) [17, 19, 31]. These do operate very efficiently for non-linear problems with a large number of unknown parameters. However, GAs may be utterly inefficient with large estimation boundaries and therefore require several iterations and large sets of candidate solutions. Several other algorithms have been studied and successfully used in estimation of the pyrolysis parameters [49–53]. All of these methods require purpose-specific software and significant computation time, and their stochastic nature means that the estimation procedure cannot be repeated exactly. The results also depend on the estimation boundaries and algorithm parameters defined by the user. However, the above mentioned shortcomings are compensated by the algorithms' advantage of not being limited to any specific model. Besides the pyrolysis kinetics, a GA can be used in estimation of any other parameters. In the fire sciences, these other parameters would typically be the thermal parameters as listed in Table 2.1.

The idea of **GA** [17, 19, 31] is based on the evolution and survival of the fittest. Each set of parameters represents one individual in a population. The individuals consist of parameters – or *genes*, as they are called in GA argot. The first population is selected randomly from the pre-defined range. The individuals are located in several subpopulations that do not share the genes in normal routines. Each individual is tested against the experimental data, and a value called the *fitness value* is calculated for measuring the goodness of the fit. The population goes through a set of operations that are stochastic, and their probabilities depend on the fitness value. These operations include *selection* (selecting the best-fitting solutions for reproduction), *cross-over* (combining two selected individuals for production of a new individual, offspring), *mutation* (changing one or more genes of some individuals into a random number), and *migration* (migrating, on the part of individuals, between subpopulations). The next generation consists of the best fitting individuals of the previous generation and of the new offspring. The operations based on the fitness value and probabilities cause the population converge towards the best fitting solutions,

and the mutation and the migration bring new genes to the subpopulations and hence prevent convergence at a local minimum. A flowchart of the algorithm is shown in Figure 2.7. This topic is further discussed in Subsection 4.4.2 and in Publication I.

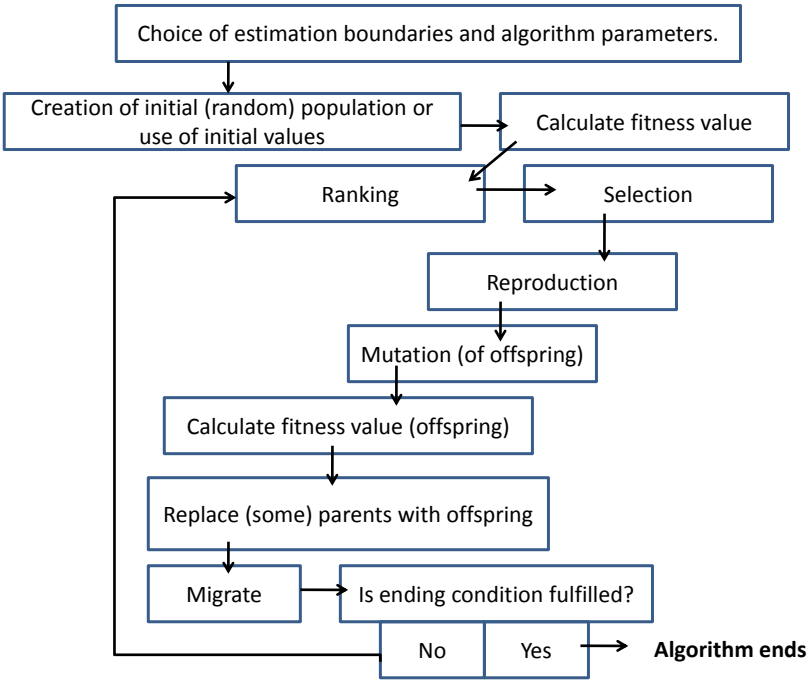

Figure 2.7. Flowchart of a genetic algorithm.

Shuffled complex evolution (SCE) is, in essence, an improved genetic algorithm [49, 54]. It starts similarly, with a random population, but is better organised and optimised with respect to the following operations. First, the individuals are ordered according to their fitness values. Then they are divided into *complexes* such that every nth individual is placed in the same group. Every individual within a complex, a probability then is assigned that determines which q individuals are to be selected for a *subcomplex*. The values are ordered by their fitness values. The worst fitting value (u_q) in the subcomplex is compared to other values within the group and a new value is calculated as

$$r = \frac{2}{1-q} \sum_{j=1}^{1-q} -u_q. \tag{2.30}$$

If r is not within the estimation boundaries, a new random value is generated instead. If the fitness value of the new value is smaller than previously

($f_r < f_q$), the new value r replaces the old value u_q. Otherwise, a new value is calculated, as

$$c = \frac{\frac{1}{1-q}\sum_{j=1}^{q-1} + u_q}{2}. \tag{2.31}$$

Comparison of the fitness values is performed as before. This operation is repeated within the subcomplex until the predetermined number of iterations are completed. After that, the same operations are performed for each of the other subcomplexes. When all the subcomplexes have been gone through, the convergence condition is checked. If this has been satisfied, the algorithm ends. If not, it starts running again from the sorting of the fitness values and distribution of candidate solutions to complexes.

This method has been applied to estimation of the parameters related to thermal degradation of several materials by Chaos et al. [49] and Lautenberger and Fernandez-Pello [50]. The SCE approach has proved to be more efficient and to provide more accurate results than GAs do.

Hybrid genetic algorithms (HGA) combine the evolutionary algorithm and local search methods (e.g., gradient methods) [52, 55–57]. They have been developed to enhance the algorithm such that it produces higher quality solutions more efficiently. The local search method can be included in any of three phases in the estimation process: before, during, or after the algorithm. Before the GA operation (*pre-hybridisation*), the local search is used for generating the initial population for the GA and therefore reducing the solution space. This is suitable for some specific problems but not in general. The second option, which some refer to as *organic hybridization*, is used as one more operator for the GA, improving the fit of each individual in each generation. Although this is computationally more efficient than a GA alone, there is no guarantee of finding the global optimum. The last method is referred to as *post-hybridisation*. Here a GA is used to provide the initial design for the local search method. This has proved to be generally the most efficient way to hybridise the GA, since the global and local searches are performed completely separately.

Saha et al. [52] have successfully applied HGA for estimation of the kinetic parameters of various plastics. They used the post-hybridisation technique and a multidimensional, unconstrained non-linear search function as a hybrid function.

Stochastic hill climber (SHC) algorithm was developed by Webster [53] for his master's thesis in 2009. The algorithm differs from GAs in the following respects:

- The initial population is generated via good engineering judgement (or by rules of thumb, discussed in Subsection 4.4.3). Webster has stated that it

is more logical to start with a well-fitting curve that has 'wrong' parameters than with a non-fitting curve that has the 'right' parameters.
- The fitness function involves an R-squared value.
- Reproduction is done via mutation only (i.e. with no cross-breeding). The parents may outlive the children if they have better fit.
- The mutation magnitude of each parameter is limited such that each can effect no more than 5% change in accuracy. This is done in order to prevent any single parameter from dominating in the estimation process.
- The mutation magnitude is multiplied by a scalar that depends on the mutation history of the parameter. If the previous mutation attempts have been successful, the scalar has a higher value than if the mutations have been unsuccessful.

This method has been applied to the estimation of cone calorimeter results by Webster himself, and by Lautenberger and Fernandez-Pello [50], with good results.

Simulated annealing (SA) differs from the previously presented algorithms in not being an evolutionary algorithm. It is, however, based on a real-life process – namely, annealing in metallurgy. In annealing, the material is first heated and then cooled, for finding of lower internal energies. In the algorithm, the initial solution is tested against a random solution. The choice of solution is based on the difference in fits and a random number that depends on a parameter referred to as *temperature*. The temperature is eventually decreased, and the probability of choosing the worse-fitting solution decreases with it [51, 58, 59]. Mani et al. [51] applied SA for estimating the kinetic parameters of lignin with good results.

Lautenberger and Fernandez-Pello [50] compared the performance of four algorithms (a GA, SCE, SHC, and a hybrid of a GA and SA). They tested these estimation methods by using generic cone calorimeter data, so that the real target values of the parameters were known. They evaluated the algorithms in terms of their effectiveness and robustness. The most rapid convergence was shown by SHC, but the final fitness was at a level similar to that with GA and HGA, and SCE turned out to perform with the best fit with any random initial population. These solutions were practically independent for the initial population, and it seems that SCE is able to find an actual global optimum for the problem. When the target values of the parameters were compared, the values estimated via SCE were the most accurate by far. The other algorithms were much less accurate with respect to correctness of the target values, with HGA producing the greatest accuracy of the three while SHC showed the least accurate fit.

2.4.3 The compensation effect

As is discussed above, the values for the activation energy may be very sensitive to small changes in experimental conditions (such as heating rate); therefore, isoconversional methods are commonly used, preferred over a single heating rate experiments. This phenomenon is also widely recognised in the literature [25, 60, 61] and observed in experiments, but no comprehensive explanation has been provided so far. There are two main, and opposite, points of view on the nature of the compensation effect; it either is caused by an experimental artefact or has a true chemical meaning. The second case is often seen as discomforting, since it means that the A and E values are not independent and therefore do not have any physical meaning in isolation. In fire modelling, the interpretation has been that the compensation effect has a chemical meaning.

The general form of the compensation effect is

$$\ln(A) = a + bE, \tag{2.32}$$

where a can be very small [60, 61]. The analytical form of the compensation effect is, according to Nikolaev et al. [60],

$$\ln(A) = \ln\left(\frac{E\beta}{RT_p^2}\right) + \frac{E}{RT_p}. \tag{2.33}$$

Slightly different form for the compensation effect has been suggested by Lyon and Safronava [62]:

$$\ln(A) = \ln\left(\frac{\beta E}{\phi RT_p^2}\right) + \frac{1}{RT_p}E, \tag{2.34}$$

where $\phi = -df(\alpha)/d\alpha$. The compensation effect depends on rate and model, as observed.

Similar behaviour has been observed more generally with other model parameters, especially with larger-scale models. The models inevitably have some degree of inaccuracy, and the parameters combine to form a model that fits to experiments. Therefore, the model parameters actually work together to compensate for the shortcomings of the model and several combinations, fitting equally well, can be found for the same experimental data. This phenomenon is demonstrated and discussed in Publication III. However, good initial guesses (e.g., by model-free methods) may help to eliminate the randomness of the solutions and keep the parameters more realistic [63].

2.5 The Monte Carlo technique

Fire modelling can be used as a part of PRA. The goal of fire-PRA is to determine the probability of the various possible consequences of a fire and discover the most significant parameters that correlate with the most severe conditions. The *Monte Carlo* (MC) technique is a tool for the statistical assessment. This method is not used for parameter estimation as the methods described previously in Section 2.4. In this dissertation, it has been used to statistically study fire spread from one cable tray to another, as described in Publication V.

The Monte Carlo technique in its simplest form means repeating an action several times at a random points in a parameter space and counting the events. A simple example of this technique is a game of tossing a coin to estimate the probability of heads or tails. The modern Monte Carlo was born in the 1940s when Stanislaw Ulam, John von Neumann, and others, started to use random numbers in the calculations of statistical physics. The most efficient use of the MC technique is to determine definite integrals that are too complex to solve analytically. [64, 65]

In applications of Monte Carlo for fire research, a simulation is repeated several times, using random numbers from certain distributions of input parameters. The number of repetitions should be high enough to cover the variable space for capturing the statistics of the events. This is computationally quite expensive, so a more optimised sampling method is used. The sampling method, called *Latin hypercubes* (LH), is a type of stratified sampling. The idea is to divide the range of each variable into as many intervals as the number of samples so that each interval has equal probability according to the distribution. From each interval, one random number is selected, and the random numbers of each parameter are paired in a random manner. As its result the sample represents the space of possible input values more extensively than traditional random sampling does, and, therefore, fewer repetitions are required. [66, 67]

For fire Monte Carlo, a software package called Probabilistic Fire Simulator (PFS) is used. It was developed at VTT Technical Research Centre of Finland. It runs Monte Carlo (or two-model Monte Carlo) with a chosen fire model, most commonly with FDS [68, 69]. This tool has been used in the simulations described in Publication V.

3. Materials

3.1 Motivation

The thermal degradation process depends on the material. The degradation varies with the polymer classes, whether the surface swells or shrinks when heated and what kinds of flame retardants, if any, are used. A brief literature survey is presented that considers these processes. Special attention is given to complex but very important materials: cables and composites. The challenges and the solutions from a modelling point of view are discussed in Section 3.5.

3.2 Thermoset and thermoplastic polymers

Synthetic polymers are classified as *thermoplastic* or *thermoset* by their behaviour when heated. When exposed to heat, thermoplastic polymers soften and melt, and they take a new form when cooled down. This may affect their burning through forming of falling droplets or burning liquid pools. Thermoset polymers, on the other hand, are cross-linked structures that do not melt when heated; they often leave residual char. Of the natural polymers, cellulose is similar in fire behaviour compared to synthetic thermoplastic polymers. A third polymer class would be the elastomers, which can be distinguished by their rubber-like properties. They can behave either like thermosets or as thermoplastics do, depending on the material. [14, 70]

3.3 Modelling shrinking and swelling surfaces

A solid surface seldom maintains its structure when exposed to heat. If a homogeneous material is converted completely to volatiles, the material thickness decreases as the fire progresses. However, many materials do not degrade completely and instead leave empty spaces (*porosity*) in the structure. Some gas from the pores may get trapped under the surface, causing the material to swell. This mechanism acts as a natural flame retardant for many charring materials, and the idea has been adopted for several synthetic flame retardants as well. More about the swelling (or intumescent) surfaces as a flame retardancy mechanism is explained in Section 3.4. Many charring materials (e.g., wood) first swell in the charring phase, and later shrink (in the presence of oxygen) when the char oxidises.

Shrinking and swelling have a significant effect on the thermal degrada-

tion of a material. Increasing porosity decreases the thermal conductivity, and a swollen surface forms a physical barrier to the heat. The simplest way to model this is to calculate the final thickness by using the information about residue fraction and final density. One can calculate the density that the material would have after the reaction if the thickness were to remain unchanged ($\rho_{s,i}$). If the final density (ρ_i) is defined to be higher than the one calculated, the material shrinks; if lower, the material swells. In FDS version 6 [71], this is done by decreasing or increasing the solid cell size in keeping with the ratio of the densities:

$$\delta = \begin{cases} \max_i \left(\frac{\rho_{s,i}}{\rho_i}\right) & \text{if } \max_i \left(\frac{\rho_{s,i}}{\rho_i}\right) \geq 1 \\ \sum_i \left(\frac{\rho_{s,i}}{\rho_i}\right) & \text{if } \max_i \left(\frac{\rho_{s,i}}{\rho_i}\right) < 1. \end{cases} \tag{3.1}$$

The cell thickness is then scaled by this factor, with the thickness from the last time step ($t-1$):

$$\Delta x(t) = \delta \Delta x(t-1), \tag{3.2}$$

and the density similarly:

$$\rho(t) = \frac{\rho(t-1)}{\delta}. \tag{3.3}$$

With this method, it is possible to model the known density or thickness change effectively by manually adjusting the thermal conductivity of the residue to be lower, but the method cannot predict the final thickness. To be able to predict the swelling or shrinking, one must model the porosity. This effort seems at the moment to be overly time consuming when compared to the benefits; therefore, the porosity model has not been included in FDS. However, Zhang et al. [8] developed a model that is able to predict the final thickness. The model takes into account the proportion of the gases that stay trapped under the surface and the conduction in the pores caused by radiation and convection.

The effect of the swelling and shrinking with FDS6 modelling is usefully demonstrated with an example. A charring material with a thickness of $2\,$cm and an initial density of $1,000\,$kg/m^3 degrades ($A = 1 \cdot 10^{10}$ s^{-1}, $E = 1 \cdot 10^5$ kJ/kmol, $N = 1$) yielding a mass fraction of 0.5 fuel gas and 0.5 residue. The thermal conductivity of the residue is $0.05\,$W/(m·K) and the surface area is assumed to remain constant. Comparison of the cone calorimeter simulations is shown in Figure 3.1. It can be seen that, although the thermal degradation process remains the same across all cases (except with swelling or shrinking), the pyrolysis and combustion are faster for the shrinking material. It also has the highest heat release rate peak, a consequence of a shorter period of releasing the same amount of heat (see the first pane in Figure 3.1). The swollen surface

also insulates the surface significantly better, as can be seen from the back-side temperatures (Figure 3.1 pane c).

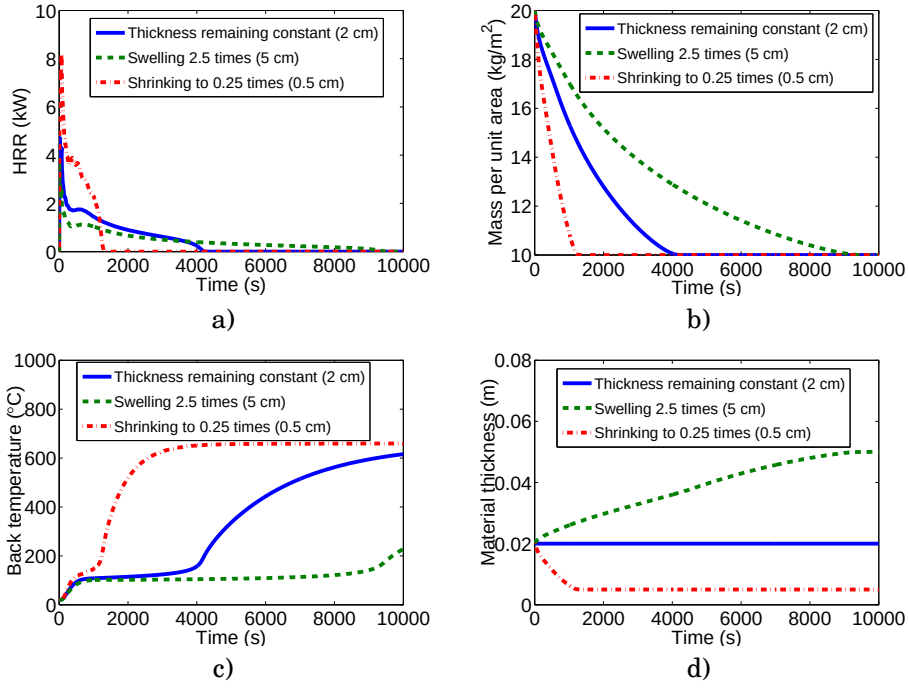

Figure 3.1. The effect of shrinking and swelling surfaces in the cone calorimeter simulations: a) heat release rate, b) mass per unit area, c) back temperature, d) thickness.

3.4 Flame retardant mechanisms

Not all fires can be prevented, but the consequences can be minimised. Several flame retardancy mechanisms have been developed for slowing down the fire spread. This section concentrates on polymers, because of their significant involvement in the fire spread, but similar methods have been used to protect other targets from the heat, such as metal structures, too (e.g., use of intumescent paints).

Use of flame retardant additives does not make the combustible material non-combustible, but it does delay the ignition and/or reduces the heat release rate in the fire. The increased time to react may be significant for the safety of the people and property involved. The choosing of flame retardant or whether one is to be used at all is not trivial. Some flame retardants have the desired effect only in quantities potentially large enough to change the mechanical properties of the polymer. Some flame retardants increase the production of smoke,

which decreases visibility in the event of fire and produces toxic gases. Therefore, the specific needs of each application have to be considered carefully. [6,72]

The flame retardants operate at many levels, in the gas or solid phase, or both. Fire spread is often described as a cycle that starts with pyrolysis in the solid phase (a) that releases flammable volatiles and that in the presence of oxygen (b) leads to flames (c). This, in turn, produces heat (d) that accelerates the pyrolysis. The flaming also may produce smoke and gas species that could be harmful to people. At the first step in the cycle (a), the goal is to affect the pyrolysis reaction in the solid phase. The reaction is modified such that char formation is promoted instead of flammable volatiles. Additionally, the char layer is a good insulator and acts as a barrier between flame and polymer. The second step (b) is to prevent the supply of oxygen to the flame and hence prevent the combustion of volatiles. This can be done via inert gases that are released during pyrolysis. By adding flame inhibiting agents to the polymer that are released near polymer degradation temperature, one can exert an effect on the flame directly (c). The last step in the cycle is to prevent heat flow back to the polymer (d). This can be done by means of either a heat sink that degrades endothermically or a physical barrier such as char or an intumescent coating. Naturally, many flame retardants act at multiple points in the fire cycle. [6,72]

At the pyrolysis stage (a) and for preventing the feedback from the flames (d), char formation is the most important mechanism for retarding the flame. Char forms an insulating barrier at the surface which delays the heat conduction to the polymer. An increased proportion of char also contributes to fewer flammable volatiles being released during pyrolysis. Significant amounts of flame retardant agents are added to the polymer, and these interact at temperatures lower than that of the polymer pyrolysis. There are two main methods by which polymers may promote char formation: dehydration and cross-linking. Dehydration is commonly associated with phosphorus derived compounds and the decreasing oxygen content in the polymer. Cross-linking stabilises the polymer by providing additional, strong bonds to the polymer chain. It has been suggested also that cross-linking increases the viscosity of the molten polymer that contributes to retarding the flow of the volatiles to the flame.

Cellulose is a good example of these mechanisms. With addition of only 2% phosphorus, the cellulose polymer is fire protected through dehydration process. It also cross-links at elevated temperatures, forming char. Nanocomposites are another example of flame retarding by char formation, more specifically by formation of high-performance carbonaceous-silicate char. Composites are discussed in greated depth in Subsection 3.5.3. [6,73]

Intumescent surfaces insulate the polymer surface with a porous, carbonaceous layer of char. The mechanism should not be confused with the char-

ring process. For an intumescent coating to form, three active components are needed: acid source, blowing agent, and charring agent. The acid source breaks down, forming a mineral acid that acts as a catalyst. This participates in the charring reaction together with the charring agent. The blowing agent produces large amounts of gaseous products that remain partly trapped under the surface, making the surface swell. [6, 8]

Another way to protect the polymer in the solid phase is to cool it down with an *endothermic* (energy-requiring) reaction. Hydrated minerals (the most commonly used are *alumina trihydrate* ($Al(OH)_3$, ATH) and *magnesium hydroxide* ($Mg(OH)_2$, MDH)) act this way, releasing water. The water also dilutes the pyrolysis gas and decreases the concentration of the flammable gas. The water content of ATH is 35% and that of MDH 31%. Their degradation temperatures and enthalpies as given in the literature vary slightly and are listed in Table 3.1. While MDH is more attractive in many applications for its higher degradation temperature and higher enthalpy, in practise ATH has been more commonly used, on account of its the lower price. [6, 7]

Table 3.1. Values in the literature for decomposition temperature and enthalpy for ATH and MDH (enthalpy is reported as required energy, positive endothermic reaction values).

	ATH		MDH	
In reference	T (°C)	ΔH (kJ/kg)	T (°C)	ΔH (kJ/kg)
[7]	180–200	1300	300–320	1450
[6]	205	1172	320	1598
[73, 74]	220	1170	330	1356

The oxygen concentration near the flame (b) can be reduced via release of an inert gas, as water or chlorides, in the gas phase, in a mechanism similar to that seen with the mineral fillers discussed earlier.

In gas phase (c), the halogens are the most prevalent group of flame inhibitors, especially chlorine and bromine. The free radicals $H\cdot$ and $OH\cdot$ have an important role in the process leading to thermal degradation and combustion. Halogens are known to react rapidly with these radicals and produce compounds that are much less active and therefore inhibit the flame. For example, PVC is flame retardant on account of its chlorine (more specifically, *hydrochloric acid*, HCl). The flame retarding effect of halogens is considerably less with large and hot fires, because the equilibrium of the halogen molecules decreases at increased temperatures. Some phosphorus chemicals are known to have similar effects in the gas phase, although they also act in the solid phase, via glass formation. [6, 14, 73, 75]

There has been much discussion about the disadvantages of the halogenated

flame retardants, mostly those containing *diphenyl oxide* (DPO), due to the toxic fumes they release during fire. At the other extreme, completely avoiding flame retardants increases the number of fires and therefore also the amount of toxic smoke. [75] The current trend is toward abandoning halogenated flame retardants because better alternatives have been developed.

3.5 Complex materials for fire modelling

The typical materials involved in fires (and fire simulations) seldom are fully characterised in their properties, homogeneous in structure, and of simple geometry, as a *poly(methyl methacrylate)* (PMMA) sheet is. In contrast, they take part in several chemical reactions and processes, contain additives, and have layered structures and complex geometry. Often the exact compound of the material is a business secret and therefore not publicly available knowledge. All of this makes the fire modelling of these materials challenging. This section of the thesis presents some of the typical applications of fire modelling. The materials and structures are reviewed from the standpoint of modelling of the fire spread.

3.5.1 PVC and its additives

A thermoplastic material with a wide range of applications, PVC is used in pipes and cables, as well as in clothes, furniture and sport equipment. Electrical cables are one of the most interesting applications from the point of view of fire modelling, since they constitute a significant fire risk at power plants and other facilities with lots of electronics. Pure PVC (C_2H_3Cl) is rigid, but often applications utilise PVC in its plasticised form ($C_{26}H_{39}O_2Cl$). Besides plasticisers, PVC material may include other additives, such as stabilisers and fillers. Rigid PVC burns, yielding char, only when an external heat source is present. If the heat source is removed, PVC extinguishes immediately. Plasticised PVC burns much better, because of the plasticisers' high heat of combustion. As is discussed in Section 3.4, PVC is inherently flame retardant, on account of the release of inert, diluting gas (HCl), and char forming. HCl is highly corrosive and therefore poses a hazard to people and property. [6, 70]

PVC has been widely studied experimentally [76–83] and in numerical analysis [81, 82, 84–87]. The degradation of pure PVC occurs in two steps. The first of these (at around 200–300°C) is dominated by a process that mainly releases HCl and hence is called dehydrochlorination. This non-combustible compound dilutes the gas phase and promotes char formation at the surface. The remaining polyene structure starts degrading immediately after this, releasing small amounts of aromatic hydrocarbons, mainly benzene ($\Delta H_c = 40$ MJ/kg [14]).

The stoichiometric amount of HCl released in PVC is 58.7%, on the assumption that all chlorine is released as HCl during the first step in the degradation. According to thermogravimetric studies performed by Miranda et al. [82] in vacuum and nitrogen, the mass loss from the first reaction is 64% and the remaining chlorine 0.14% at a 10 K/min heating rate. This process is not very sensitive to heating rate or environment (vacuum or nitrogen). The excess mass loss in the first reaction (5.44%) is identified as release of aromatics. The second major mass loss occurs at around 450°C, releasing toluene and other alkyl aromatics. The mass loss from the second reaction depends on the heating rate and environment. In Miranda et al. studies, the residue content varied (at heating rates of 1–20 K/min) from 3.1% to 6.4% in vacuum and over the range 6.9–12.4% in nitrogen. This leaves an average of 31% in vacuum and 26% in nitrogen for the second reaction mass loss. The residue content increases with the heating rate and is lower in vacuum than in normal atmospheric pressure. Naturally, the residue content in air is lower than in nitrogen, because of the oxidative effect, as can be seen in the TGA results for almost pure PVC pipe material that are presented in Figure 3.2. [6, 77, 82]

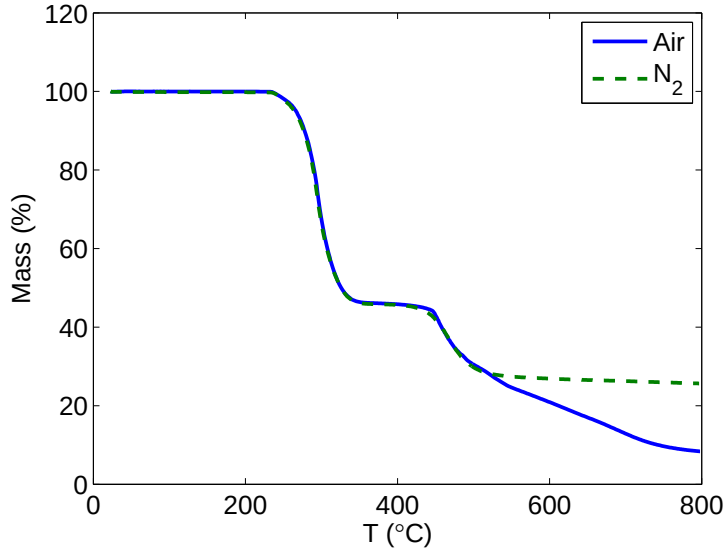

Figure 3.2. TGA experiment of almost pure PVC pipe material at 10 K/min.

What makes PVC a complex subject of modelling are the additives. In many applications (e.g., electrical cables) PVC is used in its flexible form, in which the pure PVC is mixed with plasticisers in significant amounts. Besides plasticisers, a PVC cable may include stabilisers and fillers, which affect the thermal degradation and combustion.

The most important additive from angle of the fire spread is the plasticiser, concentrations of which can be as high as 100 phr (parts per hundred parts resin). There are several commercial plasticisers available, of which one of the most commonly studied (and used) is *diethylhexyl phthalate* (DOP). The phthalates degrade at around the temperature at which the dehydrochlorination reaction occurs and releases combustible gases that burn with a flame in the presence of oxygen. Besides increasing the fire risk through the mechanism of flammable gas, plasticisers interact with the PVC resin and alter the thermal degradation process. Marcilla and Beltran [81] studied pure samples of DOP and PVC and their mixtures in TGA. The degradation temperatures of these two components are slightly different; DOP degrades at slightly lower temperatures than pure PVC. In a mixture, the temperatures almost overlap; the degradation temperature of DOP increases only slightly, but the PVC degrades clearly earlier than it does without plasticisers. The low concentrations of plasticiser and high heating rates decrease the effect. Similar destabilisation of the PVC was observed by Jimenez et al. [79]. They provided two explanations for the phenomenon: As the DOP evaporates, it leaves holes in the resin structure that act as the starting points of the HCl release. Another cause may be the reaction accelerating radicals formed at around $300\,^{\circ}\mathrm{C}$ as the DOP evaporates. Additionally, it was observed that DOP partially inhibits the formation of aromatics during the dehydrochlorination reaction.

The most significant additives in PVC mixtures, by concentration, are fillers. Reasons for the use of fillers range from improving the flame resistance (via minerals ATH and MDH), thermal stability (via calcium carbonate, $CaCO_3$), and electrical (via metal and carbon fibres) and mechanical (for example, via talc) properties to simply cost reduction. In PVC cables, the most common filler is $CaCO_3$. [88] It degrades at high temperatures, producing CO_2 and H_2O. It may also react with HCl to produce calsium chloride (CaCl). [89, 90]

Other significant groups of additives are stabilisers and metal oxides. They are not added in large quantities but do have an effect on the thermal degradation of the polymer. Stabilisers do not directly affect the degradation temperatures, but they do inhibit the formation of HCl, which is an important result from the environmental point of view. At higher concentrations (> 1 phr), these stabilisers also inhibit the benzene and toluene formation, thus decreasing the amount of combustible gases. [79] The metal oxides also suppress the formation of aromatics, for unsubstituted aromatics (benzene, and naphthalene), the effect being more significant than for alkyl-aromatics (toluene). The oxides with the greatest aromatic suppression effect also promote char formation the most. Some metal oxides (mainly ZnO) also lower the dehydrochlorination temperature. [77]

3.5.2 Electrical cables

Fire is considered one of the initial events to be examined in PRA for nuclear power plants. Electrical cables account for a significant portion of their fire load, and so cable fires have been widely studied both nationally [4] and internationally [91]. The fire itself is not the only hazard in those applications; also, failure of critical instrumentation or control cables may lead to severe consequences.

Early on cable modelling concentrated on simple, analytical models and approximations [92, 93]. With advances in processing power and CFD code, actual prediction of the fire spread, starting with the material reactions, has become more feasible. The dissertation project concentrated on the new methods for modelling cable fires more accurately.

As was noted earlier in this chapter, obtaining information about cable composition may be challenging on account of lack of information. Some cables in a nuclear power plant may have been installed decades ago and leave no way of identifying the cable composition except through extensive analysis of each cable individually. It is fortuitous that knowing the exact compound does not seem to be as critical for the modelling as it is to be able to predict the effective behaviour of the material. The small scale experiments (TGA, DSC, and possibly MCC) in combination with a bench scale experiment (use of a cone calorimeter) provide enough information for building of an accurate model.

With cables, the geometry and structure pose the biggest challenges. The cylindrical, non-uniform structure of a cable is impossible to model exactly via CFD code, in consequence of the limitations of the grid and material definitions. It is important to understand that the model is not, and does not need to be, an imitation of the reality in full; it is an approximation in which all the parameters taken together compensate for the shortcomings and uncertainties of the model (see Subsection 2.4.3).

Therefore, there are alternative ways to model a cylindrical, non-uniform object. The simplest way is to project the cylindrical geometry to Cartesian coordinates, modelling the cables as rectangular blocks. In this case, the large scale model is limited for the gas phase grid by the dimensions.

An alternative method, still under development, is to use sub-grid-scale (SGS) objects (in FDS, called Lagrangian particles) [43]. In SGS the particles behave equivalently to water droplets, but they may have surface properties of solid blocks. For particles, using a cylindrical form is feasible, and, therefore, the geometry can be interpreted more accurately. The challenges with the particles are related to radiation, flow drag and increased computation time.

The non-uniform layered structure is even more difficult to address. Since most cables do not have separate layers neatly ordered from the surface to core,

one has to approximate this too. Fortunately, other modelling parameters compensate also for this inaccuracy. The sheath layer is always on the exterior boundaries, first and last layers in the Cartesian, only the first in the cylindrical. The rest of the layers can be combined in accordance with the modeller's preferences. For example, the insulation and filler components may be taken in combination as a homogeneous layer, and the conductor may or may not be included in the model, since it does not degrade. An example of a cable model in two geometries is shown in Figure 3.3. It could be argued, that the non-combustible metal conductor needs to be included, since it operates as a heat sink and therefore participates in the process of thermal degradation, but this effect can be modelled through suitable adjustment of the thermal parameters of the other layers. In many large scale calculations, pyrolysis calculations for the solid obstacles are relatively time consuming, so it may be beneficial in those cases to keep the model as simple and thin as possible. However, all the degrading components should still be included, and with use of their actual mass fractions.

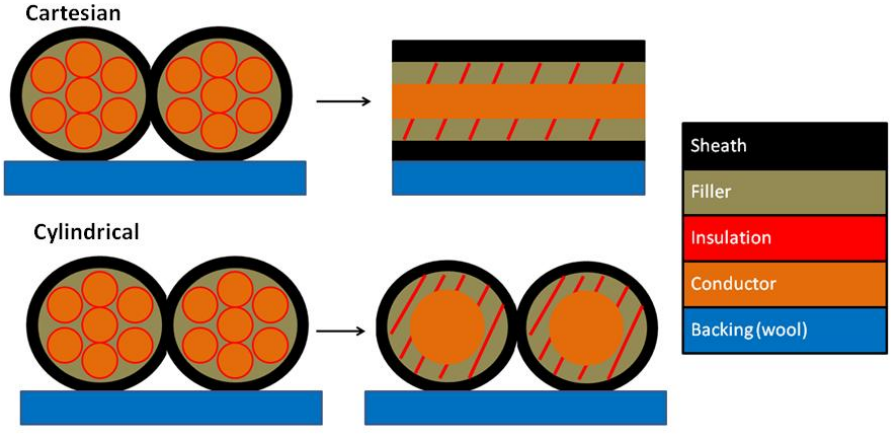

Figure 3.3. Examples of approximation of cable structure in Cartesian and cylindrical geometries.

Often in the NPP applications, it is important to know whether or not the cable can continue operating. Several models have been developed for calculating this [94, 95]. It has been shown experimentally that most PVC cables fail when the temperature within the cable exceeds 200°C. [94]

Since the cables lie in their cable tunnels for decades in varying conditions, it have to be considered that their properties may change. The important question is whether this increases the flammability of the cables. Some experimental studies have been performed that compare new and old PVC cables, and

it seems that the time of ignition is actually longer with old cables. The explanation may have to do with slow evaporation of the phthalates, leaving less combustible material in the cable. [96,97] Another question is how the evaporation influence the cable's mechanical properties. Placek and Kohout [98] studied PVC-sheathed cables after exposing them to radiation and high temperatures, corresponding to 10 years of real-world service. They noticed that mechanical properties (strength and elongation) in the sheath area were not significantly inferior to those of the new sample. However, in the insulation the effects were more significant, especially with slow ageing. These effects were connected with oxygen diffusion causing extensive degradation. The model for calculating the time of simulated ageing has been presented by Benes et al. [83].

3.5.3 Composites

Composites are made of two or more materials that are united through artificial combinations. The artificial fabrication is an important feature differentiating composites from, for example, metal alloys. Composites have the advantage of combining properties of two or more materials and therefore have qualities that individual components cannot attain alone. They can be tailored in many ways through careful choice of the components and their proportions, the distributions, morphologies, degrees of crystallinity, crystallographic texture, structure, and the composition of the interface between the components. Composites combining suitable qualities in these categories can be lightweight, stiff, strong, resistant to corrosion, durable, and thermally isolating, and they can have low thermal expansion, among other characteristics. [99, 100]

The idea behind composites is not new. The first known composites were developed by the ancient Egyptians when they reinforced their mud and clay bricks with straw and developed the first version of plywood by combining many thin layers of wood into one thick layer [101]. Composites were used in the construction of the Great Wall of China (starting in 121 BC) too, where earth-works were connected and reinforced with bricks that included, along with water and fine gravel, red willow reeds and twigs. In Mongolia, bows were made via lamination of animal horns and tendons, wood, or silk around 1200 AD [102]

Since those days, civil engineers and designers have striven to develop new forms of materials for stronger, larger, better, and more aesthetically pleasing structures. Since the 1960s, the use of polymer composites has grown very rapidly. Composites are used in applications from aircraft and race cars to sporting goods and consumer products. [101, 103, 104] Biodegradable and lignocellulosic fibre composites have been developed since the 1990s, because of the growing interest in eco-friendly materials and increased prices of oil [102].

Some challenges with composites are related to their mechanical properties, low through-thickness, poor toleration of impact damage, and anisotropic properties. One major disadvantage is their poor performance in fire. Some composite matrixes soften, creep, and distort already at relatively low temperatures (> 100–$200°$C), which can lead to problems with load-bearing installations. Organic fibres used to reinforce the composite also decompose in higher temperatures (300–$400°$C), releasing fuel gases, which leads to fire in the presence of oxygen. The consequences of this fire include heat, smoke, and toxic gases. The fire products with combination with the decreasing structural durability make the fire behaviour of this type of composites extremely dangerous. [100]

Composites are seeing increasing use in the aeronautical industry thanks to their low density and their strength, along with the possibility they present for optimising the design to achieve the best strength–weight and stiffness–weight ratios. In aeroplanes, the high flammability of composites causes a huge risk, since evacuation possibilities are limited. In 1987–1996, only 3.5% of accidents on aeroplanes originated through fire. Although the number of the accidents was small, they had the fourth largest contribution to the total casualties of all accidents, causing 339 deaths over that nine-year period. Most accidents related to fire on the aeroplanes originate from outside from a fuel tank explosion. In those cases, the integrity and thermal resistance of the cabin are fundamental for the survival of the passengers. Composites display high thermal stability and slow conduction of heat through the thickness; therefore, they are more suitable for use as thermal barriers than, e.g., metal alloys. The high flammability of the composites can be improved by various mechanisms, including heat sinks, heat barriers and fillers that act in the solid or gas phase, in various ways. [2, 7, 100, 105–107]

Research and modelling of the thermal behaviour of fibre-reinforced polymer composites had its beginnings in tandem with the defence and aerospace industries' concentration on carbon fibre materials. The first person to model mechanical properties at elevated temperatures was Springer, who did so in 1984 [108]. He related the mechanical properties empirically to mass loss. Since then, the models have improved greatly, especially in terms of elastic and viscoelastic behaviour at elevated or high temperatures. Bai and Keller [109] provide a good overview of the thermomechanical models developed thus far.

The modelling of thermal degradation of flame retardant polymer composites has been widely studied in the past few years. In 2000, Dembsey and Jacoby [110] studied ignition models for marine cored composites and concluded that the ignition models in use at the time were not able to predict the effect of skin thickness and core composition. A good compilation of analytical models for composites in various circumstances has been presented by Lattimer

and Cambell [111]. A common trend in recent years has been to model the thermal degradation of the materials by using Arrhenius-type kinetics with the three generally unknown parameters per reaction that are as discussed in Section 2.2. This approach has been successfully applied for composite materials by Kim et al. [112] and by Lautenberger et al. [113]. Trelles and Lattimer [114] have suggested an alternative model that is based on the relationship between density and temperature. That model shows good agreement with the experimental data.

4. Methods

4.1 Motivation

This chapter presents methods and applications developed during the work for this dissertation. These methods have been applied and described in detail in the Publications I-V. First is discussion of the parameter estimation process, presenting the best practise and all of the experiences collected during the modelling work, from the sample preparation all the way to the model validation on large scale. The following sections present methods for the individual phases of the modelling process. The FDS models for the experiments are briefly described, as are the parameter estimation methods used in this work. Finally, the method of combining TGA and MCC results is reviewed in brief.

4.2 The parameter estimation process

This section presents the best practise and observations gathered over the years of working with parameter estimation for various materials. A summary of the process is shown in Figure 4.1. It consists of four phases: sample preparation, experimental work, modelling and parameter estimation, and model validation.

The sample preparation is the preliminary phase to the experimental work. If the sample is not homogeneous and has several separable components, each component should be tested separately in the TGA. Therefore, the first step is to deconstruct the material. Some non-homogeneous materials cannot be deconstructed as easily, one example being fibre reinforced composites. In their case, it would be best to test the resin separately from the fibres. If the materials are not available in pure form, small solid cubic forms will work better than a powder made of the sample. The decomposition energies change due to forming of powder, which lead to different results. Also, powder does not necessarily have the same component mass fraction as the original sample, so the results may vary for that reason as well. When the components have been separated, densities and component mass fractions can be determined. At this point it is also necessary to study background information about the sample material. Relevant information would be what the typical additives are, what kinds of reactions should be expected, and so on.

The experimental work includes all of the small and bench scale experiments. The TGA and DSC experiments are performed both in nitrogen and in air, ideally at several heating rates. The maximum temperature should be

set high enough that all the reactions end before the test is complete. A similar principle holds for optional MCC results; if the reactions seem not to have ended when the test ends, or the oxygen content in the combustion chamber indicates that the material consumes all available oxygen, the test should be run again, with adjusted values. Cone calorimeter experiments should be done at least at one heat flux, but results at other heat fluxes are very useful for model validation purposes. Several, identical experiments should be conducted for determination of the experimental error. The experiment should run until the flame extinguishes completely, not only to 20 minutes as the cone calorimeter standard states. The useful measurements are the mass and heat release rate, but in some cases also front and back temperatures of the sample are helpful. An oxygen controlled cone calorimeter can be used for validating the solid phase degradation at the bench scale. The sample's preparation is a complex task, especially for cables. Ideally, each component should be tested separately also on cone calorimeter scale, but, except for the largest cables, the small size and the geometry of the cable components render this impossible. Therefore, cables are usually tested in cone calorimeter in whole form. The sample consist of several parallel 10 centimetre-long cables. The number of cables in a sample depends on their diameter; each sample is approximately $10\,\mathrm{cm}$ wide. The ends of the cables should be wrapped carefully with aluminium foil to prevent ignition from the sides (insulation or filler).

Modelling and parameter estimation is the most important phase in the whole process. It starts with determination of the reaction paths and kinetics for each component separately. The results of TGA and DSC are used for determining the number of reactions, and the results of MCC can be used in measurement of the reaction specific heats of combustion as explained in Section 4.5. The kinetic parameters are estimated from the TGA data. If the fit is acceptable, these values may be fixed in the subsequent steps. At this point, other measured properties (e.g., specific heat, reaction enthalpy, or heat of combustion) are fixed. These measurements are not mandatory, as the parameters can be also estimated from the cone calorimeter results. However, the measurements decrease the possibility of the parameter compensation and help to keep the model more realistic. The cone calorimeter model of any material can be made in several ways, as explained in Subsection 4.3.2. For cables and composites, the layered structure and geometry may not be trivial to model. When the model is chosen, the remaining parameters are estimated by fitting of the model to the experiment. If the fit is not acceptable, it may be reasonable to reconsider the cone calorimeter modelling choices.

Model validation as the final step is an important but often neglected. In its simplest form, it means comparing calculated and measured cone calorimeter

results at multiple heat fluxes that were are not used in the parameter estimation. The model should predict other heat fluxes at acceptable accuracy. At larger scale, validation is even rarer, since large scale experiments are not very commonplace. This is a very important part of the associated software development.

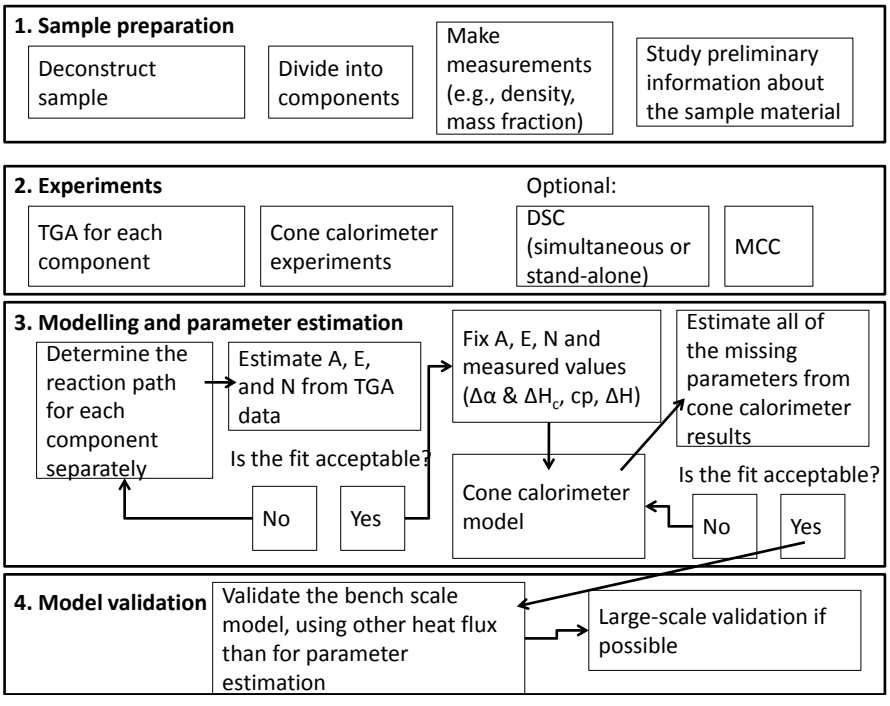

Figure 4.1. The material parameter estimation process.

4.3 FDS models of experimental methods

4.3.1 TGA and MCC

The TGA experiment is modelled for determination of the kinetics of the degradation reaction. The TGA model consists of a relatively large domain (4 m $\times$ 1 m $\times$ 1 m) and coarse grid (25 cm in the z-direction). The physical dimensions do not correspond to the real ones (the real sample cup has a volume of approximately $40\,\mu$l), but, since only the solid phase is being solved, the numerical solution is much more stable with larger dimensions than the actual sample size. Since only the pyrolysis information is desired here, the gas phase calculations are

'turned off' by setting of the ambient oxygen level to be very low. The sample is very thin (0.01 mm) and has a surface of 1 m $\times$ 1 m. The walls around the sample are heated up linearly at the desired heating rate. During the heating, the sample mass and temperature are measured. The sample must be thermally thin enough to be in thermal equilibrium with the heating walls at all times.

An MCC experiment is modelled similar to a TGA experiment for these purposes, only with a higher heating rate (typically around 60 K/min). Since the pyrolysis takes place in inert ambient, only the solid phase is solved. The heat release rate is the result of multiplying the mass loss rate by the heat of complete combustion of the reaction species, which is defined by user.

4.3.2 Cone calorimeter

The cone calorimeter model used in this work consists of two parts: the cone heater and the sample. The sample is either a slab in the bottom of the computational domain or at least one Lagrangian particle over an insulating board. The domain size is 0.3 m $\times 0.3$ m $\times 0.4$ m. The results are somewhat sensitive to the grid size, but 5 or 10 cm has been found to be fast and accurate enough. The resolution of the material model should, naturally, be based also on the final application.

The model of the cone heater depends on the sample model. Traditionally, the heat flux is added directly to the slab-like surface. This is the easiest way because the nominal heat flux of the cone heater at the surface can be determined exactly as in the cone calorimeter. For more complex geometries, especially for the Lagrangian particles, this approach does not work. In those cases, the upper walls are set to high temperatures and thus direct a heat flux to the front surface of the sample. The temperature of the walls depends on the grid cell size and other factors; hence, it should be measured for each set-up separately.

4.4 Estimation methods

The estimation methods discussed here have been developed for, and applied to, the estimation of the pyrolysis parameters. They were used extensively for the research presented in Publications I–V.

4.4.1 The generalized direct method

Various analytical methods used for obtaining the kinetic parameters of pyrolysis reactions were presented in Section 2.4. There are several, quite different approaches, some of them fast and easy to use and others providing very accurate estimates for prediction of the TGA curve. However, most of them are

somehow limited to special cases such as first-order reactions, one reaction step, or only non-noisy experimental data.

It is unfortunate that the real materials are often mixtures of several components; they may take part in multiple reactions, which cannot always be fully separated; and data can be noisy. Hence, a more general approach was developed for Publication II and compared to other known methods.

For generalisation of the method for multiple reactions, a variable for the reaction progress is introduced,

$$\alpha^* = \frac{\alpha - \alpha_{k-1}}{\alpha_k - \alpha_{k-1}}, \tag{4.1}$$

where α_k is the conversion after reaction k. The Arrhenius equation then becomes for multiple reactions

$$\frac{d\alpha}{dT} = \frac{A_k}{\beta} \frac{(\alpha_k - \alpha)_k^N}{\alpha_k - \alpha_{k-1}} exp\left(-\frac{E_k}{RT}\right). \tag{4.2}$$

One reference point can be selected from the peak of the mass gradient. At this reference point, the second derivative is 0 and the mass gradient at the peak is

$$r_{pk} \equiv max\left(\frac{d\alpha}{dT}\right). \tag{4.3}$$

The peak temperature and peak conversion, respectively, are T_p and α_p, correspondingly. From the definition of the peak, the activation energy becomes

$$E_k = N_k R \frac{r_{pk}}{\alpha_k - \alpha_{pk}} T_{pk}^2 = \frac{N_k R}{\beta} \frac{max(d\alpha/dt)}{\alpha_k - \alpha_{pk}} T_{pk}^2, \tag{4.4}$$

depending on whether the derivative is calculated with respect to time or temperature. The pre-exponential factor can be calculated from eq. 4.2 with the activation energy known:

$$A_k = r_{pk} \beta \frac{(\alpha_k - \alpha_{k-1})^{N_k - 1}}{\alpha_k - \alpha_{pk}} exp\left(\frac{E_k}{RT_{pk}}\right). \tag{4.5}$$

This method, which is from here on called *direct method* (DM), is a fast and simple way to define the pair (A_k, E_k), and reaction order can be calculated by means of some of the methods described in Subsection 2.4.1. For this method, only the location of the peak mass gradient and the total mass loss fraction of the reaction need to be known. However, if the reactions partly overlap in temperature (or time), determination of the peak may be challenging. Sometimes there is also more noise at the highest mass loss rate, making the peak value non-exact. For this reason, the idea of the DM is developed further. If the reference point could be selected more freely, e.g., before or after the peak, perhaps

the reaction overlap and possibility of noise would not be a problem. The peak of the second derivative is found from the zero of the third gradient (at T_{pp}). The activation energy then becomes

$$E_k = \frac{-b \pm \sqrt{b^2 - 4ac}}{2a}, where \begin{cases} a = \frac{(\alpha_k - \alpha_{pp})^2}{R^2 T_{pp}^2} \\ b = -\frac{2r_{pp} N_k (\alpha_k - \alpha_{pp})}{R T_{pp}^2} - \frac{2(\alpha_k - \alpha_{pp})^2}{R T_{pp}^3} \\ c = r_{pp}(N_k - 1)N_k - r_{T_{pp}} N_k (\alpha_k - \alpha_{pp}) \end{cases} \tag{4.6}$$

and the pre-exponential factor

$$A_k = r_{ppk} \beta \frac{(\alpha_k - \alpha_{k-1})^{N_k - 1}}{\alpha_k - \alpha_{ppk}} exp\left(\frac{E_k}{R T_{ppk}}\right). \tag{4.7}$$

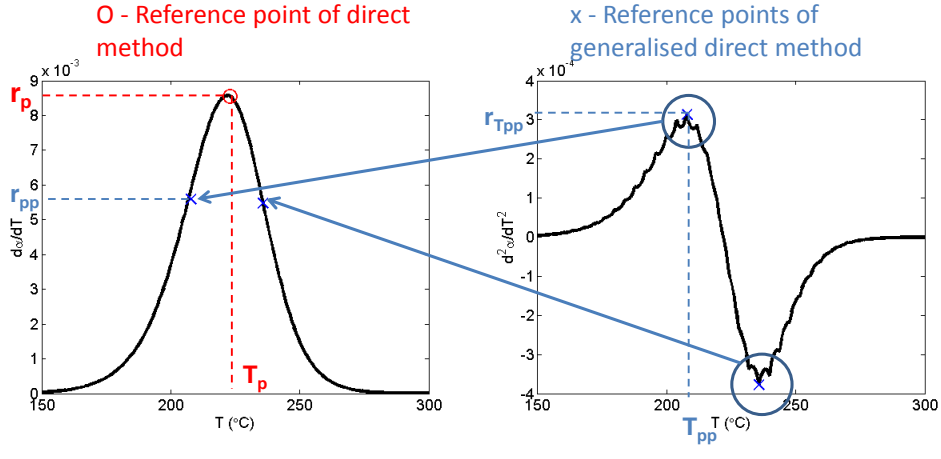

Figure 4.2. Reference points for the direct methods.

This method requires experimental data just at one heating rate. However, because of the compensation effect, several equally fitting (A, E) pairs may be found. Hence, it is important to use several heating rates. In the case of direct methods, the heating rates can be taken into account by averaging of the results (although, Opfermann [115] advise to view this approach with caution). This averaging can be directed to the parameters or to the reference points. Also, the averaging can be weighted for better extrapolation qualities. The alternative methods of weighting are listed in 4.1.

More details and results associated with these methods are provided in Publication II.

Table 4.1. Averaging weights for several heating rates. μ is the mean of the heating rates.

$w_1 = \frac{\mu}{\sum_i \beta_i}$	(direct mean)
$w_2 = \frac{1}{\lvert\beta_i-\mu\rvert \sum_i \frac{1}{\lvert\beta_i-\mu\rvert}}$	(emphasises heating rates near the mean value)
$w_3 = \frac{\lvert\beta_i-\mu\rvert}{\sum_i \lvert\beta_i-\mu\rvert}$	(emphasises heating rates far from the mean value)

4.4.2 Application of genetic algorithms

Sometimes direct methods are not suitable for the parameter estimation, as is discussed in Section 2.4. A GA application was developed for Matlab. The tool is called *PyroPlot*. It uses a free GA toolbox that can be obtained from the University of Sheffield[1]. PyroPlot exploits the toolbox for the algorithm and provides an easy-to-use graphical user interface and an interface to Fire Dynamics Simulator. PyroPlot reads, plots, and filters the data as necessary. It is optimised for the data used in fire simulations, but it can also be applied for other purposes. The GA calculates the model response by using FDS and compares the results to the experimental data. The goodness of the model fit to the experimental results is measured by fitness value. The fitness value is calculated in this application

$$fV = 1 - \sum_k \frac{1}{N_k} \frac{\sum_i (M_{exp,i} - mean(M_{exp}))^2 - (M_{exp,i} - M_{mod,i})^2}{(M_{exp,i} - mean(M_{exp}))^2}, \qquad (4.8)$$

where $\mathrm{M}_{exp,i}$ are the experimental results at each time step i and $\mathrm{M}_{mod,i}$ the corresponding model results. Several results may be compared simultaneously by scaling the fitness value by the number of results N_k. The fitness value is actually the relative error of the model fit, 0 corresponding to perfect fit.

During the simulation, PyroPlot produces plots for the best fitting individuals and indicates the progress of the process in the form of the fitness value. The iteration ends either when the maximum number of generations specified has been reached, or when the user stops it manually because a satisfactory result has been found. Typically, about 50–200 iterations are required with four subpopulations each having 20 individuals. Generating simulated data by using FDS is the bottleneck of the process, but that could be improved through parallel processing. This feature is currently under development.

The accuracy of the results depends on the estimation boundaries and the random numbers used during the process. Relatively wide estimation ranges

[1] See http://www.shef.ac.uk/acse/research/ecrg/getgat

are recommended, for yielding the best possible solution, unless the variable value is known approximately. Because of the stochastic nature of the algorithm, the results are slightly different every time. Especially if there are several solutions, with equal fit (as is typical among TGA results), the solution may converge to very different numbers each time. On occasion an overall fit cannot be found. This may be the case with the cone calorimeter results because of the geometry and layer approximations. In those cases, it is convenient to choose certain parts of the curve (e.g., ignition time and/or the location of the first peak) that have more weight in the fitness value than the other points. This helps the algorithm converge to more acceptable solutions.

PyroPlot can be obtained from Google Code[2] under the MIT License. More information about genetic algorithm and it's application to fire parameter estimation is reported in Publication I.

4.4.3 Sensitivity analysis

Despite of the method used to estimate the model parameters (thermal or kinetic), sometimes there is a need to adjust them manually for obtaining a better fit with the experimental results. In order to do that effectively, understanding of the correlations between model input and the results is required. A sensitivity study was performed for a generic, charring material in the cone calorimeter at $50\,\mathrm{kW/m^2}$ by changing one model parameter at a time. From the results of this sensitivity study, rules of thumb were formulated for summarising the results. These rules are listed in Table 4.2. Definitions for the results are shown in Figure 4.3.

The parameter values were chosen such that the two peaks were well defined. That is not always the case, if the second peak occurs very soon after the first one. The first peak of the two-peaked shape of a charring material comes from the protective char layer building up as a result of the pyrolysis. It increases the thermal resistance between the exposed surface and pyrolysis front, which leads to a decrease in the heat release rate after the maximum is reached. In the cone calorimeter, the back of the sample is often insulated, which prevents heat losses from the back side. Therefore in the end, when the pyrolysis front reaches the back, the heat release rate increases to the second peak. The two peaks overlap in time if the thermal conductivity is high for both the virgin material and residue.

The single most important parameter for all the results turned out to be the activation energy, or the pair ($A,\ E$). The emissivities of both virgin and residue components were also significant in almost all cases. For the ignition

[2] http://code.google.com/p/pyroplot/

time, the other important parameters are thermal conductivity, specific heat, and the absorption coefficient of the virgin material. The time of the first peak is additionally affected by the heat of combustion (in the cases with ambient air). The first peak's height depends also on the heat of reaction of the virgin material, and on the properties of the residue. The time of the second peak and its height depend on all the parameters except the reaction order of the virgin material, and the specific heat of the residue. For flame-out time, all the parameters are significant, apart from the specific heat of the residue.

A similar study has been performed by Stoliarov et al. [116]. They conducted an extensive literature review of the values for several polymers and simulated the model at minimum, maximum, and mean values under several radiant heat fluxes and initial thicknesses. The pyrolysis was modelled by means of the called ThermaKin software, mentioned above. It has a slightly different pyrolysis model than FDS uses. The charring process was not included in the model, but char yield was taken into account. Stoliarov and colleagues studied the variation effects on mass loss rate (MLR), instead of heat release rate. They considered four results: time to mass loss (corresponding to t_{ig}), time to peak MLR (t_{1st_p}), peak MLR (comparable to Q_{1st_p}), and average MLR (not presented in Table 4.2). The results were similar, in view of the differences in the models. For time to ignition, the most important parameter is the ratio A/E. This makes sense, because increasing E and/or decreasing A moves the reaction to higher temperatures. In fact, this ratio turned out to be the most important parameter of all the results studied. Thermal conductivity and specific heat capacity both increase the ignition time, and heat of reaction was found to have no significant effect, in both studies. The differences are in the absorption coefficient and *reflectivity* (defined as $1 - \epsilon$); where the effect is opposite that predicted in the study with FDS (see Table 4.2). For the time of peak, all of the other results are similar except those for the thermal conductivity (positive correlation with FDS and negative in the study of Stoliarov et al.) and reflectivity. The results for the peak height are similar between the two studies (except again for the reflectivity). The differences may be due to the differences in the model, mainly inclusion of the charring reaction in the model.

4.5 MCC methods

Two methods for combining TGA and MCC results have been developed. The first one discussed here is simple and easy to use, while the second is aimed at explaining the material composition more accurately. These methods are presented also in Publication IV.

Table 4.2. Rules of thumb for charring material, where + means a slight increasing, ++ substantial increasing, - slight decreasing and - - substantial decreasing effect in the result, when the particular parameter is increased.

	t_{ig}	t_{1st_p}	Q_{1st_p}	t_{2nd_p}	Q_{2nd_p}	$t_{flameout}$
Virgin material						
A	- -	- -		+	+	-
E	++	++	- -	++	-	++
N						+
k	+	+		- -	+	-
c_p	+	+	-	++	-	+
ΔH			-	+	- -	++
ΔH_c		+	++	-	++	-
κ	+		+	+	-	+
ϵ	++	++	- -	++	-	++
Residue						
k				+	++	- -
c_p			-			

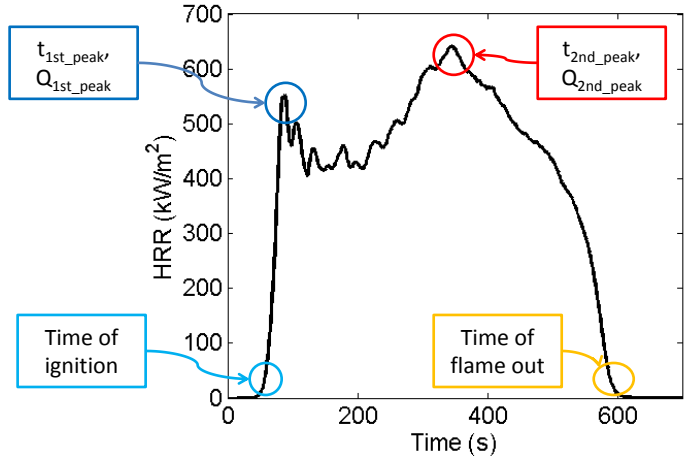

Figure 4.3. Definitions for the rules of thumb.

4.5.1 Method 1

Method 1 could be called an engineering tool. It does not require any information about the material or its composition; it is merely a way of efficiently modelling the correct amount of heat for each reaction. No special software is needed either. A simple reaction path is assumed: Each reaction step cor-

Table 4.3. Input parameters used in generation of the table of rules of thumb.

Parameter (unit)	Baseline		New value
A (s^{-1})	$1{\cdot}10^{18}$	$\rightarrow$	$1{\cdot}10^{17}$
E (J/mol)	$2.5{\cdot}10^{5}$	$\rightarrow$	$2.0{\cdot}10^{5}$
N	2	$\rightarrow$	1
k (virgin and residue) (W/m·K)	0.8	$\rightarrow$	0.4
c_p (virgin) (kJ/kg·K)	2.5	$\rightarrow$	1.8
c_p (residue) (kJ/kg·K)	2.5	$\rightarrow$	1.5
ΔH (kJ/kg)	800	$\rightarrow$	400
ΔH_c (MJ/kg)	40	$\rightarrow$	20
κ (1/m)	50000	$\rightarrow$	500
ϵ	1	$\rightarrow$	0.5

responds to one pseudo-component in the model. Each pseudo-component can yield one fuel and one inert gas. The heat of combustion (ΔH_c) is fixed for all of the reactions. Only the last reaction may yield residue.

The fuel yield ($y_{i,F}$) of each reaction (for all $i < n_r$) can be calculated from

$$y_{i,F} = \frac{Q_i/m_0}{\Delta H_c \Delta\alpha_i}, \tag{4.9}$$

where Q_i/m_0 is the MCC result (heat of complete combustion scaled by initial mass of the sample) and $\Delta\alpha_i$ the relative mass loss of reaction i as observed in TGA. The inert gas yield is thus $y_{i,I} = 1 - y_{i,F}$.

If the material does not yield residue, eq. 4.9 can be used also for the last reaction. If the material does produce residue, the yields of the last reaction become

$$\begin{cases} y_{n_r,F} = \frac{Q_{n_r}/m_0}{\Delta H_c \Delta\alpha_{n_r}}(1 - \frac{Z}{1-\sum_{i=1}^{n_r-1}\Delta\alpha_i}) \\ y_{n_r,I} = (1 - \frac{Q_{n_r}/m_0}{\Delta H_c \Delta\alpha_{n_r}})(1 - \frac{Z}{1-\sum_{i=1}^{n_r-1}\Delta\alpha_i}), \\ y_{n_r,Z} = 1 - y_{n_r,F} - y_{n_r,I} = \frac{Z}{1-\sum_{i=1}^{n_r-1}\Delta\alpha_i} \end{cases} \tag{4.10}$$

where Z is the residue yield of the original mass.

4.5.2 Method 2

Method 2 is intended for the more ambitious modeller who wants to estimate the reaction path and material composition more accurately. The reaction path can be chosen freely, including several parallel, consecutive and even competitive reactions, each yielding several gases and residue. As the reaction path is fixed and can be very complex, there is no analytical way to solve this. There-

fore, the case is constructed as an optimisation problem wherein the objective function is to minimise error between the measured and estimated values. The variables are the initial mass fractions of the components, gas yields and the heat of combustion of each gas. One can include inert gas by setting the heat of combustion to 0. The estimates for the mass loss and energy release of each reaction are

$$\begin{cases} \Delta\hat{\alpha}_i = \sum_{j=1}^{n_c} \sum_{k=1}^{n_{p,j}} y_{i,j,k} Y_{i-1,j} \\ \hat{Q}_i = \sum_{j=1}^{n_c} \sum_{k=1}^{n_{p,j}} y_{i,j,k} Y_{i-1,j} \Delta H_{c,k}, \end{cases} \tag{4.11}$$

where Y_i, j is the mass fraction of component i after reaction j. The calculation is performed recursively from the previous reaction steps;

$$Y_{i,j} = \prod_{ii=1}^{i} y_{ii,j,Z} Y_{i-1,j}. \tag{4.12}$$

The estimation can be performed with using any non-linear solver software, such as, Excel Solver or Matlab Optimization Toolbox. Since the result depends significantly on the initial values, the optimisation is performed through repetition of the process several times with random initial values from the selected range. In this application, the optimisation was made by means of a Matlab function.

4.6 Estimation of the uncertainties

4.6.1 Experimental error

On small scale, the greatest experimental error is related to the sample preparation. The experiments are, in general, highly repeatable if the conditions and the sample are kept identical. This can be seen in Figure 4.4, where the results of repeated MCC experiments are shown for samples of birch wood. The samples were taken from the same board, and some of the board was dried in an oven at $105°$C over a weekend for removal of all moisture. The total heat release of the non-dried wood varies with in the range 11.1–11.2 MJ/kg, with the maximum heat release rate being 164–178 kW/kg and the temperature at the peak between 374 and $376°$C. The heat release rate the dried wood is higher, because the original mass is purely combustible wood. If the results for non-dried wood are scaled in view of the mass of the water (6%), the results look very similar. The difference between the dried material and scaled results is 2.9% for the total heat release, 3% for the peak heat release rate and 0.2% for peak temperature. Although the dried sample is kept in a desiccator, it is quite unclear how

much moisture the dry sample absorbs during the preparations (measurement, sample positioning and heating of the furnace). Therefore, it may be more convenient to test the sample as delivered and determine the moisture content by using another sample.

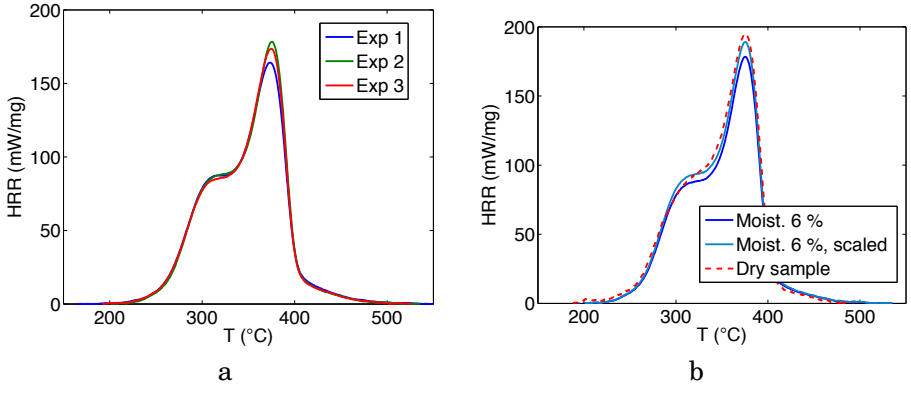

Figure 4.4. Repeated MCC experiments with birch wood. a) non-dried wood, moisture 6% and b) non-dried and dry wood.

The sample mass should be small enough for keeping the sample in thermal equilibrium with the furnace at all times. This is dependent on the thermal thickness of the sample and the heating rate. Also the load cell accuracy is significant with the smallest samples. If the accuracy is 0.1 mg, 10% error could result for the smallest samples.

In the cases involving non-homogenous materials (such as composites), the sample preparation is especially challenging. The material may be very hard to cut, one may be tempted to grate it into powder. In the approach described here, the problem may lie in preserving the sample mass fractions. For example, long fibres may be too big for the sample cup and therefore omitted, leading to lower fibre content and thus greater content of combustibles.

4.6.2 Uncertainties in the modelling

The material model's uncertainty on the larger scale depends on the accuracy of said model and the modelling software. The accuracy of FDS can be evaluated via the verification and validation guides [117, 118]. The verification guide consists of simple examples to verify that the code is implemented correctly, and the validation guide includes a comparison of the experiments and models to confirm that the physics of the several phenomena involved have been handled accurately.

Material model accuracy one the large scale depends on the accuracy of

the small and bench scale model. As is proved in Publication III, it is not the parameter values that are significant on bench scale but the overall fit. The validation work on large scale will continue.

5. Results

5.1 Motivation

This chapter includes summary of the most important results described in Publications I-V and some additional results that shed light on and explain the work done for this dissertation. The estimation methods presented in Publication I and Publication II are compared to other methods in use in terms of accuracy, effectiveness, and ease of use (in Section 5.2). The main results of the sensitivity study performed for Publication III are listed in Section 5.3. Some new results of testing of a PVC cable with the MCC methods developed in the work on Publication IV are reported in Section 5.4, and, a sensitivity study of the cable model used in the large scale MC simulations covered in Publication V is presented in Section 5.5.

5.2 Comparison of estimation methods

The range of estimation methods suitable for extraction of the parameters for pyrolysis models is wide, and often the choice is based on the personal preferences of the modeller. The methods can be divided roughly into two groups, as discussed in Section 2.4: analytical and curve-fitting algorithms. The latter can be applied to any model (including the estimation of thermal parameters), but the analytical methods are model specific. Publication II summarises some commonly used methods for the estimation of kinetic parameters and compares their results' accuracy, their efficiency, and the complexity. The set of methods included two evolutionary algorithms (a *GA* and *SCE*) and four analytical methods, of which one was derived by the author and the others were found in the literature [40, 42, 43]. These methods were tested against two sets of generic experimental data. Generic data were chosen because of the possibility of comparing the real target values to the estimated ones. The first data set was very simple and noiseless, and the reactions were well separated in time. The second data set was more complicated including noise and partly overlapping reactions. Only the analytical methods were tested for data set 2. The interpolation ability of the methods was tested at a heating rate that was within the range of experimental heating rates (20 K/min). The extrapolation ability was tested at a significantly higher rate, 100 K/min. The parameters were also evaluated on larger scale, with the cone calorimeter model and fixed thermal parameters.

The results are summarised in Table 5.1. The reference values were calculated from the generic data. For accuracy of the results, when one considers both fitness values (as in eq.4.8) and difference in the target values, the evolutionary algorithms were superior to the analytical methods. For the former, the user has to define the variable ranges and algorithm parameters. If the algorithm is used with default settings, six lower and upper boundaries have to be determined. For analytical methods, the number of parameters (the complexity) did not correlate directly with the greater accuracy of results. However, the simplest method, the first-order McGrattan-Lyon [42, 43] method, produced the worst fit. The other analytical methods performed well, with good fit in the solutions for both data sets and also for noisy data.

As for their level of accuracy for the end application, all methods tested produce acceptable results. Hence, one can state that the choice of method is basically up to the user.

Table 5.1. Comparison of the estimation methods based on two example cases. Fitness value is the relative error, 0 corresponding to perfect fit. [1]With noise 2. [2]Without parallel computing (algorithms) or automated search for reference values. [3]For algorithms, estimation boundaries etc.

	GA	SCE	DM	GDM	Friedman	McGrattan-Lyon
Fitness value w/ data set 1 (at 100 K/min)	0.0041	0.0003	0.0111	0.0082	0.0109	0.0131
Fitness value w/ data set 2[1] (at 100 K/min)	-	-	0.0143	0.0181	0.0093	0.0553
Time of preparation	10 min	10 min	0 min	0 min	0 min	0 min
Time of estimation[2]	$\approx$ 1 day	$\approx$ 1 day	10 min	15 min	15 min	5 min
Number of reference values[3]	min. 12	min. 12	10	12	16	8

5.3 Sensitivity and uncertainty of the model

For Publication III, various modelling choices were tested in modelling of a PVC cable sheath material. The versions tested included the following:

- Reaction scheme (parallel or consecutive)
- Char formation (which reaction produces char)
- Values of the kinetic parameters (A,E) pairs)
- The value of the reaction order
- The fuel yield of the first reaction.

The reaction scheme can typically be either parallel (components degrade independently of each other) or consecutive (one component degrades to another). In some cases, also competing reactions may be relevant. For example, for cellulose degradation, different reaction paths are known to dominate, depending on the temperature and heating rate. At low temperatures, the dominant process is intermolecular dehydration leading to char and gas, and in the presence of air to smouldering combustion. At high temperatures, depolymerisation p
air [119
combina

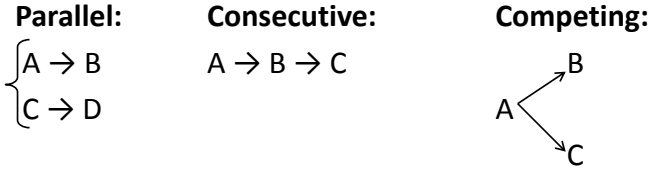

Figure 5.1. Possible reaction paths in pyrolysis modelling.

The reaction path significantly affects the kinetic parameters values, which supports the interpretation that the parameters are model-dependent rather than material properties. Equally good fits can be achieved with any reaction path, but the parameters and the reaction paths cannot be used separately. This difference is clearer with the cone calorimeter results. The consecutive reaction path results in significantly slower degradation when the same thermal parameters are used. This happens because the next reaction is always limited by the previous one in the consecutive reaction path, and at high heating rates and with fixed thermal parameters the reactions overlap more in the parallel path than is possible with the consecutive path. With fitting of the thermal parameters for each reaction path, equally good fit is again reached.

Another modeller decision is that on distribution of char forming. When a parallel reaction path is used, the char can be formed from any reaction(s). On small scale, this does not make any difference, and with the version of FDS (version 5) used for the simulations reported upon in Publication III it did not make any difference on cone calorimeter scale either when the char conductivity was high enough. Version 6 of FDS includes a new ability for modelling swelling surfaces. Char is known to swell and form an insulating layer at the material's surface. The amount of swelling depends on the density of the residue component, and, therefore, it does make a difference at which reaction char is former,

and in what quantities (as seen earlier, in Figure 3.1).

As mentioned above, the values of A and E are unambiguous because of the compensation effect [60], so several pairs that fit equally well can be found. Two sets of parameters (N being 1) were estimated by means of GA and an analytical approach. The results showed that if the reaction path and order are the same, and the kinetic parameters fit equally well on small scale, they cause no difference on the larger scale either. Naturally, small differences in the fit at small scale may lead to larger differences on the larger scale. In addition, this study confirmed that the results are not sensitive to the estimation method, as discussed in Section 5.2, above.

The reaction order is the parameter that compensates for the inaccuracy in modelling of the chemical reactions. In other words, it is the parameter that lumps several reactions together and defines the sharpness of the TGA curve. The results show that this is an important parameter: two sets of parameters that on small scale had equally good fit, resulted in very different heat release and mass loss rate curves in the cone calorimeter context with the same thermal parameters. The lower reaction rate led to slower degradation of the sample material.

Although pure PVC releases only a small quantity of combustible gases during the first reaction, this is often not the case for the real PVC cable material. These materials contain large amounts of additives, including plasticisers that degrade at around the same temperatures as pure PVC (dehydrochlorination reaction), releasing highly flammable gases. This should be taken into account when one builds a PVC model, even if it is not detectable in the TGA results. Alternative methods for defining the fuel yield are presented in Section 4.5, but a fast way to estimate the fuel content of the sample is fitting to the heat release rate curve of the cone calorimeter results. Also making a big difference for the results is whether one allows fuel gas release from the first reaction too.

Summarising the results, one can state that most of the modeller choices do not have any significant effect on the bench scale experimental results but they do have an effect on the parameter values used. This means that the parameters really are model-dependent and should not be considered independent material characteristics, and it means in consequence that these values should not be mixed or used outside the intended application.

5.4 Estimation of the cable composition via MCC

The MCC methods were applied to a PVC sheath of an electric cable (#701) for Publication IV. Now method 2 has been used for estimating the reaction path for another cable, identified as MCMK, which was also used in the sensi-

tivity study of Publication III. The TGA experiments were performed at heating rates of 2, 10, and 20 K/min, and the MCC analysis was repeated three times with a pyrolysis temperature of 75 to 900°C, 900°C combustion temperature, and 20 cm^3/min flow of oxygen to the combustor. In TGA, three clear peaks can be observed and in MCC two. An additional, very weak peak may be observed near the end of the MCC experiment at around 700°C, but it is so weak that it can be ignored. The averages of the experimental results are listed in Table 5.2.

Table 5.2. Experimental MCC results for the MCMK sheath (the values are averages over three repetitions and heating rates).

	Reaction 1	Reaction 2	Reaction 3	Total
T_p $(°C)$	282	462	728	-
$\Delta\alpha$ in TGA	0.56	0.10	0.07	0.74
$\Delta\alpha$ in MCC	-	-	-	0.74
Q/m_0 (MJ/kg) in MCC	10.5	4.2	0	14.7

The iterative estimation process explained in Section 4.5 was repeated $5,000$ times, and the accuracy (or fit) of the final result is $1.5 \cdot 10^{-7}$. The results are listed in Table 5.3, where they are compared with the estimation results for cable #701. The mass fractions in the original material are denoted by Y_i, and the fuel and inert gas yields with $y_{F,ij}$ and $y_{I,ij}$, respectively. Index i is the component index and j the reaction index. The results are quite different: They showed that according to assumptions on the reaction paths, the MCMK to consist of 29% PVC ($i = 1$), 39% plasticiser ($i = 2$) and 32% $CaCO_3$ ($i = 3$), while the corresponding mass fractions for cable #701 are 51% , 27% and 22%, respectively. The experimental results for both cable sheaths are shown in Figure 5.2. From the figures it can be observed that MCMK sheath has less mass loss and higher heat release during the first reaction. This explains the result of the higher mass fraction of plasticiser. The second-reaction mass loss is higher for the #701 sheath, but the heat released during the reactions is almost the same. Hence, the heat of combustion of the PVC residual must be higher. The third mass loss is higher for the MCMK; therefore, the amount of $CaCO_3$ is probably higher in the MCMK. It should be kept in mind that while method 2 allows more truthful reaction paths, the real accuracy always depends on the assumptions made by modeller. The cable sheath compositions presented here may or may not correspond to the real composition, but the resulting model is able to predict correct mass loss and heat release rate using more complex reaction path, as intended.

Table 5.3. Estimation results for MCMK cable sheath compared with the results for cable #701 sheath.

	Estimation boundaries	Initial values	Result (MCMK)	Result (#701)
Y_1	[0.2,0.7]	0.26	0.29	0.51
Y_2	[0.1,0.5]	0.38	0.39	0.27
Y_3	-	0.35	0.32	0.22
y_{I11}	[0.57,0.61]	0.60	0.58	0.60
y_{F11}	[0,0.07]	0.00	0.00	0.04
y_{F12}	[0.5,0.9]	0.85	0.81	0.75
y_{I33}	[0.05,0.3]	0.21	0.22	0.18
$\Delta H_{c,11}$	[25,50]	49.40	32.54	49.10
$\Delta H_{c,12}$	[25,50]	30.38	42.00	35.80
$\Delta H_{c,21}$	[25,50]	30.62	26.90	30.20

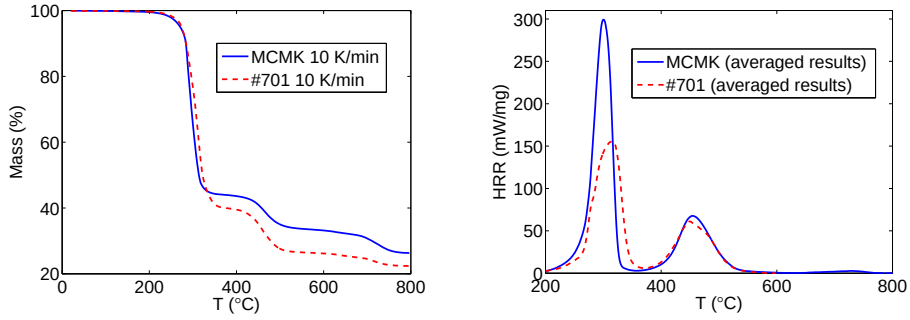

Figure 5.2. Comparison of experimental results for two PVC sheaths. a) TGA at 10 K/min, and b) MCC at 60 K/min.

5.5 Application to a cable tunnel

Publication V applied the parameter estimation results to large scale simulation at a cable tunnel fire of a nuclear power plant. The diversity of the cables found at a real nuclear power plant was taken into account through variation of some of the cable model parameters in the MC simulations. A sensitivity study for the parameter values in cone calorimeter results is presented here.

A cable model used in Publication V was studied via MC technique with the same parameter ranges as in the paper. The sample was generated by means of Latin hypercubes, and the sample size was 100. The variables were the thermal conductivity of the charring pseudocomponents of the sheath (*sheath 1* and *sheath 2*) and the thicknesses of the first three layers (sheath, insulation

plus filler, and sheath). All distributions were assumed to be uniform since the idea was only to study the correlations between input and output. Four output quantities were defined: time to ignition (defined as the time until HRR $> 10\,\mathrm{kW/m^2}$ the first time), maximum heat release rate, time of maximum heat release rate, and time of flame out (the time until HRR $< 10\,\mathrm{kW/m^2}$ in the end of the experiment). The correlations are shown as a scatter plot in Figure 5.3 and as correlation coefficients in Figure 5.4. It can be seen that the thermal conductivity has the greatest correlation with all of the output quantities, and the strongest correlation is with the time of ignition, as expected. The layer thicknesses correlated most strongly with the maximum heat release rate, and the second layer's thickness correlates also with the time of the maximum heat release rate. There is a little uncertainty related to definition of the maximum heat release rate, because of noise in the simulated data. For the flame-out time, the only significant parameter was thermal conductivity.

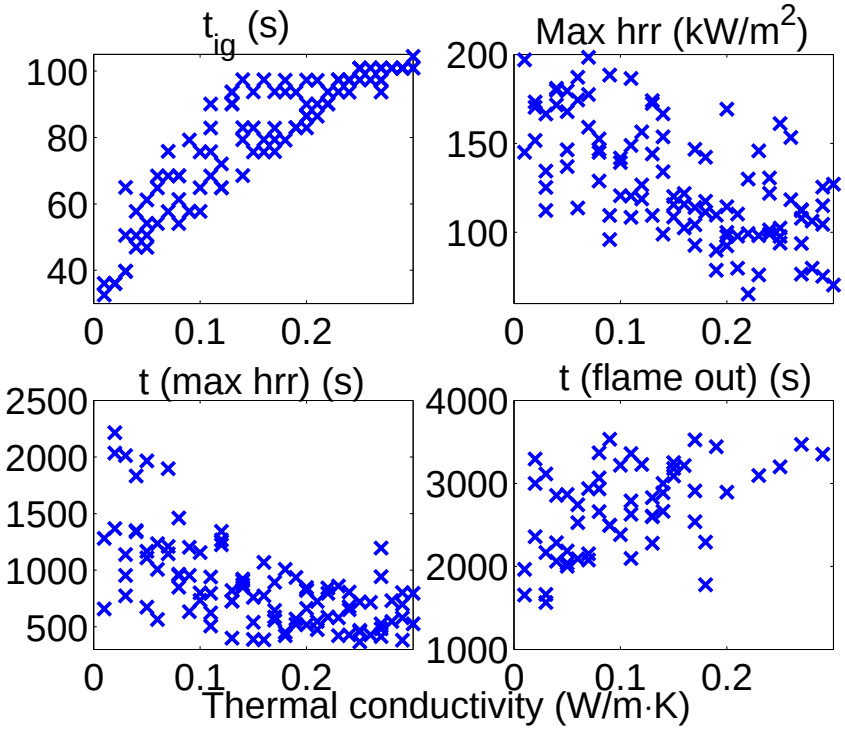

Figure 5.3. Output quantities versus thermal conductivity.

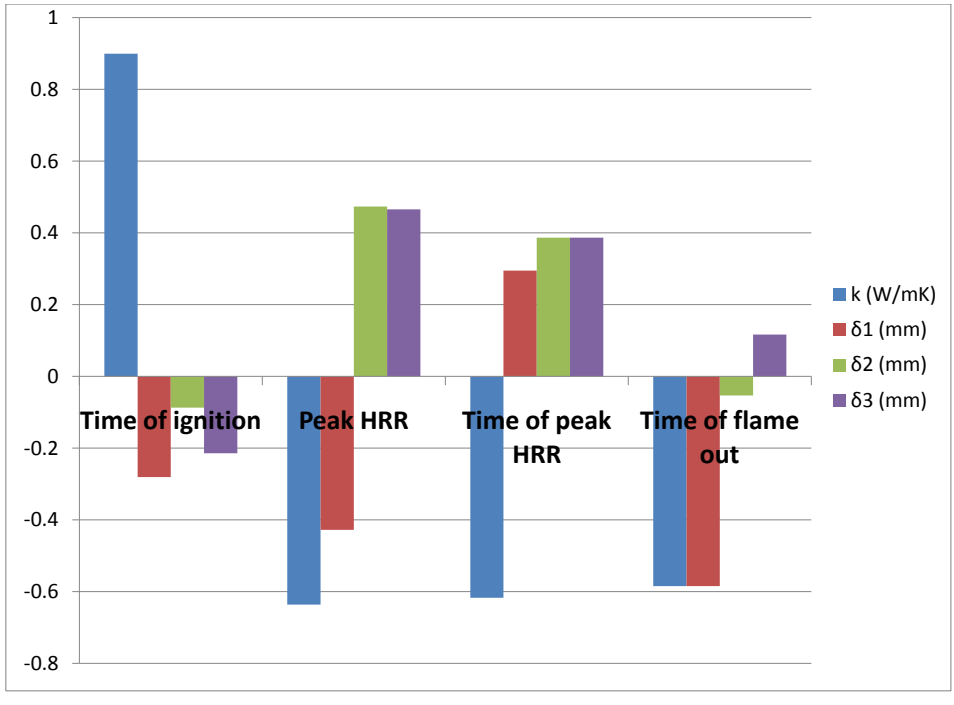

Figure 5.4. Coefficients of correlation between input values and results. k is the thermal conductivity of the first sheath layer, and δ_1, δ_2, and δ_3 are the thicknesses of the three first layers.

6. Conclusions and future work

6.1 Conclusions and discussion

Since fires cause significant harm to people and property, being able to recognise the risks is essential if one is to limit the consequences. For prediction of the fire spread, it is necessary to model the pyrolysis of the solid phase, starting with the chemical degradation reactions. This dissertation has focused on studying the methods of pyrolysis modelling, including the estimation methods, and best practises throughout the modelling process. The methods have been applied to one real-world-scale application in simulation of a cable tunnel fire at a nuclear power plant.

Publication I and Publication II present methods for estimation of the pyrolysis model parameters. The semi-analytical models are simple and fast to use, and they are able to find estimates for the kinetic parameters that show accurate enough fit to the experimental data. Some of them even work for slightly overlapping or noisy data. An additional benefit with these methods is that the result does not depend on the estimation process or on boundary values; the result is always the same. However, for more complicated reaction paths or noisy data, the estimation algorithms offer a more robust method. Those algorithms demand more time and resources but are almost certainly able to find an accurate fit for the experimental data. They can also be used for the estimation of other parameters besides kinetics. The main drawback and criticism of the pyrolysis modelling is that the kinetic parameters are rendered ambiguous by the compensation effect. Depending on the stochastic nature of the algorithm and estimation boundaries, the algorithm may end up reaching a different solution every time. However, the work done in this dissertation project and the discussion above indicate that the bench and large scale results are not sensitive to the kinetic parameters themselves, just relevant for the fit to the experimental data.

Publication III covers the modelling of a PVC material. Several modelling choices are studied there and compared on bench scale. It turned out that the model is sensitive to many choices (e.g., reaction path or order) when the same thermal parameters are used. However, results with equally good fit may be found for all the alternatives if the thermal parameters are fitted separately. This confirms that the parameters are model-specific and not material-specific. It is important that one does not take the parameters out of context and use them in a different model, since they do not mean anything on their own. This

study proved again that any particular estimation method is not significant for finding the fit on the larger scale. As long as the reaction path and order are the same and the result shows equally good fit on the small scale, the difference in order of magnitude does not matter with the pair (A, E).

The methods combining the results of TGA and MCC were presented in Publication IV. These two methods were developed for different modelling needs: method 1 is very simple and can be used only for calculating the correct amount of heat from each reaction. The second method is more complex, and has the ambitious goal of modelling the reaction path as accurately as is reasonable. It can also be used for estimating the composition of an unknown material.

The methods presented in the dissertation were tested in a real world scenario for a nuclear power plant (see Publication V). The cable trays were modelled by means of the genetic algorithm and small and bench scale data. The model was used as a basis for Monte Carlo simulations. The results provided valuable information about the failure probabilities of the cables and the most significant variables behind the most severe conditions. More specifically, this study was used as a part of PRA for an actual nuclear power plant in Finland [4].

The methods and applications developed in this dissertation project have a real impact on the fire safety of the materials and public buildings in use. Capability of accurately modelling and predicting the flame spread with different fire loads improves the evaluation and identification of the risks and makes the allocation of resources more effective. The cable simulations have already contributed to the calculation of more realistic probabilities of fire spread, in the updating of the PRA for the Finnish nuclear power plant. [120]

6.2 Future work and trends in pyrolysis modelling

Work to validate the current fire spread models continues on the large scale. The SGS modelling is expected to solve the current problems found in the CFD modelling of the cables. Being able to model composite structures accurately could save significant amount of effort and expenses in real scale testing in the development phase.

The OECD project PRISME 2[1] will provide excellent large scale experimental results for fires affecting multiple cable trays and electrical cabinets. The tests are performed for various room configurations, and several measurements are made in the course of any given test. The resulting data will be used for validating the entire process of pyrolysis modelling and parameter estimation as described in Section 4.2, from the solid phase thermal degradation reactions

[1] see http://www.oecd-nea.org/jointproj/prisme-2.html

through prediction of fire spread in large installations.

Being able to model the thermal degradation reactions of a material accurately opens new opportunities also in the area of material development and design. Modelling the flame retardancy mechanisms may be especially valuable for the design of new, flame retardant materials. Correctly predicting the cooling effect of an endothermic reaction or the insulating effect of an insulating char barrier enables large scale testing via simulations before the material is even produced. The concentrations of the additives can be studied numerically first, which should decrease the effort of experimental trial and error.

Applications of the presented methods can also be found outside the fire safety engineering. For example, they could be used in developing new methods for extracting biofuels from the biomass as well. Understanding the thermal degradation process of the biomass provides new possibilities for testing the alternative methods by modelling instead of performing experiments. [121–123]

An even smaller scale tool for studying the thermal degradation of materials is molecular dynamics [13]. It calculates the behaviour of the molecules numerically, on the basis of knowledge of the interactions (forces) between the molecules. It allows study on such time and dimension scales as could not be addressed otherwise. The tools of MD could indeed be used in studies of flame retardants. Studying additives' effect in the resin at molecular level may significantly aid in understanding the operation of the current flame retardants and in developing new and better ones.

Bibliography

[1] E. Kokki. Palokuolemat ja ihmisen pelastamiset tulipaloissa 2007–2010. *Pelastusopisto, tutkimusraportti*, 3, 2011.

[2] I. Lopez de Santiago, I. Saez de Ocariz Granja, A. Arbildi Fernandez, F. Fernandez Sanchez, A. Cortes Rueda, and K. Fernandez Horcajo. Fire penetration in an aircraft made in composite. *Proceedings of the Interenational Congress on Combustion and Fire Dynamics in Santander*, 2010.

[3] T. Hakkarainen, J. Hietaniemi, S. Hostikka, T. Karhula, T. Kling, J. Mangs, E. Mikkola, and T. Oksanen. Survivability for ships in case of fire. final report of surship-fire project. *VTT Research Notes 2497*, 2009.

[4] E.-K. Puska and V. Suolanen. Safir 2010. the finnish research programme on nuclear power plant safety 2007-2010. *VTT Research Notes 2571*, 2011.

[5] S.V. Hoa. *Principles of the Manufactoring of Composite Materials*. DEStech Publications, Inc., 2009.

[6] E.S. Papazoglou. Chapter 4. flame retardants for plastics. In C.A. Harper, editor, *Handbook of Building Materials for Fire Protection*, pages 4.1–4.88. McGraw-Hill, New York, 2004.

[7] P. Hornsby. Chapter 7. fire retardant fillers. In C.A. Wilkie and A.B. Morgan, editors, *Fire Retardancy of Polymeric Materials, Second Edition*, page 163–185. CRC PressINC, 2009.

[8] Y. Zhang, Y.C. Wang, C.G. Bailey, and A.P. Taylor. Global modelling of fire protection performance of intumescent coating under different cone calorimeter heating conditions. *Fire Safety Journal*, 50(0):51–62, 2012.

[9] A. Paajanen, T. Korhonen, M. Sippola, S. Hostikka, M. Malendowski, and R. Gutkin. Fds2fem - a tool for coupling fire and structural analyses. *Proceedings of CMM-2013 - Computer Methods in Mechanics, Poznan, Poland*, 2013.

[10] J. Vaari, S. Hostikka, T. Sikanen, and A. Paajanen. Numerical simulations on the performance of waterbased fire suppression systems. *VTT TECHNOLOGY 54*, 2012.

[11] T. Korhonen, S. Hostikka, S. Heliövaara, and H. Ehtamo. Fds+evac: An agent based fire evacuation model. In W.W.F. Klingsch, C. Rogsch, A. Schadschneider, and M. Schreckenberg, editors, *Pedestrian and Evacuation Dynamics 2008*, pages 109–120. Springer Berlin Heidelberg, 2010.

[12] S. Hostikka, T. Kling, and A. Paajanen. Simulation of fire behaviour and human operations using a new stochastic operation time model. *PSAM-11 -ESREL 2012 Conference. 25-29 June. Helsinki*, 2012.

[13] K.D. Smith, M. Bruns, S.I. Stoliarov, M.R. Nyden, O.A. Ezekoye, and P.R. Westmoreland. Assessing the effect of molecular weight on the kinetics of backbone scission reactions in polyethylene using reactive molecular dynamics. *Polymer*, 52(14):3104–3111, 2011.

[14] D. Drysdale. *An Introduction to Fire Dynamics. 3rd edition.* John Wiley and Sons, Ltd, UK., 2011.

[15] C.L. Beyler and M.M. Hirschler. Section 1. chapter 7. thermal decomposition of polymers. In *The SFPE Handbook of Fire Protection Engineering, 2nd edition*, pages 1.99–1.119. National Fire Protection Association, USA, 1995.

[16] Reaction-to-fire tests - heat release, smoke production and mass loss rate. *ISO 5660-1*, 2002.

[17] C. Lautenberger, G. Rein, and C. Fernandez-Pello. The application of a genetic algorithm to estimate material properties for fire modeling from bench-scale fire test data. *Fire Safety Journal*, 41(3):204–214, 2006.

[18] K. McGrattan, S. Hostikka, J. Floyd, H. Baum, R. Rehm, W. Mell, and R. McDermott. *Fire Dynamics Simulator (Version 5) Technical Reference Guide. Volume 1: Mathematical Model*. NIST Special Publication 1018-5.

[19] C. Lautenberger. *A Generalized Pyrolysis Model for Combustible Solids*. PhD thesis, University of California, Berkeley, 2007.

[20] S.I. Stoliarov, S. Crowley, R.E. Lyon, and G.T. Linteris. Prediction of the burning rates of non-charring polymers. *Combustion and Flame*, 156(5):1068–1083, 2009.

[21] L.J. Rodriguez-Aragón and J. López-Fidalgo. Optimal designs for the arrhenius equation. *Chemometrics and Intelligent Laboratory Systems*, 77(1-2):131–138, 2005.

[22] F. Jensen. Activation energies and the arrhenius equation. *Quality and Reliability Engineering International*, 1(1):13–17, 1985.

[23] R.R. Keuleers, J.F. Janssens, and H.O. Desseyn. Comparison of some methods for activation energy determination of thermal decomposition reactions by thermogravimetry. *Thermochimica Acta*, 385(1-2):127–142, 2002.

[24] S. Li and P. Järvelä. Application of a model-free isoconversional method to the cure of phenolic systems. *Journal of Polymer Science Part B: Polymer Physics*, 39(13):1525–1528, 2001.

[25] Z. Liu, Q. Wang, Z. Zou, and G. Tan. Arrhenius parameters determination in non-isothermal conditions for the uncatalyzed gasification of carbon by carbon dioxide. *Thermochimica Acta*, 512(1-2):1–4, 2011.

[26] C. Sierra. Temperature sensitivity of organic matter decomposition in the arrhenius equation: some theoretical considerations. *Biogeochemistry*, 108:1–15, 2012. 10.1007/s10533-011-9596-9.

[27] R. Skomski, R.D. Kirby, and D.J. Sellmyer. Activation entropy, activation energy, and magnetic viscosity. *Journal of Applied Physics*, 85(8):5069–5071, 1999.

[28] D. Stawski and R. Jantas. Potato starch thermooxidation: Selection of the optimal calculation method for activation energy determination. *Potato Research*, 52:355–365, 2009. 10.1007/s11540-009-9139-0.

[29] K.B. McGrattan, T. Kashiwagi, H.R. Baum, and S.L. Olson. Effects of ignition and wind on the transition to flame spread in a microgravity environment. *Combustion and Flame*, 106(4):377–391, 1996.

[30] G. Rein, A. Bar-Ilan, C. Fernandez-Pello, J.L. Ellzey, J.L. Torero, and D.L. Urban. Modeling of one-dimensional smoldering of polyurethane in microgravity conditions. *Proceedings of the Combustion Institute*, 30((2)):2327–2334, 2005. 30th International Symposium of Combustion Institute 2005.

[31] G. Rein, C. Lautenberger, A.C. Fernandez-Pello, J.L. Torero, and D.L. Urban. Application of genetic algorithms and thermogravimetry to determine the kinetics of polyurethane foam in smoldering combustion. *Combustion and Flame*, 146(1-2):95–108, 2006.

[32] S.I. Stoliarov and R.E. Lyon. Thermo-kinetic model of burning. Technical Report DOT/FAA/AR-TN08/17, Federal Aviation Administration, 2008.

[33] R.E. Lyon and R.N. Walters. Pyrolysis combustion flow calorimetry. *Journal of Analytical and Applied Pyrolysis*, 71(1):27–46, 2004.

[34] R.E. Lyon, N.R. Walters, S.I. Stoliarov, and N. Safronava. Principles and practise of microscale combustion calorimetry. Technical Report DOT/FAA/TC-12/53, Federal Aviation Administration, 2013.

[35] S.I. Stoliarov, S. Crowley, R.N. Walters, and R.E. Lyon. Prediction of the burning rates of charring polymers. *Combustion and Flame*, 157(11):2024–2034, 2010.

[36] M. Janssens. Section 3. chapter 2. calorimetry. In *The SFPE Handbook of Fire Protection Engineering, 2nd edition*, pages 3.16–3.36. National Fire Protection Association, USA, 1995.

[37] E. Mikkola. Effects of oxygen concentration on cone calorimeter results. *Proceedings of the Sixth International Interflam Conference*, pages 49–56, 1003.

[38] F. Bell and R. Sizmann. Determination of activation energy from step annealing. *Physica status solidi (b)*, 15(1):369–376, 1966.

[39] J.H. Flynn and L.A. Wall. A quick, direct method for the determination of activation energy from thermogravimetric data. *Journal of Polymer Science Part B: Polymer Letters*, 4(5):323–328, 1966.

[40] H.L. Friedman. New methods for evaluating kinetic parameters from thermal analysis data. *Journal of Polymer Science Part B: Polymer Letters*, 7(1):41–46, 1969.

[41] R.E. Lyon. Heat release kinetics. *Fire and Materials*, 24(4):179–186, 2000.

[42] R.E. Lyon, N. Safronava, and E. Oztekin. A simple method for determining kinetic parameters for materials in fire models. *Fire Safety Science*, 10:765–777, 2011.

[43] K. McGrattan, R. McDermott, W. Mell, G. Forney, J. Floyd, S. Hostikka, and A. Matala. *Proceedings of the 12^{th} International Interflam Conference*.

[44] R. Sundberg. Statistical aspects on fitting the arrhenius equation. *Chemometrics and Intelligent Laboratory Systems*, 41(2):249–252, 1998.

[45] J.V. Li, S.W. Johnston, Y. Yan, and D.H. Levi. Measuring temperature-dependent activation energy in thermally activated processes: A 2d arrhenius plot method. *Review of Scientific Instruments*, 81(3):033910, 2010.

[46] O. E. Rodionova and A. L. Pomerantsev. Estimating the parameters of the arrhenius equation. *Kinetics and Catalysis*, 46:305–308, 2005. 10.1007/s10975-005-0077-9.

[47] M. Starink. Activation energy determination for linear heating experiments: deviations due to neglecting the low temperature end of the temperature integral. *Journal of Materials Science*, 42:483–489, 2007. 10.1007/s10853-006-1067-7.

[48] Z. Gao, T. Kaneko, D. Hou, and M. Nakada. Kinetics of thermal degradation of poly(methyl methacrylate) studied with the assistance of the fractional conversion at the maximum reaction rate. *Polymer Degradation and Stability*, 84(3):399–403, 2004.

[49] M. Chaos, M.M. Khan, N. Krishnamoorthy, J.L. de Ris, and S.B. Dorofeev. Evaluation of optimization schemes and determination of solid fuel properties for cfd fire models using bench-scale pyrolysis tests. *Proceedings of the Combustion Institute*, 33:2599–2606, 2011.

[50] C. Lautenberger and C. Fernandez-Pello. Optimization Algorithms for Material Pyrolysis Property Estimation. *Fire Safety Science*, 10:751–764, 2011.

[51] T. Mani, P. Murugan, and N. Mahinpey. Determination of distributed activation energy model kinetic parameters using simulated annealing optimization method for nonisothermal pyrolysis of lignin. *Industrial and Engineering Chemistry Research*, 48(3):1464–1467, 2009.

[52] B. Saha, P.K. Reddy, and A.K. Ghoshal. Hybrid genetic algorithm to find the best model and the globally optimized overall kinetics parameters for thermal decomposition of plastics. *Chemical Engineering Journal*, 138(1–3):20–29, 2008.

[53] R.D. Webster. Pyrolysis model parameter optimization using a customized stochastic hill-climber algorithm and bench scale fire test data. Master's thesis, Graduate school of the University of Maryland, Collegepark, 2009.

[54] Q.Y. Duan, V.K. Gupta, and S. Sorooshian. Shuffled complex evolution approach for effective and efficient global minimization. *Journal of Optimization Theory and Applications*, 76:501–521, 1993.

[55] T.A. El-Mihoub, A.A. Hopgood, L. Nolle, and A. Battersby. Hybrid genetic algorithms: A review. *Engineering Letters*, 13(2):124–137, 2006.

[56] C.-H. Wang and J.-Z. Lu. A hybrid genetic algorithm that optimizes capacitated vehicle routing problems. *Expert Systems with Applications*, 36(2, Part 2):2921–2936, 2009.

[57] G. Whittaker, R. Confesor Jr., S.M. Griffith, R. Färe, S. Grosskopf, J.J. Steiner, G.W. Mueller-Warrant, and G.M. Banowetz. A hybrid genetic algorithm for multiobjective problems with activity analysis-based local search. *European Journal of Operational Research*, 193(1):195–203, 2009.

[58] F. Jin, S. Song, and C. Wu. A simulated annealing algorithm for single machine scheduling problems with family setups. *Computers and Operations Research*, 36(7):2133–2138, 2009.

[59] R. Tavakkoli-Moghaddam, A.R. Rahimi-Vahed, A. Ghodratnama, and A. Siadat. A simulated annealing method for solving a new mathematical model of a multi-criteria cell formation problem with capital constraints. *Advances in Engineering Software*, 40(4):268–273, 2009.

[60] A.V. Nikolaev, V.A. Logvinekol, and V.M. Gorbatchevl. Special features of the compensation effect in non-isothermal kinetics of solid-phase reactions. *Journal of Thermal Analysis and Calorimetry*, 6(4):473–477, 1974.

[61] A.K. Galwey and M.E. Brown. Arrhenius parameters and compensation behaviour in solid-state decompositions. *Thermochimica Acta*, 300(1-2):107–115, 1997.

[62] R.E. Lyon and N. Safronava. A comparison of direct methods to determine n-th order kinetic parameters of solid thermal decomposition for use in fire models. *Journal of Thermal Analysis and Calorimetry*, 114(1):213–227, 2013.

[63] J.R. Opfermann, E. Kaisersberger, and H.J. Flammersheim. Model-free analysis of thermoanalytical data-advantages and limitations. *Thermochimica Acta*, 391(1–2):119 – 127, 2002.

[64] D.P. Landau and K. Binder. *A Guide To Monte Carlo Simulations In Statistical Physics*. Cambridge University Press, 2000.

[65] N. Metropolis and S. Ulam. *Journal of the American Statistical Association*. Number vol. 44. American Statistical Association, 1949.

[66] M.D. McKay, R.J. Beckman, and W.J. Conover. A comparison of three methods for selecting values of input variables in the analysis of output from a computer code. *Technometrics*, 1979.

[67] M. Stein. Large sample properties of simulations using latin hypercube sampling. *Technometrics*, 29(2):143–151, 1987.

[68] S. Hostikka and O. Keski-Rahkonen. Probabilistic simulation of fire scenarios. *Nuclear Engineering and Design*, 224(3):301–311, 2003.

[69] S. Hostikka, T. Korhonen, and O. Keski-Rahkonen. Two-model monte carlo simulation of fire scenarios. *Fire Safety Science*, 8:1241–1252, 2005.

[70] R.E. Lyon. Chapter 3. plastics and rubber. In C.A. Harper, editor, *Handbook of Building Materials for Fire Protection*, pages 3.1–3.51. McGraw-Hill, New York, 2004.

[71] K. McGrattan et al. *Fire Dynamics Simulator User's Guide.* NIST Special Publication 1019.

[72] D. Price, G. Anthony, and P. Carty. Chapter 1. introduction: polymer combustion, condensed phase pyrolysis and smoke formation. In A.R. Horrocs and D. Price, editors, *Fire retardant materials*, pages 10–30. Woodhead Publishing Limited, England, 2001.

[73] M. Lewin and E.D. Weil. Chapter 2. mechanism and models of action in flame retardancy of polymers. In A.R. Horrocs and D. Price, editors, *Fire retardant materials*, pages 31–68. Woodhead Publishing Limited, England, 2001.

[74] S.V. Levchik. Chapter 1. introduction to flame retardancy and polymer flammability. In A.B. Morgan and C.A. Wilkie, editors, *Flame Retardant Polymer Nanocomposites*, pages 1–30. Wiley, 2007.

[75] P. Georlette. Chapter 8. applications of halogen flame retardants. In A.R. Horrocs and D. Price, editors, *Fire retardant materials*, pages 264–292. Woodhead Publishing Limited, England, 2001.

[76] R.P. Lattimer and W.J. Kroenke. The formation of volatile pyrolyzates form poly(vinyl chloride). *Journal of Applied Polymer Science*, 25(1):101–110, 1980.

[77] G. Montaudo and C. Puglisi. Evolution of aromatics in the thermal degradation of poly(vinyl chloride): A mechanistic study. *Polymer Degradation and Stability*, 33(2):229–262, 1991.

[78] A. Marcilla and M. Beltran. Pvc-plasticizer interactions during the thermal decomposition of pvc plastisols. influence of the type of plastizicer and resin. *Polymer Degradation and Stability*, 53(2):261–268, 1996.

[79] A. Jimenez, J. Lopez, J. Vilaplana, and H.-J. Dussel. Thermal degradation of plastisols. effect of some additives on the evolution of gaseous products. *Journal of Analytical and Applied Pyrolysis*, 40–41(0):201–215, 1997.

[80] E.O. Elakesh, T.R. Hull, D. Price, G.J. Milnes, and P. Carty. Effect of plasticizers on the thermal decomposition of chlorinated polyvinylchloride. *Journal of Vinyl and Additive Technology*, 11(1):21–27, 2005.

[81] A. Marcilla and M. Beltran. Effect of the plasticizer concentration and heating rate on the thermal decomposition behaviour of pvc plastisols. kinetic analysis. *Polymer Degradation and Stability*, 60(1):1–10, 1998.

[82] R. Miranda, J. Yang, C. Roy, and C. Vasile. Vacuum pyrolysis of pvc i. kinetic study. *Polymer Degradation and Stability*, 64(1):127–144, 1999.

[83] M. Benes, V. Plaek, G. Matuschek, A. A. Kettrup, K. Gyoryova, W. D. Emmerich, and V. Balek. Lifetime simulation and thermal characterization of pvc cable insulation materials. *Journal of Thermal Analysis and Calorimetry*, 82(3):761–768, 2005.

[84] A. Marcilla and M. Beltran. Thermogravimetric kinetic study of poly-(vinyl chloride) pyrolysis. *Polymer Degradation and Stability*, 48(2):219–229, 1995.

[85] A. Marcilla and M. Beltran. Kinetic models for the thermal decomposition of commercial pvc resins and plasticizers studied by thermogravimetric analysis. *Polymer Degradation and Stability*, 53(2):251–260, 1996.

[86] M. Beltran and A. Marcilla. Kinetic models for the thermal decomposition of pvc plastisols. *Polymer Degradation and Stability*, 55(1):73 – 87, 1997.

[87] S. Kim. Pyrolysis kinetics of waste pvc pipe. *Waste Management*, 21(7):609–616, 2001.

[88] G. Wypych. *PVC Formulary*. ChemTec Publishing, 2009.

[89] N.N. Greenwood and A. Earnshaw. *Chemistry of the Elements*. Pergamon Press Ltd, 1984.

[90] M. Pansu and J. Gautheyrou. Chapter 17. carbonates. In *Handbook of Soil Analysis*, pages 593–604. Springer Berlin Heidelberg, 2006.

[91] K. McGrattan, A. Lock, N. Marsh, M. Nyden, Bareham S., M. Price, A.B. Morgan, M. Galaska, K. Schenck, and D. Stroup. Cable heat release, ignition, and spread in tray installations during fire (christifire), phase 1: Horizontal trays. *NUREG/CR-7010*, 1, 2012.

[92] N. Alvares and C. Fernandez-Pello. Fire initiation and spread in overloaded communication system cable trays. *Experimental Thermal and Fluid Science*, 21(1-3):51–57, 2000.

[93] P. Van Hees, J. Axelsson, A. M. Green, and S. J. Grayson. Mathematical modelling of fire development in cable installations. *Fire and Materials*, 25(4):169–178, 2001.

[94] P. Andersson and P. Van Hees. Performance of cables subjected to elevated temperatures. *Fire Safety Science*, 8:1121–1132, 2005.

[95] K. McGrattan and J. Dreisbach. Cable response to live fire (carolfire) volume 3: Thermally-induced electrical failure (thief) model. *NUREG/CR-6931*, 3, 2008.

[96] S.P. Nowlen. The impact of thermal aging on the flammability of electric cables. *NUREG/CR-5629, SAND90-2121*, 1991.

[97] J. Mangs and A. Matala. Ageing effects on flame spread and pyrolysis of pvc cables. *VTT Research Reports VTT-T-07229-10*, 2010.

[98] V. Placek and T. Kohout. Comparison of cable ageing. *Radiation Physics and Chemistry*, 79(3):371–374, 2010. IONIZING RADIATION AND POLYMERS Proceedings of the 8th International Symposium on Ionizing Radiation and Polymers Angra dos Reis, Rio de Janeiro, Brazil, 12-17 October 2008.

[99] D.D.L. Chung. *Composite Materials. Science and Applications. 2nd edition.* Springer, USA., 2010.

[100] A.P. Mouritz and A.G. Gibson. *Fire Properties of Polymer Composite Materials*. Springer, The Netherlands, 2006.

[101] Karbhari V.M. and Seible F. Fiber reinforced composites - advanced materials for the renewal of civil infrastructure. *Applied Composite Materials*, 7(2/3):95–124, 2000.

[102] K.G. Satyanarayana, G.G.C. Arizaga, and F. Wypych. Biodegradable composites based on lignocellulosic fibers—an overview. *Progress in Polymer Science*, 34(9):982–1021, 2009.

[103] T. Ford. Aerospace composites. *Aircraft Engineering and Aerospace Technology*, 69(4):334–342, 1997.

[104] G. Savage. Formula 1 composites engineering. *Engineering Failure Analysis*, 17(1):92–115, 2010.

[105] S. Bocchini and G. Camino. Chapter 4. halogen-containing flame retardants. In C.A. Wilkie and A.B. Morgan, editors, *Fire Retardancy of Polymeric Materials, Second Edition*, pages 75–105. CRC PressINC, 2009.

[106] P. Joseph and J.R. Ebdon. Chapter 5. phosphorus-based flame retardants. In C.A. Wilkie and A.B. Morgan, editors, *Fire Retardancy of Polymeric Materials, Second Edition*, pages 107–127. CRC PressINC, 2009.

[107] S. Bourbigot and S. Duquesne. Chapter 6. intumescence-based fire retardants. In C.A. Wilkie and A.B. Morgan, editors, *Fire Retardancy of Polymeric Materials, Second Edition*, pages 129–162. CRC PressINC, 2009.

[108] G.S. Springer. Model for predicting the mechanical properties of composites at elevated temperatures. *Journal of Reinforced Plastics and Composites*, 3(1):85–95, 1984.

[109] Y. Bai and T. Keller. Modeling of mechanical response of frp composites in fire. *Composites Part A: Applied Science and Manufacturing*, 40(6–7):731 – 738, 2009.

[110] N.A. Dembsey and D.J. Jacoby. Evaluation of common ignition models for use with marine cored composites. *Fire and Materials*, 24(2):91–100, 2000.

[111] B. Lattimer and T. Cambell. Chapter 4. fire modelling of composites. In Gibson A.G. Mouritz, A.P., editor, *Fire Properties of Polymer Composite Materials*, pages 103–132. Springer, The Netherlands, 2006.

[112] E. Kim, C. Lautenberger, and N. Dembsey. Property estimation for pyrolysis modeling applied to polyester frp composites with different glass contents. *Composites and Polycon 2009. American Composites Manufacturers Association*, 2009.

[113] C. Lautenberger, E. Kim, N. Dembsey, and C. Fernandez-Pello. The role of decomposition kinetics in pyrolysis modeling - application to a fire retardant polyester composite. *Fire Safety Science*, 9:1201–1212, 2009.

[114] J. Trelles and B.Y. Lattimer. Modelling thermal degradation of composite materials. *Fire and Materials*, 31(2):147–171, 2007.

[115] J. Opfermann. Kinetic analysis using multivariate non-linear regression. i. basic concepts. *Journal of Thermal Analysis and Calorimetry*, 60(2):641–658, 2000.

[116] S.I. Stoliarov, N. Safronava, and R.E. Lyon. The effect of variation in polymer properties on the rate of burning. *Fire and Materials*, 33(6):257–271, 2009.

[117] K. McGrattan et al. *Fire Dynamics Simulator Volume 2: Verification.* NIST Special Publication 1018.

[118] K. McGrattan et al. *Fire Dynamics Simulator Volume 3: Validation.* NIST Special Publication 1018.

[119] C. Di Blasi. Physico-chemical processes occurring inside a degrading two-dimensional anisotropic porous medium. *International Journal of Heat and Mass Transfer*, 41(24):4139–4150, 1998.

[120] L. Tunturivuori. Updating of the fire pra of the olkiluoto npp units 1 and 2. *PSAM-11 -ESREL 2012 Conference. 25-29 June. Helsinki*, 2012.

[121] D. Mohan, C.U. Pittman, and P.H. Steele. Pyrolysis of wood-biomass for bio-oil: A critical review. *Energy & Fuels*, 20(3):848–889, 2006.

[122] C. Di Blasi. Modeling chemical and physical processes of wood and biomass pyrolysis. *Progress in Energy and Combustion Science*, 34(1):47–90, 2008.

[123] C. Di Blasi. Combustion and gasification rates of lignocellulosic chars. *Progress in Energy and Combustion Science*, 35(2):121–140, 2009.

PUBLICATION I

Estimation of Pyrolysis Model Parameters for Solid Materials Using Thermogravimetric Data

In: Fire Safety Science – Proceedings of the
Ninth International Symposium,
pp. 1213–1224.

Estimation of Pyrolysis Model Parameters for Solid Materials Using Thermogravimetric Data

ANNA MATALA, SIMO HOSTIKKA and JOHAN MANGS
VTT
P.O.Box 1000
FI-02044 VTT, Finland

ABSTRACT

Determination of the material parameters is one of the key challenges of numerical fire simulation attempting to predict, rather than prescribe the heat release rate. In this work, we use common fire simulation software and genetic algorithms to estimate the kinetic reaction parameters for wood components, birch wood, PVC and black PMMA. Parameters are estimated by modelling thermogravimetric experiments and minimizing the error between the experimental and numerical results. The implementation and choice of the parameters for the genetic algorithm as well as the scheme to describe wood pyrolysis are discussed.

KEYWORDS: pyrolysis model, genetic algorithms, fire simulation, thermogravimetry

NOMENCLATURE

$A_{\alpha\beta}$	Frequency factor (s^{-1})	**Greek**	
A_p	Penalty of parameter A	ρ	Mass concentration or density (kg/m^3)
$E_{\alpha\beta}$	Activation energy (kJ/mol)	ω	Weight in fitness function
ΔH	Heat of reaction (kJ/kg)	**subscripts**	
M	Mass fraction (kg/kg)	α	Material index
$\overline{M}$	Average of mass fraction (kg/kg)	β	Reaction index
m	Sample mass (kg)	0	Initial value
N	Number of variables in a model.	i	Index over time series
$n_{\alpha\beta}$	Reaction order	*exp*	Experimental
R	Universal gas constant (8.31431 J/K.mol)	*max*	Upper bound
S_α	Mass production for material α	*min*	Lower bound
T	Temperature (K)	*mod*	Model
fV	Fitness value		

INTRODUCTION

The numerical simulation of fires is used extensively as a tool in performance based design of buildings and ships. Although such a design often relies on the use of prescribed design fires, there is an increasing need for a capability to predict the fire spread. There are several challenges associated with the fire spread simulations, including the difference in scales of close field heat transfer and the largest resolved scales of the geometry, physical and numerical modelling of the mass and heat transfer phenomena within the condensed phase and the definition of the necessary model parameters. During the recent update of the Fire Dynamics Simulator (FDS) to version 5 [1], the treatment of the condensed phase pyrolysis reactions was significantly changed, allowing the definition of a wide range of reactions of varying complexity. Increased complexity has an evident drawback of increased number of model parameters. Quite often, these parameters can not be found directly from literature because the parameters are not material constants by nature. Instead, they are always associated with a specific model of the material, and they should be determined using the exactly same or very similar model.

The reaction parameters for fire models are often estimated by varying the parameters until the model reproduces the measured behaviour in some laboratory experiment. Small scale experiments are typically preferred for the estimation while larger experiments serve as validation tests. It depends on the type of the test, whether it can yield estimates for the thermal parameters or kinetic reaction parameters or both.

FIRE SAFETY SCIENCE–PROCEEDINGS OF THE NINTH INTERNATIONAL SYMPOSIUM, pp. 1213-1224
 / DOI:10.3801/IAFSS.FSS.9-1213

Mathematically, the parameter estimation process can be presented as an optimization problem. In the recent papers of Lautenberger *et al.* [2] and Rein *et al.* [3], Genetic Algorithms (GA) were used for the optimization to estimate the thermal material properties from bench scale experiments [2] and kinetic parameters from thermogravimetric experiments [3]. In this work, we use the ideas of the above mentioned authors to determine the kinetic reaction parameters for the modelling of pyrolysis behaviour of selected solid materials, including wood and its components, polyvinylchloride (PVC) and polymethyl methacrylate (PMMA). The reactions are modelled using FDS and the practical aspects associated with the use of genetic algorithms are studied.

METHODS

Experiments

In this work, the kinetic parameters of selected solid materials were determined using Thermogravimetric Analysis (TGA) [4]. In addition, Differential Scanning Calorimetry (DSC) was used to determine the heat of reaction. In both experiments, just 10-50 mg of sample material is needed. A small furnace is heated at constant heating rate (heating rate typically 2-20 K/min) so that the temperature of the sample is in equilibrium with the environment all the time. The purge gas can be air or nitrogen (N_2). These thermoanalytical experiments were carried out at the Laboratory of Inorganic and Analytical Chemistry, Helsinki University of Technology, using Netzsch STA 449C equipment. The sample materials are listed in Table 1.

TGA measures the sample mass as a function of temperature. In this paper, the results are presented as a fraction of the current mass to the initial mass

$$M = \frac{m}{m_0} \tag{1}$$

The main difference between TGA experiments conducted in air and in N_2 is that in air, direct oxidation reactions may take place parallel or after the pyrolysis reaction. Oxidation decreases the mass of material, so the residual mass is usually smaller in air than in N_2. This is true for all the sample materials discussed in this work. In DSC, temperature of a sample is kept identical with reference sample and the energy needed for that is measured. In DSC data it is possible to see if the reaction is endothermic or exothermic. Sometimes it is even possible to measure the heat of reaction by integrating over the peak in the DSC curve. Nitrogen should be used as a purge gas if the heat of reaction is going to be measured. However, sometimes many parallel reactions take place simultaneously or the measurement is not accurate enough, and the DSC graph does not give the expected results.

Table 1. Sample properties. The moisture-% is wet based.

Material	Description	ρ (kg/m^3)	Moisture-%
Cellulose (Avicel® PH-101)	High purity cellulose powder.	360	4
Lignin (alkali)	Powder, 4 % sulphur, carbon typically 45 % - 65 %	494	8
Xylan from birch wood	Powder, xylose residues ≥90 %	312	7
Birch	-	550	3
PVC	Almost pure PVC pipe material.	1440	0
Black PMMA	ICI, Perspex	1180	0

Kinetic modelling of pyrolysis reactions

The condensed phase materials are modelled as mixtures of material components. In the modelling of condensed phase reactions, the rate of an individual condensed phase reaction β converting material α to something else is expressed as an Arrhenius equation

$$r_{\alpha\beta}(T) = A_{\alpha\beta}\left(\frac{\rho_\alpha}{\rho_{s0}}\right)^{n_{\alpha\beta}} e^{-\frac{E_{\alpha\beta}}{RT}} \quad (2)$$

where ρ_α is the mass concentration of component α and ρ_{s0} the original density of the material. The rate of change for the mass concentration of component α is

$$\frac{\partial}{\partial t}\left(\frac{\rho_\alpha}{\rho_{s0}}\right) = -\sum_\beta r_{\alpha\beta} + S_\alpha \quad (3)$$

where S_α is the production rate of material α. is In words, the mass is consumed by all the reactions converting material α to something else and created by the reactions converting something else to α. If none of the reactions leaves solid residue, the sample volume is reduced correspondingly, thus retaining constant density.

Kinetic parameters A, E and n depend both on the material and the assumed reaction scheme. They must be determined using some sort of experimental data. To estimate the kinetic parameters for Eq. (1), a numerical model of the TGA experiment was created using Fire Dynamic Simulator (FDS) version 5.0.2 [1]. The model is very simple, consisting of only few gas phase control volumes and a single surface element to describe the sample material. A thin layer of sample material is heated by radiation from the surroundings with linearly increased temperature. The layer is thin enough to remain in equilibrium with the surroundings with a tolerance of few Kelvins. Gas phase convection and reactions are neglected and the sample backing is adiabatic.

Correct interpretation of the model output is important when comparing the experimental results and model predictions. TGA results are presented as mass fractions M. The model, in turn, provides us with a sample density ρ which is sum of the individual mass concentrations. Direct comparison between M and ρ/ρ_0 is possible if the sample volume does not change. For non-charring materials, such as PMMA, the sample volume is reduced and the mass fractions leading to ρ/ρ_0 must be based on the initial sample volume.

Parameter estimation

The parameter estimation was performed by minimizing the error between a measured and simulated TGA result using Genetic Algorithm (GA) as a minimization technique. GA was chosen because it is effective for problems with several unknown variables, and can usually find a global minimum instead of converging to some local minimum. Recently, GA has been used for the parameter estimation of condensed phase reactions by Lautenberger *et al*. [2] and Rein *et al*. [3].

Genetic algorithms are based on the idea of evolution and the procedure and the terminology is adapted from references [2], [3] and [5]. The process is iterative, and each iteration round corresponds to one *generation*. The first generation is initialized by generating random numbers for candidate solutions (*individuals*). An individual is a vector with real numbers corresponding to the unknown variables of the model. The individuals of a generation form a *population*. Population can be divided from the beginning into smaller *subpopulations* to keep up the variety of candidate solutions. Each generation goes through several processes. First, the goodness of an individual is tested using a *fitness function* returning a *fitness value*. According the fitness value, the individuals are ranked, and the best of them are selected to produce *offspring*. The offspring are formed by *crossover*, where the chosen individuals are set to pairs and each pair are changing *alleles* (values of variables) according the conditions of crossover. After that occur *mutations*, stochastically according to a predetermined mutation rate. In mutation, one value in an individual is replaced by a new random number. Then fitness values are calculated for the offspring and the best parents and offspring are chosen to the next generation. If population is divided into isolated subpopulations, some individuals *migrate* then between subpopulations bringing new genes and so maintaining variety. After each generation, the best individual is plotted, which enables the user to observe the action of algorithm. The process is repeated until the maximum number of iterations is finished or the user is satisfied with the result and stops the algorithm from outside.

The fitness function compares experimental data to model and returns a metrics of how good is the fit. This is often made by using least mean squares. Based on the numerical experiments, another feature was added to the fitness function: The results of the parameter estimation process are not unambiguous and several well-fitting parameters can be found for the same material. On the other hand, high values of pre-exponential factors A were found to make the FDS simulations more prone for numerical fluctuations. An additional term was thus added to the fitness function to prefer the smaller values of A. The formula for the fitness value is

$$fV = \omega_1 \left(1 - \frac{\sum_i \left(M_{\mathrm{exp}} - \overline{M}_{\mathrm{exp}} \right)^2 - \sum_i \left(M_{\mathrm{exp}} - M_{\mathrm{mod}} \right)^2}{\sum_i \left(M_{\mathrm{exp}} - \overline{M}_{\mathrm{exp}} \right)^2} \right) + \omega_2 A_p \tag{4}$$

where M is mass fraction in TGA experiment and i goes over all the data. ω_1 and ω_2 are the weights of fitness function so that $\omega_1+\omega_2=1$. A_p is the penalty of high parameter A, and has a form

$$A_p = \frac{A - A_{\mathrm{min}}}{A_{\mathrm{max}}} \tag{5}$$

where A is the current value of the pre-exponential factor, A_{min} is its lower bound and A_{max} the upper bound. Weight ω_2 should be in same order of magnitude as the differences in the fitness values of the best solutions. In the tests, these differences were around 15/1000. Too high weight would lead to small pre-exponential factors giving inaccurate predictions.

The population size and the division of one big population into smaller subpopulations are important when fast convergence to a possible local minimum must be avoided. Inside one population, the solution converges quite fast towards the best candidate solution. If there are many independent populations, the probability that one of the solutions is near the global minimum, is much higher. In test simulations, division to subpopulations was found to be even more important than the population size. The populations without separation converged very fast, no matter how big the number of individuals was in the population. On the other hand, when there were at least four subpopulations, each of them could have as few as 20 individuals and the diversity was still maintained well enough. Mutation rate is used to control the maintenance of diversity. It expresses the probability of an individual to mutate during one generation. If the mutation rate is too low, the solution may converge to a local minimum, and if it is too high, good solutions may be lost. A good rule of thumb is to choose a mutation rate close to ratio $1/N$, where N is number of variables.

When TGA experiments are available at many different heating rates, the fitness value should be calculated considering all the rates, thus ensuring that the model is good in general, not only with one heating rate. To illustrate this, in Fig. 1 is shown a comparison of measured (solid lines) and simulated (dash lines) TGA results. The simulation used kinetic parameters that provided very good results at 2 K/min heating rate but poor predictions of the residue mass at others.

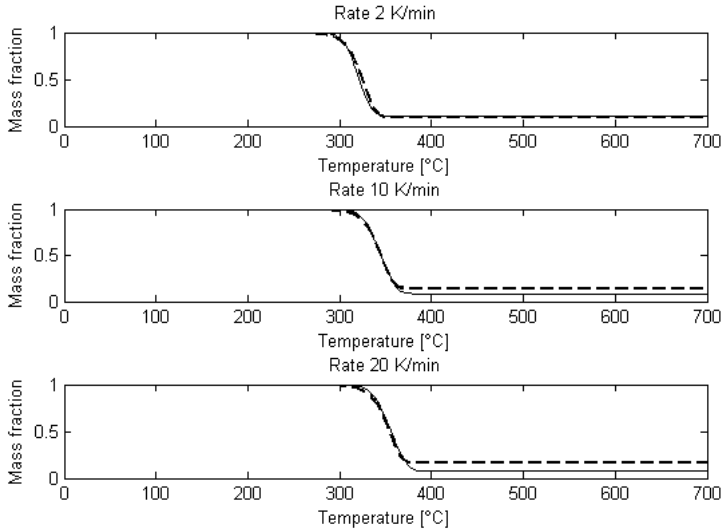

Fig. 1. TGA graphs of same kinetic parameters with different heating rates.

The Genetic Algorithm application was implemented using Genetic Algorithm Toolbox for Matlab, developed by the Department of Automatic Control and Systems Engineering of The University of Sheffield, UK [6]. The toolbox is available for free at http://www.shef.ac.uk/acse/research/ecrg/getgat.html. The parameters used in the estimation are listed in Table 2. Many different combinations were studied and the listed parameters were found to give the best results in estimation of kinetic parameters. The variable and function names are consistent with the Genetic Algorithm toolbox.

Despite the simplicity of the FDS model used for TGA simulation, the computational cost of the parameter estimation was quite high because the model had to be solved for every individual of every generation, and with each heating rate separately. Estimations for this work took from about 10 h to one day to run on a single CPU of a modern workstation.

Table 2. Parameters of Genetic Algorithm application.

Parameter	**Symbol in GA Toolbox**	**Value**
Number of individuals.	NIND	20
Generation gap: The fractional difference between the new and old population sizes.	GGAP	0.8
Crossover rate.	XOVR	0.7
Mutation rate.	MUTR	1/Number of variables
Maximum number of generations.	MAXGEN	1200
Insertion rate: Fraction of offspring reinserted into the population.	INSR	0.9
Number of subpopulations.	SUBPOP	4
Migration rate.	MIGR	0.2
Number of genes per migration.	MIGGEN	20

RESULTS

Heats of reaction were achieved by integrating the reaction peaks of DSC data in nitrogen. Heat of reaction ΔH is the integral divided by consumed mass. Consistent values of ΔH were obtained at all the heating rates only for cellulose and birch. The value for cellulose was -482 kJ/kg and for birch -230 kJ/kg. Negative sign here means endothermic reaction. For comparison, di Blasi [7] has used ΔH = -418 kJ/kg for lignocellulosic fuel, which is relatively close to the value obtained here. However, it is considerably different from our value for birch.

The kinetic parameters of several materials were estimated using genetic algorithm. TGA experiments were made in nitrogen (N_2) because the focus was on the modelling of the pyrolysis (degradation) reactions. For each of the kinetic parameters, a range of possible values was defined, as shown in Table 3. The ranges can be chosen according the literature values, if available, or initial estimates. In the tests, the ranges were set unnecessarily wide on purpose to be able to study the variety of solutions. Unfortunately, the choice of the range may affect the results, as was demonstrated by running two version of the black PMMA with different bounds for the reaction order *n*. Experimental results at four different heating rates (2, 5, 10 and 20 K/min) were used for the estimation. The iterations normally converged during the first 50 generations, but often the iteration process was continued at least up to 100, sometimes even 1000 generations. Most of the materials include some amount of moisture, and the evaporation of water was modelled as a one step reaction with own kinetic parameters. The numerical results are presented in Table 5 and as model behaviour in figures below.

Table 3. Estimation ranges for sample materials.

Material	A (s^{-1})	E (kJ/mol)	n	residue
Cellulose	$[10^{10},10^{20}]$	[100,300]	[0,7]	[0,1]
Lignin (alkali)	$[10^{10},10^{20}]$	[100,300]	[0,7]	[0,1]
Xylan from birch wood	$[10^{10},10^{20}]$	[100,300]	[0,7]	[0,1]
Birch (all reactions)	$[10^{10},10^{20}]$	[100,300]	[0,5]	[0,1]
PVC (all reactions)	$[10^{8},10^{20}]$	[100,300]	[0,4]	[0,1]
Black PMMA –estimation 1	$[10^{2},10^{10}]$	[100,300]	[0,2]	-
Black PMMA –estimation 2	$[10^{2},10^{10}]$	[100,300]	[0,7]	-

Components of wood

The three main components of wood are cellulose, hemicellulose and lignin. Roughly 40-44 % of hardwood is cellulose, 23-40 % hemicellulose and 18-25 % lignin [8]. All the components of wood produce char in combustion but lignin yields most of the char. The sample of hemicellulose was xylan, which is dominant hemicellulose specie in birch wood. The samples of components were in powder form, so the densities and thermal characteristics may differ from real. However, the kinetics' were assumed to be the same. Cellulose was modelled using di Blasi's model [7] and simple one-step model. The di Blasi model was slightly more accurate, but did not differ from the one-step model significantly. For other components, simple one-step reactions were assumed. With lignin and xylan, the experimental TGA data is not the best possible: Unexpected mass losses in the ends of the graphs are seen, which makes it more difficult to decide the residual mass. The results at 2 K/min heating rate are shown in Fig. 2. All the models succeed to predict the total mass loss quite well and the reactions take place in correct temperature range. The dominant shapes of graphs are correct but small errors can be found close to the end of the pyrolysis period. The numeric values of the kinetic parameters are given in Table 5.

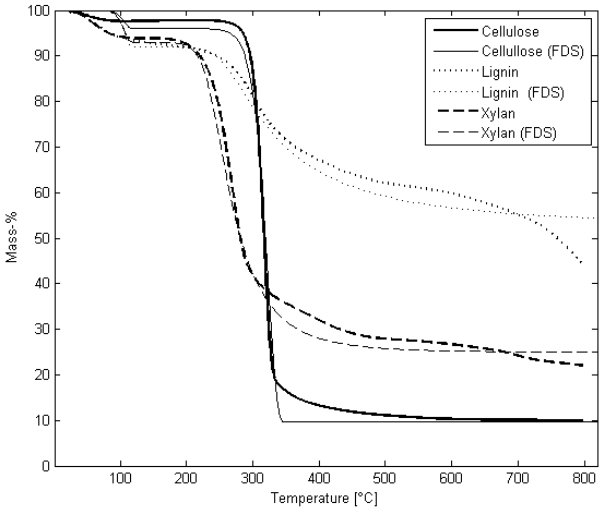

Fig. 2. TGA models of components of wood in N_2. Heating rate is 2 K/min.

Birch

Birch is typical Finnish hardwood specie. When the temperature rises, the moisture of wood evaporates [8]. After this, the fibres start to degrade. The volatiles are now generated, and they consist of a combustible mixture of gases, vapours and tars. A solid carbon char matrix remains, and its volume is smaller than original volume of wood. The sample density was 550 kg/m^3, which is higher than any of the component densities studied above. That is because the powders form of component samples.

For modelling the pyrolysis of birch four different schemes were used: Scheme 1 was a sum of the one-step reactions of components (cellulose, hemicellulose and lignin) yielding independently certain amount of char. Besides of char, fuel gases are released. In this scheme, the mass fractions of the component variables were also estimated using GA, in order to achieve the total density of birch. Scheme 2 was a one-step reaction converting virgin solid to char. Schemes 3 and 4 were presented by Liu *et al*. in Ref. [9]. In Scheme 3, there are two separate pseudo-components, which both produce char and fuel gases in parallel. In Scheme 4, there is only one material that has two consecutive reactions. The reaction formulas are summarized in Fig. 3.

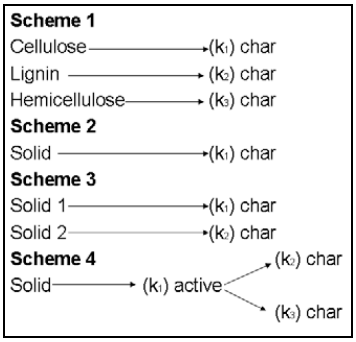

Fig. 3. Reaction schemes for birch.

A comparison of the measured and predicted TGA curves at 2 K/min heating rate is shown in Fig. 4, and the fitness values corresponding to the last iteration are listed in Table 4. In scheme 1, the best model had the composition 44 % cellulose, 18 % lignin and 38 % xylan. Other parameters are listed in Table 5. According to a visual comparison and the fitness values, Scheme 2 gives the best prediction of the TGA curve, which suggests that the components in wood are behaving like a homogenous solid material rather than a mixture of three. Scheme 1 gave the worst results of all the studied schemes, and its fitness value was more than 10 times the fitness value of Scheme 2.

Table 4. Fitness values of TGA results of birch schemes.

Scheme	1	2	3	4
Fitness value	0.0691	0.0069	0.0119	0.0123

PVC

The sample was almost pure polyvinyl chloride (PVC) pipe material. PVC undergoes two reactions: Release of hydrochloric acid between 200 and 300°C and the pyrolysis reaction of the remaining solid at about 400°C. The pyrolysis products are HCl, benzene and toluene [8]. Reactions were modelled by two pseudo-components, of which the first does not yield any tar and the second does.

The mass fraction of volatiles was assumed to be 0.54 (taken directly from the graphs). A comparison of the measured and predicted TGA curves at the end of the parameter estimation is shown in Fig. 5. The solid lines denote the experimental data and the dash lines the model. Good predictions of the PVC pyrolysis are achieved at all heating rates. The numeric values of the kinetic parameters are given in Table 5.

Black PMMA

PMMA (Polymethyl methacrylate) is a non-charring thermoplastic that melts and then burns. The pyrolysis product is 100 % monomer [8] with no significant residue yield. Different from charring materials where the density decreases, in PMMA model the sample thickness decreases instead. This may cause problems when modelling TGA test where the sample is very thin from the beginning. As a result, care must be taken to define a sufficiently high sampling frequency for the numerical results.

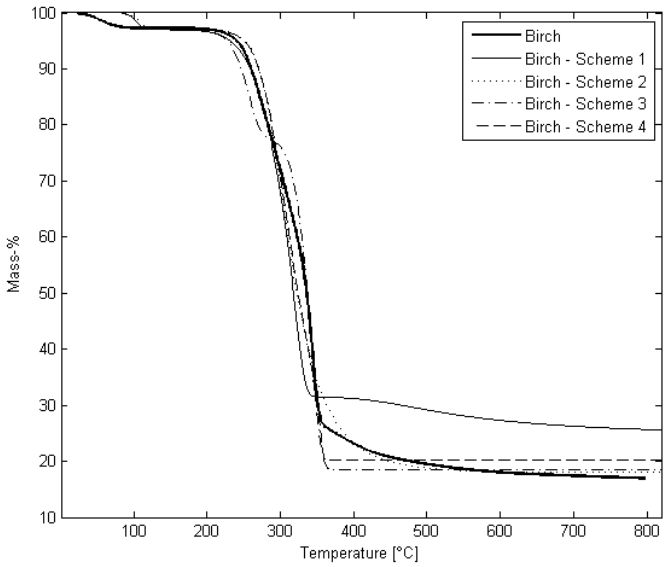

Fig. 4. TGA models of birch in N_2. Heating rate is 2 K/min.

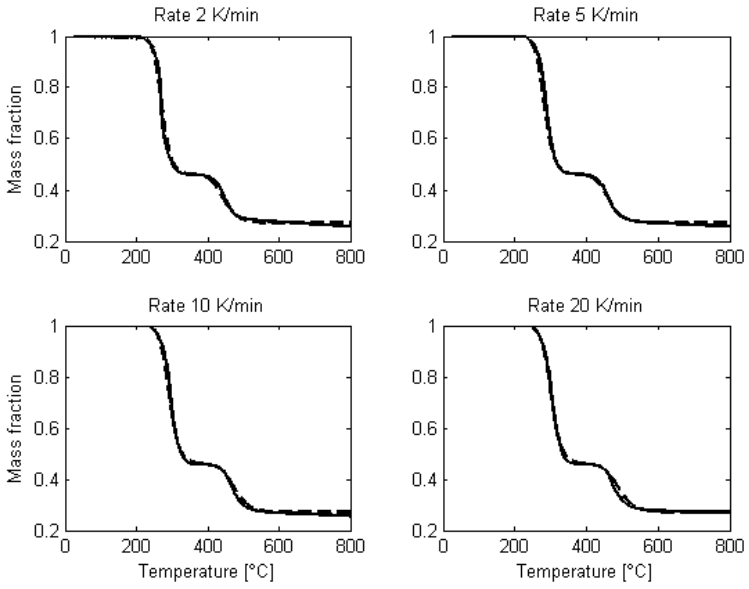

Fig. 5. TGA model of PVC in N_2.

The estimation was made twice using different range for the reaction order parameter *n*. In the first run, the range was [0, 2] and in the second, it was [0, 7]. The result of estimation run 1 is shown in Fig. 6. Again, the solid line denotes the experimental data and the dash line the model. An accurate prediction of the mass loss is achieved at heating rates 5 and 10 K/min, and reasonably well at heating rates 2 and 20 K/min. The results of the estimation run 2 look very much the same and the model is considered as accurate as in estimation run 1. That suggests that the parameter sets can be chosen among various alternatives and the genetic algorithm can find solutions from desired range. The numeric values of the kinetic parameters are given in Table 5.

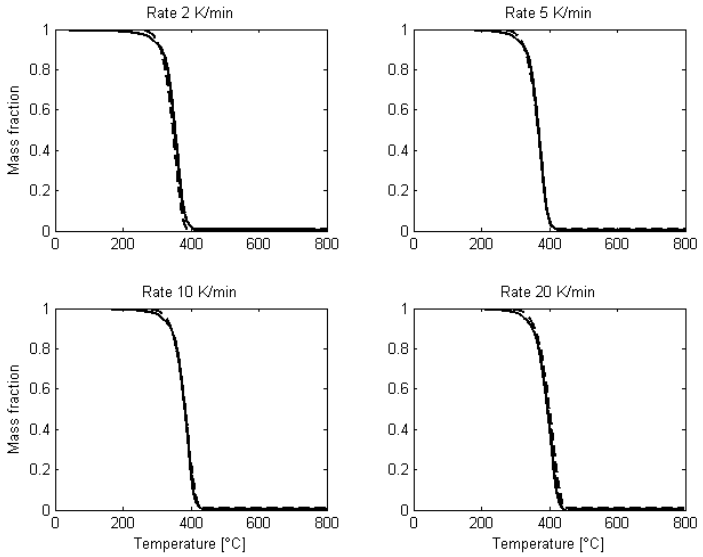

Fig. 6. TGA of black PMMA in N_2.

CONCLUSIONS

Kinetic pyrolysis model parameters were estimated for six different solid materials using FDS fire model and genetic algorithm for the estimation. The estimation parameters, such as variable bounds and time step size, were carefully chosen to minimize the effect of the estimation procedure. The results were promising and indicated that the thermogravimetric experiments and genetic algorithm can successfully be used for the parameter estimation in fire engineering. As the material models were created using the actual fire simulation tool, the results can be directly used in applications. The estimation process is computationally expensive, taking several hours to a day on a single computer, but needs to be performed only once for each material. Validation of the current parameters and estimation of the lacking ones is still needed to build a full parameter set for fire spread computation.

Different reaction schemes were considered for the hardwood charring process. Best results were obtained using a simple one-step reaction for the pyrolysis. From the engineering viewpoint this is a very good result because the model simplicity means smaller number of unknown parameters to estimate and computational savings. Some of the resulting parameter values were quite different from those previously presented in literature. This demonstrates that the kinetic parameters are model dependent and should not be considered as fundamental material properties. The parameters should therefore be used only in models with similar structure. In addition, the estimation results are not unambiguous and there may be many suitable sets of parameters that predict the mass loss accurately.

Table 5. Kinetic parameters of materials, estimated using genetic algorithm.

Material	A (s^{-1})	E (kJ/mol)	n	residue
Moisture	$1 \cdot 10^{20}$	162	1	0
Cellulose	$2.68 \cdot 10^{14}$	195	0.85	0.1
Lignin	$2.18 \cdot 10^{10}$	138	7	0.567
Xylan	$5.78 \cdot 10^{13}$	164	4.166	0.268
Birch – scheme 2	$7.51 \cdot 10^{11}$	161	3.12	0.172
Birch – scheme 3 – k_1	$8.64 \cdot 10^{16}$	230	1	0.19
Birch – scheme 3 – k_2	$1.3 \cdot 10^{12}$	150	1	0.19
Birch – scheme 4 – k_1	$9.26 \cdot 10^{18}$	142	1	1
Birch – scheme 4 – k_2	$3.91 \cdot 10^{10}$	148	1	0.268
Birch – scheme 4 – k_3	$1.05 \cdot 10^{14}$	210	1	0
PVC (chlorides) k_1	$6.12 \cdot 10^{16}$	198	2.18	0
PVC (solid) k_2	$3.63 \cdot 10^{13}$	219	2.08	0.589
Black PMMA – estimation 1	$2.43 \cdot 10^{9}$	146	1.758	0
Black PMMA – estimation 2	$1.35 \cdot 10^{9}$	143	4.01	0

ACKNOWLEDGMENT

We thank Dr. Tuula Leskelä of Helsinki University of Technology (TKK), for performing the thermoanalytical experiments. This work was funded by the State Nuclear Waste Management Fund (VYR).

REFERENCES

[1] McGrattan, K., Hostikka, S., Floyd, J., Baum, H. and Rehm, R. Fire Dynamics Simulator (Version 5) Technical Reference Guide. National Instititute of Standards and Technology, MD. USA. NIST Special Publication 1018-5. 86 p. (Draft: August 26, 2007).

[2] Lautenberger, C., Rein, G., Fernandez-Pello, C., (2006). The application of a genetic algorithm to estimate material properties for fire modeling from bench-scale fire test data. Fire Safety Journal 41: 204-214. doi:10.1016/j.firesaf.2005.12.004

[3] Rein, G., Lautenberger, C., Fernandez-Pello, C., Torero, J., Urban, D., (2006). Application of genetic algorithms and thermogravimetry to determine the kinetics of polyurethane foam in smoldering combustion. Combustion and Flame 146: 95-108. doi:10.1016/j.combustflame.2006.04.013

[4] Kellner, R., Mermet J.-M., Otto, M., Valcárcel, M., Widmer, H. M., Analytical Chemistry: A Modern Approach to Analytical Science, Second edition. Wiley-VCH Verlag GmbH & Co. KGaA, Weinheim, 2004.

[5] Reeves, Colin R., Rowe, Jonathan E., Genetic algorithms - principles and perspective. Kluwer Academic Publishers. Kluwer Academic Publishers, 2002.

[6] Chipperfield, A., Fleming, P., Pohlheim, H., Fonseca, C. Genetic Algorithm Toolbox for Use with Matlab. Version 1.2. User's Guide. Department of Automatic Control and Systems Engineering, University of Sheffield.

[7] Di Blasi, C., (1998) Physico-chemical processes occurring inside a degrading two-dimensional anisotropic porous medium. International Journal of Heat and Mass Transfer 41: 4139-4150. doi:10.1016/S0017-9310(98)00142-2

[8] Harper, C. (ed.) Handbook of building materials for fire protection. McGraw-Hill Handbooks. The McGraw-Hill Companies Inc., 2004.

[9] Liu, N., Chen, H., 2007. Two-step kinetic models for thermal decomposition of forest combustibles: Three kinetic schemes. 7th Asia-Oceania Symposium on Fire Science and Technology, Hong Kong.

PUBLICATION II

Generalized direct method for pyrolysis kinetic parameter estimation and comparison to existing methods

In: Journal of Fire Sciences, Vol. 30, No. 4,
pp. 339–356.

JOURNAL OF FIRE SCIENCES

Article

Journal of Fire Sciences
30(4) 339–356

DOI: 10.1177/0734904112439840
jfs.sagepub.com
SAGE

Generalized direct method for pyrolysis kinetic parameter estimation and comparison to existing methods

Anna Matala[1], Chris Lautenberger[2] and Simo Hostikka[1]

Date received: 04 November 2011; accepted: 01 February 2012

Abstract

Solid-phase pyrolysis is often modelled using the Arrhenius degradation equation with three unknown parameters: reaction order, activation energy and pre-exponential factor. Since the parameters are model dependent and not directly measurable, several estimation methods have been developed over the years for extracting them from the experimental small-scale data. Lately, the most commonly used methods have been based on optimization and curve fitting. These methods are very efficient for complex problems with multiple reactions but may require significant computational time. Direct (analytic) methods are simpler and faster but often have more restrictions and limited accuracy. This article presents a new, generalized direct method and its performance evaluated along with other commonly used estimation methods. The real usability of the methods is tested also in the presence of small noise.

Keywords

Pyrolysis, modelling, parameter estimation

Introduction

Solid-phase pyrolysis is often modelled using the Arrhenius reaction rate equation with three unknown, model-specific parameters. These parameters are called *kinetic parameters* as they define the reaction kinetics. Direct measurement of these parameters using any common experimental apparatus is not possible. Knowing the reaction chemistry helps to define the reaction path but for an engineering solution, this may be far too complicated and

[1]VTT Technical Research Centre of Finland, FI-02044 VTT, Finland
[2]Reax Engineering Inc., Berkeley, CA, USA

Corresponding author:
Anna Matala, VTT Technical Research Centre of Finland, PO Box 1000, Espoo, FI-02044 VTT, Finland.
Email: anna.matala@vtt.fi

ambitious. In real pyrolysis, several reactions occur simultaneously and may overlap in time and temperature. From the fire modeller's point of view, it is not necessary or even worthwhile to describe all those reactions but rather approximate the process using as few and as simple reactions as possible. It is a well-known fact that the model parameters are able to compensate the other shortcomings and simplifications in the model.[1,2] As the kinetic parameters are associated with a specific reaction scheme having no fundamental physical significance, their values can indeed be chosen freely in order to get the best possible description of reality using the model in hand.

For obtaining the kinetic parameters, one needs to extract them from small-scale experimental data. The most commonly used small-scale experiment is non-isothermal *thermogravimetric analysis* (TGA), which measures the loss of a very small (few milligrams) sample during constant rate heating. There are basically two approaches to property estimation: curve fitting (mainly evolutionary algorithms)[3–8] and analytical methods.[8–11] Both have their advantages: curve fitting has very few limitations related to the reaction path or estimated parameters and can operate very effectively for complicated, overlapping reactions and noisy data. Their shortcoming is that they often require significant computational time for the iteration process to converge and some specific software for performing the estimation. It may also be discomforting that – due the compensation effect and other factors – several equally fitting solutions may be found (meaning the solution is not unique). Furthermore, the process is stochastic, which means that the results and the estimation routine cannot be repeated with exactly same results. Analytical methods, on the other hand, use *reference points* (such as the peak reaction rate) in experimental data to define kinetic parameters. They do operate well for simple, non-noisy and non-overlapping data and give unique solutions without requiring lengthy iterations. They also require just a pencil and paper for obtaining the solutions, so they are fast and efficient solution for an engineer. However, they are often limited to some specific reaction path and well-separated reactions. Noise in the data can lead to difficulties.

In this work, a generalized direct (analytical) method (GDM) for estimating reaction kinetics from TGA data is presented and its performance is compared to alternative common estimation methods. The methods are assessed in terms of accuracy of the results, time consumed and level of user participation and knowledge needed. All the simulations in this work have been made using the pyrolysis model of fire dynamic simulator (FDS) version 6.0.0.[12]

Estimation methods

Direct method

The direct method (DM) considers a multiple step (k being the reaction index), Nth order reaction path, where the reaction steps are well separated. By reactions being well separated, we mean that the reaction $k - 1$ is completed before reaction k starts. This method is based on the same idea as Friedman used for the one-step reaction.[11] The char-yielding reaction of converting material A into material B and fuel gas is described as

$$A \rightarrow (1 - \nu_k)B + \nu_k gas$$

for each reaction k. The conversion after the reaction k is defined as

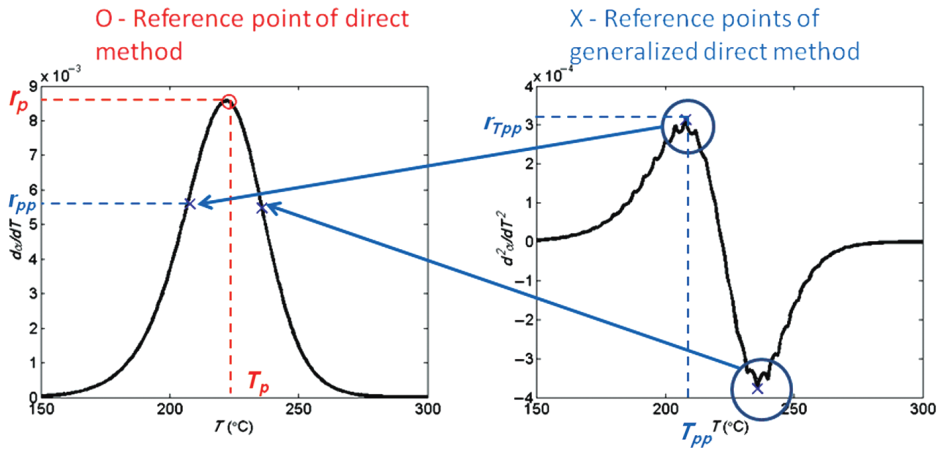

Figure 1. Reference points of the direct methods.

$$\alpha_k = 1 - \frac{m_k}{m_0} \tag{1}$$

where m_k is the mass after reaction k is complete and m_0 is the initial mass of the sample. A reaction progress variable α_k^* corresponding to the mass released from one-step reaction can be defined as

$$\alpha_k^* = \frac{\alpha - \alpha_{k-1}}{\alpha_k - \alpha_{k-1}} \tag{2}$$

An Arrhenius form of the decomposition reaction rate can be written for multiple reactions as

$$\frac{d\alpha_k^*}{dt} = A_k\left(1 - \alpha_k^*\right)^{N_k} \exp\left(-\frac{E_k}{RT}\right) \tag{3}$$

Replacing the reaction progress variable with the relation from equation (2) and dividing both sides by the heating rate $\beta = dT/dt$, the Arrhenius equation becomes

$$\frac{d\alpha}{dT} = \frac{A_k}{\beta}\frac{(\alpha_k - \alpha)^{N_k}}{(\alpha_k - \alpha_{k-1})^{N_k - 1}} \exp\left(-\frac{E_k}{RT}\right) \tag{4}$$

To connect these analytical expressions to the thermogravimetric data, a *reference point* needs to be specified. In DM, the reference point for each of the reactions is chosen from the peak of the differential thermogravimetric (DTG) curve, as shown in Figure 1. The first derivative (with respect to temperature) of the conversion at the reference point of kth reaction is called *reference value* and is denoted as r_{pk}.

$$r_{pk} \equiv \max\left(\frac{d\alpha}{dT}\right) \tag{5}$$

The corresponding temperature and conversion values are denoted as T_{pk} and α_{pk}, respectively. The second derivative of the conversion α is zero at reference point. Using these definitions, we can solve the above equation for activation energy

$$E_k = N_k R \frac{r_{pk}}{\alpha_k - \alpha_{pk}} T_{pk}^2 \tag{6}$$

Alternatively, the calculation can be made using the reference value based on the first *time* derivative of the conversion

$$E_k = \frac{N_k R}{\beta} \frac{\max(d\alpha/dt)}{\alpha_k - \alpha_{pk}} T_{pk}^2 \tag{7}$$

By substituting the activation energy into equation (4), we obtain an equation for pre-exponential factor

$$A_k = r_{pk} \beta \frac{(\alpha_k - \alpha_{k-1})^{N_k - 1}}{(\alpha_k - \alpha_{pk})} \exp\left(\frac{E_k}{RT_{pk}}\right) \tag{8}$$

Now, the only unknown parameter is the reaction order N_k. In certain applications, it can be assumed to be one, but for more general approach, some methods from the literature are presented. Gao et al.[13] listed theoretical limits for the conversion as a function of the reaction order. A very simple curve fit can be made for approximating the reaction order

$$N_k \approx 13.25\left(1 - \alpha^*_{p,k}\right)^3 - 4.16\left(1 - \alpha^*_{p,k}\right)^2 + 2.3\left(1 - \alpha^*_{p,k}\right) - 0.077 \tag{9}$$

where α^*_{p} is the reaction progress variable from equation (2) at the peak. More elaborate methods have been presented by Friedman.[11] For three different points (1, 2, 3) of a single experimental TGA curve, the reaction order can be calculated as

$$N_k = \frac{\ln\left(\frac{r_{3k}}{r_{1k}}\right) - \frac{T_{2k}(T_{3k} - T_{1k})}{T_{3k}(T_{2k} - T_{1k})} \ln\left(\frac{r_{2k}}{r_{1k}}\right)}{\frac{T_{2k}(T_{3k} - T_{1k})}{T_{3k}(T_{2k} - T_{1k})} \ln\left(\frac{1 - \alpha^*_{1k}}{1 - \alpha^*_{2k}}\right) - \ln\left(\frac{1 - \alpha^*_{1k}}{1 - \alpha^*_{3k}}\right)} \tag{10}$$

If one point is the peak value, N can be estimated using only two reference points (1, p)

$$N_k = \frac{\ln\left(\frac{r_{pk}}{r_{1k}}\right)}{\frac{T_{pk}\left(T_{pk} - T_{1k}\right) r_{Tp}}{T_1\left(1 - \alpha^*_{pk}\right)} - \ln\left(\frac{1 - \alpha^*_{1k}}{1 - \alpha^*_{pk}}\right)} \tag{11}$$

Generalized Direct Method (GDM)

The DM is very sensitive to the correct definition of the conversion and the peak value. If the reactions are overlapping at later stage, it may be more convenient to choose the reference point where the reactions do not yet overlap. That is, either before or after the peak value. If the reference point is chosen from where the third derivative is zero (see Figure 1), the activation energy can be calculated as (neglecting the reaction index k for brevity)

Table 1. Weighting functions for different heating rates

wt1	$w_i = \frac{\mu}{\sum_i \beta_i}$ (direct mean)
wt2	$w_i = \frac{1}{\lvert\beta_i-\mu\rvert \sum_i \frac{1}{\lvert\beta_i-\mu\rvert}}$ 1 (heating rates near mean value get greater weight)
wt3	$w_i = \frac{\lvert\beta_i-\mu\rvert}{\sum_i (\lvert\beta_i-\mu\rvert)}$ (heating rates far from mean value get greater weight)

μ is the mean of the heating rates.

$$E = \frac{-b \pm \sqrt{b^2 - 4ac}}{2a} \tag{12}$$

where

$$\begin{cases} a = \frac{\left(\alpha_k - \alpha_{pp}\right)^2}{R^2 T_{pp}^4} \\ b = -\frac{2 r_{pp} N_k \left(\alpha_k - \alpha_{pp}\right)}{R T_{pp}^2} - \frac{2\left(\alpha_k - \alpha_{pp}\right)^2}{R T_{pp}^3} \\ c = r_{pp}^2 (N_k - 1) N_k - r_{Tpp} N_k \left(\alpha_k - \alpha_{pp}\right) \end{cases}$$

Here T_{pp} is the reference point and r_{pp} and r_{Tpp} are the first and second derivatives of the conversion at the reference point, respectively. The second gradient r_T has two peaks and the sign ($\pm$) in equation (12) depends on which peak is chosen. If the first (positive) peak is chosen, the sign is positive. After this, A_k can be calculated at the point T_{pp} as in equation (8) and N_k as previously described for DM. This will be called GDM.

Data reduction

It is customary to perform the TGAs at different heating rates, typically between 1 and 20 K/min. In fires, the heating rates can, at least for short periods of time, be as high as 1000 K/min. In this work, some approaches to the reduction of the estimation results obtained from different heating rates are studied. First of all, the results from all the heating rates must be somehow averaged for a general result. The averaging can be performed either to the calculated parameter values (A, E, N) or to the reference values (α, T, r).

In addition, the effect of the heating rate range can be considered by giving more or less importance to the extreme heating rates. Different weighting methods examined are listed in Table 1.

The error (*fitness value*) between target and estimated curves is calculated as sum of errors in conversions scaled by average relative deviation

$$fV = \frac{\sum_j \left|\alpha_{\mathrm{mod},j} - \alpha_{\exp,j}\right|}{\sum_j \alpha_{\exp,j}} \tag{13}$$

with the summation going over the values obtained at different temperatures. Small fitness value means good fit in this work.

Table 2. Analytical methods used in this work

Method	E	A	Values to specify/reaction
Direct method	$E_k = N_k R \frac{r_{pk}}{\alpha_k - \alpha_{pk}} T_{pk}^2$	$A_k = r_{pk} \beta \frac{(\alpha_k - \alpha_{k-1})^{N_{k-1}}}{(\alpha_k - \alpha_{pk})^{N_k}} \exp\left(\frac{E_k}{RT_{pk}}\right)$	5: r_p, T_p, α_p, α_k, α_{k-1}
Generalized direct method	$E = \frac{-b \pm \sqrt{b^2 - 4ac}}{2a}$ a, b and c as in equation (12)	$A_k = r_{ppk} \beta \frac{(\alpha_k - \alpha_{k-1})^{N_{k-1}}}{(\alpha_k - \alpha_{ppk})^{N_k}} \exp\left(\frac{E_k}{RT_{pp}}\right)$	6: r_{pp}, r_{Tpp}, T_{pp}, α_{pp}, α_k, α_{k-1}
Friedman[11]	$E_k = -R \frac{\ln\left(\frac{r_{2k}}{r_{1k}}\right) + N_k \ln\left(\frac{\alpha_k - \alpha_{1k}}{\alpha_k - \alpha_{2k}}\right)}{\frac{1}{T_{2k}} - \frac{1}{T_{1k}}}$	$A_k = \beta \frac{r_{1k}(\alpha_k - \alpha_{k-1})^{N_{k-1}}}{\exp\left(-\frac{E}{RT_{1k}}\right)(\alpha_k - \alpha_{k-1})^{N_k}}$	8: r_{1T}, r_{2T}, T_1, T_2, α_{1k}, α_{2k}, α_k, α_{k-1}
McGrattan et al.[8] and Lyon et al.[10]	$E_k = \frac{RT_{pk}^2 e r_{pk}}{\alpha_k - \alpha_{k-1}}$ $N = 1$	$A_k = \frac{\beta e r_{pk}}{\alpha_k - \alpha_{k-1}} \exp\left(\frac{E_k}{RT_{pk}}\right)$	4: r_p, T_p, α_{1k}, α_{k-1}

Other commonly used estimation methods

Several authors have proposed other analytical methods for obtaining the kinetic parameters. Some of the methods are listed in Table 2. These methods are generally easy and quick to use, and they provide relatively unique solutions. Friedman developed his method for a single-step model, but here, it is scaled for multiple steps for generality. McGrattan et al. and Lyon et al.[9,10] presented essentially the same equations with slightly different derivations and nomenclature. They both assumed first-order reaction kinetics. Lyon et al. additionally limited the reaction path to just one reaction but offered an alternative method for extracting the reaction parameters using the heat release rate from microscale combustion calorimeter (MCC).[10,14] Those equations may have great value for some applications but are not evaluated here since they require different experimental apparatus than the other methods.

Besides the analytical methods, several curve-fitting algorithms have been applied for the kinetic parameter estimation. Evolutionary algorithms are most commonly used, including genetic algorithms (GA),[3–7] hybrid genetic algorithms (HGA)[7] and shuffled complex evolution (SCE).[7,8] Their main idea is based on the survival of the fittest. The algorithm starts from a random set of trial solutions and tests their fitness against the experimental curve. The probability of the stochastic processes depends on this fitness value; the better the fitness value, the greater the probability of the trial solution surviving to the next iteration round. Other processes are crossover (creating new trial solution by uniting two older solutions), mutation (one or more parameters are replaced by a random number) and migration (trial solutions change place between two groups of the solutions). These algorithms are very efficient for complex problems with many parameters, overlapping reactions and even noisy data. They are a bit more complicated to use than the analytical methods and require significant amount of computer resources.

Results and discussions

Simple synthetic material

Four analytical methods, presented by equations (6) to (12) and Table 2, and two optimization methods (GA and SCE) were tested using a synthetic material sample with two

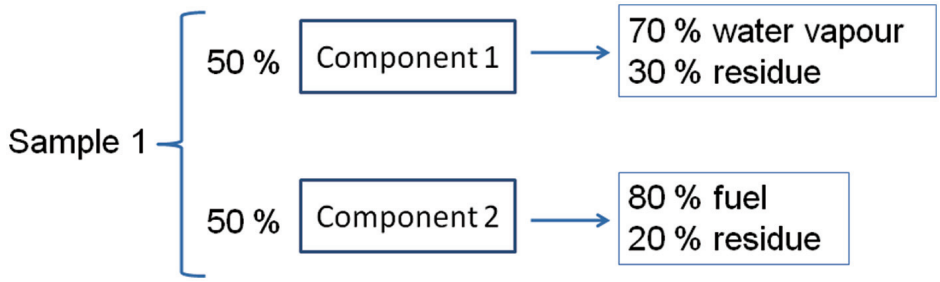

Figure 2. Reaction path for the simple synthetic material.

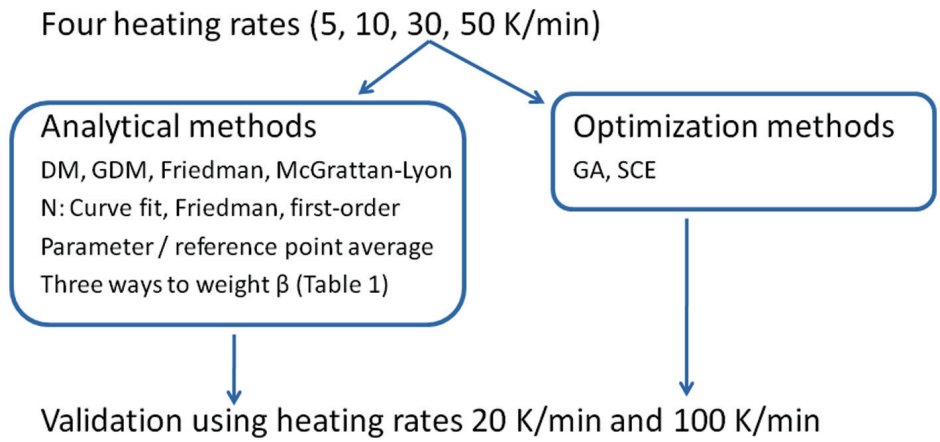

Figure 3. Test scheme for the estimation methods.
DM: direct method; GDM: generalized direct method; GA: genetic algorithms; SCE: shuffled complex evolution.

well-separated reactions. The synthetic material was chosen because of known target values, simple shape and non-noisy data. The reaction path is shown in Figure 2. Two pseudocomponents are assumed with mass losses of 0.35 and 0.4, respectively, of the original mass, and they were assumed to be known. The first reaction produces water vapour (as some flame retardants) and the second reaction produces fuel gas. The reaction order was calculated using equations (9) and (10) and assuming a first-order reaction for comparison for those models that it was applicable.

The synthetic target data were generated for four different heating rates (5, 10, 30 and 50 K/min), and the results were generalized using the weighting functions (Table 1) for either directly for the estimated parameter values or for the reference points and values. The real performance of the parameters was then tested using target data at 20 K/min and 100 K/min. A summary of the test scheme is shown in Figure 3.

The parameter estimation produced in total 62 sets of kinetic parameters, and they were tested for two different heating rates (20 and 100 K/min). The predicted DTG curves with best fitting parameter sets of each method are presented in Figure 4. In addition to the overall result covering the whole temperature range (Figure 4(a)), the detailed results of

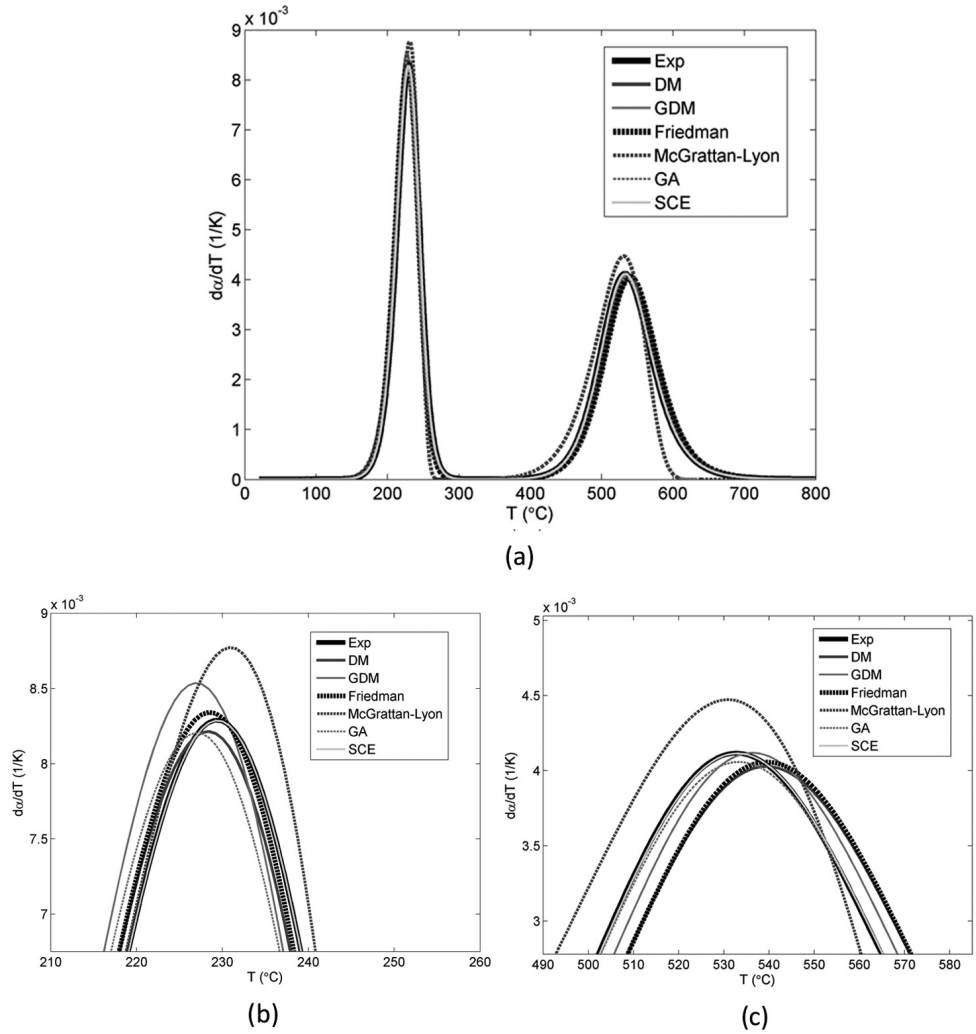

Figure 4. Comparison of estimation methods and experimental curve at 20 K/min. (a) Overall results, (b) first peak and (c) second peak.
DM: direct method; GDM: generalized direct method; GA: genetic algorithms; SCE: shuffled complex evolution.

the reaction rate peaks are shown in Figure 4(b) and (c). The reaction order in best fitting model for GDM was calculated using the Friedman's equation (equation (10)), and the curve fit (equation (9)) was used for DM and Friedman's method. Based on a visual judgement, all the methods reproduced the TGA experiment very well, suggesting that they are adequate for engineering purposes. The fit and the calculated fitness values were significantly better using optimization methods (GA, SCE) than the analytical methods. SCE reproduced the synthetic TGA data most accurately at both validation heating rates. The best fitting parameter sets of each method are listed in Table 3. Between analytical methods, the GDM showed the best performance both at 20 K/min and at 100 K/min heating

Table 3. Best fitting parameter sets of each method

	Target values	DM, equations (6) and (8)	GDM, equations (8) and (12)	Friedman (Table 2)	McGrattan –Lyon (Table 2)	GA	SCE
A_1 (s^{-1})	1.50×10^{15}	3.10×10^{14}	4.11×10^{15}	5.83×10^{14}	2.67×10^{12}	3.41×10^{15}	1.47×10^{15}
E_1 (kJ/kmol)	1.60×10^5	1.53×10^5	1.63×10^5	1.56×10^5	1.36×10^5	1.62×10^5	1.60×10^5
N_1	1.50	1.43	1.50	1.43	1.00	1.59	1.50
A_2 (s^{-1})	1.00×10^{12}	2.48×10^{11}	1.17×10^{12}	3.15×10^{11}	6.05×10^7	4.52×10^{11}	9.93×10^{11}
E_2 (kJ/kmol)	2.10×10^5	2.03×10^5	2.12×10^5	2.05×10^5	1.51×10^5	2.05×10^5	2.10×10^5
N_2	2.00	1.92	2.00	1.92	1.00	1.97	2.00
fV (20 K/min)	–	0.0086	0.0070	0.0085	0.0299	0.0024	0.0003
fV (100 K/min)	–	0.0111	0.0082	0.0109	0.0131	0.0041	0.0003
fV (HRR)	–	0.0832	0.0591	0.0819	0.2463	–	–
fV (MLR)	–	0.0045	0.0022	0.0047	0.0151	–	–
Number of reference points (excluding *N*)		10	12	16	8	–	–
Comments		N_{cf} equation (9), Ref. ave, wt3	N_f equation (10), Ref. ave, wt2	N_{cf} equation (9), Ref. ave, wt3	*N* = 1, Par. ave, wt3	–	–

DM: direct method; GDM: generalized direct method; GA: genetic algorithms; SCE: shuffled complex evolution; HRR: heat release rate; MLR: mass loss rate.
'Ref. ave' means that reference values were averaged. 'Par. ave' means that parameters were averaged. Small fitness value means good fit.
The used reaction order *N* and information about the parameter averaging are listed in the comments (Table 1).

Table 4. Fitness values of the analytical methods with different weight functions

Averaging		DM	GDM	Friedman	McGrattan–Lyon
	fV (20 K/min)				
Parameters	wt1	0.0236	0.0570	0.0174	0.0314
	wt2	0.0210	0.0536	0.0229	0.0316
	wt3	0.0182	0.0486	0.0207	0.0299
Reference values	wt1	0.0100	0.0108	0.0099	0.0453
	wt2	0.0129	0.0070	0.0130	0.0409
	wt3	0.0086	0.0084	0.0085	0.0491
	fV (100 K/min)				
Parameters	wt1	0.0311	0.0689	0.0227	0.0132
	wt2	0.0282	0.0638	0.0292	0.0131
	wt3	0.0250	0.0603	0.0267	0.0131
Reference values	wt1	0.0128	0.0122	0.0123	0.0297
	wt2	0.0181	0.0082	0.0174	0.0242
	wt3	0.0111	0.0094	0.0109	0.0342

DM: direct method; GDM: generalized direct method.
The *N* is calculated as in Table 3.

rates. McGrattan–Lyon method provided the fit with the largest error, but this is to be expected since it is limited to first-order reactions. Of the other analytical methods, only Friedman's method performed reasonably well when $N = 1$ was assumed.

The effects of the weight functions and two different means of averaging were examined by calculating the fitness values for the validation results of each of the analytical methods. The fitness values with different weight functions are listed in Table 4. For all the other methods except MGrattan–Lyon, the results were much more accurate when the reference values were first averaged prior to calculating the parameters. For the McGrattan–Lyon method, straight averaging of the parameters resulted in better fits. The different weight functions also had some significant effect on the resulting fitness values. Surprisingly, for DM and Friedman's method, it seems that the wt2 (emphasizing the heating rates closer to mean value) has the better extrapolating ability than wt3 (emphasizing the heating rates far from mean value). For GDM, the opposite was true.

While the analytical methods were very quick to use, the optimization methods required significant computational time even when parallel processing was used to speed up the computations. The set-up time for all the methods was more or less the same. For the analytical methods, the added complexity means increasing number of reference points to be chosen (listed in Table 2). The method of McGrattan and Lyon is the simplest with only four values to specify per reaction, while Friedman's method is the most complicated one with eight values per reaction. The curve fit reaction order (equation (9)) requires only three reference points, while the Friedman's equation (equation (10)) needs eight. Of course, the use of the analytical methods could be automated reducing the workload.

The significance of the differences in estimated kinetic parameters was studied by applying the results of the analytical methods to a simulated cone calorimeter test. The

Table 5. Thermal parameters used in the simulations

	ρ (kg/m^3)	ε	k (W/m/K)	c_p (kJ/kg/K)	H_r (kJ/kg)	H_c (MJ/kg)
Component 1	1000	1.0	0.5	3.0	1500	25
Component 2	1000	1.0	0.1	2.0	200	30
Residue 1	300	0.8	0.3	1.2	–	–
Residue 2	200	0.9	0.7	1.5	–	–

cone heater was not simulated. Instead, a 50 kW/m^2 external heat flux was applied to the sample surface in the condensed phase solver. The gas space of the cone calorimeter was simulated with a 1-cm grid resolution to capture the flame heat flux. The thermal parameters of the simulated material are listed in Table 5. The comparison of the simulated cone calorimeter results are shown in Figure 5, and fitness values are shown in Table 3. GDM provides the most accurate prediction of the heat and mass loss rates. The first-order method of McGrattan and Lyon gives the least accurate prediction, as expected according to the TGA results. However, the differences between the methods are relatively small and could be compensated by the thermal parameter values if they were separately estimated using the cone calorimeter data. The differences in the sample's front and back temperatures were insignificant.

Noisy synthetic material

The performance of the analytical estimation methods was also tested in a more realistic case with two, slightly overlapping reactions using synthetic TGA signal that includes noise. According to the previous tests, the optimization methods are known to result in better fitness in most cases and are therefore excluded from this study. The sample is assumed to consist of two pseudocomponents, and the reaction path is seen in Figure 6. The mass losses during the two reactions were 0.25 times the original mass and that was assumed to be known. As in the simple test case, the first reaction yields water vapour and the second fuel gas. The sample data were created at 5 and 50 K/min heating rates and tested at 20 and 100 K/min. The reference points were given equal weights.

Typically TGA experiments have very little noise. According to our own experience on TGA data, the noise is usually associated with the high mass loss rate during the degradation and is by no means constant during the experiment. Two noise types were tested:

$$\begin{aligned}
&\text{Noise } 1 = 1 \cdot 10^{-4} \sin(T) \\
&\text{Noise } 2 = 0.0003 \sin(2 \cdot 0.01 \cdot \pi T) + \sin(2 \cdot 0.022 \cdot \pi T) \cdot \begin{cases} 0, \text{when } T \notin T_{\text{deg}} \\ 0.01 + 1 \cdot 10^{-4} x, \text{when } T \in T_{\text{deg}} \end{cases} \\
&x \sim N(0, 1)
\end{aligned} \tag{14}$$

The noise was added to the conversion α. It was generated similarly for both heating rates, but the random numbers were different. Noise 1 is small sinusoidal noise with relatively high frequency. Noise 2 has two parts: small, low frequency sinusoidal noise where nothing is degrading and higher frequency noise with some randomness in the area where

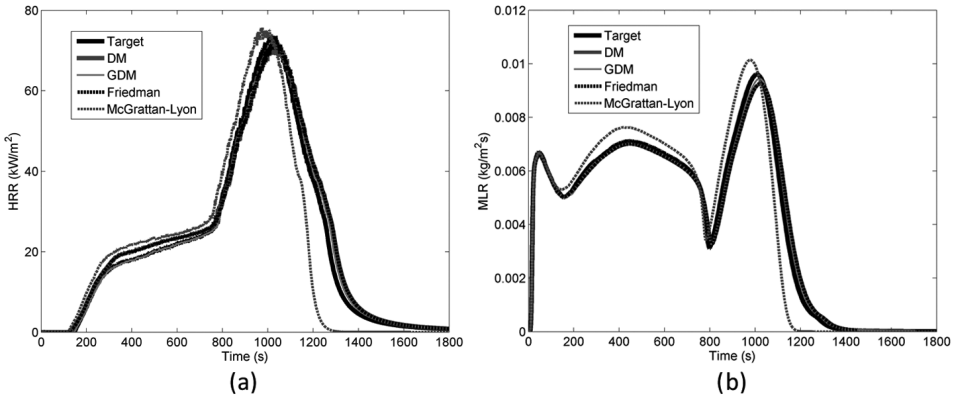

Figure 5. Effect of different sets of kinetic parameters in cone calorimeter model at 50 kW/m^2. (a) HRR and (b) MLR.
DM: direct method; GDM: generalized direct method; HRR: heat release rate; MLR: mass loss rate.

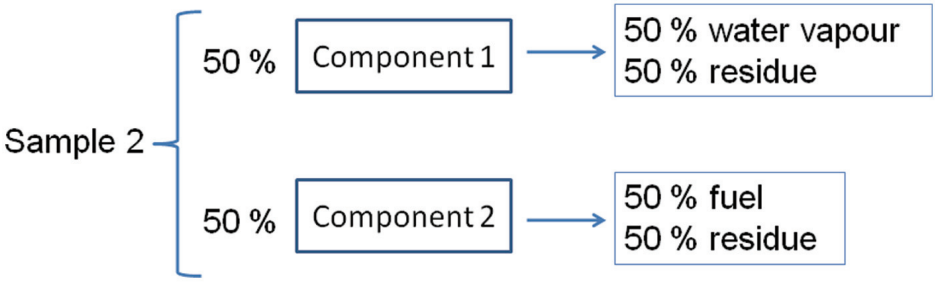

Figure 6. Reaction path for slightly overlapping synthetic material.

the sample is degrading. The noise levels can be seen in Figure 7. Noise 2 is significantly greater than Noise 1, and it is based on an analysis of real, noisy TGA data. Fitness values were calculated compared to the original, non-noisy data. The noisy data were tested using all the methods listed in Table 2. Due to the strong overlapping of the reactions, the reaction order (N) could not be accurately calculated using the Friedman's method, and therefore, the curve fit method in equation (9) was used for all methods.

The parameter estimation results are listed in Table 6 and visually presented for Noise 2 in Figure 8. When no noise was added, all the methods where $N \neq 1$ predicted the DTG curve very accurately. Small sinusoidal noise (Noise 1) did not cause significant error for DM or Friedman's method, but for GDM, the error increased especially in the second peak. This is probably due to the fact that the magnitude of the error caused by the high-frequency noise increases with each successive derivative, and therefore, small error in the mass data causes greater error in the second derivative. It is also more difficult to define the location of the peak from very noisy data.

Noise 2 was more challenging for all other methods except GDM. The results are shown in Figure 8. The effect of the noise depends on the location of the greatest error, whether it is

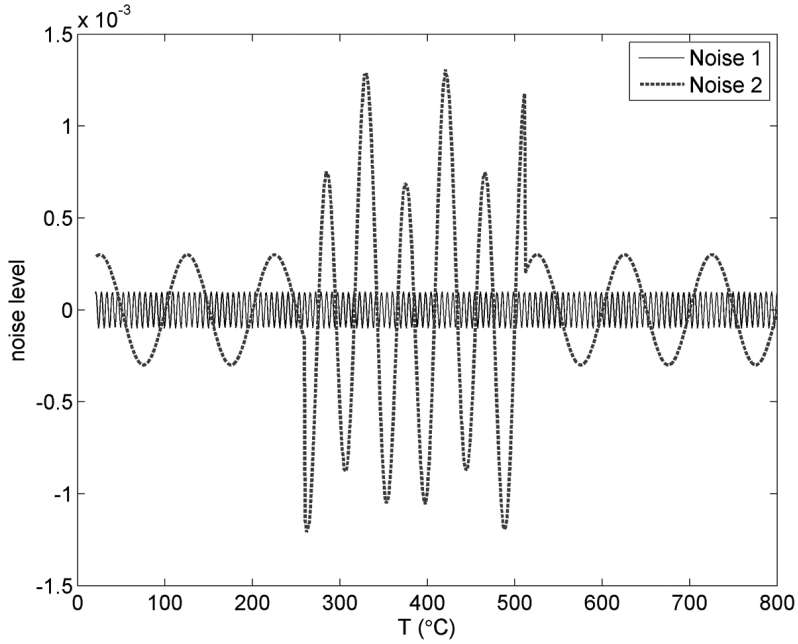

Figure 7. Noise 1 and Noise 2.

located exactly at the reference point or not. In some cases, the noise can even improve the accuracy of the method, as can be seen for the DM and Friedman's method for Noise 1 at 100 K/min, compared to the results without any noise. All the methods produced acceptable accuracy for simulation purposes at both noise types.

The sets of kinetic parameters estimated with Noise 2 were tested in cone calorimeter at 50 kW/m^2 heat flux level. The simulations were made using 1 cm grid size. The thermal parameters were the same as for the simple test case (Table 5), and the heat release rate and mass loss rate at 50 kW/m^2 are shown in Figure 9. The fitness values of the cone calorimeter results with Noise 2 are listed in Table 6. Only the kinetic parameters estimated using McGrattan–Lyon method caused slightly higher rate and earlier flame out compared to the target results. As expected according to the TGA results, GDM provided the best fit also in the cone calorimeter results. The significance of this difference is very small, as the thermal parameters are known to compensate the inaccuracies in the kinetic model. The kinetic parameters did not have any significant effect on the front and back temperatures of the sample.

Summary and conclusions

A DM for estimation of kinetic parameters was generalized for multiple reactions and compared with other commonly used estimation methods. Both analytical methods and optimization algorithms were compared. For analytical methods, different methods for calculating the reaction order were also presented and assessed and different weight functions for the heating rates tested. Synthetic experimental data based on known kinetic parameters were used. The first test was a simple two-step reaction with well-separated reactions and no noise.

Table 6. Target $1.50.10^{15}$ $2.00.10^{5}$ 1.50 $1.00.10^{10}$ $1.60.10^{5}$ 2.00 – Estimated parameters when noise is added to the sample data

		A_1 (s^{-1})	E_1 (kJ/kmol)	N_1	A_2 (s^{-1})	E_2 (kJ/kmol)	N_2	fV (20 K/min)	fV (100 K/min)
No noise	Target	1.50×10^{15}	200×10^{3}	1.50	1.00×10^{10}	1.60×10^{5}	2.00	–	–
	DM	3.50×10^{14}	1.92×10^{5}	1.35	6.65×10^{11}	1.59×10^{5}	1.96	0.0104	0.0117
	GDM	8.29×10^{14}	1.96×10^{5}	1.35	7.25×10^{11}	1.85×10^{5}	1.96	0.0105	0.0151
	Friedman	6.19×10^{14}	1.95×10^{5}	1.35	2.78×10^{9}	1.54×10^{5}	1.96	0.0103	0.0137
	McGrattan–Lyon	1.34×10^{13}	1.75×10^{5}	1.00	4.55×10^{6}	1.17×10^{5}	1.00	0.0576	0.0465
Noise 1	DM	5.59×10^{14}	1.94×10^{5}	1.35	2.36×10^{10}	1.66×10^{5}	2.01	0.0104	0.0100
	GDM	5.29×10^{14}	1.94×10^{5}	1.35	1.22×10^{17}	2.55×10^{5}	2.01	0.0183	0.0314
	Friedman	6.10×10^{14}	1.95×10^{5}	1.35	8.92×10^{9}	1.60×10^{5}	2.01	0.0106	0.0119
	McGrattan–Lyon	2.19×10^{13}	1.78×10^{5}	1.00	8.46×10^{6}	1.20×10^{5}	1.00	0.0578	0.0492
Noise 2	DM	2.31×10^{15}	2.01×10^{5}	1.45	5.07×10^{11}	1.83×10^{5}	2.40	0.0169	0.0143
	GDM	7.76×10^{14}	1.96×10^{5}	1.45	1.67×10^{16}	2.43×10^{5}	2.40	0.0120	0.0181
	Friedman	1.25×10^{16}	2.10×10^{5}	1.45	7.48×10^{12}	1.98×10^{5}	2.40	0.0149	0.0093
	McGrattan–Lyon	1.79×10^{13}	1.76×10^{5}	1.00	7.90×10^{6}	1.19×10^{5}	1.00	*0.0634*	0.0553

DM: direct method; GDM: generalized direct method.

Table 7. Fitness values of cone calorimeter results with Noise 2

	fV (HRR)	*fV* (MLR)
DM	0.0790	0.0032
GDM	0.0386	0.0007
Friedman	0.0629	0.0028
McGrattan–Lyon	0.3166	0.0146

HRR: heat release rate; MLR: mass loss rate; DM: direct method; GDM: generalized direct method.

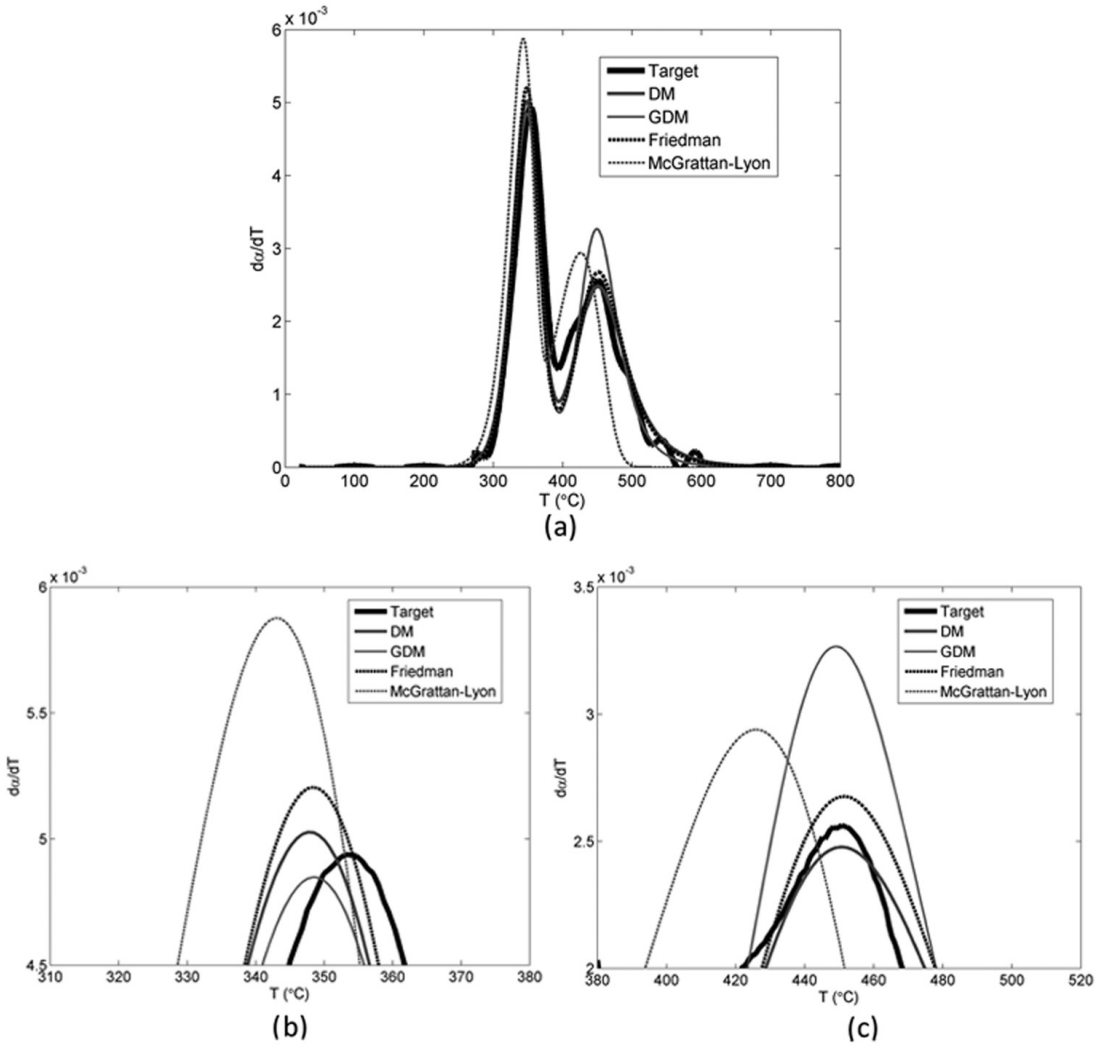

Figure 8. Estimation results with different analytical methods for data with Noise 2 at 20 K/min. (a) Overall results, (b) first peak and (c) second peak.
DM: direct method; GDM: generalized direct method.

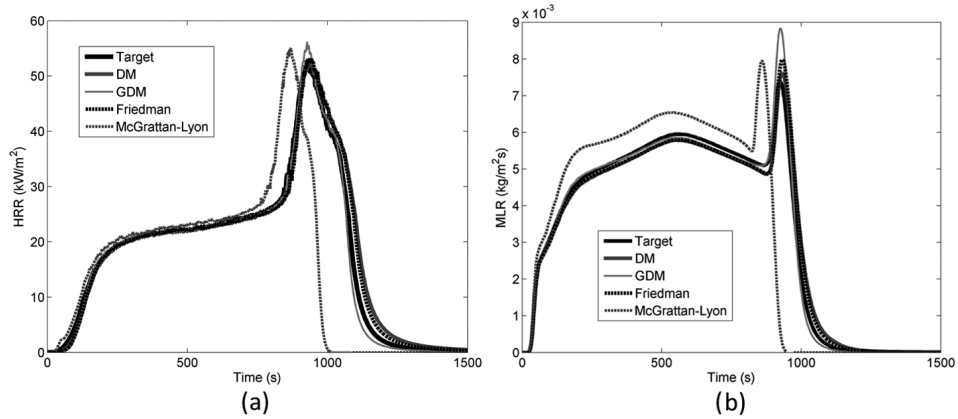

Figure 9. The performance of the estimation results in cone calorimeter model at 50 kW/m^2. (a) HRR and (b) MLR.
HRR: heat release rate; MLR: mass loss rate; DM: direct method; GDM: generalized direct method.

The second test had two slightly overlapping reactions. Two types of noise were added to the data for testing the performance in a more realistic case with experimental noise.

For the simple sample case, the parameters were estimated at four different heating rates and then averaged using different weight functions. The results were then used at two other heating rates to test the extrapolating ability of the results. Optimization methods turned out to produce better fitting results, but all the methods, including the analytical methods were able to find parameters that produce a sufficiently accurate fit for most engineering applications. The McGrattan–Lyon method was the simplest and fastest to use without any software. All the analytical methods take just few minutes to obtain results, while the optimization methods take hours or days for running the algorithm.

The noisy sample was tested only using the analytical methods. The parameters were estimated at two heating rates, and the fitness of the solution was tested at two other heating rates. Without noise, all the analytical methods, excluding the first-order McGrattan–Lyon method, reproduced the TGA results very accurately. In case of small high-frequency noise (Noise 1), most method still performed very well but the performance of the GDM was greatly hampered. In case of Noise 2, consisting of lower frequency components, the predictions were significantly less accurate for all the methods except for the GDM. The phase of the noise signal with respect to the selected reference points has somewhat random effect on the performance of the estimation methods. In both test cases, the mass losses of the reactions were assumed to be known exactly. The uncertainties of the methods may be higher if the mass losses are also estimated from the experimental data.

The differences in the TGA predictions did not cause significant errors in the cone calorimeter scale. Furthermore, the thermal parameters are known to be able to compensate small differences in the kinetic models, and therefore, the errors can be reduced if some of the thermal parameters are estimated using the cone calorimeter data itself.

This work demonstrates that the analytical methods can be used efficiently as substitutes to the computationally expensive optimization methods when estimating the parameters of pyrolysis kinetics. There are several methods to choose from, and the choice depends on the

required accuracy, complexity and the experimental data. Methods with fewer reference values work better in case of noisy data and overlapping reactions, while more complicated methods yield more accurate results for clean, simple data. Removing the high-frequency noise from the mass data by filtering is recommended in order to improve the performance of methods relying on higher-order derivatives of the mass data, such as the GDM.

Funding

The work of A. Matala and S. Hostikka was funded by the European Union under 7th Framework project FIRE-RESIST and by the State Nuclear Waste Management Fund of Finland. The work of C. Lautenberger was funded by the National Science Foundation under Grant No. 0730556.

Conflict of interest

Any opinions, findings and conclusions or recommendations expressed in this material are those of the authors and do not necessarily reflect the views of the National Science Foundation (NSF).

References

1. Nikolaev AV, Logvinenko VA and Gorbatchev VM. Special features of the compensation effect in non-isothermal kinetics of solid-phase reactions. *J Therm Anal* 1974; 6: 473–577.
2. Matala A and Hostikka S. Pyrolysis modeling of PVC cable materials. *Fire Saf Sci* 2011; 10: 917–930.
3. Lautenberger C, Rein G and Fernandez-Pello C. The application of a genetic algorithm to estimate material properties for fire modeling from bench-scale fire test data. *Fire Safety J* 2006; 41: 204–214.
4. Rein G, Lautenberger C, Fernandez-Pello C, et al. Application of genetic algorithms and thermogravimetry to determine the kinetics of polyurethane foam in smoldering combustion. *Combust Flame* 2006; 146: 95–108.
5. Matala A, Hostikka S and Mangs J. Estimation of pyrolysis model parameters for solid materials using thermogravimetric data. *Fire Saf Sci* 2009; 9: 1213–1223.
6. Lautenberger C and Fernandez-Pello C. Generalized pyrolysis model for combustible solids. *Fire Safety J* 2009; 44: 819–839.
7. Lautenberger C and Fernandez-Pello C. Optimization algorithms for material pyrolysis property estimation. *Fire Saf Sci* 2011; 10: 751–764.
8. Chaos M, Khan MM, Krishnamoorthy N, et al. Evaluation of optimization schemes and determination of solid fuel properties for CFD fire models using bench-scale pyrolysis tests. *P Combust Inst* 2011; 33(2): 2599–2606.
9. McGrattan K, McDermott R, Mell W, et al. Modeling the burning of complicated objects using Lagrangian particles. In: *Conference proceedings of the twelfth international interflame conference*, 2010, pp.743–753.
10. Lyon RE, Safronava N and Oztekin E. A simple method for determining kinetic parameters for materials in fire models. *Fire Saf Sci* 2011; 10: 765–777.
11. Friedman HL. New methods for evaluating kinetic parameters from thermal analysis data. *J Polym Sci Pol Lett* 1969; 7(1): 41–46.
12. McGrattan K, McDermott R, Hostikka S, et al. *Fire dynamics simulator (version 5) user's guide*. 2011. NIST Special Publication 1019.
13. Gao Z, Kaneko T, Hou D, et al. Kinetics of thermal degradation of poly(methyl methacrylate) studied with the assistance of the fractional conversion at the maximum reaction rate. *Polym Degrad Stabil* 2004; 84: 399–403.
14. Lyon RE and Walters RN. Pyrolysis combustion flow calorimetry. *J Anal Appl Pyrol* 2004; 71: 27–46.

Nomenclature

A is pre-exponential factor (s^{-1})
c_p is specific heat capacity (kJ/K/kg)
E is activation energy (kJ/k mol)
fV is fitness values
H_r is heat of reaction (kJ/kg)
H_c is heat of combustion (MJ/kg)
k is thermal conductivity (W/K/m)
m is mass (kg)
n is number of reactions
N is reaction order
r is reaction rate (1/s)

R is Gas constant (8.3145 J/(mol·K))
t is time (s)
T is temperature (K, °C)
w is weighting parameter

Greek
α is conversion (g/g)
β is heating rate (K/s)
ε is emissivity
μ is mean value of heating rates (K/s)
v is Fuel yield

Subscripts
0 is initial, virgin
cf is curve fit
deg is degradation range (temperature)
exp is experimental
f is Friedman's method
i is heating rate index
j is index of a conversion curve
k is reaction index
model is model value
p is peak value
pp is peak of the second derivative
t is time derivative
T is temperature derivative

Author biographies

Anna Matala is a Research Scientist at VTT Technical Research Centre of Finland and PhD candidate at Aalto University School of Science. She received her MSc degree in Systems and Operations Research from Helsinki University of Technology in 2008. Her research concentrates on pyrolysis modelling and parameter estimation in fire simulations.

Chris Lautenberger is currently a Principal Engineer at Reax Engineering Inc. He received his MSc in Fire Protection Engineering from Worcester Polytechnic Institute in 2002 and PhD in Mechanical Engineering (combustion) from University of California in Berkeley in 2007. One of Dr Lautenberger's areas of expertise is computer fire modelling and its application to forensic fire reconstruction. He is a leading fire expert in the rapidly growing field of fire growth modelling where computational fluid dynamics is used to predict how fires would spread under different conditions.

Simo Hostikka is a Principal Research Scientist at VTT Technical Research Centre of Finland. He received an MSc degree in 1997 and a PhD in 2008 from the Department of Engineering Physics and Mathematics of the Helsinki University of Technology. He is one of the main developers of the Fire Dynamics Simulator (FDS) and his expertise covers all the fields of fire modelling.

PUBLICATION III

Pyrolysis Modelling of PVC Cable Materials

In: Fire Safety Science – Proceedings of the Tenth International Symposium, pp. 917–930.

Pyrolysis Modelling of PVC Cable Materials

ANNA MATALA, and SIMO HOSTIKKA
VTT Technical Research Centre of Finland
P.O.Box 1000
FI-02044 VTT, Finland

ABSTRACT

One of the most commonly used materials in electrical cables is flexible PVC. In this work, the effects of the modelling decisions and parameter estimation methods on the pyrolysis modelling of two PVC cables were studied. The kinetic and thermal parameters were estimated from TGA and cone calorimeter experiments. The role of the plasticizers was shown to be important for the early HRR. The effects of the reaction path and reaction order were only minor in the TGA results but significant effects were found in the cone calorimeter results, unless a specific set of thermal parameters was estimated. The results show that the thermal parameters estimated for one kinetic model should not be used for another, unless the kinetic models only differ in fuel yields or different pairs of kinetic coefficients with same reaction order.

KEYWORDS: pyrolysis, modelling, heat release rate, reaction parameters, electrical cables.

NOMENCLATURE LISTING

A	frequency factor (s^{-1})
c	specific heat capacity (kJ/kg·K)
E	activation energy (kJ/kmol)
H_r	heat of reaction (kJ/kg)
H_c	heat of combustion (kJ/kg)
k	thermal conductivity (W/m·K)
N_m	number of material components
N_r	number of reactions
N_s	reaction order
R	gas constant (8.3145 J/(mol·K))
T	temperature (K, °C)

Greek

β	heating rate (K/s)
ε	emissivity
ρ	density (kg/m^3)

subscripts

i	component i
j	reaction j
p	reference
s	solid

INTRODUCTION

Polyvinyl chloride (PVC) is one of the most versatile thermoplastic materials due to its processability and range of different applications. PVC is widely used in electrical cables in the form of flexible PVC. Flexible PVC is produced by adding 30–40 wt. % additives, especially plasticizers to lower the glass-transition temperature [1]. Flexible PVC ignites more easily and burns at higher rate than rigid PVC because the plasticizers are usually combustible [2].

Electrical cables are the primary fire load in many fire engineering applications. The numerical simulation of the PVC cable fires requires the modelling of the cable pyrolysis, which is extremely challenging due to the geometrical complexity and the wide range of different PVC compositions and plasticizers. As the cable manufacturers seldom provide information about the exact chemical composition of the material, the fire modelling must be based on testing the modelling decisions against available experimental evidence. The modelling decisions are related to the degree of geometrical complexity, the number of independent material components, number of reactions and the reaction paths. The different approaches for modelling the kinetics of PVC degradation have been studied by Marcilla and Beltrán [3] who concluded that two parallel reactions are needed to describe the first stage of PVC degradation, and a single reaction for the second. The degree of model complexity should be in balance with the amount of experimental evidence and the allowable estimation and computing times. For instance, electrical cables have typically a cylindrical shape but non-symmetric inner structure with several layers of materials. How much of the layer structure is retained in the pyrolysis model, is a modelling decision. Once the model structure has been fixed, the problem becomes a parameter estimation problem, as explained in Refs. [4–8].

FIRE SAFETY SCIENCE-PROCEEDINGS OF THE TENTH INTERNATIONAL SYMPOSIUM, pp. 917-930
 / DOI: 10.3801/IAFSS.FSS.10-917

This work studies the sensitivity of the pyrolysis model to modelling decisions concerning the reaction path, reaction order and estimation method. The goal is to find the best practises of modelling complex materials such as PVC. Different modelling decisions are tested in the light of their capability to reproduce the experimentally observed behaviour in Cone calorimeter. First, models assuming a parallel reaction path are estimated for the two sample materials taking into account the softeners. An alternative reaction path is then created and the results compared to the parallel model keeping the thermal parameters fixed. The sensitivity on the kinetic parameters is studied by using two alternative estimation methods. The significance of the reaction order parameter is examined.

MATERIALS AND METHODS

Materials

The fire behaviour of two electrical cables is studied: a four conductor power cable (MCMK 4 × 1.5 mm^2) and a three conductor power cable (AHXCMK 10 kV 3 × 95/70 mm^2), referred as Cable 1 and Cable 2, respectively. Cable 1 has a PVC sheath and insulation, and an unknown filler material. From Cable 2, only the PVC sheath is studied in this work. The cable dimensions and weights of the cable components are listed in Table 1.

Table 1. Mass fractions of the cable components. *D* denotes cable diameter.

		Sheath	**Filler**	**Insulation**	**Conductor**	**Other plastic**
Cable 1	Material	PVC	-	PVC	Copper	-
D =13 mm	Thickness (mm)	2.5	10	3[b]	15[b]	-
	Linear mass (kg/m)	0.0898	0.0321	0.0297	0.0647	0.0009
	Linear mass (%)	41.3	14.8	13.7	29.7	0.4
	Density (kg/m^3)	1316 ± 25	1745 ± 100	1375 ± 100	-	-
Cable 2[a]	Material	PVC	PE	PE	Aluminium and copper	-
D =54 mm	Thickness (mm)	2.0[b]	Not measurable	1.0[b]	1.5[b]	-
	Linear mass (kg/m)	0.649	0.228	0.662	0.1097	0.063
	Linear mass (%)	22.8	8.0	23.3	38.6	2.2
	Density (kg/m^3)	1500 ± 30	950 ± 50	1039 ± 50	-	-

[a] The other components than sheath are listed just for completeness, although not studied in this work.
[b] Measured from a photograph.

Experimental

The degradation of each of the material components was studied using simultaneous thermal analysis (STA) including thermogravimetric analysis (TGA) and differential scanning calorimetry (DSC). A small sample (~10 mg) was placed in a furnace and heated at constant rate. The sample mass and energy release were measured during the heating. The experiments were carried out both in air and nitrogen at heating rates between 2–20 K/min, using Netzsch STA 449C equipment.

Cone calorimeter experiments of Cable 1 were performed for eight 10 cm long samples of Cable 1 placed next to each other to construct a roughly 10 cm × 10 cm exposed area. Due to the large diameter of Cable 2, it was possible to test the sheath layer alone. Radiative heat flux was 50 kW/m^2 and ignition by spark igniter. The heat release rate (HRR) and mass loss rate (MLR) were recorded until all the flames disappeared. Since the experimental mass data was quite noisy, the MLR was determined by fitting a piecewise continuous polynomial to the mass results and taking the MLR as a first derivative [9]. The second-order polynomials had continuous first derivative. The second-derivative discontinuities were allowed in a few locations chosen by visual inspection of the data.

Modelling

Formulation

All the simulations were made using Fire Dynamics Simulator (FDS), version 5.5.2 [10]. In the model, the reaction rate of the pyrolysis reactions is calculated using Arrhenius equation

$$r_{ij} = A_{ij}\left(\frac{\rho_{s,i}}{\rho_{s0}}\right)^{N_{s,ij}} \exp\left(-\frac{E_{ij}}{RT_s}\right), \tag{1}$$

where subscript i denotes the i^{th} material component and j the j^{th} reaction. $\rho_{s,i}$ is the solid density of the component, and $\rho_{s,0}$ is the original density of the layer [10]. The solid phase heat conduction is solved in one dimension, according to the heat conduction equation

$$\rho_s c_s \frac{\partial T_s}{\partial t} = \frac{\partial}{\partial x} k_s \frac{\partial T_s}{\partial x} + \dot{q}_s''' , \tag{2}$$

where the chemical source term $\dot{q}_s'''$ is

$$\dot{q}_s'''(x) = -\rho_{s0} \sum_{i=1}^{N_m} \sum_{j=1}^{N_r} r_{ij}(x) H_{r,ij} . \tag{3}$$

A mixture fraction based combustion model was used in the Cone calorimeter simulations.

Models of the Experiments

A simple model of the TGA experiment in Nitrogen atmosphere was created. The gas phase heat and mass transport were neglected in the model and the experiment was assumed to be 0-dimensional, in which case the dimensions of the simulation domain do not affect the results. The bottom of the domain was assigned with the sample material and the side walls and ceiling were heated according to the specified heating rate. As the TGA experiments were carried out for each component separately, the model included just one homogenous layer of material.

The Cone calorimeter model had dimensions of 30 × 30 × 40 cm^3. The sample (10 × 10 cm^2) was placed in the middle of the bottom boundary and all the other walls were open. The computational mesh was extremely coarse (10 cm). A refinement of the mesh was not found to change the results significantly at an external heat flux of 50 kW/m^2, but the computing time of the estimation process increased substantially. It is clear that a computation with such a coarse mesh cannot capture the details of the flame in the real Cone calorimeter experiment. However, it can provide an effective description of the flame heat flux to the sample surface because the combustion model burns most of the fuel within the one or two 10 cm cells above the sample, and because the source term of the gas phase radiation transport equation includes a specified fraction (usually 0.35) of the local heat release rate. The spark igniter was not included in the model because the ignition happens as soon as the fuel meets oxygen.

Cable 1 was modelled as a complete cable, neglecting the small amount of additional plastics. The approximation of Cable 1 structure as a planar surface is illustrated in Fig. 1. The first and third layers consist of cable sheath material. The inner layer is a homogenous mixture of the insulation and filler materials. Conductors are not combustible and thus neglected in the model for simplicity and to save computational time in large scale simulations. According our previous simulations, the effect of the conductor on the model performance is not significant. The properties of the 2 cm thick backing layer were ρ = 800 kg/m^3, k_s = 0.1 W/m·K and c_s = 1 kJ/kg·K. Cable 2 model included only one layer of sheath and the backing.

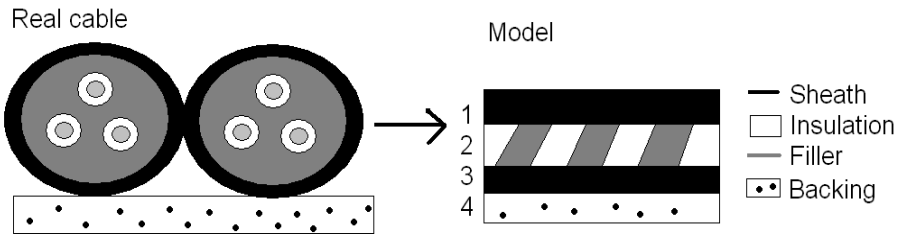

Fig. 1. Principle of creating FDS model of electrical cables in the cone calorimeter.

Model Parameters

The reaction rate formula in Eq. 1 contains three free parameters: A, E, and N_s. In this work, they are called 'kinetic parameters' as they define the reaction kinetics. The remaining free parameters are thermal conductivity k_s, specific heat capacity c_s and the heat of reaction H_r. Other important parameters are the heat of combustion (H_c) and surface emissivity (ε). The heat of combustion is defined as the energy released per unit mass of reacting material in the gas phase combustion. Material-dependent heat of combustion was used to ensure that the correct amount of heat is released. The emissivity was assumed to be equal to surface absorptivity. These parameters are called 'thermal parameters'.

Three commonly used methods for determining the kinetic parameters from TGA data are the analytical and model-free methods and the estimation by optimization. When estimating the parameters by optimization, a model with free parameters is fitted to the experimental results. This method, utilizing e.g. genetic algorithm (GA) as an optimization method, has been used in many of the recent works [4–7]. Genetic algorithms are based on the idea of survival of the fittest. Originally a random set of parameters is tested against the experiment, and the best fitting sets survive to the next iteration round. The method is effective in non-linear problems with several unknown parameters. The algorithm works well with any kind of reaction paths or parameter ranges. The drawback may be a long estimation time, and the stochastic nature of the algorithm. The number of iterations needed cannot be predicted as all the operations depend on the random numbers and probability distributions. This method can be used also for the estimation of other parameters and using other experimental results, such as Cone calorimeter. The GA parameters in this work are the same as used in Ref. [6] except for the mutation rate that was set to 0.25.

An analytical method for the determination of kinetic parameters was introduced by McGrattan et al. [11]. It assumes that all the material components undergo parallel one-step reactions with reaction order 1. This method has an advantage of being very fast; often just a couple of trials are needed. The parameters are calculated from a reference temperature (T_p), reference mass loss ratio (Y_p) and the reference mass loss rate (r_p). The reference temperature is the reaction peak temperature of TGA gradient, and the mass values are the corresponding mass and mass gradient values. According those values, the A and E can be calculated as

$$\begin{cases} E = \dfrac{RT_p^2}{\beta}\dfrac{r_p}{Y_p} \\ A = \dfrac{r_p}{Y_p}\exp\left(\dfrac{E}{RT_p}\right) \end{cases}. \tag{4}$$

The model-free methods are based on simple analytical calculations. Equation 1 can be written as

$$\ln(r_{ij}) - N_s \ln\left(\frac{\rho_{s,i}}{\rho_{s0}}\right) = \ln(A) - \frac{E}{RT_s}. \tag{5}$$

The reaction order N_s is a modelling choice. After choosing N_s, the unknown parameters, A and E can be determined by fitting a straight line to the plot of the left hand side against $1/T_s$. This method is relatively fast and does not assume anything of the reaction order. However, it is quite sensitive for the choice of the temperature area considered and the details of the fitting process. Practical aspects of model-free methods were recently discussed by Kim [12].

Thermal parameters can be either directly measured or estimated from a Cone calorimeter test. Typical measured values are the specific heat capacity and the heat of reaction that can be obtained using DSC. The measurement of thermal conductivity is possible for building materials, for instance, but unpractical for small plastic samples, such as the components of electrical cables, or materials undergoing thermal degradation in the interesting temperature range. The effective heat of combustion, derived from the Cone calorimeter results, can sometimes be used as a material property if the relative proportions of the pyrolyzing materials are known over the time of the experiment. Alternatively, the heats of combustion can be estimated like the other thermal parameters by considering the difference between the measured and simulated effective heats of combustion as one of the measures of model fitness.

RESULTS AND DISCUSSION

Parallel Reactions - Model

The TGA results of the sheath materials of Cables 1 and 2 were found to be very close to each other. Therefore, the kinetic parameters were only estimated for Cable 1 and used for the sheaths of both cables. The sheath material was assumed to be a homogenous mixture of three independent components. A parallel reaction path with free reaction orders was used. A genetic algorithm was used for the estimation. The reaction path and the kinetic parameters are shown in Fig. 2 and the comparison of experimental and simulated TGA results in Fig. 3. The results fit slightly better for Cable 1, for which the parameters were estimated, but the difference to Cable 2 is not large. The reaction paths and kinetic parameters of the Cable 1 filler and insulation materials are shown in Figs. 4 and 5, respectively.

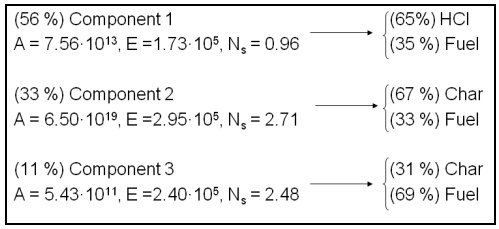

Fig. 2. Parallel model reaction path and kinetic parameters for the cable sheath. A in s^{-1} and E in kJ/kmol.

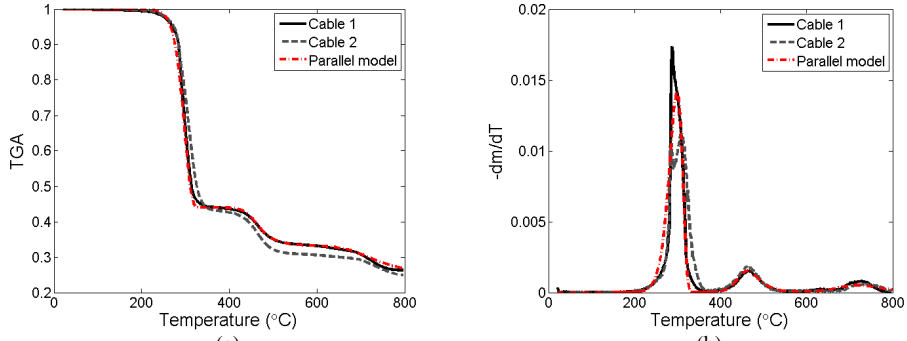

Fig. 3. TGA results (10 K/min) for cable sheaths and FDS fit: (a) TGA; (b) Gradient of TGA.

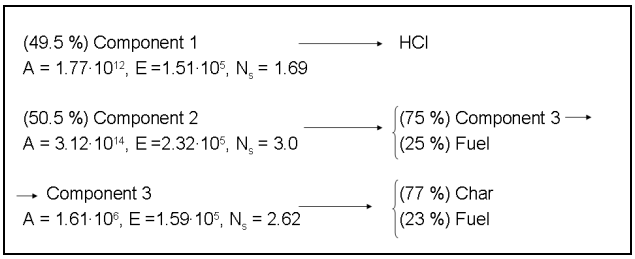

Fig. 4. Reaction path and kinetic parameters for the insulating material. A in s^{-1} and E in kJ/kmol.

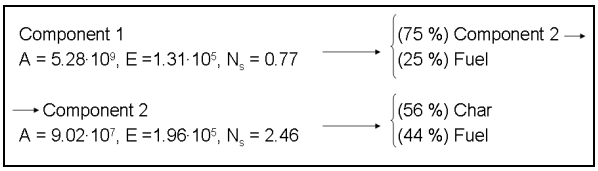

Fig. 5. Reaction path and kinetic parameters for the filler. A in s^{-1} and E in kJ/kmol.

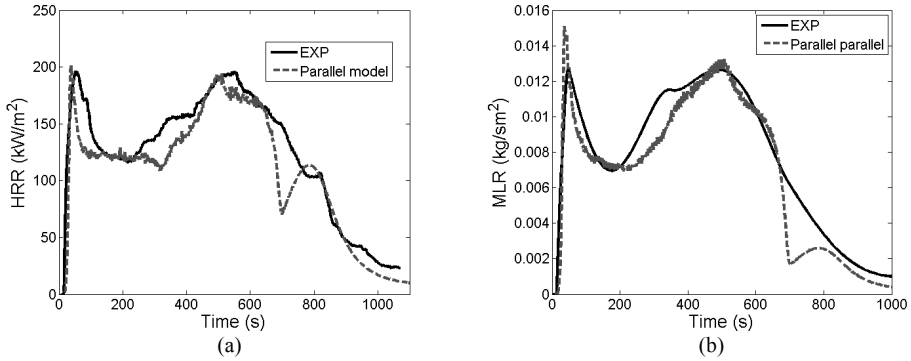

Fig. 6. Comparison of experimental and simulated Cone calorimeter results of Cable 1 at 50 kW/m^2: (a) heat release rate; (b) mass loss rate.

The thermal parameters were estimated from the Cone calorimeter experiments. The emissivities of the initial material components were set to 1.0, but non-unity emissivities were allowed for the chars. This choice was made because earlier sensitivity studies had shown that the results are sensitive to the emissivity of char but not to the emissivity of the virgin material. Besides, the virgin emissivity only plays a role during the short time before the ignition. As the conductivities and the specific heats were treated as constants over temperature, the estimated values must be treated as averages over corresponding temperature ranges. The middle layer of Cable 1 is a mixture of 48.1 % insulator and 51.9 % filler. The layer thicknesses from first to last are 2.73 mm, 3.2 mm and 2.73 mm. A comparison of simulated and measured HRR and MLR is shown in Fig. 6. The model predicts very accurately both the ignition time and shapes of the two peaks in the curves. Including data for different radiation levels would probably reduce the model fitness into a single curve but improve the parameter generality. Inclusion of surface temperature measurement, as in [7], would add another dimension to the fitness assessment. However, performing such measurements for thermoplastic samples with complex structure may be challenging.

For Cable 2, only the sheath layer (2.9 mm thick) was modelled. A comparison of the experimental and model HRR and MLR is shown in Fig. 7. Again, ignition time is accurately predicted and the overall shapes of the curves are satisfactory, although not as accurate as for Cable 1. The thermal parameters are listed in Table 2. Some of the conductivity and heat of combustion values are equal to the lower or upper

bounds of the corresponding estimation ranges. This means that the optimization algorithm could not find a good agreement within the estimation range, and it might be possible to obtain a better fitting model with a wider estimation range. It is interesting that even though the reaction paths and kinetic parameters were identical for the two cables, the thermal parameters resulting from the estimation process turned out be quite different. The most significant difference can be found for H_c of the first component of the sheath. For Cable 1, at 35 % fuel yield it is 40 MJ/kg while for Cable 2 with the same fuel yield only 15 MJ/kg.

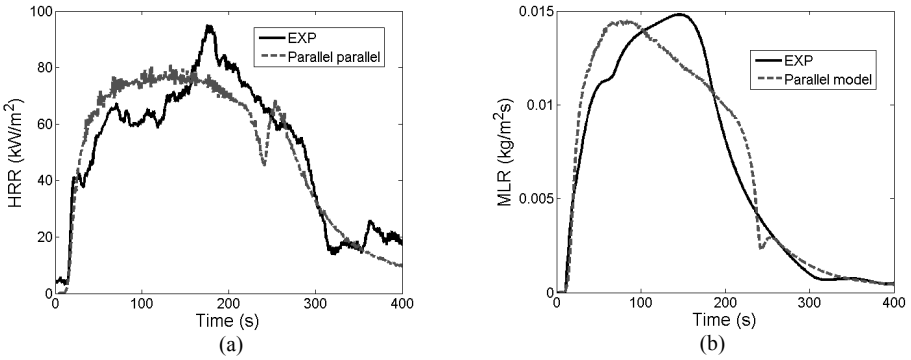

Fig. 7. Comparison of experimental and simulated Cone calorimeter results of sheath of Cable 2 at 50 kW/m^2: (a) heat release rate; (b) mass loss rate.

Table 2. Thermal parameters of the cable models. 'Sheath (N = 1)' of Cable 1 is related to the section Effect of the Kinetic Parameters. The emissivities for Components 1–3 are all 1.0.

	Component 1				**Component 2**			
	k_s (W/m·K)	c_s (kJ/kg·K)	H_r (kJ/kg)	H_c (MJ/kg)	k_s (W/m·K)	c_s (kJ/kg·K)	H_r (kJ/kg)	H_c (MJ/kg)
Cable 1								
Sheath (N free)	0.25	2.0	800	40	0.15	2.8	700	45
Sheath (N = 1)	0.14	3.5	1110	45	0.1[a]	0.8	1760	45[b]
Insulation	0.77	3.3	450	-	0.4	2.5	300	45[b]
Filler	0.65	2.5	800	30	0.45	0.81	300	40
Cable 2								
Sheath	0.1[a]	1.5	1630	15	0.26	1.6	740	23.9
	Component 3				**Residue**			
	k_s (W/m·K)	c_s (kJ/kg·K)	H_r (kJ/kg)	H_c (MJ/kg)	k_s (W/m·K)	c_s (kJ/kg·K)	ε	
Cable 1								
Sheath (N free)	0.15	2.09	700	40[b]	0.9	2.0	1.0	
Sheath (N = 1)	0.42	0.8	950	45[b]	0.8[b]	2.0	0.99	
Insulation	0.79	0.8	300	40	0.67	1.3	1.0	
Filler	-	-	-	-	0.25	1.3	1.0	
Cable 2								
Sheath	0.21	1.37	1860	27.8	0.79	2.0	0.98	

[a] At lower bound of estimation range.
[b] At upper bound of estimation range.

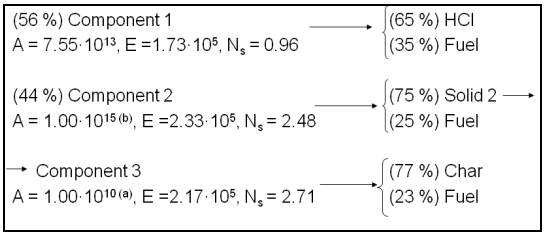

Fig. 8. Consecutive model reaction path and kinetic parameters for the cable sheath; [(a)] at lower bound of the estimation range; [(b)] at upper bound of estimation range.

Effect of the Reaction Scheme

The parallel model the reaction path describing the sheath pyrolysis consists of three parallel reactions, which is the simplest possible model being able to reproduce the three distinct reactions observed in the TGA curve. In the absence of information about the true chemical formulations and reactions, which is often the case in fire modelling, the reaction path is modeller's choice. The only evidence for or against the chosen scheme comes from the fitting process. Alternative schemes, such as a consecutive reaction path, must be evaluated based on their fitting capability and the credibility of the best-fitting model parameters. A consecutive reaction path was therefore applied to the sheath reactions, yielding the kinetic parameters shown in Fig. 8. The estimated values for the pre-exponential factors of components 2 and 3 correspond to the upper and lower bounds of the estimation range, indicating that the algorithm could not find satisfactory fit in the range of these parameters. For better agreement with consecutive reactions, the range of these parameters should be extended. A comparison of the parallel and consecutive model predictions of TGA at 10 K/min heating rate is shown in Figs. 9a–b. Both reaction paths can accurately predict the experimental results. The other model parameters were the same for both models, as listed in Table 2. The effect of the reaction path on the simulated cone calorimeter results is shown in Figs. 9c–f. Even though the TGA curves are quite close to each other, the cone calorimeter results differ significantly. In the consecutive reaction path, the third reaction is limited by the second one. Parallel reaction path does not have this limitation and this could explain the differences in the cone calorimeter results. For Cable 1, the consecutive reaction scheme yields lower heat release and mass loss rates and longer extinction times than the parallel scheme. The differences are in the same direction but less significant for the sheath of Cable 2.

In theory, the degradation of rigid PVC could be modelled as a two-stage process: the first releasing HCl and the second producing combustible fuel vapour and residue. Flexible PVC contains softeners, such as phthalates, with degradation products such as benzene, naphthalene and anthracene that may be combustible and must be considered in the pyrolysis modelling. In the presence of Oxygen and heat these compounds can burn, having a heat of combustion over 40 MJ/kg [13]. In the pyrolysis modelling, the release of combustible products is considered by specifying a non-zero fuel yield for the first reaction of PVC. In the most accurate model for the cable sheaths, the fuel yield of the first reaction was 35 %. The effect of this parameter for the HRR prediction is demonstrated in Fig. 10 showing the HRR results for both cables at three different fuel yields 0 %, 15 % and 35 % of the first reaction step. The smaller-than-optimal yield of fuel can, to some extent, be compensated by adjusting the heat of combustion of the corresponding material. The values should however be chosen from a reasonable range, i.e. smaller or equal to 50 MJ/kg.

In the parallel model, both solid components produce independently fuel and char. One could also choose the mass fractions so that only the second solid reaction produces char, and the other one fuel. The cone calorimeter results are not sensitive to this choice for any of the cable models.

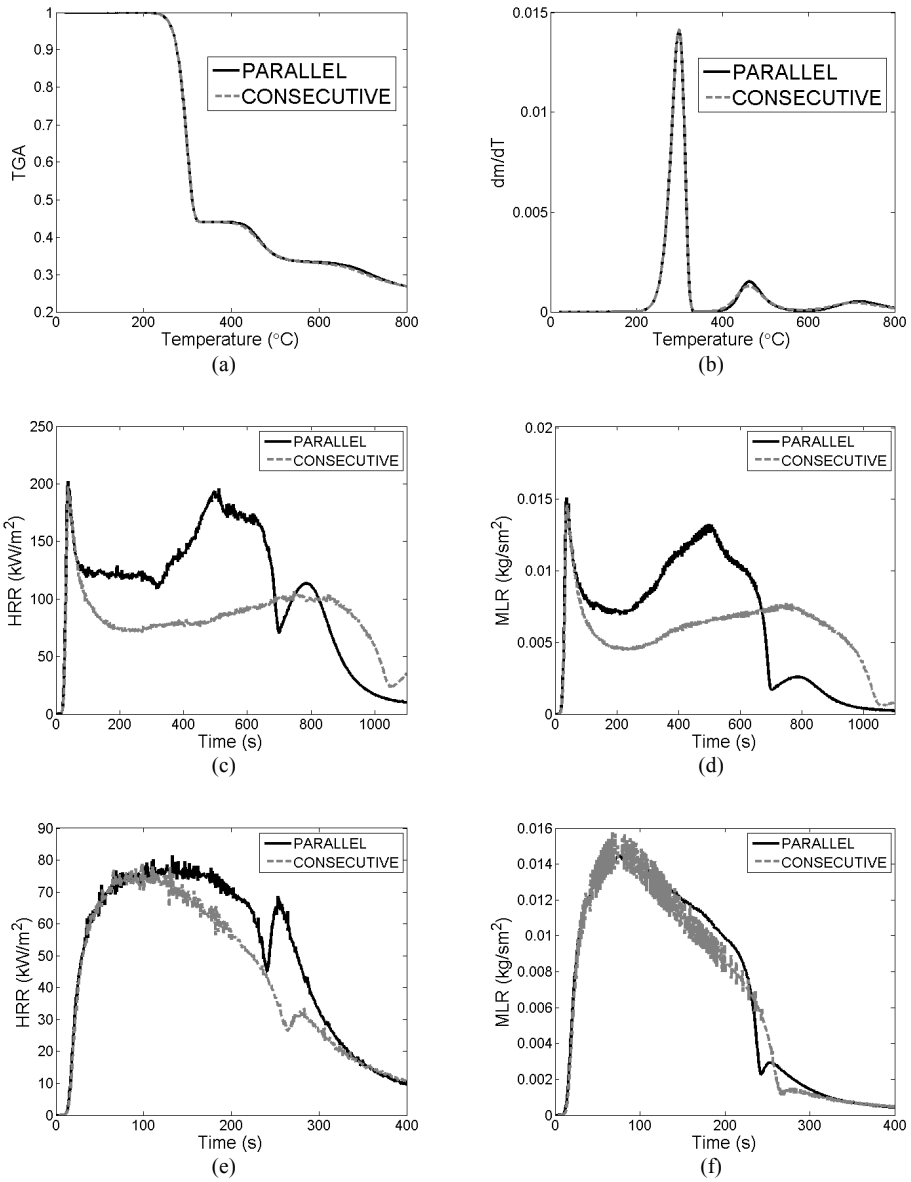

Fig. 9. Sensitivity of the cable pyrolysis for the reaction path in TGA (a and b) and cone calorimeter (c–f): (c) HRR of Cable 1; (d) MLR of Cable 1; (e) HRR of Cable 2 sheath; (f) MLR of Cable 2 sheath.

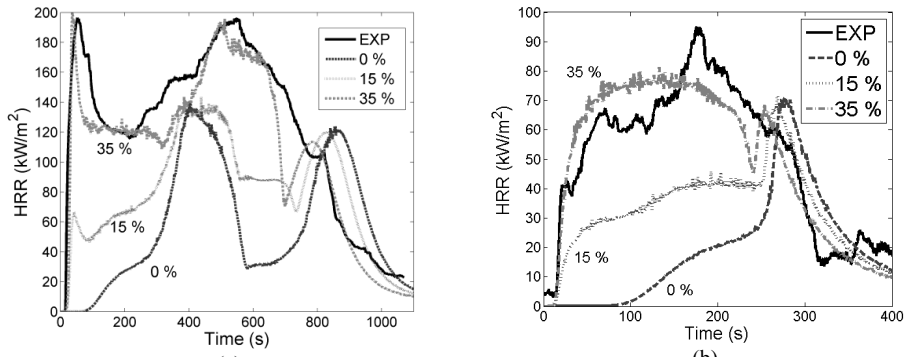

Fig. 10. Effect of first reaction fuel yield at 50 K/min: (a) Cable 1; (b) Cable 2 sheath.

Effect of the Kinetic Parameters

Due to the so-called 'compensation effect', the values of A and E are usually not important just by themselves, but their ratio is significant [14]. Many different sets of kinetic parameters can thus produce equally accurate prediction for TGA results. Two different sets of kinetic parameters were estimated with constraint $N_s = 1$. One was estimated using the genetic algorithm (GA) and another one using the analytical method. The reaction paths were parallel and the differences were only allowed in the kinetic parameters and fuel allocation of the components. The results are shown in Fig. 11 and kinetic parameters listed in Table 3. The TGA predictions are quite similar with the two sets of parameters. Using the thermal parameters listed in Table 2, the cone calorimeter results do not show any significant difference either, indicating that there is no preference over one of the estimation methods. Due to the use of a non-optimized set of thermal parameters, neither of the results shown in Figs. 11c–d are close to the experimental result, though. Both estimation methods have their advantages. The GA takes a longer time than the analytical method, but is more flexible for the changes in the reaction path and the reaction order. The analytical method provides fast results, but the model has to be limited to parallel reaction path with reaction order 1.

A comparison between Table 3 and Fig. 2 shows that the mass allocations between components 2 and 3 have been exchanged. The integrated mass loss and heat release are still quite close to each other due to the different fuel yields. This peculiarity is caused by the nature of the parallel reaction scheme, for which the assignment of reactions between the reactions observed in TGA by the stochastic optimization cannot be pre-determined, if the parameter ranges are wide enough. This should be kept in mind when interpreting the results of the stochastic optimization methods.

Table 3. Kinetic parameters with $N_s = 1$.

	A (s^{-1})	E (kJ/kmol)	Residue yield
Method: GA			
Component 1 (56 %)	1.08×10^{15}	1.85×10^{5}	0 %
Component 2 (11 %)	5.93×10^{11}	1.99×10^{5}	6 %
Component 3 (33 %)	1.08×10^{12}	2.73×10^{5}	83 %
Method: Analytical			
Component 1 (56 %)	9.80×10^{18}	2.24×10^{5}	0 %
Component 2 (10 %)	3.40×10^{36}	5.40×10^{5}	0 %
Component 3 (34 %)	1.67×10^{9}	2.21×10^{5}	79 %

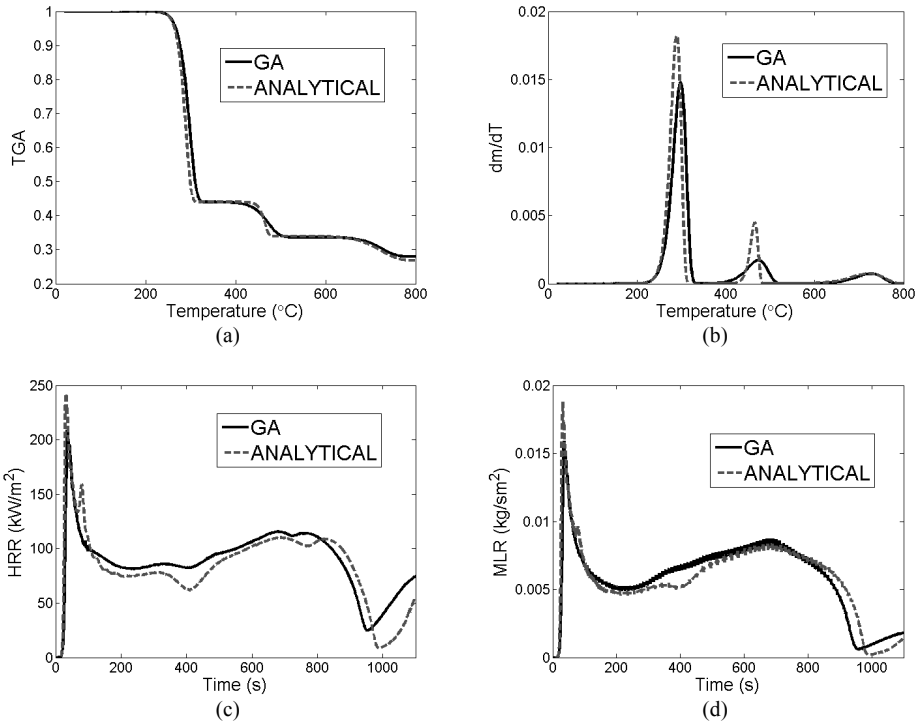

Fig. 11. Sensitivity of the simulation results to different sets of parameters for Cable 1: (a) TGA at 10 K/min; (b) gradient of TGA at 10 K/min; (c) HRR at 50 kW/m^2; (d) MLR at 50 kW/m^2.

The reaction order affects the sharpness of the TGA curve. In Fig. 12, models with two different reaction orders are compared. For 'N free', the kinetic parameters were those shown in Fig. 2 and for 'N = 1', the parameters estimated by GA, shown in Table 3 were used. Thermal parameters were the same in both models (Table 2). TGA curves (Fig. 12a–b) are very close to each other, but the cone results (Fig. 12c–d) show more differences. Both heat release and mass loss rates are higher when N_s is freely chosen. The magnitude of the differences is somewhat surprising, considering the very close match in TGA. The 'N = 1' model gives lower HRR than the version with free N, even though the heat of combustion and all the other thermal parameters are the same. The explanation can be found in the different sources of fuel in these two models, as indicated by Fig. 2 and Table 3. The total fuel yields are the same for the two models (otherwise TGA curves would be different) but the heats of combustion of the components 2 and 3 are different (45 and 40 MJ/kg, respectively, Table 2).

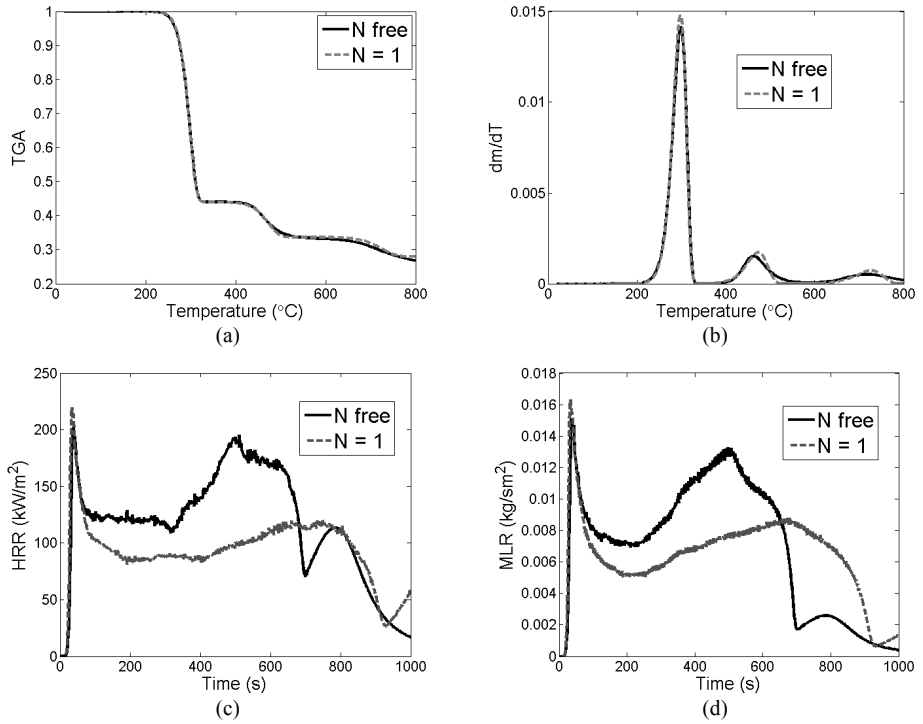

Fig. 12. Comparison of results with different reaction orders for Cable 1: (a) TGA at 10 K/min; (b) gradient of TGA at 10 K/min; (c) heat release rate at 50 kW/m^2; (d) mass loss rate at 50 kW/m^2.

The relatively strong effect that the kinetic parameters have on the cone calorimeter simulation can be 'compensated' by adjusting other parameters. When the thermal parameters for sheath were estimated separately for the both kinetic schemes, 'N free' and 'N = 1', the HRR and MLR predictions (Fig. 13) come very close to each other and closer to the experimental curve. The parameter values, in turn, are significantly different. They are listed in Table 2 as 'Cable 1 Sheath (N = 1)'. The greatest differences are found in the specific heat capacities of the initially existing material components (i.e. not residue), the heat of reaction of the second component and the thermal conductivity of the third component.

From a theoretical viewpoint, it may be discomforting to see that the thermal parameters can 'compensate' for the choices concerning the reaction scheme or the values of the kinetic coefficients. This problem should be examined from the viewpoint of the experimental and model uncertainty: If one wants to test the capability of a model to explain observed experimental evidence, one must also take into account the uncertainty associated with the experimental data and conditions, and the model input parameters. If the model can or cannot be fit to the test data within the given uncertainty bounds of the thermal parameters, that is all we can say. Of course, if one can directly measure any of the parameters with a sufficient accuracy, the size of the parameter space would be reduced, and the weight of the given scenario increased as an evidence of the model validity. Direct measurements of the properties are therefore highly recommended whenever possible.

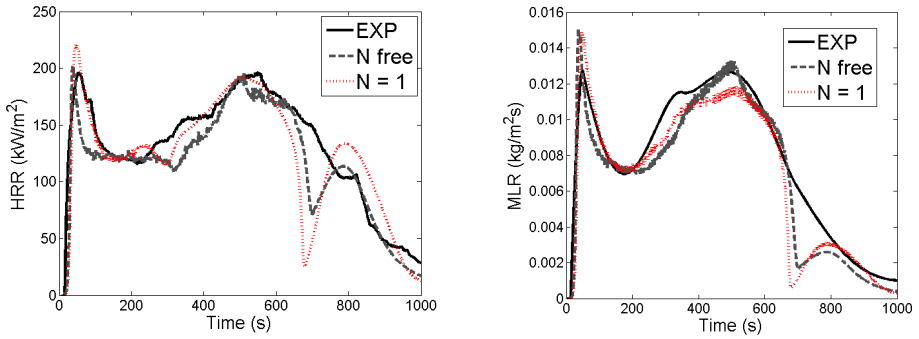

Fig. 13. Cone calorimeter results at 50 kW/m^2 with separately estimated thermal parameters for the two sets of kinetic parameters: (a) heat release rate; (b) mass loss rate.

CONCLUSIONS

The effects of the modelling decisions and methods on the pyrolysis modelling of two PVC cables were studied. The kinetic and thermal parameters were estimated from the TGA and cone calorimeter experiments. The TGA results of the cable sheaths were so close to each other that the same kinetic parameters were used for both cables. With three structural components describing the structure of the complete cable (sheath, insulation and filler) and two to three material components for each structural components, the estimation algorithm was able to find a set of parameters that accurately reproduced the mass loss and heat release rate curves at one radiation level.

The effect of the reaction path was studied by comparing the results obtained with parallel and consecutive reaction schemes. The effect on the TGA results was shown to be very small. However, a substantial effect was observed in the cone calorimeter results, where the consecutive scheme produced significantly lower heat release and mass loss rates. The plasticizers that are used in the production of flexible PVC were found to have a strong effect on the early part of the HRR curves. These additives can make up 30–40 wt. % of the flexible PVC, and should therefore be taken into account in the pyrolysis model as a non-zero fuel yield for the first degradation reaction. The exact allocation of the fuel between the components was found to be unimportant, as long as the correct yields of fuel and residue were retained.

When first-order reactions were assumed and two sets of parameters estimated, no significant differences were found. Both estimation methods accurately reproduced the TGA curve. The different values of reaction order made more difference. The TGA predictions were almost equal, but the heat release and mass loss were greatly reduced when the reaction order was forced to one without estimating a separate set of thermal parameters. When the separate thermal parameters were estimated for the two different sets of kinetic parameters, equally good fits to the experimental data were again achieved, but the estimated values of the thermal parameters were very different.

The reaction path, estimation method and the parameter sets can be chosen in many ways when estimating the pyrolysis model parameters from the cone calorimeter results. Thermal parameters can, to some extent, compensate the choices made for the kinetic model. Nothing implies that one way to make the choice would be better than another. This is a topic that requires more research and discussion. However, the results demonstrate that the thermal parameters estimated for one kinetic model should not be used for another, unless the difference between the kinetic models considers only fuel yields or different pairs of A and E with same N_s. It is very important to check the model behaviour when changing the model details or the simulation code version. Also, the universality of the thermal parameters could be improved by considering a wider set of experimental data during the parameter estimation process, such as sample temperatures, different heat flux levels and different atmospheres.

ACKNOWLEDGEMENTS

This work has been partially funded by the State Nuclear Waste Management Fund (VYR). Authors would like to thank Tuula Leskelä from Aalto University School of Science and Technology for the thermogravimetric experiments, and Konsta Taimisalo and Johan Mangs from VTT for help when conducting cone calorimeter experiments.

REFERENCES

[1] DeLassus, P.T., and Whiteman, N.F., "Physical and Mechanical Properties of Some Important Polymers," *Polymer Handbook (4th ed.)*, Brandrup, J., Immergut, E.,H. Grulke, E.A., Abe, A., Bloch, D.R. (ed.) Wiley, New York, 1999, pp. 159-169.

[2] Papazoglou, E., Flame Retardants for Plastics. *Handbook of building materials for fire protection*, Harper, C.A. (ed.), McGraw-Hill, New York, NY, 2004. pp. 4.1-4.88.

[3] Marcilla, A., and Beltrán, M., (1995) Thermogravimetric kinetic study of poly(vinyl Chloride) pyrolysis. Polymer Degradation and Stability 48: 219-229. http://dx.doi.org/10.1016/0141-3910(95)00050-V

[4] Lautenberger, C., Rein, G., and Fernandez-Pello, C., (2006). The application of a genetic algorithm to estimate material properties for fire modeling from bench-scale fire test data. Fire Safety Journal 41: 204-214. http://dx.doi.org/10.1016/j.firesaf.2005.12.004

[5] Rein, G., Lautenberger, C., Fernandez-Pello, C., Torero, J., and Urban, D., (2006). Application of genetic algorithms and thermogravimetry to determine the kinetics of polyurethane foam in smoldering combustion. Combustion and Flame 146: 95-108. http://dx.doi.org/10.1016/j.combustflame.2006.04.013

[6] Matala, A., Hostikka, S. and Mangs, J., 2009. Estimation of Pyrolysis Model Parameters for Solid Materials Using Thermogravimetric Data. *Fire Safety Science* 9: 1213-1223. http://dx.doi.org/10.3801/IAFSS.FSS.9-1213

[7] Lautenberger, C., and Fernandez-Pello, C., (2009) Generalized pyrolysis model for combustible solids. Fire Safety Journal 44: 819-839. http://dx.doi.org/10.1016/j.firesaf.2009.03.011

[8] Chaos, M., Khan, M.M., Krishnamoorthy, N., de Ris, J.L., and Dorofeev, S.B., "Evaluation of optimization schemes and determination of solid fuel properties for CFD fire models using bench-scale pyrolysis tests," *Proceedings of the Combustion Institute 33 (2)*, 2011, pp. 2599-2606. http://dx.doi.org/10.1016/j.proci.2010.07.018

[9] Baroudi, D., 1993. "Piecewise least squares fitting technique using finite interval method with Hermite polynomials," VTT Technical Research Centre of Finland, VTT Publications 135, Espoo, Finland. 27 p.

[10] McGrattan, K., Hostikka, S., Floyd, J., Baum, H., Rehm, R., Mell, W., and McDermott, R., "Fire Dynamics Simulator (Version 5) Technical Reference Guide. Volume 1: Mathematical Model," NIST Special Publication 1018-5. Gaithersburg, MD, 2010.

[11] McGrattan, K., McDermott, R., Mell, W., Forney, G., Floyd, J., Hostikka, S., and Matala, A. "Modeling the burning of complicated objects using Lagrangian particles," *Proceedings of the Twelfth International Interflam Conference*, 2010, pp. 743-753.

[12] Kim, E., Shivkumar, S., and Dembsey, N., "Thermal degradation kinetics modeling for pyrolysis modeling using fire retarded thermoset polymer resins," *Proceedings of the Twelfth International Interflam Conference*. 2010, pp. 475-486.

[13] Appendix C. DiNenno, P.J. (ed.) *SFPE Handbook of Fire Protection Engineering* (4th ed.), National Fire Protection Association, Quincy, MA 02269, 2008.

[14] Nikolaev, A.V., Gorbatchev, V.M. and Logvinenko, V.A. (1974) Special features of the compensation effect in non-isothermal kinetics of solid-phase reactions, Journal of Thermal Analysis 6: 473-477. http://dx.doi.org/10.1007/BF01914927

PUBLICATION IV

Modelling polymeric material using Microscale combustion calorimetry and other small scale data

Manuscript,
submitted to Fire and Materials
in June 2013.

MODELLING POLYMERIC MATERIAL USING MICROSCALE COMBUSTION CALORIMETRY AND OTHER SMALL SCALE DATA

Anna Matala and Simo Hostikka
VTT Technical Research Centre of Finland
P.O. Box 1000, FI-02044 VTT
anna.matala@vtt.fi

Keywords: pyrolysis modelling, Microscale combustion calorimetry, cables, PVC

Abstract

A challenge encountered by many practicing fire engineer carrying out fire modelling is that the combustible fuel is not completely well-known. Practical materials may, for instance, be identified as some well-known polymer, but this is usually not the whole truth from the viewpoint of the fire behaviour. Besides of the nominal polymer, the blend may include large quantities of different additives that affect the thermal degradation and combustion of the material. Until now, the effect of these additives has been taken into account in the modelling by adjusting the thermal parameters when fitting the model to the cone calorimeter results. Such a model captures the joint effect of all the components, but cannot distinguish between the combustible volatiles from additives and main polymer, which may lead to inaccurate prediction if the conditions, such as the heating rate, are significantly different. In this work we use Microscale Combustion Calorimetry for building a more accurate model of the polymer pyrolysis by combining the heat release rate measurements with the mass loss rate measured in Thermogravimetric Analysis. Two methods are developed and tested using a generic sample and a real PVC sheath of an electric cable. The results show that the methods are able to calculate the heat release rate correctly for the tested materials, and also estimating the sample composition to some extent.

Symbols

A	Pre-exponential factor (s^{-1})	*Greek*	
c_p	Specific heat capacity (kJ/kg/K)	α	Conversion
E	Activation energy (kJ/mol)	β	Heating rate (K/s)
ΔH	Heat of reaction (kJ/kg)	ε	Emissivity
ΔH_c	Heat of combustion (kJ/kg)	ρ	Density (kg/m^3)
k	Thermal conductivity (W/m/K)		
m	Mass (kg)	*Subscripts*	
$\dot{m}$	Mass loss rate (kg/s)	0	Initial
n_c	Number of components	eff	Effective value
n_{O2}	Reaction order of oxidation	F	Fuel gas
n_p	Number of (gaseous) products.	i	Reaction index
n_r	Number of reactions	I	Inert gas
N	Reaction order	j	Component index
Q_c	Heat release (kJ)	Z	Residue
$\dot{Q}_c$	Heat release rate (kW)		
Q/m_0	Total heat release in MCC (MJ/kg)		
Z	Residue yield (of total mass)		
T	Temperature (K)		

ΔT Temperature range
X_{O2} Oxygen volume fraction
y yield
Y Mass fraction

INTRODUCTION

Polymeric materials often include large amount of additives besides of the nominal polymer. The electrical cables, for instance, contain significant mass fractions of plasticizers, stabilizers and fillers. These additives are not reported by the manufacturer, and their concentrations are business secrets. This is a challenge commonly encountered by practicing fire engineer carrying out fire modelling. The problem is most pronounced in situations where the composition of the combustibles is not known at all, such as the fire investigation. The same problem is also faced when modelling industrial fires where the fuel may be formally known. The actual contents of the commercial material may be a very complicated blend of polymers and additives, as illustrated above for the electrical cables. A full chemical analysis of the combustible fuels could be used to reveal the contents of the fuels, at least qualitatively, but carrying out such an analysis would be impractical for many reasons. Simple and robust methods are therefore needed to determine the relevant pieces of information to support the fire modelling.

In this work, we use electrical cables as an example of material to be modelled. The additives of the cable components (e.g. phthalates, a plasticizer) are often combustible and may have other joint effects on the polymer degradation as well. In the pyrolysis modelling of the cable materials, these additives are usually taken into account simply by fitting the model to the experimental data [1]-[3]. The cone calorimeter has been until now the most commonly used experimental method that measures the heat release rate. The problem in cone calorimeter scale is that it only provides information about the effective heat of combustion, the joint effect of all the components degrading simultaneously. It does not provide information about the degradation temperatures or separate the heat release by reactions or components, which make the distinguishing between the components challenging.

Microscale Combustion Calorimetry (MCC) is a relatively new, experimental small scale device that was developed at Federal Aviation Administration (FAA) [4],[5]. It provides information about the heat release as a function of temperature, similarly to Thermogravimetric Analysis (TGA). By combining the information about mass loss and the simultaneous heat release, the heat of combustions of each reaction can be determined. Moreover, this information can be used in estimation of the sample composition and mass fractions.

In this work, the heat release rate measured by MCC is combined with mass loss measured by Thermogravimetric Analysis (TGA) at each reaction step. Two alternative methods are presented for building a reaction path using these results. The first one is a general model, which does not require any knowledge of the actual polymeric mixture. The second method is targeted for building a more complete and accurate model, and requires information about typical additives and their thermal degradation and heat of combustion. The results of both methods help to allocate the sample heat release to correct temperatures. Additionally, the second method can be used to estimate the mass fractions of main components in a polymer blend. These methods are applied to a generic sample in order to verify and validate the methods, and to a real PVC sheath of an electric cable. The results are compared in small and bench scale using experimental data and numerical simulations. The effect of surface oxidation is also taken into account in the cone calorimeter simulations.

METHODS

Experimental methods

TGA is the most common small scale experiment for determining the reaction kinetics of the pyrolysis reaction. In TGA, a small sample (5-10 mg) is placed into a furnace that has either air or nitrogen atmosphere. The furnace is heated linearly at relatively slow heating rate, typically at 1-30 K/min. The small sample and slow heating rate ensure that the sample is in thermal equilibrium with the furnace. The mass of the sample is measured during the heating, and the experiment results the mass loss as a function of temperature. [6]

MCC, also known as *Pyrolysis-combustion flow calorimetry*, was developed at FAA in the beginning of the millennium [4],[5]. A small sample (5-10 mg) is placed into a pyrolyzer that operates similarly to TGA under either inert of oxidative ambient. The heating rates are higher than typically in TGA experiment, usually 1 K/s. The pyrolysis gases are then led to a combustor that has high temperature (up to 1000 °C) and sufficient oxygen ambient. The gases are completely combusted in few seconds, and the result is the heat release rate (often scaled with the sample mass) as a function of temperature.

Cone Calorimeter is the most commonly used bench scale experiment in fire research. A 10 x 10 cm^2 sample is placed under a cone heater that directs a heat flux of 35-75 kW/m^2 to the sample surface. The sample is ignited using an electric spark. During the experiment, mass and heat release rates are measured. [7]

Combining TGA and MCC results

MCC measures the heat release rate scaled by the initial mass of the sample. For complete burning at heat of combustion ΔH_c and fuel yield $y_{i,F}$, the result can be expressed as

$$\frac{\dot{Q}_{c,i}}{m_0} = \frac{\dot{m}_{i,F}}{m_0}\Delta H_{c,i} = \frac{\dot{m}}{m_0} y_{i,F}\Delta H_{c,i}, \qquad (1)$$

where m_F corresponds to the mass loss that is responsible of the heat release (the production of the fuel gas). The total heat release of the reaction i (when temperature range of the reaction is T_{i-1} - T_i) can be written

$$\frac{Q_{c,i}}{m_0} = \int_{t_{i-1}}^{t_i} \frac{\dot{Q}_c}{m_0} dt = y_{i,F}\Delta H_{c,i} \int_{t_{i-1}}^{t_i} \frac{\dot{m}}{m_0} dt\,. \qquad (2)$$

The material is considered to be composed of j pseudo-components that each degrades in one or more reactions yielding potentially fuel gas (combustible), inert gas (e.g. water vapour) and residue. The yields of the products are denotes as y_{ijF}, y_{ijI} and y_{ijZ}, respectively. Naturally a component may yield several different fuel gases during one reaction, but in the accuracy of the model only the gross effect is significant. The total conversion ($\alpha = 1 - \frac{m}{m_0}$) of the reaction is

$$\Delta\alpha_i = \int_{t_{i-t}}^{t_i} \frac{\dot{m}}{m_0} dt = \frac{m_i - m_{i-1}}{m_0} = \sum_j (y_{ijF} + y_{ijI}) x_j, \qquad (3)$$

where x_i is the mass fraction of the component j. The overall fuel yield of the reaction is therefore

$$y_{iF} = \frac{Q_{c,i} / m_0}{\Delta H_{c,i} \Delta \alpha_i}. \qquad (4)$$

These results can be used in several ways, depending on the provided background information about the sample material. Therefore two methods were developed: *Method 1* is a general method for an unknown sample material. It does not require any information about the sample, just few assumptions by the user. *Method 2* targets to a more complete model with accurate information about the sample components. It makes assumptions about the reaction paths of the thermal degradation of the components and, in the best case, it can be used for determining the composition of the material.

Method 1 (blind approach)

For method 1, we assume that each reaction represents one pseudo-component, which release at most one fuel and one inert gas ($y_{i,F}+y_{i,I} = 1$ when $i<n_r$). Only the last reaction ($i = n_r$) yields also char. The reactions are well separated in time and each component degrades independently from the others. The modeller has to decide only two factors: The fuel gas (or the heat of combustion) and the inert gas (or the molar mass). These gases are assumed to be the same for all components and reactions. The reaction path of the Method 1 is shown in Figure 1.

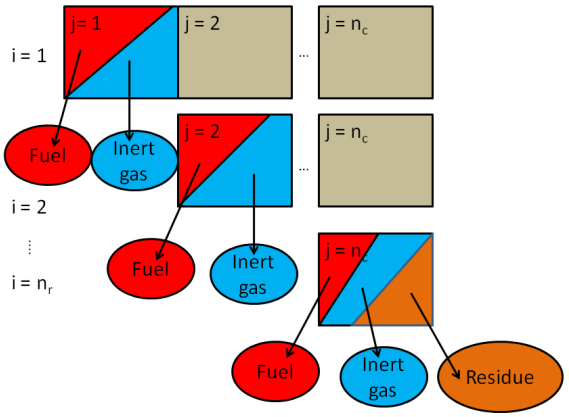

Figure 1. The reaction path assumption in Method 1.

The method is very straightforward: Since the mass loss of the reaction i ($i<n_r$) is equal to the mass fraction of the pseudo-component (x_i), eq. (4) can be used straight. For each reaction, an integral of the heat release rate, mass loss of the reaction and the constant heat of combustion are needed. For the last, residue yielding reaction the yields are calculated as

$$\begin{cases} y_{n_r F} = \dfrac{(Q_{c,n_r}/m_0)}{\Delta H_c \Delta\alpha_{n_r}}\left(1-\dfrac{Z}{1-\sum_{i=1}^{n_r-1}\Delta\alpha_i}\right) \\ y_{n_r I} = \left(1-\dfrac{(Q_{c,n_r}/m_0)}{\Delta H_c \Delta\alpha_{n_r}}\right)\left(1-\dfrac{Z}{1-\sum_{i=1}^{n_r-1}\Delta\alpha_i}\right) \\ y_{n_r Z} = 1-y_{n_r F}-y_{n_r I} = \dfrac{Z}{1-\sum_{i=1}^{n_r-1}\Delta\alpha_i} \end{cases}. \qquad (5)$$

Method 2 (advanced approach)

For method 2, an initial evaluation of the material composition has to be made. This method tries to follow the real reaction paths of the main components as accurately as possible while avoiding unnecessary complex model. The main components are those mainly responsible of the mass loss and heat release. Their typical reaction path and thermal degradation of the components can be studied from the literature. It assumed, that each component degrades in one or more reactions yielding several gases (both fuel and inert) and residue. The heat of combustion of inert gas is 0. Serial reaction paths are also possible, and several components may degrade simultaneously in the same reaction. A possible reaction path of the method 2 is shown in Figure 2.

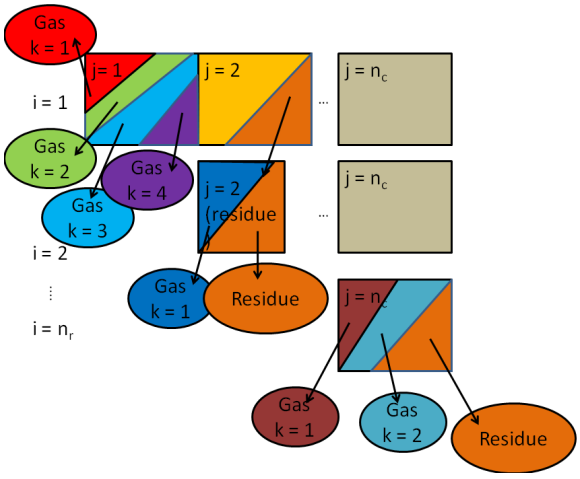

Figure 2. A possible reaction path in method 2.

The total heat release in each reaction *i* is estimated as

$$\hat{Q}_i = \sum_{j=1}^{n_c} \sum_{k=1}^{n_{p,j}} Y_{i-1,j} y_{i,j,k} \Delta H_{c,k} \ , \tag{6}$$

where $Y_{i,j}$ is the remaining mass fraction of the component j after reaction i. It is calculated from the initial mass fraction ($Y_{0,j}$) as

$$Y_{i,j} = \prod_{ii=1}^{i} y_{ii,j,Z} Y_{0,j} \ . \tag{7}$$

The estimate for the conversion (or mass loss) is

$$\Delta\hat{\alpha} = \sum_{j=1}^{n_c} \sum_{k=1}^{n_{p,j}} y_{i,j,k} Y_{i-1,j} \ . \tag{8}$$

The composition (initial mass fractions) can be solved by minimizing the error between the measured values and the calculated estimates as in

$$\min \sum_{i=1}^{n_r} \left(\frac{\left|\Delta a_i - \Delta\hat{a}_i\right|}{\Delta a_i} - \frac{\left| Q_i / m_0 - \hat{Q}_i \right|}{Q_i / m_0} \right). \tag{9}$$

This optimization problem can be solved e.g. using Matlab (function *fminsearch*) or Excel (solver). The solutions of the software depend strongly on the initial values. Therefore a Matlab script was generated to test several random initial values from the pre-defined range. The solution with smallest error is then selected as the final solution. The script is very fast to run; the time to perform 1000 iterations is few minutes.

The original mass fractions can also have some constrains according to the typical concentrations in similar applications. Sometimes the components or their products may react together resulting different reaction paths than the components individually. Also the reaction rate and other experimental circumstances are known to affect on gas and residue yields.

Numerical simulations

For verification and validation purposes, the TGA, MCC and cone calorimeter experiments were modelled using Fire Dynamics Simulator (FDS). All the numerical simulations are performed using FDS version 6.0 (release candidate 4, svn 15111) [8].

If the thermal equilibrium is maintained in TGA, it can be simulated using a 0-dimensional model. In order to make a 0-dimensional model of the sample with FDS, which is basically a 2 or 3-dimensional flow solver coupled with 1-dimensional pyrolysis model, the physical dimensions of the TGA were significantly altered to decouple the gas phase conditions from the sample response. In practice, the TGA sample modelled as a 0.1 mm thick slab with surface area of 2 m^2. The dimensions of the simulation domain were 4 m x 1 m x 1 m. All the gas phase reactions were prevented (nitrogen ambient), thus removing the dependence of the simulation on the gas phase cell size. The surrounding walls were heated linearly according to a slow, pre-determined heating rate from 20°C to 820°C. The thickness of the sample was small enough to keep it in thermal equilibrium with the environment. This was verified by measuring the temperatures of both the sample and the walls. The mass of the sample was monitored during the heating.

MCC experiment is identical to the TGA model in geometry, sample definition and omitting the gas phase calculation. The heat release rate is calculated as

$$\dot{q} = \dot{m}\Delta H_c . \qquad (10)$$

The heat release rate could be measured also directly by allowing gas phase calculation. However, then the grid cell size would be important parameter for the accuracy of the results, and the calculation would become significantly slower. The domain should also be divided to inert and oxidative ambient, which would increase the domain size even further. Therefore, this simplistic method for MCC experiment is chosen.

When the simulated TGA and MCC results are compared, it can be observed that in FDS the high heating rates move the reaction to higher temperatures. This behaviour can be observed in the experiments as well, but not nearly as much. The sample is in thermal equilibrium with the furnace, as can be observed in Figure 3 a. However, the increasing the heating rate of a simulation from 10 K/min to 60 K/min moves the curve about 50 K to higher temperatures (Figure 3b). This can be explained with the kinetic parameters. Sometimes, the reaction is slow compared to the heating rate. Although the reaction rate of the thermal degradation reaction is independent on the reaction rate, the temperature of the sample increases faster than the reaction can occur. Therefore at high heating rates it seems like the reaction has moved to higher temperatures.

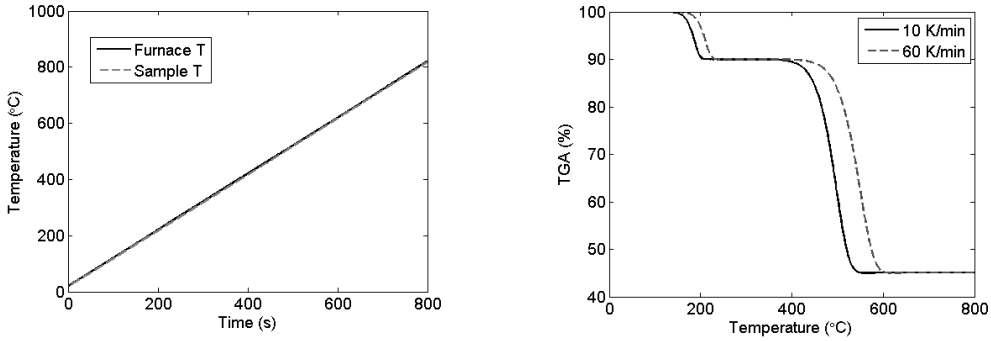

Figure 3. Results of TGA/MCC simulation. a) Comparison of furnace and sample temperature at 60 K/min. b) TGA at 10 and 60 K/min.

In cone calorimeter experiments usually the cable is tested as whole, not divided into components as in the small scale experiments. The cables and all other complex structures are modelled as rectangular slabs. That works relatively well in coarse applications, but the solution is always limited by the grid size. Also the geometry is strongly simplified when the cylindrical object consisting of multiple components is treated as a laminate of separate, rectangular layers. This model has a domain of 0.3x0.3x0.4 m^3 and grid size of 5 cm. The grid size is quite coarse but it should be similar to the one in the final application. The cone heater is modelled as an external heat flux (50 kW/m^2) directed to the surface of the sample. The structure of the layers is symmetric.

MATERIALS

Generic materials

Three generic materials are developed. These samples represent ideal samples, where all reaction steps are well-defined and known. They do not correspond to any real material, and the parameters are listed only for completeness. Generic sample 1 is used to verify the calculations and simulation methods in a very simple case. The Generic sample 2 is made for verification with a more complex case where the first reaction has a small mass loss with high heat of combustion, and the second

reaction high mass loss with low heat of combustion. The accuracy of the reaction path for a PVC-like material is assessed with Generic sample 3. Other than kinetic parameters are same for all the samples and components, including char ($\varepsilon = 1.0$, $c_p = 1.0$ kJ/kg·K, $k = 1.0$ W/m·K, $\rho_0 = 100$ kg/m^3, $\Delta H = 0$ kJ/kg).

Generic 1 is the simplest test case with only one reaction step. It yields 0.9 of the mass fuel gas with heat of combustion 35 MJ/kg. The parameters are listed in Table 1 .

The second test case, Generic 2, yields little mass and lots of energy at the first reaction step, and the second releases lots of mass and little energy. The reaction parameters are listed in Table 1 and visually shown in Figure 4a.

For testing the method for more complex sample, a third generic material (Generic 3) is used. The kinetics or other parameters do not represent any specific material, and the kinetic parameters of components 1 and 3 are identical to those of Generic 2. The reaction path resembles the one of plasticized PVC. It has two initial components (Comp 1 and Comp 2) as the PVC polymer and the plasticizer. They start to thermally degrade in close to the same temperatures. The earlier reaction yields some fuel gas, inert gas (as Hydrocloric acid (HCl) in PVC) and residual polymer that degrades further in higher temperatures. The second initial component releases fuel gas and no residue during the first reaction step. All the parameters are listed in Table 1 and the simulated results are shown in Figure 4b.

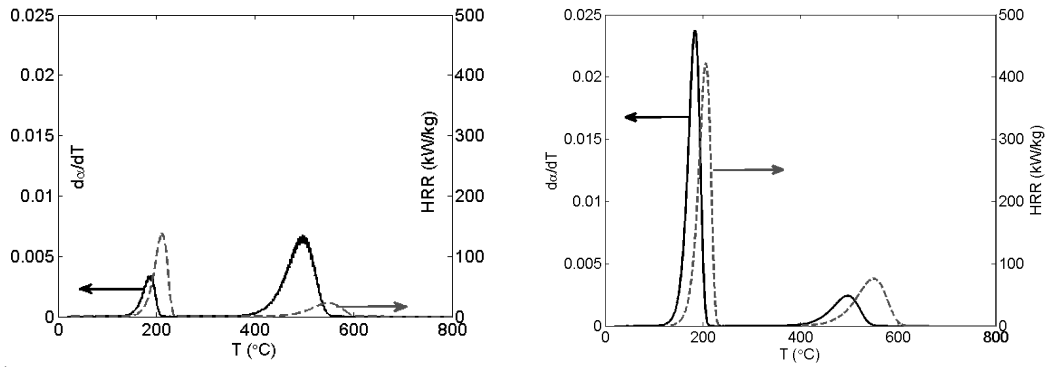

Figure 4. Generic samples. TGA results are shown on the left axes and MCC results on the right. a) Generic 2 sample. b) Generic 3 sample.

Table 1. Reaction parameters and resulting mass loss and energy release of each reaction for the generic samples 1, 2 and 3.

	Generic 1	*Generic 2*		*Generic 3*		
	Comp 1	*Comp 1*	*Comp 2*	*Comp 1*	*Comp 2*	*Comp 3*
Mass fraction in virgin material	1.0	0.5	0.5	0.7	0.3	0.0
A (s^{-1})	$1.0 \cdot 10^{10}$	$1.0 \cdot 10^{15}$	$1.0 \cdot 10^{10}$	$1.0 \cdot 10^{15}$	$1.0 \cdot 10^{16}$	$1.0 \cdot 10^{10}$
E (J/mol)	$1.6 \cdot 10^{5}$	$1.48 \cdot 10^{5}$	$1.8 \cdot 10^{5}$	$1.48 \cdot 10^{5}$	$1.55 \cdot 10^{5}$	$1.8 \cdot 10^{5}$
gas yield	0.9 (fuel)	0.2 (fuel)	0.1 (fuel) 0.8 (inert)	0.02 (fuel) 0.58 (inert)	1.0 (fuel)	0.6 (fuel)
ΔHc (MJ/kg)	35	45	35	30	35	42
Residue?	Char	Char	Char	Comp 3	No residue	Char
Peak Temperature (°C) at 10 K/min	420	180	500	180	180	500
Δα	0.9	0.1	0.45	0.72		0.17

Q/m_0	31.5	4.5	1.75	13.02	5.88

PVC sheath

Real plasticized PVC can be significantly more complex than the generic example presented above. Therefore the methods are applied to a real thermoplastic cable with PVC sheath and PE insulation. The cable is the number #701 in the Christifire campaign (GENERAL CABLE® BICC® BRAND SUBSTATION CONTROL CABLE 7/C #12AWG 600V 30 MAY 2006). It has 7 conductor and diameter of 14 mm. All the other details can be found from the ref. [9]. The experimental data set included TGA results at 10 K/min and three repeated MCC results at 60 K/min for sheath and insulation. The experimental small scale results are listed in Table 2. In addition, cone calorimeter results at 25 KW/m^2, 50 KW/m^2 and 75 KW/m^2 were available. The experimental results for the PVC sheath are shown in Figure 5. An average of the three repetitions of the MCC experiment was used.

Table 2. Experimental results for PVC sheath and PE insulation of cable #701.

	Sheath			Insulation		
	Reac 1	Reac 2	Reac 3	Reac 1	Reac 2	Reac 3
$\Delta\alpha$	0.600	0.137	0.040	0.570	0.120	0.052
Q/m_0 (MJ/kg)	9.195	4.905	0.000	8.233	4.770	0.000

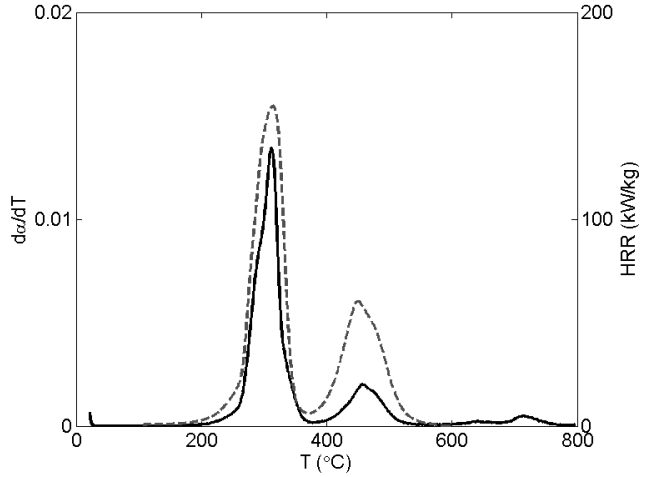

Figure 5. Experimental TGA (10 K/min) and MCC (60 K/min) results for PVC sheath. The experimental results are slightly filtered.

Understanding the basics of PVC blend degradation is important if more accurate reaction path is required. The theoretical background of the degradation of PVC and the most significant additives is therefore briefly presented here.

The thermal degradation of pure and plasticized PVC has been studied widely in the literature, experimentally ([10]-[16]) and numerically ([15]-[21]). Overall, the thermal degradation of the PVC is a two stage process. The first reaction around 320 °C is often called dehydrochlorination reaction, because it is mainly responsible of release of HCl. The remaining polyene structure starts degrading immediately releasing small amounts of aromatic hydrocarbons, mainly benzene. The second major reaction occurs around 450 °C, and is the pyrolysis of the polyene residue. The main product of this reaction is toluene. [10],[12],[17] Studied in vacuum [16], the mass loss of the first reaction was 64

%, which is higher than the stoichiometric value 58.7 %. Therefore the amount of benzene release in the first reaction was 5.3%. The mass loss of the second reaction was 30.3 % leaving 5.7 % residue.

Various additives have effect on the thermal degradation of PVC. The most important additive in many PVC applications (including cables) is the plasticizer. The concentrations can be as high as 100 phr (parts per hundred parts of resin). There are several commercial plasticizers available, and one of the most commonly studied of them is Di-2-ethylhexyl phthalate (DOP). Marcilla and Beltrán compared pure samples of DOP and PVC resin to mixtures at different concentrations and heating rates [15]. The plasticizer degrades around the same temperatures as the dehydrochlorination reaction, but carefully looking two peaks can be observed; DOP evaporates slightly before HCl. When the peak temperatures are compared, it can be seen that in mixture the reactions are closer to each other, almost overlapping: DOP evaporates slightly later, and HCl slightly earlier than separately. Low concentrations of DOP decrease this effect. Also, at higher heating rates the decrease in resin degradation temperature is not as significant as at the lower heating rates. One explanation for the decreasing HCl release temperature is that when the DOP evaporates, it leaves holes to the polymer blend structure. These holes are the initiation centres of the dehydrochlorination process and the reaction becomes faster. Another explanation is that the radicals formed around 300 °C at the DOP evaporation promote the reaction. DOP is also known to partially inhibit the release of the aromatics formation. [12],[13],[15]

PVC blend also includes some amount of fillers. Calcium Carbonate ($CaCO_3$) is the most commonly used with PVC. It is used to improve the impact resistance and thermal stability. Typical concentrations are 20-30 wt% in rigid and 30-40 wt% in flexible PVC. [22] It may react with HCl producing calcium chloride. It also degrades at high temperatures (above 840 °C) producing CO_2 and H_2O.

Other significant additives are stabilizers and metal oxides, although their concentrations are not very high. The stabilizers do not affect on the degradation temperatures, but they seem to inhibit the formation of the HCl. In higher concentrations (> 1 phr) they also seem to inhibit the formation of benzene and toluene [13]. Metal oxides suppress the amount of released aromatic hydrocarbons. Some oxides also lower the temperature of the dehydrochlorination reaction. Those metal oxides that suppress most benzene formation also promote char under nitrogen ambient. [10] The role of these additives is not investigated in this paper.

The insulation layer is nominally a polyethylene (PE) blend. Pure PE degrades around 400-500 °C without leaving residue. The additives are assumed to be similar to those of PVC for simplicity. [23]

RESULTS

Generic samples

The calculation and simulation methods were first verified by using the Generic 1 sample. The results show that the correct amount of heat can be allocated to each reaction using both methods. Additionally, it showed that the FDS model indeed calculates the mass and heat release as expected.

The Generic 2 sample undergoes two reactions. Both of them yield fuel and residue, the second also inert gas. The experimental results and the target values were listed in Table 1. These results are confirmed by integrating over the reaction steps of the FDS results. The mass fractions of the components are assumed known (0.5 for both components), and the other parameters are listed in

Table 3. For both methods the reaction specific mass loss and heat release are calculated correctly with these parameters. Method 2 only slightly (3 %) overestimates the mass loss of the reaction 2 (0.46), but the total heat release is exactly 1.75 MJ/kg.

Table 3. Estimation results and estimation boundaries for method 2 of sample Generic 2.

	y_{I11}	y_{F11}	y_{I22}	y_{F22}	$\Delta H_{c,11}$ (MJ/kg)	$\Delta H_{c,22}$ (MJ/kg)
Exact value	0.00	0.20	0.80	0.10	45.00	35.00
Method 1	0.03	0.97	0.46	0.04	46.45	46.45
Method 2	0.01	0.19	0.81	0.12	47.02	30.07
Est. boundaries	[0,1]	[0,0.3]	[0,1]	[0,0.3]	[30, 50]	[30, 50]

The Generic 3 sample undergoes three fuel yielding reactions. Two first reactions (Comp 1 and Comp 2) are overlapping and inseparable in time or temperature. The net energy release in the first reaction should be (according to Table 1) 13.02 MJ/kg and in the second 5.88 MJ/kg, making the total heat release of the sample 18.90 MJ/kg. The corresponding mass losses should be 0.72 and 0.17. An integral over the peaks confirm these results.

For **Method 1**, we assume that the heat of combustion of the fuel gas is 40 MJ/kg. For the first reaction, the parameters are $Q_{c,1}/m_0$ = 13.02 MJ/kg, $\Delta\alpha_1$ = 0.72 and ΔH_c = 40 MJ/kg. According to eq. (4), the fuel yield (y_{1F}) is 0.45 (and the yield of the inert gas is therefore 0.55). For the second reaction, we have to take the char yield into account. The total char yield of the material (Z) is 0.11. The fraction of the fuel of all the gas released in the second reaction is by eq. (4) 0.865. The yields are then calculated as in eq. (5)

$$\begin{cases} y_{2F} = 0.865\left(1-\dfrac{0.11}{1-0.72}\right) = 0.53 \\ y_{2I} = (1-0.865)\left(1-\dfrac{0.11}{1-0.72}\right) = 0.08 \\ y_{2Z} = 1-0.53-0.08 = 0.39 \end{cases}.$$

The results are summarized in Table 4.

Table 4. The yields and mass fractions for generic sample 3 using Method 1.

	y_F	y_I	y_Z	Y
Reaction 1	0.45	0.55	0.0	0.72
Reaction 2	0.53	0.08	0.39	0.28

For **method 2** we assume that the material is a PVC polymer with some plasticizer. We set the estimation boundaries as listed in Table 5. The estimation problem was solved using a Matlab function and a script that tried random initial values and chose the values that gave the smallest error. The iteration with random initial values was performed 5000 times, and the best solution gave an error of $5.8 \cdot 10^{-8}$. The values for the final estimation results can be seen in Table 5. The results are relatively near the target values considering the width of the estimation boundaries.

Table 5. Estimation boundaries, initial values and the final results for the Generic 3 sample. The first subscript denotes to reaction and second to component (PVC = 1, plasticizer = 2).

Variable	Boundaries	Initial value used	Target value	Estimation result	Error
Y_1 ("PVC")	[0.5, 0.8]	0.59	0.70	0.70	0 %
Y_2 ("Plasticizer")	-	0.41	0.30	0.30	0 %
y_{I11}	[0.57, 0.61]	0.58	0.58	0.60	-3 %
y_{F11}	[0, 0.05]	0.00	0.02	0.00	100 %
y_{F12}	[0.5, 0.9]	0.67	0.60	0.61	-2 %
ΔH_{c11} (MJ/kg)	[20, 45]	30.27	30.0	27.60	8 %
ΔH_{c12} (MJ/kg)	[20, 45]	34.28	35.0	34.59	1 %
ΔH_{c21} (MJ/kg)	[20, 45]	36.05	42.0	43.04	-2 %

The results with Method 1 and Method 2 were next tested by investigating if the resulting parameters can reproduce the mass loss and heat release characteristics of the generic data. This was done by calculating the TGA and MCC experiments using both reaction paths. The kinetic parameters are assumed to be known exactly (for Method 1, only those of the Comp 1 are used for the first reaction). The results confirm that although the reaction paths and assumptions are different, the essential information (mass loss and heat release) can be repeated correctly using both methods. The results are shown in Figure 6.

In addition to the mass and energy calculation, the capability of method 2 was validated by comparing the estimated and target values. The errors between these two values are listed in Table 5. In general, the estimated values are within 10 % to the real ones. However, the greatest error is with the fuel yield of the Comp 1 in reaction 1. As the amount of fuel from the PVC is very small, this error is irrelevant.

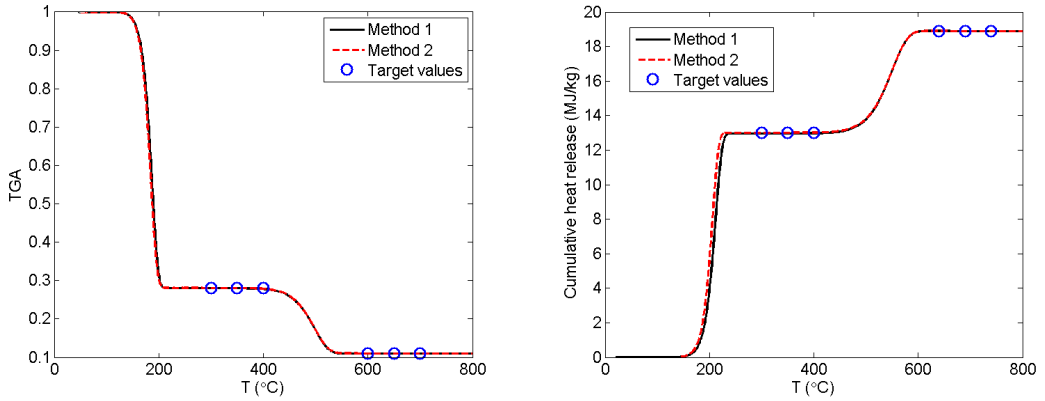

a) b)

Figure 6. Verification of the estimation results. a) Mass loss (TGA at 10 K/min in N_2). b) Energy release (MCC at 60 K/min in air).

Application to a real PVC sheath

Small scale model

As seen in Figure 5, the TGA results show three reaction peaks, MCC results only two. As listed in Table 2, the measured heat releases are 9.195 MJ/kg in the first reaction and 4.905 MJ/kg in the second. The mass losses are 0.6, 0.137 and 0.04, correspondingly. The kinetic parameters (A, E, N) were estimated using Genetic Algorithm (GA) ([2],[9]) for both methods (different reaction paths) separately. The kinetic parameters are known to compensate the other parameter values so that there may be several sets of equally fitting parameters. To minimize this effect, the parameters should be estimated at several heating rates. Unfortunately, the experimental data set only included on heating rate at 10 K/min. However, from the MCC results (at 60 K/min) it can be seen, that the reactions happen almost simultaneously as seen in Figure 5. Therefore the parameters are estimated at these two heating rates, using the same experimental results from 10 K/min.

The reaction path parameters were estimated similarly for the insulating material that was known to be PE. It had similarly three mass loss peaks, the third one without heat release. The mass losses of the reactions were 0.57, 0.12 and 0.052. The heat releases of the two first reactions were 8.233 MJ/kg and 4.77 MJ/kg.

Method 1: The fuel in this model was assumed to be propane (46.45 MJ/kg) and the inert gas water vapour. The fuel yields are calculated according eq. (4) and eq. (5) and the results are listed in Table 6. The reaction path and the kinetic parameters are shown in Figure 7. The comparison between experimental and simulated small scale results are seen in Figure 9.

With similar assumptions of the fuel gas as for the sheath material, the fuel yields of the insulation material are 0.31 and 0.86 in two first reactions. The third reaction does not yield fuel gas, and residue yield is 0.83. The kinetic parameters are listed in Table 8.

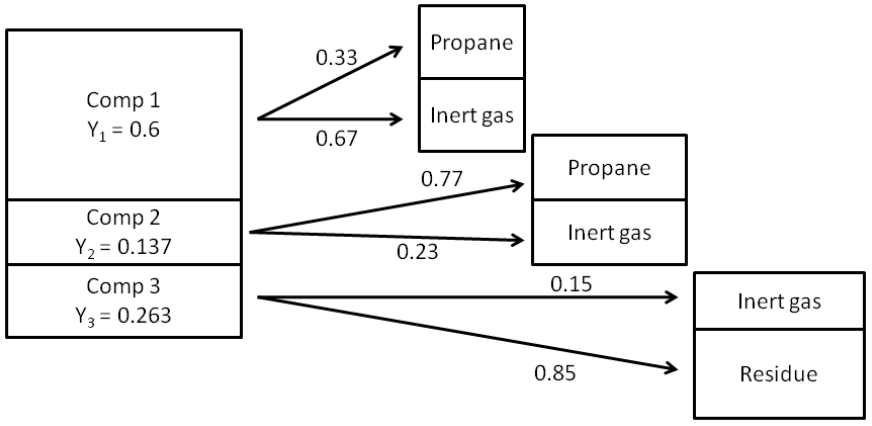

Figure 7. Reaction path and kinetic parameters for the PVC sheath using Method 1.

Table 6. Estimation results for PVC sheath and PE insulation using Method 1.

	Reaction i	Y_i	y_{Fi}	y_{Ii}	y_{Ri}
Sheath (PVC)	1	0.600	0.33	0.67	0.00
	2	0.137	0.77	0.23	0.00
	3	0.263	0.00	0.15	0.85
Insulation (PE)	1	0.57	0.31	0.69	0.00
	2	0.12	0.86	0.14	0.00
	3	0.31	0.00	0.17	0.83

Method 2: The reaction path of the real PVC sheath was assumed similar to the Generic 2 sample, and the third additional reaction (with no measured heat release) was assumed to be due to $CaCO_3$ thermal degradation. The estimation boundaries are listed in Table 7. The optimization was performed using the Matlab script mentioned before. In 5000 iterations, the minimum was found with error (eq. (9)) of $2.4 \cdot 10^{-7}$. The resulting values are listed in Table 7 and the reaction path and kinetic parameters are shown in Figure 8. The comparison between experimental and simulated small scale results are shown in Figure 9.

The insulating material was known to be PE. Pure PE is thermoplastic and therefore does not yield residue. The first reaction corresponds to the temperature range of the plasticizer, and second to the degradation of the PE. The third reaction is again assumed to be due to $CaCO_3$. As the two fuel yielding components do not yield any char (at least, not in their pure form), the mass losses of the reactions are used as the mass fractions of the components. The calculation of the heat of combustions is very straight-forward and they can be calculated using eq. (4). As result, the heats of combustions for two first reactions are 14.45 MJ/kg and 39.73 MJ/kg, respectively. The residue yield of the last reaction is 0.83.

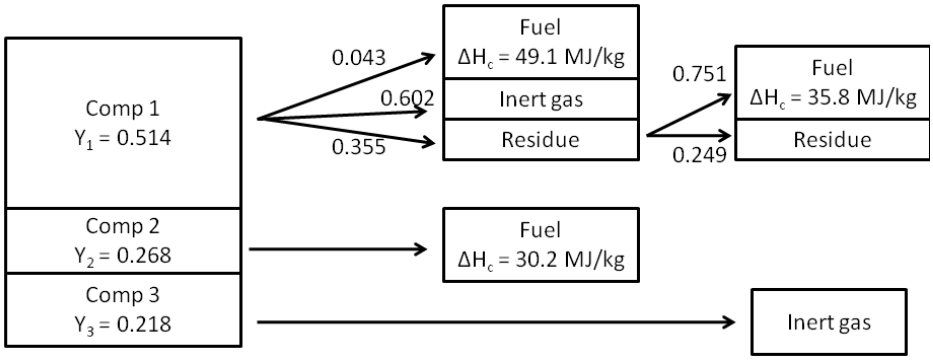

Figure 8. Reaction path and kinetic parameters for a PVC sheath using Method 2.

Table 7. Estimation boundaries, initial values and the final estimated values of the PVC sheath using Method 2.

	Estimation boundaries	Initial values	Estimation result
Y_1	[0.2, 0.7]	0.508	0.514
Y_2	[0.1, 0.5]	0.323	0.268
Y_3	-	0.169	0.218
y_{I11}	[0.57,0.61]	0.606	0.602
y_{F11}	[0, 0.07]	0.040	0.043
y_{F12}	[0.5, 0.9]	0.786	0.751
y_{I13}	[0.05, 0.3]	0.186	0.184
ΔH_{c11} (MJ/kg)	[25, 50]	48.9	49.1
ΔH_{c12} (MJ/kg)	[25, 50]	31.2	35.8
ΔH_{c21} (MJ/kg)	[25, 50]	32.1	30.2

Table 8. The kinetic parameters for PVC sheath and insulation using Method 1 and Method 2.

Material	Method	Component (i) Reaction (j)	A (s^{-1})	E (mol/kJ)	N
Sheath (PVC)	Method 1	i = j= 1	$3.6 \cdot 10^{21}$	$2.4 \cdot 10^{5}$	2.87
		i = j = 2	$1.2 \cdot 10^{29}$	$3.8 \cdot 10^{5}$	4.10
		i = j = 3	$5.1 \cdot 10^{21}$	$3.0 \cdot 10^{5}$	2.67
	Method 2	i = 1,2, j = 1	$2.1 \cdot 10^{26}$	$2.8 \cdot 10^{5}$	3.69
		i = 1, j = 2	$2.0 \cdot 10^{25}$	$3.2 \cdot 10^{5}$	4.91
		i = 3, j = 3	$9.8 \cdot 10^{24}$	$2.9 \cdot 10^{5}$	0.96
Insulation (PE)	Both methods	i = j = 1	$1.26 \cdot 10^{25}$	$2.7 \cdot 10^{5}$	3.20
		i = j = 2	$1.9 \cdot 10^{27}$	$3.6 \cdot 10^{5}$	3.7
		i = j =3	$1.6 \cdot 10^{12}$	$2.1 \cdot 10^{5}$	4.41

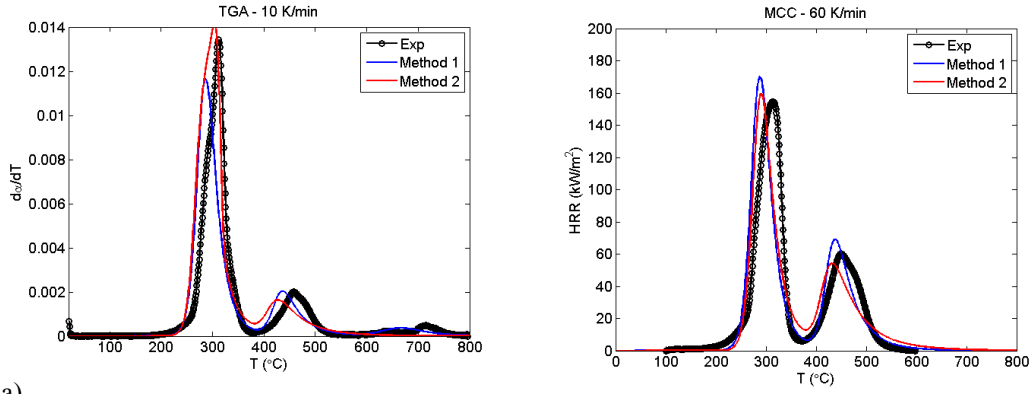

a) b)

Figure 9. Comparison of the experimental and simulated results for real PVC sheath. a) TGA. b) MCC.

Bench scale model

The cone calorimeter experiments were performed at 25, 50 and 75 kW/m^2 heat fluxes. The experimental results are listed at Table 9. The mass fractions of the components were 0.24 (sheath), 0.18 (insulation) and 0.58 (conductor). Conductor is non-combustible. The total mass loss of the sheath is 77.7 % and of insulation 74.2 % and total heat release 14.1 MJ/kg and 13.0 MJ/kg,

respectively. Multiplying by mass fractions and the initial mass 270 g, the mass loss is 84.8 g (32 %) and the total heat release 1.52 MJ. The effective heat of combustion (total heat release scaled by the mass loss) is then 17.9 MJ/kg. This is less than in cone calorimeter experiments at 25 and 50 kW/m^2. The extra heat released is related to the oxidation of char. This phenomenon is addressed in the next section.

Table 9. Experimental cone calorimeter results.

	25 kW/m^2	50 kW/m^2	75 kW/m^2
m_0 (g)	263.9	269.0	262.2
Δm (g)	71.0	91.2	89.0
$\Delta m/m_0$ (g/g)	0.27	0.34	0.34
Q_{tot} (MJ)	1.92	1.71	1.59
$\Delta H_{c,\,eff}$ (MJ/kg)	27	18.75	17.9

The cone calorimeter models were developed based on the small scale results and mass fractions. The results are listed in Table 10 and graphically presented in Figure 10. The cone calorimeter models where calculated using FDS 6 with 5 cm grid resolution. The parameters were fitted at 50 kW/m^2 heat flux, and validated using results of 25 and 75 kW/m^2 heat fluxes.

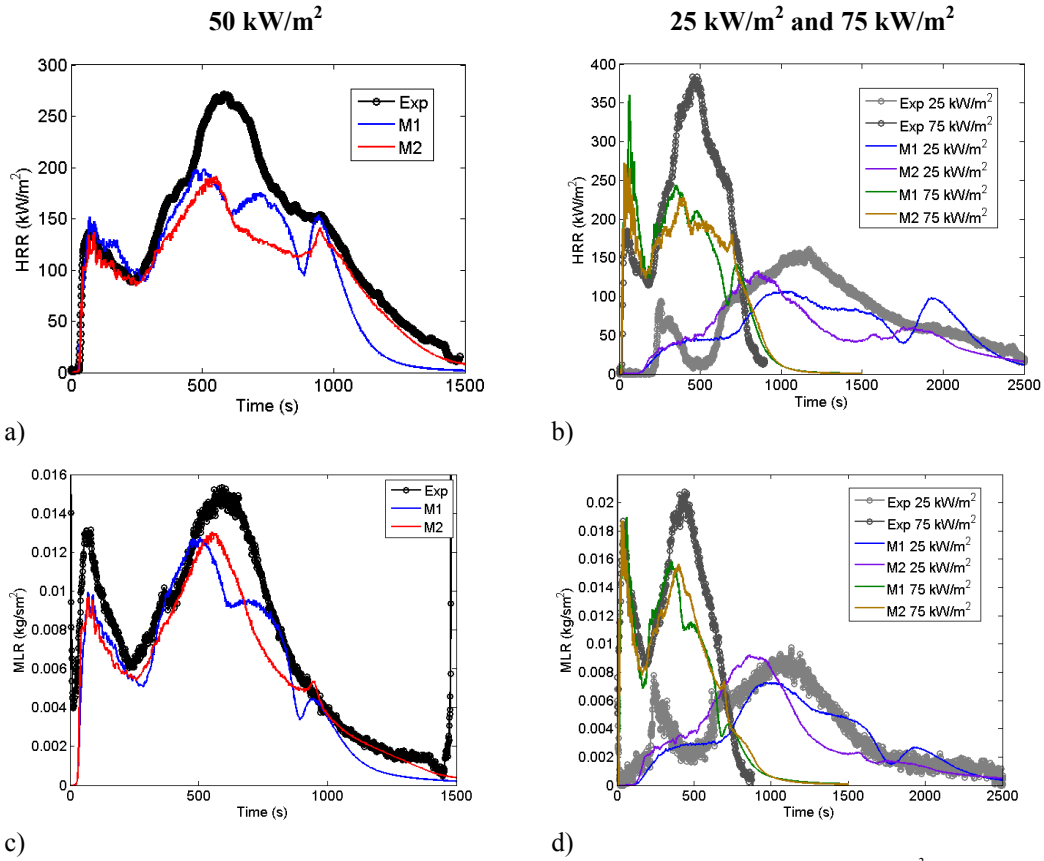

Figure 10. Cone calorimeter results for Method 1 and Method 2. a) Heat release rate at 50 kW/m^2. b) Heat release rate at other heat fluxes. c) Mass loss rate at 50 kW/m^2. d) Mass loss rate at other heat fluxes.

Table 10. Thermal parameters of cable 701.

			Method 1	Method 2		
				Polymer	Plasticizer	$CaCO_3$
Sheath	Reaction 1	k (W/(mK))	0.147	0.146	0.185	0.48
		c_p (kJ/(kgK))	3.22	3.4	2.8	3.5
		ΔH (kJ/kg)	1607	206	1112	1669
		ε	0.7	1.0	1.0	1.0
	Reaction 2	k (W/(mK))	0.175	0.2	-	-
		c_p (kJ/(kgK))	3.45	2.26	-	-
		ΔH (kJ/kg)	1425	1783	-	-
		ε	1.0	1.0	-	-
	Reaction 3	k (W/(mK))	0.103	-	-	-
		c_p (kJ/(kgK))	3.5	-	-	-
		ΔH (kJ/kg)	43	-	-	-
		ε	1.0	-	-	-
	Residue	ρ (kg/m^3)	344	70		274
		k (W/(mK))	0.122	0.188	-	0.188
		c_p (kJ/(kgK))	3.5	2.0	-	2.0
		ε	0.85	1.0	-	1.0
Insulation	Reaction 1	k (W/(mK))	0.783	0.246	-	-
		c_p (kJ/(kgK))	3.36	1.9	-	-
		ΔH (kJ/kg)	1408	1760	-	-
		ε	1.0	1.0	-	-
	Reaction 2	k (W/(mK))	1.0	-	0.59	-
		c_p (kJ/(kgK))	3.4	-	3.0	-
		ΔH (kJ/kg)	1516	-	691	-
		ε	1.0	-	1.0	-
	Reaction 3	k (W/(mK))	0.087	-	-	0.285
		c_p (kJ/(kgK))	2.74	-	-	2.9
		ΔH (kJ/kg)	445	-	-	353
		ε	1.0	-	-	1.0
	Residue		297	-	-	297
		k (W/(mK))	0.01	-	-	0.338
		c_p (kJ/(kgK))	1.29	-	-	1.29
		ε	1.0	-	-	1.0

Surface oxidation

It was noticed that the heat release and mass loss in cone calorimeter was higher than according to small scale results should be. This was speculated to be due to surface oxidation, and this can be confirmed by comparing TGA results in air and nitrogen. In air the mass loss of the sheath is 7.7% higher than in nitrogen. This corresponds to 1.7 % (4.6 g) mass loss in the whole cable. The heat released in cone calorimeter is about 0.17 MJ more than that of the models. Dividing the heat by the mass loss gives heat of oxidation about 37 MJ/kg.

The newest version of FDS 6 is currently able to model the oxidation as function of available oxygen [8]. The reaction rate defined by Arrhenius parameters is multiplied by a function of oxygen volume fraction of the first gas cell

$$r_{ij} = A_{ij}\left(\frac{\rho_i}{\rho_0}\right)^{n_{ij}} \exp\left(-\frac{E_{ij}}{RT}\right) X_{O_2}^{n_{O_2,ij}} . \qquad (11)$$

In normal pyrolysis reaction order of oxidation is 0. Deeper under the surface the oxygen concentration depends on the diffusion depth, also defined by user. The parameters are found by comparing the model with the last reaction of TGA experiment in air. For method 1, the oxidation reaction is one parallel reaction more. For method 2, the char yielded by PVC and $CaCO_3$ is converted into ash. The parameters of this reaction are listed in Table 10 and visually shown in Figure 11. The pyrolysis reactions do not fit exactly to the experimental data. Part of the reason may be the ignition model of FDS. In FDS, whenever oxygen is present, the fuel gas ignites. In real TGA this hardly happens, since the temperatures of most degradation steps are below the autoignition temperature. However, also in the experiment the fuel reacts with oxygen in some level, releasing heat. For these reasons, the only significant part of the curve is in the end, corresponding to the surface oxidation.

The cone calorimeter results are shown in Figure 12. It seems that the oxidation alone does not explain the different mass loss and heat release results in the cone calorimeter.

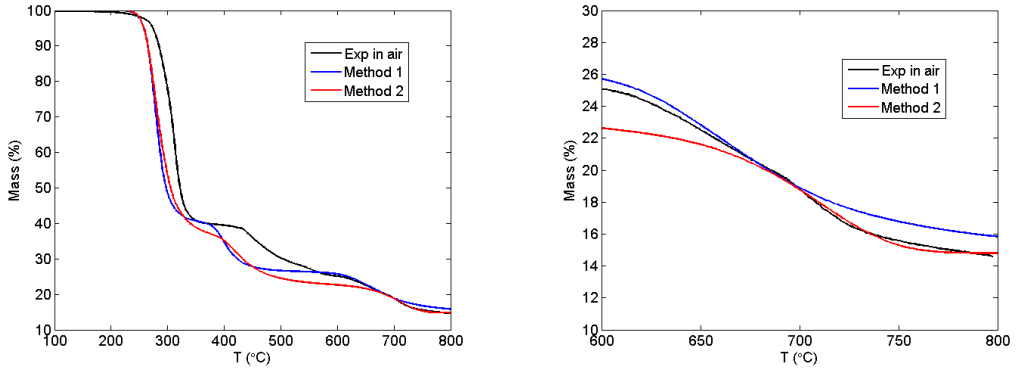

Figure 11. Implementing the oxidation reaction. a) TGA in air. b) Zoomed in to the end of the experiment.

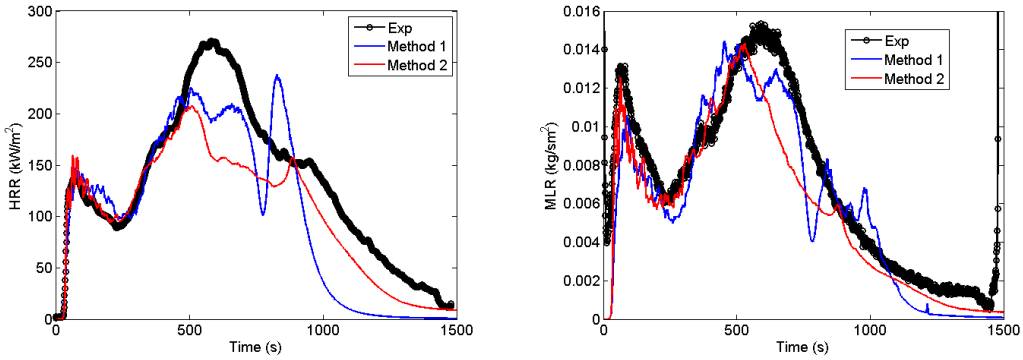

a) b)

Figure 12. Cone calorimeter results with oxidation at 50 kW/m2. a) Heat release rate. b) Mass loss rate.

Table 11. Parameters for surface oxidation of cable sheath.

	Method 1	Method 2
22.9 % of initial mass		
A (s^{-1})	$6.0 \cdot 10^{12}$	$2.5 \cdot 10^{10}$
E (kJ/kmol)	$2.5 \cdot 10^{5}$	$2.3 \cdot 10^{5}$
N	1.4	1.0
n_{O2}	1.5	1.5
y_F	0.34	0.34
k (W/m·K)	1.0	0.2
c_p (kJ/kg·K)	1.0	2.5
ΔH (kJ/kg)	0	1500
ash		
k (W/m·K)	0.122	0.6
c_p (kJ/kg·K)	3.5	3.0
ε	0.85	1.0

CONCLUSIONS

Unknown composition of the sample material is often a challenge in the pyrolysis and fire modelling. Since it is not practical to perform a complete chemical analysis of each material, alternative methods have been searched. An experimental tool, MCC, has been exploited for measuring the heat of combustion of each reaction and estimation of the sample composition.

Two new methods for combining MCC and TGA results were developed. First one is a simple and practical engineering solution that just measures the net heat release of each reaction. This approach is usually enough in order to make an accurate pyrolysis model. The second one has more ambitious goal to understanding better the sample material. It requires some knowledge about the chemical components and the degradation path of the material. This method may be more useful in the academic research projects than in engineering applications. Both methods were applied to two generic materials with known reaction paths and parameters, and to one real PVC mixture of an electric cable.

Both methods were verified to calculate the heat release of each reaction correctly. The method 2 was also validated by comparing the estimated and target values of the mass fractions, fuel yields and the heat of combustions of the reactions. The differences were very small considering that the parameters are known to compensate each other.

The methods 1 and 2 were finally used in the pyrolysis modelling of a real PVC cable. The results are realistic and predicting the small scale experiments accurately. The models were applied also in the bench scale using cone calorimeter results. The surface oxidation of char was also modelled. Surface oxidation is a significant phenomenon in the end of the cone calorimeter experiment and can be observed visually by the glowing surface. However, in the model this did not seem to make great difference because of the definition of the reaction paths.

Acknowledgements

The authors would like to thank Dr. Kevin McGrattan from NIST for the MCC and cone calorimeter results for cable #701 and Dr. Tuula Leskelä (Aalto University School of Science and Technology) for the TGA results. The work has been partially funded by the Nuclear Waste Management Fund of Finland (VYR).

References

1. Matala, A. and Hostikka, S. Pyrolysis Modelling of PVC Cable Materials. *Fire Safety Science -- Proceedings of the Tenth International Symposium*, International Association for Fire Safety Science, 2011, p. 917-930. DOI: 10.3801/IAFSS.FSS.10-917

2. Matala, A., Hostikka, S., Mangs, J. Estimation of Pyrolysis Model Parameters for Solid Materials Using Thermogravimetric Data. *Fire Safety Science -- Proceedings of the Ninth International Symposium*, International Association for Fire Safety Science, 2008, p. 1213-1224. DOI:10.3801/IAFSS.FSS.9-1213

3. Lautenberger, C., Rein, G., Fernandez-Pello, C. The application of a genetic algorithm to estimate material properties for fire modeling from bench-scale fire test data. Fire Safety Journal 41 (2006) 204-214. doi:10.1016/j.firesaf.2005.12.004

4. Lyon, R.E., Walters, R.N. Pyrolysis combustion flow calorimetry. Journal of analytical applied pyrolysis 71 (2004) 27-46 dx.doi.org/10.1016/S0165-2370(03)00096-2

5. Lyon, R.E., Walters, R.N., Stoliaroc, S.I., Safronava, N. Principles and Practise of Microscale Combustion Calorimetry. Federal Aviation Administration report DOT/FAA/TC-12/53, Springfield, Virginia, 2013. 89 p.

6. D. Drysdale. An Introduction to Fire Dynamics. 3rd edition. John Wiley and Sons, Ltd, UK., 2011.

7. Reaction-to-fire tests - heat release, smoke production and mass loss rate. ISO 5660-1, 2002.

8. NIST Special Publication 1019. Fire Dynamics Simulator. User's Guide. (2012)

9. McGrattan, K., Lock, A., Marsh, N., Nyden, M., Morgan, A.B., Galaska, M., Schenck, K. Cable Heat Release, Ignition, and Spread in Tray Installations During Fire (CHRISTIFIRE). Phase 1: Horizontal Trays. NUREG/CR-7010, Vol. 1. (2012)

10. Lattimer, R.P., Kroenke, W.J. The Formation of Volatile Pyrolyzates from Poly(vinyl Chloride). Journal of Applied Polymer Science, Vol. 25, 101-110 (1980)

11. Mountado, G., Puglisi, C. Evolution of Aromatics in the Thermal Degradation of Poly(vinyl chloride): A Mechanistic Study. Polymer Degradation and Stability 33 (1991) 229-262

12. Marcilla, A., Beltrán, M. PVC-plasticizer interactions during the thermal decomposition of PVC plastisols. Influence of the type of plastizicer and resin. Polymer Degradation and Stability 53 (1996) 261-268.

13. Jiménez, A., López, J., Vilaplana, J., Dussel, H.-J. Thermal degradation of plastisols. Effect of some additives on the evolution of gaseous products. Journal of Analytical and Applied Pyrolysis 40-41 (1997) 201-215.

14. Elakesh, E.O., Hull, T.R., Price, D., Milnes, G.J. Carty, P. Effect of Plasticizers on the Thermal Decomposition of Chlorinated Polyvinylchloride. Journal of Vinyl & Additive Technology (2005).

15. Marcilla, A., Beltrán, M. Effect of the plasticizer concentration and heating rate on the thermal decomposition behavior of PVC plastisols. Kinetic analysis. Polymer degradation and Stability 60 (1998) 1-10.

16. Miranda, R., Yang, J., Roy, C., Vasile, C. Vacuum pyrolysis of PVC I. Kinetic study. Polymer Degradation and Stability 64 (1999) 127-144.

17. Marcilla, A., Beltrán, M. Thermogravimetric kinetic study of poly(vinyl chloride) pyrolysis. Polymer Degradation and Stability 48 (1995) 219-229.

18. Marcilla, A., Beltrán, M. Kinetic models for the thermal decomposition of commercial PVC resins and plasticizers studied by thermogravimetric analysis. Polymer Degradation and Stability 53 (1996) 251-260.

19. Beltrán, M., Marcilla, A. Kinetic models for the thermal decomposition of PVC plastisols. Polymer Degradation and Stability 55 (1997) 73-87.

20. Kim, S. Pyrolysis kinetics of waste PVC pipe. Waste Management 21 (2001) 609-616.

21. Matala, A., Hostikka, S. Pyrolysis Modelling of PVC Cable Materials. Fire Safety Science 10 (2011).

22. Wypych, G. PVC Formulary. ChemTec Publishing. (2009) pp. 379.

23. Marcilla, A., Ruiz-Femenia, R., Hernández, J., García-Quesada, J.C. Thermal and catalytic pyrolysis of crosslinked polyethylene. Journal of Analytical Applied Pyrolysis 76 (2006) 254-259. doi:10.1016/j.jaap.2005.12.004

PUBLICATION V

Probabilistic simulation of cable performance and water based protection in cable tunnel fires

In: Nuclear Engineering and Design,
Vol. 241, No. 12, pp. 5263–5274.

Nuclear Engineering and Design 241 (2011) 5263–5274

Contents lists available at SciVerse ScienceDirect

Nuclear Engineering and Design

journal homepage: www.elsevier.com/locate/nucengdes

Probabilistic simulation of cable performance and water based protection in cable tunnel fires

Anna Matala*, Simo Hostikka

VTT, P.O. Box 1000, FI-02044 VTT, Finland

ARTICLE INFO

Article history:
Received 19 January 2011
Received in revised form 29 August 2011
Accepted 11 September 2011

ABSTRACT

Nuclear power plants contain a significant amount of fire load in form of electrical cables. The performance of the cables is interesting both from the fire development and system failure viewpoints. In this work, cable tunnel fires are studied using numerical simulations, focusing on the fire spreading along power cables and the efficiency of the water suppression in preventing the cable failures. Probabilistic simulations are performed using Monte Carlo technique and the Fire Dynamics Simulator (FDS) as the deterministic fire model. The primary fire load, i.e. the power cables are modelled using the one-dimensional pyrolysis model, for which the material parameters are estimated from the experimental data. Two different water suppression systems are studied. The simulation results indicate that using either suppression system decreased the heat release rate in the tunnel to less than 10% of the non-suppressed case. Without water suppression, the cables of the second sub-system were damaged in almost all fires, but when either of the studied water suppression systems was used, the probability of the cable failures was decreased to less than 1%. This result indicates that in current scenario, the probability of losing both sub-systems is determined directly by the suppression system unavailability.

1. Introduction

The safety of nuclear power plants relies heavily on concepts such as defence-in-depth and redundancy. For fire safety, the defence-in-depth means that attempts are made both to prevent the ignition of fires and to prepare for their consequences. Fire may also challenge the redundancy if it can penetrate through the barriers between the redundant parts. Sometimes the components of two subsystems can be located in the same room. This can challenge the safety of the plant especially when dealing with cables placed in the cable spreading rooms and cable tunnels. If the cables belonging to the other subsystem catch fire, they can be assumed to have already failed electrically. From the viewpoint of Probabilistic Risk Assessment (PRA), the probability of the failure in the other subsystem is extremely interesting (Paté-Cronell and Dillon, 2006) and several different methods have been used for the computation of the failure probability. One of the methods is based on the use of a severity factor which is the likelihood of those heat release rates for a given fire source that can cause a failure of a given target. As mentioned in the guidance document by the U.S. Nuclear Regulatory Commission (NRC, 2005), the application of severity factors has been a point of debate in past PRA approaches because fire severity-likelihood relationships are heavily influenced by expert judgment. Additional difficulty comes from the fact that neither the fire sources nor the targets may be explicitly specified in spaces such as cable tunnels because both of them can exist anywhere in the space.

The risk of losing both subsystems can be reduced by several means, such as physical separation between the subsystems, choice of cable materials and the use of fire suppression systems. The requirement for the physical separation is typically 6.2 m (20 ft), as suggested by the U.S. NRC in 10 CFR 50.48 (Appendix A and R). If the minimum distance cannot be fulfilled, some barriers should be placed between the cable trays. In some installations, information and control (IC) cables are placed inside metal cable conduits, which act also as thermal barriers. The sufficiency of the 6.2 m separation distance between the polyvinyl chloride (PVC) cable trays was studied by Shen (2006) using Fire Dynamic Simulator (FDS) simulations. In this work, the separation distance is fixed according to the actual case from a Finnish nuclear power plant (NPP), and the focus is in the simulation of fire spreading and fire suppression.

The cable materials are a versatile group of different kinds of plastics. Although modern, flame-retardant and non-corrosive cable sheath materials are on the market, the cables of the existing

Abbreviations: CFD, Computational Fluid Dynamics; DSC, Differential Scanning Calorimetry; FDS, Fire Dynamics Simulator; GA, Genetic Algorithm; HCl, hydrochloric acid; HRR, heat release rate; IC, information and control (cable); LHC, Latin Hypercube (sampling); MC, Monte Carlo (simulation); MLR, mass loss rate; NPP, nuclear power plant; PFS, Probabilistic Fire Simulator; PMMA, polymethyl methacrylate; PRA, Probabilistic Risk Assessment; PVC, polyvinyl chloride; RTI, response time index; TGA, Thermogravimetric Analysis.

* Corresponding author. Tel.: +358 405152535.
E-mail address: anna.matala@vtt.fi (A. Matala).

0029-5493/$ – see front matter © 2011 Elsevier B.V. All rights reserved.
doi:10.1016/j.nucengdes.2011.09.014

Nomenclature

A	pre-exponential factor (s^{-1})
c_p	specific heat capacity (kJ/(kg K))
C	C-factor of sprinkler
E	activation energy (kJ/mol)
d	thickness (m)
ΔH	heat of reaction (kJ/kg)
ΔH_c	heat of combustion (MJ/kg)
k	thermal heat conductivity (W/(m K))
L	length characteristic of the smoke detector geometry
N	reaction order
q'''	source term in heat conductive equations
Q_{max}	maximum heat release rate of the initial burner (kW)
R	universal gas constant, 8.314510 J/(mol K)
RTI	RTI value of the sprinkler detector ($(ms)^{1/2}$)
T_a	activation temperature of the sprinkler detector (°C)
t_{peak}	time of the maximum heat release rate of the burner (s)
u	the free stream velocity (in sprinkler and smoke detector)
x	co-ordinate along the tunnel (m)
y	horizontal co-ordinate across the tunnel. Residue yield (kg/kg)
Y_c	mass fraction of smoke in the sensing chamber of the detector
Y_e	Mass fraction in the external free stream (of smoke detector)
z	vertical co-ordinate (m)
x_b, z_b	horizontal and vertical co-ordinates of the initial burner

Greek letters

β	volume fraction of water in the gas stream
ρ	density (kg/m^3)
σ	Stefan–Boltzmann constant, 5.67051×10^{-8} W/(m^2K^4)

power plants are often made of conventional plastics, such as PVC. Loss of the hydrochloride acid (HCl) gas from heated PVC acts as "in-built" flame-retardant, thus reducing the burning rate as compared to many other non-flame retardant polymers. However, burning PVC produces lots of smoke and toxic gases. Quite recently, Ferng and Liu (2011) used the FDS code to investigate the burning characteristics of the electrical cables in cone calorimeter experiments. In their article, they compared several gas phase measurements of cable and polymethyl methacrylate (PMMA) samples, but did not report how the cables were described in the simulations. In this work, the thermal decomposition of PVC cables is modelled using the pyrolysis model of the FDS code. The model parameters are estimated from small scale experiments (Matala et al., 2008). The occurrence of electrical failures in the target subsystem is predicted using temperature criteria, as demonstrated by Andersson and Van Hees (2005). This method was recently validated in Dreisbach and McGrattan (2008) and Dreisbach et al. (2010).

The suppression systems may be designed either to suppress the fire or to protect the subsystems from each other, or both. In fire-PRA, it is important to consider that the reliability of the active systems is not perfect. The sprinkler system, for instance, may suffer from system or component failures. The water suppression system of the room may fail to activate or problems may appear in individual nozzles or valves. The efficiency of the system also depends on the details of the design, such as nozzle placement, nozzle characteristics, sensitivity of the activating components or water flow rate. Chien et al. (2006) used FDS to study the effects of shielding and sprinkler spacing and pressure on the fire development in a NPP cable room.

In this work, we propose a probabilistic method of numerical simulation that gives the conditional probability of second subsystem failure, in case of *any* ignition in the cables of the tunnel. Monte Carlo (MC) simulations are performed using Probabilistic Fire Simulator – PFS (Hostikka and Keski-Rahkonen, 2003) for the statistical operations and FDS (McGrattan et al., 2007, 2010) as the deterministic fire model. The most important boundary conditions of the fire simulations are treated as random variables and the deterministic simulations are repeated many times with different input parameters. The statistical distributions of the random variables are based on the geometrical properties of the cable tunnel under consideration or expert opinions. The work demonstrates how the state-of-the-art deterministic fire simulation can be used in the probabilistic framework. The goals of the work are

1. to evaluate the effectiveness of two different water based suppression systems in the protection of the second subsystem in case of power cable fire,
2. to find out the probabilities of cable failures in cases when the suppression system does or does not operate, and
3. to evaluate the conditions affecting the operation of fire fighters.

The numerical tools used in this work are shortly described in Section 2. The details of the cable tunnel under consideration and its features, including the fire source, suppression system and the fire detection are described in Section 3. This section also describes how these aspects are implemented as boundary conditions for numerical simulations. The selection of random variables is described in Section 4 and the results of the probabilistic simulations in Section 5. The conclusions are presented in Section 6.

2. Overview of the numerical methods

2.1. Fire Dynamics Simulator (FDS)

FDS is developed as a co-operation between NIST (National Institute of Standards and Technology) and VTT Technical Research Centre of Finland. It models fire-driven flows by solving numerically a low-Mach number form of the Navier–Stokes equations. The time dependent field of thermal radiation is solved using Finite Volume Method for radiation accompanied by the gray gas model for the gas phase emission, absorption and scattering. The governing equations are explained in detail in the Technical Reference Guide of FDS (McGrattan et al., 2007). Here we only provide a brief summary of the models used for computing the specific features of the simulation.

In the current simulations, the fire development is predicted by the code itself – not prescribed by the user. In terms of Computational Fluid Dynamics (CFD) boundary conditions, this means that the inflow rate of fuel gas at cable surfaces is computed using a pyrolysis model. The heat conduction inside the solid materials is solved using the one-dimensional heat conduction equation

$$\rho_s c_s \frac{\partial T_s}{\partial t} = \frac{\partial}{\partial x} k_s \frac{\partial T_s}{\partial x} + q_s''', \quad (1)$$

where x is the internal distance from the material surface, $T_s(x,t)$ is the solid phase temperature and ρ_s, c_s and k_s are material properties. Source term q_s^m consists of heats of reaction due to the thermal decomposition reactions. Each solid surface can consist of multiple layers, and each can consist of a mixture of multiple material

components. Each of the components can undergo several reactions yielding solid residue or gaseous products, such as fuel for the gas phase combustion. The reaction rates are calculated using Arrhenius equation

$$\frac{\partial}{\partial t}\left(\frac{\rho_i(x,t)}{\rho_0}\right) = A\left(\frac{\rho_i(x,t)}{\rho_0}\right)^N \exp\left(-\frac{E}{RT_s(x,t)}\right), \quad (2)$$

where A is the pre-exponential factor, E is the activation energy, N is the reaction order and R is the universal gas constant. ρ_i is the mass concentration of the ith solid phase species and ρ_0 is the initial density of the layer.

The coefficients in Eqs. (1) and (2) are not well known constants that would be listed in handbooks. Instead, they must be estimated from experimental data. In this work, the experimental methods used were Thermogravimetric Analysis (TGA) along with Differential Scanning Calorimetry (DSC) and cone calorimeter. In the beginning of the estimation process, the reaction paths were determined from qualitative analysis of TGA and DSC results. The kinetic parameters A, E and N were then estimated from the TGA data. The remaining unknown parameters were estimated from the cone calorimeter data, which was obtained both for each of the major cable components separately and for the complete cable. This stage involves modelling of the cone calorimeter experiment and making the most important pyrolysis model approximations concerning the representation of real cables as one-dimensional objects.

Each degradation reaction requires the total of eight unknown parameters (A, E, N, y, k_s, c_s, ΔH, ΔH_c). As there are several components in each cable and each component may degrade with multiple degradation steps, the number of estimates and therefore the complexity of the estimation task increase rapidly. Furthermore, the target equations are strongly non-linear with local minima which make the traditional, gradient-based optimization methods inefficient in finding the best combination of model parameters. For these reasons, the parameter estimation was mainly done using Genetic Algorithm (GA) (Matala et al., 2008), which has proved to be an effective tool for the parameter estimation for fire engineering needs. GA is based on the idea of evolution or the survival of the fittest. A group of randomly chosen candidate solution converges towards a local optimum during the iteration steps. The operations are stochastic and the probabilities are based on the fitness of the model. In this work, the number of individuals of each four subpopulation was 20 making altogether 80 candidate solutions. The iterations were manually interrupted after necessary convergence was achieved, typically after 100–200 generations. The other parameter values used for GA in this work are more profoundly listed in paper of Matala et al. (2008). Thermal parameters can be also estimated manually using predetermined information concerning the effects of the various parameters on the cone calorimeter result. For example, high thermal conductivity is known to produce longer ignition times. This method can be used instead of the numerically expensive GA or to supplement it.

When estimating parameters from the experimental data, it is important to understand the approximations and limitations of the model. The cone calorimeter model used here approximates the cable geometry as a rectangular slab with homogenous layers. The assessment of the pyrolysis model validity should be based on the accuracy of predicted time to ignition and time evolution of three quantities: heat release rate, mass loss rate and effective heat of combustion.

Automatic sprinklers are activated when the temperature of the sensing element of the device T_l exceeds the predetermined activation temperature. The heat conducted away from the element by the mount is not taken into account. The temperature is estimated from the differential equation

$$\frac{dT_1}{dt} = \frac{\sqrt{|u|}}{\mathrm{RTI}}(T_g - T_l) - \frac{C_2}{\mathrm{RTI}}\beta|u|, \quad (3)$$

where T_g is the gas temperature, u is the stream velocity and β is the volume fraction of liquid water in the gas stream. Response time index (RTI) defines the sensitivity of the detector and C_2 is constant 6×10^6 K/(m/s)$^{1/2}$.

The transport of liquid water is computed using a Lagrangian method, where the water spray consists of a sampled set of spherical droplets. For each type of sprinkler head/nozzle, the user defines the median droplet diameter d_m, droplet speed and angular direction where the droplets are inserted. The droplet size distribution consists of a combination of Rosin–Rammler and log-normal distributions, and is expressed with Cumulative Volume Fraction

$$F(d) = \begin{cases} \dfrac{1}{\sqrt{2\pi}} \displaystyle\int_0^d \frac{1}{\sigma d'} \exp\left(-\frac{|\ln(d'/d_m)|^2}{2\sigma^2}\right) dd', & d \le d_m \\ 1 - \exp\left(-0.693\left(\dfrac{d}{d_m}\right)^{\gamma}\right), & d_m < d \end{cases}, \quad (4)$$

where empirical constants are $\sigma = 0.6$ and $\gamma = 2.4$. The variation in pipe pressure P due to the opened sprinkler heads/nozzles affects the droplet boundary conditions: flow rate and droplet speed are proportional to $P^{1/2}$, and the median diameter to $P^{-1/3}$.

2.2. Probabilistic Fire Simulator

The MC simulations were carried out using PFS – tool that has been developed at VTT. In addition to the actual Monte Carlo simulations, PFS can be used as an interface for several fire models, including FDS (Hostikka and Keski-Rahkonen, 2003; Hostikka, 2008). PFS can handle all three phases in the MC simulations: sampling, simulation and results post-processing. The user interface is an excel spreadsheet that uses macros. In the interface, there is an individual sheet dedicated for each operation, and user can easily apply it to match the requirements of each task. In this work the sampling is done using Latin Hypercube (LHC), which reduces the necessary sample size compared to traditional Monte Carlo sampling (McKay et al., 1979; Stein, 1987). PFS creates the necessary input for FDS simulations using the previously created random values and user-defined template. After that, PFS performs the FDS simulations for all the input files separately. For more efficiency and parallel processing, this part can also be done separately from the earlier phase. In the post-processing phase the program reads the outputs from all simulations and performs the statistical analysis comparing the input variables and output values.

3. Fire scenario and modelling

3.1. Cable tunnel

The dimensions of the simulated tunnel are 95 m × 2.8 m × 5.5 m (height). The room has IC and power cables from two independent subsystems physically separated by a 1.3 m wide corridor. The cables are placed along the long sides of the tunnel, one subsystem at each side. The subsystems have 10 trays of IC cables in the bottom and 5 trays of power cables on the top, as illustrated in Fig. 1. The tunnel walls are made of 30 cm concrete. The properties of concrete (thermal conductivity, specific heat capacity and density) are treated as random variables to consider the uncertainty associated with their numeric values.

For the computations the tunnel was divided into three CFD meshes. The first mesh is the most important one and contains the cable trays and sprinkler heads. It is 15 m long and discretized with

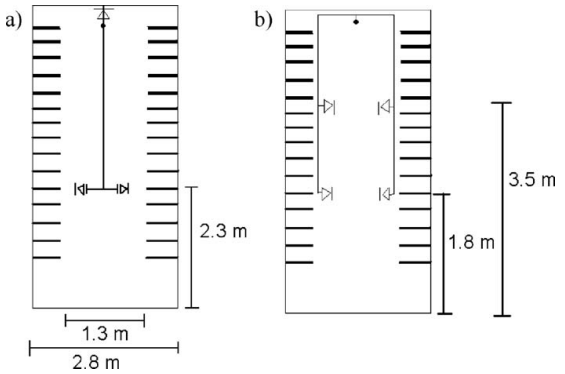

Fig. 1. Cross-section of the cable tunnel and the sprinkler nozzles of System 1 (a) and System 2 (b).

10 cm grid cells. It is assumed to be large enough to reveal all the relevant dynamics of the fire, cable failures and suppression system. The spatial resolution is coarse when considering the geometrical length scales of the flames between the cable trays, but sufficiently fine to capture the main characteristics of the fire spreading, provided the igniting fire source is large enough. The two remaining meshes are necessary just for the correct amount of available air. They have coarser grid size and no cable trays or sprinklers to speed up the simulations. The lengths of these meshes are 5 m and 75 m, and computational resolutions 0.30 m and 0.60 m, respectively.

3.2. Electrical cables

3.2.1. Power cables

Numerical simulation of fire spreading on cable trays is the most challenging part of the fire simulations and practically unvalidated class of FDS applications. Due to the involvement of a wide range of different physical scales, it is extremely difficult to numerically predict the development of the fire from small ignition. Our philosophy of modelling the spreading cable fire was to prescribe the initial fire up to the size where the fire can be resolved by the CFD mesh used for the tunnel scale simulation and realistic predictions of the thermal environment can be expected. Beyond that point, the development of the fire is predicted by the cable pyrolysis model.

The initial source of the fire in these simulations is a local fire on one of the power cable trays. The fire starts from a small local ignition and develops to a scale that corresponds to a roughly 2-m long section of 3 trays of PVC cables. It is prescribed as a burner with heat release rate curve following roughly an experimental result from a horizontal cable fire test (Mangs and Keski-Rahkonen, 1997). The approximation of the experimental curve is shown in Fig. 2. To account for the geometrical and material related variations between the experiment and the target tunnel, and the uncertainty concerning the actual ignition mechanism, some randomness is added by setting the peak heat release rate and the time of the peak as triangularly distributed random variables. The details and exact values are discussed in Section 4. Other times and the shape of the curve are kept similar to the experimental curve. The fire starts always from the same subsystem. The burner size is $0.75 \times 0.75\ \mathrm{m}^2$ and its x- and z-location are random variables.

It is important to notice that the initial fire source is not coupled with the activation of the suppression systems. The model is therefore likely to underestimate the efficiency of the sprinklers.

Each of the power cable trays is assumed to contain one layer of power cables. In reality the cable tunnels contain many different types of cables but in the simulations they are approximated using

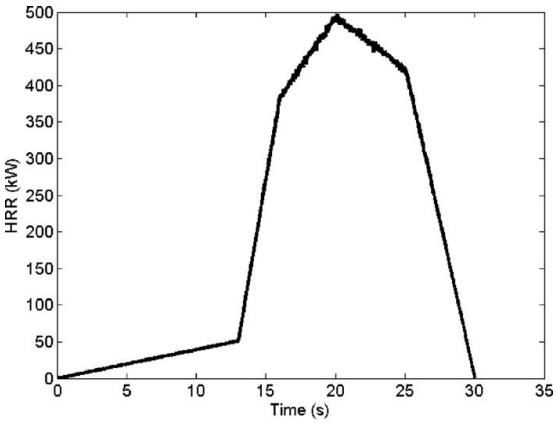

Fig. 2. Approximation of the experimental power cable heat release rate.

a numerical model of NOKIA AHXCMK 10 kV $3 \times 95/70\ \mathrm{mm}^2$ power cable (Fig. 3). The cable components and their properties in the original cable are listed in Table 1.

The reaction paths and kinetic parameters of the degradable components (sheath, insulation and filler) were estimated from separate TGA results. The reaction paths used for the components are shown below

$$\begin{aligned} \text{Sheath} &= \begin{cases} \text{volatile component}\,(56\%) \\ \text{solid}\,1\,(11\%) \rightarrow \text{char} + \text{fuel gas} \\ \text{solid}\,2\,(33\%) \rightarrow \text{char} + \text{fuel gas} \end{cases} . \\ \text{Insulation} &= \text{solid} \rightarrow \text{char} + \text{fuel gas} \\ \text{Filler} &= \text{solid} \rightarrow \text{char} + \text{fuel gas} \end{aligned} \tag{5}$$

A comparison between the experimental and simulated TGA results in Fig. 4a shows that the model can predict the TGA curves very accurately. The simplification of replacing hundreds of chemical reactions just by few is very strong but necessary considering the complexity of the whole simulation problem. It is desirable to have a model that tries to reproduce the main characteristic behaviour of the degrading cable in a computationally affordable way, requiring as few parameters as possible.

The thermal parameters were estimated from the cone calorimeter experiments that were performed separately for each of the components (sheath, filler rods and insulation with conductor), considering three different quantities: heat release rate, mass loss rate and effective heat of combustion. A comparison of the measured and predicted heat release rates for the components are shown in Fig. 4b. Thermal and kinetic model parameters are listed in Table 2. Finally, the geometrical parameters of the 1D-approximation were estimated using the data of the complete cable, shown in Fig. 4c. The 1D model of the cable consists of four layers:

1. sheath 2.5 mm,

Table 1
Components and mass fractions of the NOKIA AHXCMK 10 kV $3 \times 95/70\ \mathrm{mm}^2$ cable.

Component	Mass fraction (kg/kg)	Linear mass (g/m)	Thickness (mm)
Sheath (PVC)	0.228	600	2.5
Copper binding	0.15	400	–
Filler rods	0.08	210	10
Insulator (PEX)	0.25	650	3
Conductor	0.27	710	15
Plastics and crepe paper	0.022	58	–

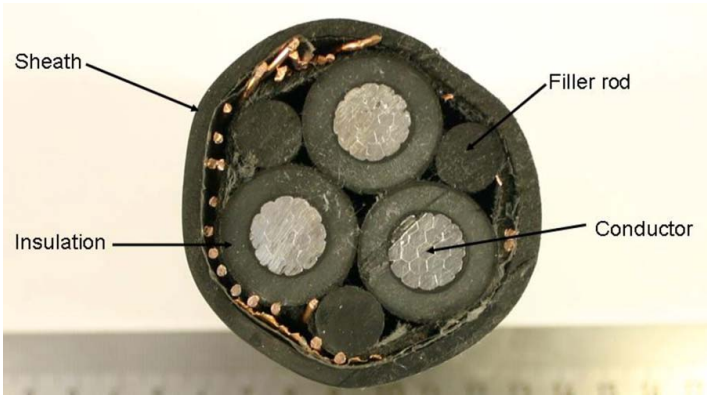

Fig. 3. Cross-section of the NOKIA AHXCMK 10 kV 3 × 95/70 mm² power cable.

2. insulation and filler 12 mm,
3. sheath 5.0 mm,
4. metal 8.234 mm.

When the model created in cone calorimeter was applied to the cable tunnel simulations, the 1D pyrolysis model was associated with both top and bottom surfaces of the obstacles representing the cable trays. As the same material point was allowed to burn from two sides of the obstacles, the layer thicknesses were divided by two to ensure the conservation of combustible mass.

The gas phase combustion reaction is specified as

$$C_2H_3Cl + 2.75O_2 \rightarrow 2CO_2 + 1.5H_2O + Cl + 5\%\,\text{soot} + 40\,\text{MJ/kg heat} \quad (6)$$

where the product chlorine acts as a simple non-reacting species, while in reality, the chlorine appears as HCl.

3.2.2. IC cables

IC cables are a versatile group of electrical cables. They are located inside of a cable conduit in the 10 lowest cable trays at both sides of the corridor. The conduits are made of steel sheets, 1 mm thick at the bottom and 2 mm on the sides and top. Because of the cable conduit, the IC cables do not contribute to the fire. However, the heating of the cables inside the conduit is computed for the prediction of cable failures. The IC cables are simulated with a 1D heat transfer solver as a layer of non-reacting PVC covered by a layer of steel. The thermal properties for non-reacting PVC were $k_s = 0.16\,\text{W/(m K)}$, $c_s = 1.05\,\text{kJ/(kg K)}$ and $\rho_s = 1400\,\text{kg/m}^3$. The cable failures are assumed to take place when the temperature at the depth corresponding to electrical insulation layer reaches a pre-defined critical temperature. The method is essentially the same as proposed by Andersson and Van Hees (2005) and further developed by U.S. NRC in Dreisbach and McGrattan (2008), but makes use of the thermal properties of the specific cables in the current scenario. In the works of Andersson and Van Hees and U.S. NRC, the thermoplastic cables, such as PVC cables, were found to have a critical temperature around 200 °C. In this work, two different failure criteria, 180 °C and 220 °C, were used in order to study the sensitivity of the failure probability. The cable temperatures were monitored in all locations of the tunnel, and the highest observed temperature was compared against the chosen failure criteria.

3.3. Suppression systems

Two different water suppression systems were studied. Both systems consist of a control valve and open nozzles. The control valves are located in the middle of the corridor, 10 cm below the ceiling and 3.5 m from each other in *x*-direction, as illustrated in Fig. 1. The control valve detects the temperature under the ceiling and discharges the water to the open nozzles below. In the model, the suppression system was only included to the first mesh. To the length of the first mesh it means four independently operating units.

The spray nozzles were characterized for the model using simple experiments. The flow rates at known pressure were first measured to determine the nozzle *K*-factors. The water distributions of the nozzles were then measured by covering the floor by empty pans and spraying the water through the nozzle at known water pressure. After pre-determined time, the amount of the water in the pans was measured and the water distribution as a function of horizontal distance from the nozzle was determined. The model parameters (spray angle, droplet velocity, droplet insertion offset and droplet median diameter) were estimated from the experimental results where the nozzle was in pendent position. The model was then validated using the results of a horizontally positioned nozzle. The RTI value and sprinkler activation temperature are variables in the MC simulations.

Table 2
Model parameters for the NOKIA AHXCMK 10 kV 3 × 95/70 mm² cable.

Material	Layer	ρ	A	E	n	y	k_s	c_s	ΔH	ΔH_c
Sheath 1 (56%)	1, 3	1501	1.78×10^9	127	1	0	0.1	2.5	200	–
Sheath 2 (11%)	1, 3	1501	8.64×10^{12}	290	1	0.474	0.05	1.0	300	20
Sheath 3 (33%)	1, 3	1501	6.61×10^8	159	1	0.618	0.05	1.0	1700	50
Insulation	2	1039	6.53×10^{12}	218	0.308	0	0.2	3.5	2500	35
Filler	2	950	6.27×10^{12}	220	0.135	0	0.15	3.0	2000	35
Metal	4	3042	–	–	–	–	10.0	8.5	–	–
Char	1, 3	385	–	–	–	–	0.4	1.5	–	–

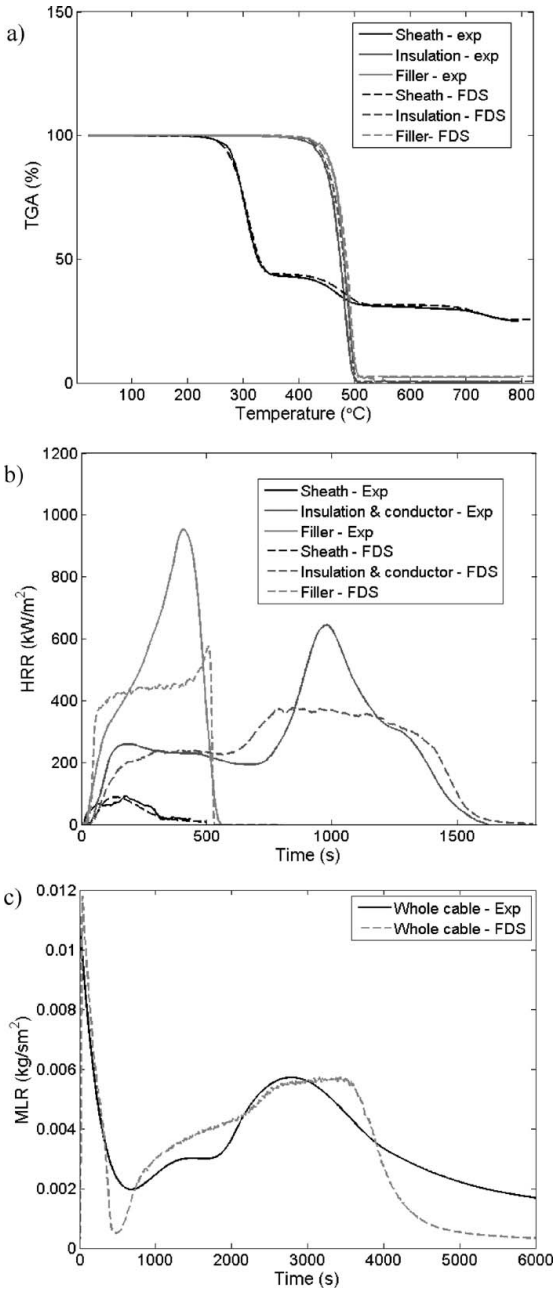

Fig. 4. Comparison of the experimental and simulated results. (a) TGA in nitrogen at heating rate 10 K/min. (b) Heat release rate of the components from cone calorimeter at 50 kW/m^2 heat flux. (c) Mass loss rate of the whole cable from cone calorimeter at 50 kW/m^2 heat flux.

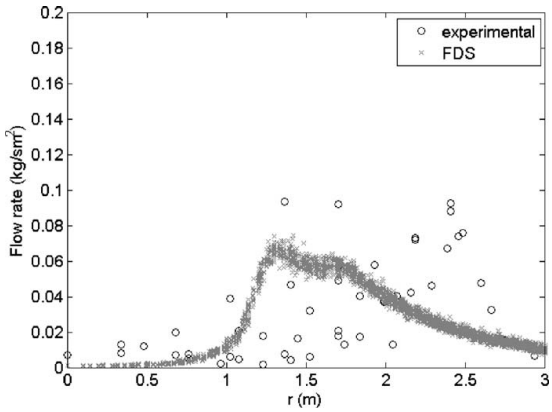

Fig. 5. Flow rate as a function of horizontal distance from the nozzle of the Suppression System 1.

3.3.1. Suppression System 1

The water suppression System 1 consists of control valves and two open nozzles for each. The control valve sprays water downwards. The two nozzles are located in the middle of the corridor, at height of 2.3 m from the floor spraying towards the cable trays. The control valve is slow (RTI around 150 $(ms)^{1/2}$) and the nominal activation temperature is 68 °C. The nozzles are type Walther LU 25 NW 15 with K-value 25 l/min/bar$^{1/2}$.

In the experiment, the nozzle was installed to pendent position at 134 cm height from the floor. The nozzle was spraying water during 7 min in about 5 bar pressure. Result of this experiment is shown in Fig. 5. The total water flow at the same pressure was measured during 30 s to be 27.77 kg which corresponds to flow rate 56 l/min. The spray of this nozzle is not homogeneous and the spray of the model has been also divided into two parts so that the water flow near the nozzle is smaller than farther away. The best fitting model is shown in Fig. 5 and the model parameters are listed in Table 3.

3.3.2. Suppression System 2

The suppression System 2 consists of control valves under the ceiling and four open nozzles controlled by one control valve. This control valve does not spray water. The nozzles are fastened to the trays pointing to the trays at the opposite side, at two different heights. The lower pair of nozzles is at height 1.8 m and the upper at 3.5 m from the floor. The pair of nozzles is not exactly towards each other, but they have some 1.7–1.8 m distances in x-direction. The control valve is fast (RTI not over 50 $(ms)^{1/2}$) and the nominal activation temperature is 68 °C. The open nozzles are type Tyco D-3 Protectospray 180° No. 32 with K-value 80.6 l/min/bar$^{1/2}$.

In the experiment, this nozzle was installed at 1.765 m from the floor. The nozzle was on during 3:05 min with pressure 3.7 bar. The flow rate was measured with the barrel. During 52 s the water accumulation was 152.8 kg which corresponds to flow rate 159 l/min. The flow area of this nozzle is much wider than that of the nozzle in System 1. The best fitting model is shown in Fig. 6 and the model parameters of this nozzle are listed in Table 3.

The effective pressure in the pipes depends on how many sprinklers or nozzles are operating at the moment. The pressure when no sprinklers are operating is 10 bar. The pressure as a function of operating sprinklers is shown in Table 4.

Table 3
Model parameters of the nozzles in the suppression systems.

	Spray angle (°)	Droplet velocity (m/s)	Flow rate at 5 bar	Droplet median diameter (μm)	Offset
Nozzle (System 1)	20% 40–50 80% 50–75	40	56	700	0.1
Control valve (System 1)	60–80	14	56	700	0.1
Nozzle (System 2)	1% 0–9 36% 9–60 63% 60–90	23	160	500	0.1

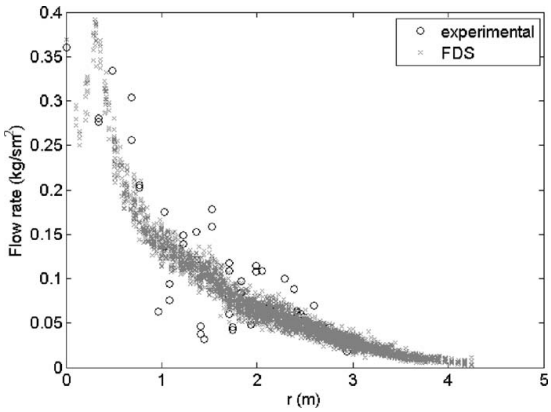

Fig. 6. Flow rate as a function of horizontal distance from the nozzle of the Suppression System 2.

3.4. Fire detection

In addition to the suppression system, the tunnel is also equipped with OMNI-type fire detectors having three activation criteria: ion, optical and temperature. When any of the criteria is fulfilled, the detector alarms. In the simulations, three separate detectors are placed under the ceiling, to the middle of the length of the first computational mesh. The ion detector is called *smoke* detector in FDS. The FDS implementation is an idealization of a spot-type smoke detector. The change in the mass fraction of smoke in the sensing chamber can be found by solving

$$\frac{dY_c}{dt} = \frac{Y_e(t) - Y_c(t)}{L/u}, \tag{7}$$

where Y_c is the mass fraction of smoke in the sensing chamber, Y_e is the mass fraction in the external free stream, L is length characteristic of the detector geometry and u is the free stream velocity. The detector activates when Y_c rises above the threshold value. The optical smoke detector is called *beam*. The user has to specify the emitter and receiver positions and the total obscuration at which the detector will alarm. FDS integrates the obscuration over the path length using the predicted soot concentration in each grid cell along the path. The temperature in the *heat* detector follows the equation

$$\frac{dT_l}{dt} = \frac{\sqrt{|u|}}{\mathrm{RTI}}(T_g - T_l), \tag{8}$$

where subscript l denotes to link and g to gas. As no information was available of the original detector parameters, the values were estimated by expert judgment and listed in Table 5.

3.5. Tenability criteria for human actions

The conditions of the fire environment were monitored inside the tunnel to allow the estimation of the probability of successful fire extinction by fire fighters. Three physical conditions were considered: gas temperature, incident thermal radiation and visibility. The physical conditions were monitored at 7.5–9.25 m horizontal distance from the middle point of the fire source, depending on the location of the source. The conditions at three vertical heights from the floor were monitored: 0.5 m, 1.0 m and 1.5 m.

Since there are no generally accepted values for the tenability limits, rather crude values were here used to give a rough estimation of the time when the possibilities of the fire fighters to find and extinguish the fire are seriously decreased. The tolerable conditions were defined to be (at 0.5–1.5 m from the floor)

- temperature $\leq 100\,^{\circ}\mathrm{C}$,
- visibility ≥ 1 m,
- radiative heat flux $\leq 10\,\mathrm{kW/m^2}$.

4. Probabilistic simulations

The Monte Carlo simulations were performed with two suppression systems and without any. Monte Carlo technique was implemented using Probabilistic Fire Simulator version 4. The random variables and the associated distributions are listed in Table 6. A FDS model was created and input template was added to the user interface of PFS. During the simulation, the FDS input parameters depending on some of the random variables were linked to the realized values of the random variables. The sample size was set in each simulation to 100 LHC samples, and corresponding amount of FDS input files was created by PFS. The simulations were carried out using FDS versions 5.2.4–5.4.3, using parallel processing. After all the simulations were completed, the results were read and post-processed using PFS.

The model had 14 random variables (listed with their distributions in Table 6). The distributions are mostly uniform or triangular as more accurate information was not available. For concrete wall properties several different literature values were available and some of them are listed in Table 7. The parameter ranges were chosen to cover most of the literature values. The thicknesses of the power cable layers vary ±50% of the thicknesses of the NOKIA AHXCMK 10 kV $3 \times 95/70\,\mathrm{mm^2}$ power cable model. The sprinkler properties RTI and T_a, and the horizontal distance x are not vari-

Table 4
Effective pressure as a function of operating nozzles and sprinklers.

Number of operating nozzles	Pressure (bar)
1	10
4	8
7	6

Table 5
Parameters used for the OMNI-detector.

	Quantity	Threshold value	Parameters
Smoke	Chamber obscuration	3.28%/m	Length = 1.8 m
Beam	Path obscuration	33%	–
Heat	Link temperature	68 °C	RTI = 150 $(\mathrm{ms})^{1/2}$

Table 6
Random variables and their distributions in the Monte Carlo simulations. Parameters are listed in form of min, max for uniform and peak, min, max for triangular distribution.

	Distribution	Parameters
Burner		
x_b	Uniform	0, 1.75
z_b	Discrete	
Q_{max}	Triangular	500, 300, 700
t_{peak}	Triangular	1200, 900, 1500
Sprinkler		
RTI – slow	Triangular	150, 120, 180
RTI – fast	Triangular	37.5, 25, 50
T_a	Triangular	68, 61, 75
Concrete wall		
k	Uniform	1.4, 1.8
c_p	Uniform	0.6, 1.0
ρ	Uniform	2100, 2500
Power cable		
k (sheath)	Triangular	0.05, 0.01, 0.3
d (sheath 1)	Uniform	0.625, 1.875
d (insulation)	Uniform	3.0, 9.0
d (sheath 2)	Uniform	1.25, 3.75

ables in the simulations without sprinklers. The slow RTI value is used in the simulations with suppression System 1 and the fast with suppression System 2.

The calculation of the droplets is the most computationally expensive part of the simulations. To reduce the calculation time, a stopping condition was created to turn the nozzles off after the fire has certainly died. The stopping condition consists of three criteria, and each of them has to be fulfilled before the condition is taking effect. The criteria are:

- Time is greater than the burner flame-out time.
- The fire heat release rate is less than 1 kW.
- The temperature in the ceiling is less than 25 °C.

The stopping condition was only used in the simulation of suppression System 2.

5. Results and discussion

5.1. Simulation results

When either of the suppression systems was used, the peak heat release rates (HRRs) during the simulations were reduced to about 10% of the non-sprinklered values. The cumulative probability distributions of the peak HRR are shown in Fig. 7. The highest peak HRR without sprinklers was more than 60 MW while with suppression System 1 it was around 5 MW and with suppression System 2 less than 4 MW.

The most significant correlation coefficients between the peak HRR and the random variables are listed in Table 8. The most significant variable to peak HRR was in all the simulations the z-coordinate of the ignition point. It deserves consideration that without a suppression system and with System 1, the correlation was negative, meaning that higher ignition point leads to smaller fire. This is probably due to the reduced amount of combustible cables above the burner that could be easily heated up and ignited.

Table 7
Some literature values for concrete properties.

	Harmathy (1995)	Iwankiw et al. (2004)
ρ (kg/m^3)	2150–2450	2323
k (W/m K)	1.37, 1.4–2.5	1.64
c_p (W/m K)	0.88, 0.6–0.85	0.84

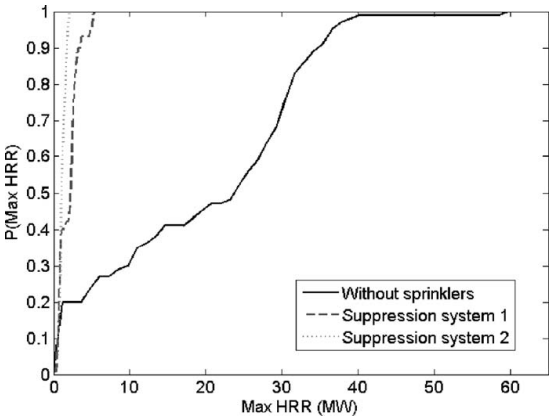

Fig. 7. Comparison of the cumulative probability distributions of the peak heat release rate.

With System 2, the correlation was positive. The reason lies in the placement of the upper open nozzles: System 2 does not have any nozzle just below the ceiling as System 1, but there is an extra pair of nozzles at the height 3.5 m protecting the lower power cable trays from igniting. However, they cannot protect the cable trays close to the ceiling from igniting. The peak HRR with System 2 is not sensitive to other variables, but in the other simulations the specific heat capacity of concrete wall and the peak HRR of the initial burner are also significant. The simulations with System 1 are also sensitive to the thickness of the first sheath layer and the density of concrete wall.

Without sprinklers, all the power cables and 60% of the IC cables passed both failure limits (180 °C and 220 °C). The power cable failures occurred in the time frame 700–1500 s and IC cable failures in the time frame 1000–1800 s. With suppression systems, no failures occurred. The peak power cable temperatures were 120 °C in case of System 1 and 170 °C in case of System 2. IC cables remained far below the failure temperatures with both suppression systems, the maximum being 50–60 °C. The cumulative probability distributions of the peak cable temperatures at the insulation layer are shown in Fig. 8. The high temperatures in the case with no suppression system correspond to conditions where the cables would be burning, and the temperature is controlled by the local flame heat transfer, not global conditions affected by the random boundary conditions. System 2 protects the IC cables slightly better than System 1. However, the power cables are much better protected with System 1. This confirms that the upper nozzles at this position are not necessarily enough for protecting the ceiling.

The significant correlations for the cable temperatures are listed in Table 9. The power cable correlations in the non-sprinkled case are not given, due to the above mentioned reason. The most significant parameters are the z-coordinate of the ignition point, concrete wall's specific heat capacity and the thickness of the first

Table 8
Significant correlations between the peak HRR and random variables. Confidence level ≥0.95 to be unequal to zero.

	No suppression	System 1	System 2
z_b	−0.86	−0.85	0.30
c_p (concrete)	−0.21	0.20	–
Q_{max}	0.24	0.24	–
ρ (concrete)	–	−0.21	–
d (sheath 1)	–	−0.29	−0.20
x	–	–	−0.29

Table 9
Significant correlations with the maximum temperature of the cables with confidence level ≥0.95.

	IC cable			Power cable	
Parameter	No suppression	System 1	System 2	System 1	System 2
z_b	−0.93	−0.97	−0.66	−0.91	0.65
c_p (concrete)	−0.22	0.24	–	–	–
Q_{max}	0.21	–	–	–	–
d (sheath 1)	–	–	–	−0.40	–
d (insulation and filler)	–	–	0.30	–	–

sheath layer. In the light of the correlation coefficients, the peak temperatures behave in a similar manner as the peak HRR: high ignition point causes smaller temperatures, except for System 2, where the fires became more severe and the power temperatures higher. Interestingly, the high ignition point does not cause higher temperatures for the IC cables protected by System 2.

In most of the cases all four sprinkler units activated. The cumulative probability distributions of both suppression systems are shown in Fig. 9. With System 2, the probability of only one or two activated units is a bit higher than with the System 1. The significant correlations are listed in Table 10. Both systems are sensitive to the ignition point z-coordinate. System 1 is also negatively correlated with the x-coordinate of the ignition point and the concrete specific heat capacity. System 2 is correlated with RTI of the control valve and the peak HRR of the initial burner.

In the simulations without sprinklers, only the temperature criteria were met (2–49% probability depending on the altitude). On

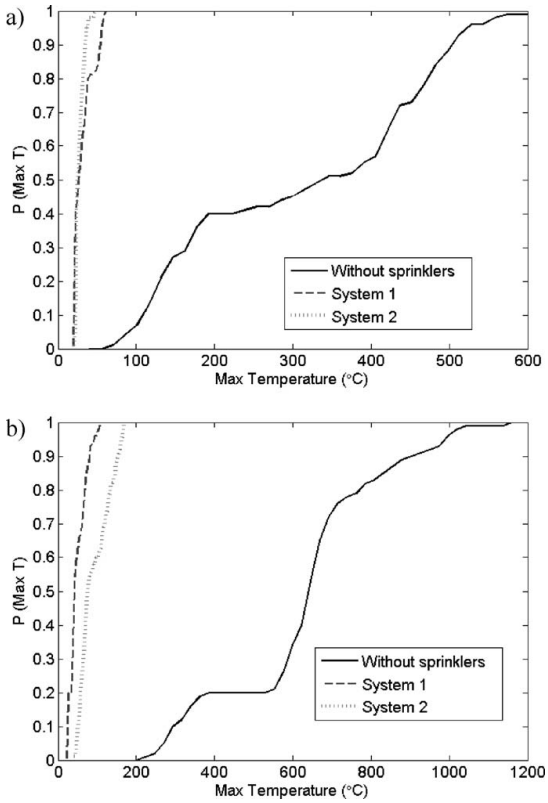

Fig. 8. The cumulative probability distributions of the peak internal cable temperatures. (a) IC cables. (b) Power cables.

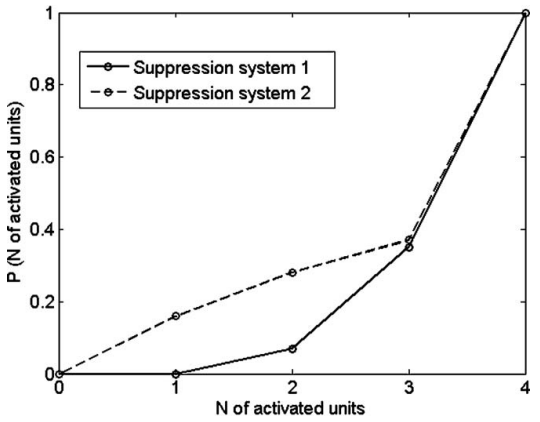

Fig. 9. Cumulative probability distributions for number of activated suppression units (control unit and nozzles).

Table 10
Significant correlations between the number of activated sprinklers and random variables with confidence ≥0.95 of not being zero.

	System 1	System 2
z_b	−0.74	–
x_b	−0.24	–
c_p (concrete)	−0.21	–
Q_{max}	–	0.19

the other hand, in the simulations with any suppression system, the only condition to exceed the limits was the visibility, which was lost in all cases. The cumulative distributions for the time when the tenability criteria were met are shown in Fig. 10. The visibility is lost fastest (between 12 and 25 min from the beginning) in the simulations with System 2. With System 1 the visibility is lost a bit later, between 16 and 30 min from the beginning. Without suppression systems, the temperature exceeds 100 °C in less than 50% of the simulations. If it happens, it happens after 20 min from the beginning. These times are in the same range with the cable failure times, meaning that if the fire brigade can reach the fire compartment before the failures, they also have good possibilities to actually reach actual fire location. The poor visibility in case of activated sprinklers will make finding the fire source very difficult.

The cable failures may be prevented if the fire is detected early and the fire brigade has time to operate. The details about the OMNI detector used for detecting the fire is described in Section 3.4. The detector activates when any of the three criteria (heat, ion or optical) exceeds the critical value. The activation times of the fire detectors are shown in Fig. 11. The ion and optical detectors were always the first ones to go off – the heat detector was much slower and did not always reach the critical value when sprinklers were used. For the case without water suppression, the ion detector was always slightly faster than the optical detector, with mean difference of 13 s. The ion detector was faster than optical in 64%

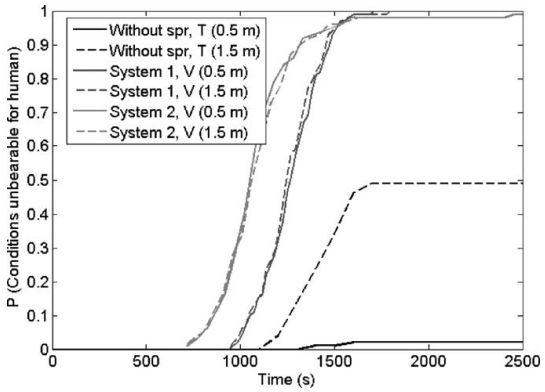

Fig. 10. Cumulative probability distributions for the time that the conditions for human get intolerable 7.5 m away from the ignition point. T, temperature criterion; V, visibility criterion.

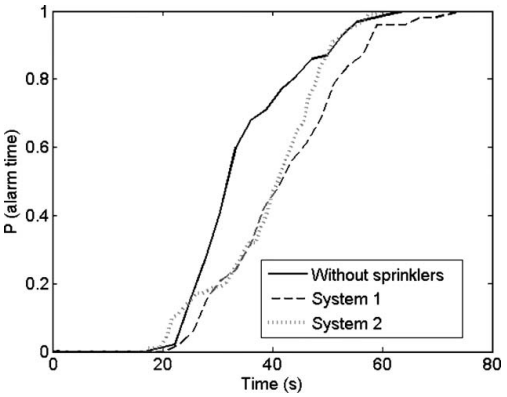

Fig. 11. Cumulative probability distributions of smoke alarm activation times.

of the cases when suppression System 1 was used, and in only 8% with suppression System 2. The mean delays were the same order of magnitude as for the non-suppressed case. These results are in line with the results of Fig. 10, where the visibility is lost much faster with suppression System 2 than with System 1. Soot yield is assumed to be 5% in the simulations. At the time of the OMNI detector activations, none of the sprinklers has been activated and all the systems are similar in this sense. The only difference comes from the x-location of the burner which is constant in the simulations without sprinklers. The small differences in the cumulative distributions are caused by the different random variables. The alarm activates between 20 and 80 s from the ignition of the fire. The heat release rates at the time of the alarms are less than 10 kW.

5.2. Sensitivity study

The random variables of the Monte Carlo simulation covered the uncertainty associated with the unknown location and properties of the initial fire, properties of the sprinkler heads and surrounding walls and the variability in the power cables. The simulations were performed using the existing (System 1) or proposed (System 2) design values of the sprinkler system. Additional simulations were performed to study the sensitivity of the simulation outcome on

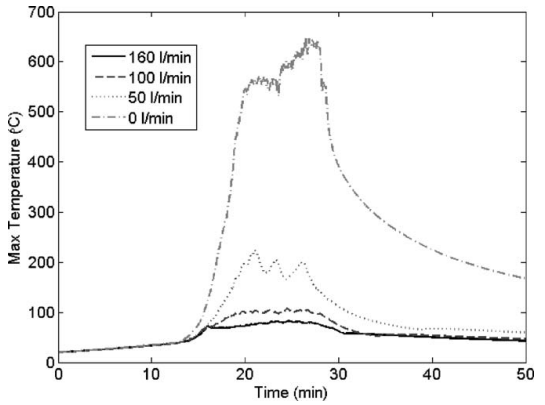

Fig. 12. The maximum power cable temperatures at different flow rates of the nozzles.

the two of the sprinkler system design values: water flow rate and installation height.

The flow rate of the nozzles depends strongly on the pressure in the pipes. If the pressure drops due to some fault or because too many nozzles are operating at the same time, the suppression system may not be able to protect the room as designed. The same simulation of the suppression System 2 was repeated with flow rates varying between 0 and 160 l/min. As long as the flow rate was at least 50 l/min, it was found to have no significant effect on the heat release rate or the peak temperature of the IC cables, but the difference between 50 l/min and 0 l/min is remarkable. The effect of the flow rates is seen best from the peak temperature of the power cables (Fig. 12). The nozzles with flow rate of 50 l/min or less are not able to protect the power cables from exceeding the failure temperature in this case.

Above, it was suspected that the efficiency of the suppression System 2 may be sensitive to the height of the upper nozzles. The same simulation was repeated varying the height of the upper nozzles. The results are shown in Figs. 13 and 14. However, the differences were not significant and the temperatures remained well below the failure limit in all cases.

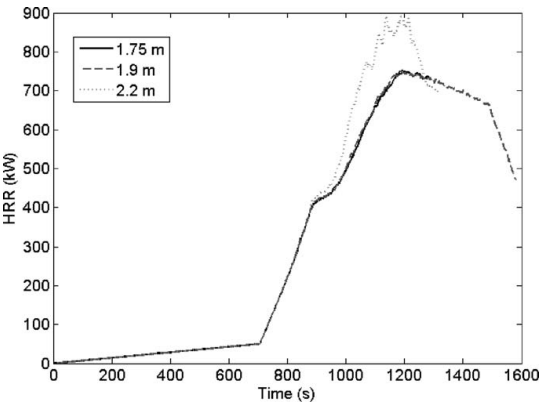

Fig. 13. Heat release rate in the simulation with different upper nozzle heights. The legend indicates the distances from ceiling.

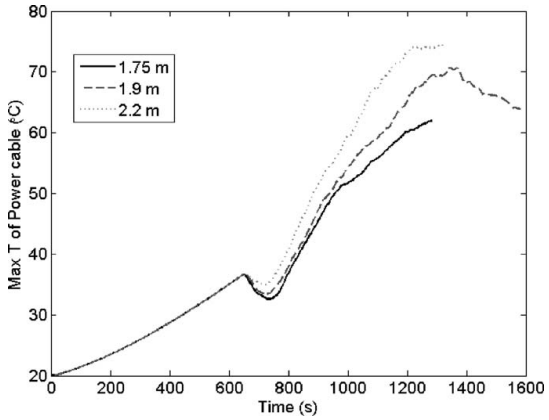

Fig. 14. The maximum temperature of the power cables with different upper nozzle distances from the ceiling. The legend indicates the distances from ceiling.

6. Conclusions

Cable fires inside a cable tunnel of a nuclear power plant were simulated using Monte Carlo technique and FDS code as a deterministic tool. The fire development on the power cables was predicted using a pyrolysis model, and the performance of the water based suppression systems was simulated using physical modelling of the sprinkler activation and two-phase flows. Three separate MC simulations were performed with 100 LHC samples for each, to find out the differences between two water suppression systems and the case without any suppression system. Some of the model parameters associated with the placement of the ignition point, tunnel properties and cable properties, were treated as random variables with probability distributions. The results included the probability distributions of the peak heat release rate in the room, cable failure times, alarm times and the conditions for a fire fighter entering the room.

In the case without fire suppression, the predicted peak heat release rates varied between 2 and 60 MW. When suppression was used, the peak HRRs were generally less than 10% of the ones without suppression. The suppression effect on the cable failures was clear as well. Without suppression, almost all power cables and 60% of the IC cables of the second sub-system failed due to the thermal damage, but failures did not occur when either of the two suppression system was used. From the viewpoint of the plant PRA, this is an extremely interesting result because it means that that the probability of losing both sub-systems is determined by the unavailability of the suppression system.

The temperature of the cables in the second sub-system was mostly dependent on the height of the ignition point, but the direction of the effect was dependent on the suppression system. The internal temperatures of the power cables were higher with suppression System 2. According to the current results, the performance of a suppression system similar to System 2 may be very sensitive to the actual distance of the upper nozzles from the ceiling. As the system has no ceiling nozzle, it cannot prevent fire spread and failures in the highest cable trays if the upper nozzles are designed to be placed too low.

In most simulations, the conditions would remain tolerable for a fire fighter reaching the fire before cable failures. In the simulations without suppression system, the temperature exceeded 100 °C with a 50% probability. In the simulations with suppression system, the heat was not a problem but the visibility was lost in all the cases. The smoke alarms were activated quite early in all fires, between 20 and 80 s from the ignition.

Overall, the current results concerning the efficiency of the sprinkler systems should be considered conservative because the power of the ignition source is not affected by the sprinkler activation. In reality, the ignition source already could be suppressed by the sprinklers. This finding indicates that the accurate simulation of fire development from its early phases is extremely important for the completeness and accuracy of the probabilistic, simulation based fire risk assessment. Despite the many advances in our capability to simulate fire spreading and fire dynamics, the focus of the fire research should remain in this topic, as it is still far from solved.

Another topic where more research and, in particular, full scale validation of the models is needed, is the simulation of water suppression. Both the physical and numerical simulation problems observed during this work indicate that the models of the two-phase flows and suppression effects are far from mature. The importance of the water suppression system was evident because the PVC cables burn easily and impose a high fire risk. They are still widely used in the nuclear installations around the world, but in the new or renovated installations, the fire performance of the electrical cables may be significantly better due to the use of flame retardant materials. The safety importance of the suppression system may be much smaller in such cases, but the risks in these situations have not been generally evaluated.

Acknowledgements

We thank Dr. Tuula Leskelä of Aalto University, for performing the thermoanalytical experiments. We also thank Dr. Johan Mangs and Mr. Konsta Taimisalo from VTT for the cone calorimeter experiments. This work was funded by the State Nuclear Waste Management Fund (VYR).

References

Andersson, P., Van Hees, P.,2005. Performance of cables subjected to elevated temperatures, fire safety science. In: Proceedings of the Eighth International Symposium. International Association for Fire Safety Science, pp. 1121–1132, doi:10.3801/IAFSS.FSS.8-1121.

Chien, S.-W., Huang, Y.-H., Shen, T.-S., Lin, C.-Y., Cheng, T.-M., 2006. How does a sprinkler system perform in a nuclear power plant? Journal of Applied Fire Science 15 (3), 201–217, doi:10.2190/AF.15.3.c.

Dreisbach, J., McGrattan, K., 2008. Cable Response to Live Fire (CAROLFIRE) Volume 3: Thermally-Induced Electrical Failure (THIEF) Model., NUREG/CR-6931, Vol. 3 NISTIR 7472.

Dreisbach, J., Hostikka, S., Nowlen, S.P., McGrattan, K., 2010. Electrical cable failure – experiments and simulation. In: 12th International Interflam Conference, pp. 1857–1865.

Ferng, Y.M., Liu, C.H., 2011. Investigating the burning characteristics of electric cables used in the nuclear power plant by way of 3-D transient FDS code. Nuclear Engineering and Design 41, 88–94, doi:10.1016/j.nucengdes.2010.08.021.

Harmathy, T.Z., 1995. Properties of building materials. In: The SFPE Handbook of Fire Protection Engineering, 2nd edition, Section 1, Chapter 10 and Appendix B (table B-7).

Hostikka, S., Keski-Rahkonen, O., 2003. Probabilistic simulation of fire scenarios. Nuclear Engineering and Design 224, 301–311.

Hostikka, S., 2008. Development of fire simulation models for radiative heat transfer and probabilistic risk assessment. VTT publications 683, Doctoral dissertation.

Iwankiw, N., Beitel, J., Gewain, R., 2004. Structural materials. In: Harper, C. (Ed.), Handbook of Building Materials for Fire Protection. McGraw-Hill Handbooks, New York.

Mangs, J., Keski-Rahkonen, O., 1997. Fullscale fire experiments on vertical and horizontal cable trays. VTT publications 324, Espoo, 58 pp. + app. 44 pp.

Matala, A., Hostikka, S., Mangs, J.,2008. Estimation of pyrolysis model parameters for solid materials using thermogravimetric data. In: Fire Safety Science – Proceedings of the Ninth International Symposium. International Association for Fire Safety Science, pp. 1213–1223.

McGrattan, K., Hostikka, S., Floyd, J., Baum, H., Rehm, R., Mell, W., McDermott, R., 2007. Fire Dynamics Simulator (Version 5), Technical Reference Guide. Volume 1: Mathematical Model. National Institute of Standards and Technology, Gaithersbug, MD, NIST Special Publication 1018-5.

McGrattan, K., McDermott, R., Hostikka, S., Floyd, J., 2010. Fire Dynamics Simulator (Version 5) User's Guide. National Institute of Standards and Technology, Gaithersburg, MD, NIST Special Publication 1019-5.

McKay, M., Beckman, R., Conover, W., 1979. A comparison of three methods for selecting values of input variables in the analysis of output from a computer code. Technometrics 21 (2), 239–245.
Paté-Cronell, M.E., Dillon, R.L., 2006. The respective roles of risk and decision analyses in decision support. Decision Analysis 3 (4), 220–232.
Shen, T-S., 2006. Will the second cable tray be ignited in a nuclear power plant? Journal of Fire Sciences 24, 265–274.
Stein, M., 1987. Large sample properties of simulations using Latin Hypercube sampling. Technometrics 29 (2), 143–151.
U.S. NRC, 2005. EPRI/NRC-RES Fire PRA Methodology for Nuclear Power Facilities: Volume 2: Detailed Methodology. Electric Power Research Institute (EPRI)/U.S. Nuclear Regulatory Commission, Office of Nuclear Regulatory Research (RES), Palo Alto, CA/Rockville, MD, EPRI – 1011989 and NUREG/CR-6850.

Series title and number
VTT Science 44

Title	**Methods and applications of pyrolysis modelling for polymeric materials**
Author(s)	Anna Matala
Abstract	Fire is a real threat for people and property. However, if the risks can be identified before the accident, the consequences can be remarkably limited. The requirement of fire safety is particularly important in places with large number of people and limited evacuation possibilities (e.g., ships and airplanes) and for places where the consequences of fire may spread wide outside of the fire location (e.g., nuclear power plants). The prerequisite for reliable fire safety assessment is to be able to predict the fire spread instead of prescribing it. For predicting the fire spread accurately, the pyrolysis reaction of the solid phase must be modelled. The pyrolysis is often modelled using the Arrhenius equation with three unknown parameters per each reaction. These parameters are not material, but model specific, and therefore they need to be estimated from the experimental small-scale data for each sample and model individually. The typical fuel materials in applications of fire safety engineers are not always well-defined or characterised. For instance, in electrical cables, the polymer blend may include large quantities of additives that change the fire performance of the polymer completely. Knowing the exact chemical compound is not necessary for an accurate model, but the thermal degradation and the release of combustible gases should be identified correctly. The literature study of this dissertation summarises the most important background information about pyrolysis modelling and the thermal degradation of the polymers needed for understanding the methods and results of this dissertation. The articles cover developing methods for pyrolysis modelling and testing them for various materials. The sensitivity of the model for the modelling choices is also addressed by testing several typical modeller choices. The heat release of unknown polymer blend is studied using Microscale Combustion Calorimetry (MCC), and two methods are developed for effectively using the MCC results in building an accurate reaction path. The process of pyrolysis modelling is presented and discussed. Lastly, the methods of cable modelling are applied to a large scale simulation of a cable tunnel of a Finnish nuclear power plant. The results show that the developed methods are practical, produce accurate fits for the experimental results, and can be used with different materials. Using these methods, the modeller is able to build an accurate reaction path even if the material is partly uncharacterised. The methods have already been applied to simulating real scale fire scenarios, and the validation work is continuing.
ISBN, ISSN	ISBN 978-951-38-8101-6 (Soft back ed.) ISBN 978-951-38-8102-3 (URL: http://www.vtt.fi/publications/index.jsp) ISSN-L 2242-119X ISSN 2242-119X (Print) ISSN 2242-1203 (Online)
Date	November 2013
Language	English, Finnish abstract
Pages	85 p. + app 87 p.
Keywords	pyrolysis modelling, simulation, polymer, cables, composites, probabilistic risk assessment (PRA)
Publisher	VTT Technical Research Centre of Finland P.O. Box 1000, FI-02044 VTT, Finland, Tel. +358 20 722 111

Julkaisun sarja ja numero
VTT Science 44

Nimeke	**Pyrolyysimallinnuksen metodeita ja sovelluksia polymeereille**
Tekijä(t)	Anna Matala
Tiivistelmä	Tulipalot aiheuttavat todellisen uhan ihmisille ja omaisuudelle. Mikäli riskit voidaan tunnistaa jo ennen onnettomuutta, tulipalon ikäviä seurauksia voidaan rajoittaa. Paloturvallisuuden merkitys korostuu erityisesti paikoissa, joissa on paljon ihmisiä ja rajoitetut evakuointimahdollisuudet (esim. laivat ja lentokoneet), ja laitoksissa, joissa tulipalon seuraukset voivat levitä laajalle palopaikan ulkopuolellekin (esim. ydinvoimalaitokset). Jotta materiaalien palokäyttäytymistä voitaisiin luotettavasti tarkastella erilaisissa olosuhteissa, pitää palon leviäminen pystyä ennustamaan sen sijaan, että paloteho määrättäisiin ennalta. Palon leviämisen ennustamiseksi täytyy materiaalin kiinteän faasin pyrolyysireaktiot tuntea ja mallintaa. Pyrolyysi mallinnetaan usein käyttäen Arrheniuksen yhtälöä, jossa on kolme tuntematonta parametria jokaista reaktiota kohti. Nämä parametrit eivät ole materiaali- vaan mallikohtaisia, ja siksi ne täytyy estimoida kokeellisista pienen mittakaavan kokeista jokaiselle näytteelle ja mallille erikseen. Paloturvallisuusinsinöörin kannalta erityisen hankalaa on, että palavat materiaalit eivät useinkaan ole hyvin määriteltyjä tai tunnettuja. Esimerkiksi sähkökaapeleiden polymeeriseokset voivat sisältää suuria määriä erilaisia lisäaineita, jotka vaikuttavat materiaalin palokäyttäytymiseen merkittävästi. Kemiallisen koostumuksen tunteminen ei ole välttämätöntä luotettavan mallin aikaansaamiseksi, mutta aineen lämpöhajoaminen ja erityisesti palavien kaasujen vapautuminen tulisi tuntea tarkasti. Väitöskirjan tiivistelmäosa kokoaa yhteen tärkeimmät taustatiedot pyrolyysimallinnuksen ja polymeerien palokäyttäytymisen ymmärtämisen tueksi. Tässä väitöstyössä on kehitetty menetelmiä pyrolyysiparametrien estimoimiseksi ja näitä metodeita on testattu erilaisilla materiaaleilla. Mallinnusvalintojen merkitystä mallin tarkkuuteen on myös tutkittu herkkyysanalyysin keinoin. Osittain tuntemattomien polymeeriseosten lämmön vapautumista on tutkittu käyttäen mikrokalorimetria. Mikrokalorimetritulosten hyödyntämiseksi kehitettiin kaksi metodia, joiden avulla voidaan saada aikaan entistä tarkempia reaktiopolkuja. Lopuksi pyrolyysimallinnusta on hyödynnetty sovellusesimerkissä suomalaisen ydinvoimalan kaapelitilan täyden mittakaavan kaapelisimuloinneissa. Tulokset osoittavat, että tässä työssä kehitetyt menetelmät ovat käytännöllisiä, tuottavat riittävän tarkkoja sovituksia koetuloksille ja niitä voidaan soveltaa monien erilaisten materiaalien mallintamiseen. Näitä menetelmiä käyttämällä mallintaja pystyy mallintamaan tuntemattomienkin materiaalien palokäyttäytymistä riittävän tarkasti. Menetelmiä on jo sovellettu todellisten, suuren mittakaavan palotilanteiden simuloimiseksi, ja validointityö jatkuu edelleen.
ISBN, ISSN	ISBN 978-951-38-8101-6 (nid.) ISBN 978-951-38-8102-3 (URL: http://www.vtt.fi/publications/index.jsp) ISSN-L 2242-119X ISSN 2242-119X (painettu) ISSN 2242-1203 (verkkojulkaisu)
Julkaisuaika	Marraskuu 2013
Kieli	Englanti, suomenk. tiivistelmä
Sivumäärä	85 s. + liitt. 87 s.
Avainsanat	pyrolyysimallinnus, simulaatiot, polymeerit, kaapelit, komposiitit, todennäköisyyspohjainen riskianalyysi (PRA)
Julkaisija	VTT PL 1000, 02044 VTT, puh. 020 722 111